CARBON DIOXIDE ASSISTED BLENDING OF BIODEGRADABLE POLYESTERS

by

SHONA HOLLIE MURPHY

UNIVERSITY OF BIRMINGHAM

A thesis submitted to the University of Birmingham

for the degree of

DOCTOR OF PHILOSOPHY

School of Metallurgy and Materials
College of Engineering and Physical Sciences
University of Birmingham
September 2014

ABSTRACT

Blends of biodegradable polyesters; poly(ε-caprolactone) (PCL) and poly(lactic acid) (PLA) were produced by a variety of preparation methods; solution casting, melt blending and blending in the presence of carbon dioxide using a single screw extruder. The blends were characterised using scanning electron microscopy (SEM), mechanical testing, differential scanning calorimetry (DSC), Fourier Transform infrared spectroscopy (FTIR), rheology and size exclusion chromatography (SEC). Comparison of the blends produced via the different preparation techniques indicated that carbon dioxide was able to improve the morphology and mechanical properties of the PLA/PCL blends.

The influence of carbon dioxide on the reptation time of poly(ε-caprolactone) was investigated using oscillatory rheology. It was shown that by introducing CO_2 into the polymer melt, the reptation time was significantly reduced, providing evidence that CO_2 was interacting with this polymer. Further analysis of the data showed that the activation energy to flow was reduced, which was consistent with the reduction in the reptation times.

Flash DSC, a relatively new thermal analysis technique, was used to explore areas of polymer science that are otherwise unachievable using conventional DSC. It showed the ability to prevent reorganisation and crystallisation in partially crystalline polymers such as poly(ε-caprolactone) and was able to evaluate the activation energy of the glass transition temperature for different amorphous and partially crystalline grades of PLA.

ACKNOWLEDGEMENTS

I would like to express my sincere gratitude to all who have supported me throughout my PhD. In particular, I would like to thank my supervisors, Dr. Mike Jenkins and Dr. Gary Leeke for their guidance and encouragement.

I would also like to give my appreciation to Frank Biddlestone who has provided me with invaluable technical assistance, advice and friendship.

I am extremely grateful to the University of Nottingham for allowing access to their high pressure rheology equipment and to Dr. Catherine Kelly for her assistance with these measurements, in addition to her advice and support with numerous experiments throughout my PhD. Many thanks to Kayleigh McEwan at Warwick University who also provided valuable assistance and access to SEC equipment.

I would also like to thank Prof. Jim Hay for his insightful discussions on my work and to those who have provided emotional support, friendship and guidance; Dr. Stephen Kukureka, Mrs Anne Cabezas and Prof. Paul Bowen.

I hold great appreciation for the Institution of Mechanical Engineers (IMechE), the Institute of Materials, Minerals and Mining (IOM^3), Dr. Gary Leeke from Chemical Engineering (UoB) and the EPSRC, who provided financial support, enabling me to attend and present my work at the 28th international conference of the Polymer Processing Society (PPS-28) in Pattaya, Thailand. The experience is something I am incredibly grateful for.

Finally, my upmost appreciation goes to my family and friends for their continuous support and encouragement over my time at the University of Birmingham. I reserve my deepest love and appreciation for my parents, who have played a key role in my achievements to date. Their constant support and belief is something I will always be grateful for and something I will never forget.

CONTENTS

CHAPTER 1 - INTRODUCTION

CHAPTER 2 – MATERIALS, EXPERIMENTAL TECHNIQUES AND METHODS

CHAPTER 6 – CONCLUSIONS AND FURTHER WORK

CHAPTER 1 - INTRODUCTION

1.1 The origins of bio-polymer science

Many polymers, or macromolecules, are naturally occurring and essential for life and some have been exploited by humans for thousands of years. Those found in plants and animals, such as DNA, enzymes, polysaccharides (starches and cellulose) are examples of crucially important polymers occurring in living organisms [1]. Other naturally occurring polymers that have been exploited by man include rubber, resins, wood, cotton, proteins, silk and leather [2].

Initial developments in the 19th century were made by chemically modifying the natural products; Thomas Hancock and Charles Goodyear, discovered that the properties of natural rubber could be improved by cross linking it with sulphur, a process called vulcanization [1]. Other semi-synthetic polymers and associative patents were also produced during this time; polymers such as cellulose nitrate and cellulose acetate; the 'viscose process' for producing textile fibres and cellophane film, Parkesine and celluloid. However, the first fully synthetic polymer to be commercialised, was not until 1910, when Leo Baekeland produced phenol-formaldehyde resin, known as Bakelite [3]. Synthetic polymers were subsequently produced from the cracking of crude oil, natural gas and coal distillation, in particular from olefins, dienes, aromatics *etc.* [4]. The following years saw the production of new polymers and an understanding that their unique properties arose from the long chain nature of the materials. This was followed by the production of conventional linear polymers during the 1930s to the 1950s. The development of polycondensation and polyaddition reactions enabled new polymers such as poly(vinyl chloride), polystyrene, poly(methyl methacrylate), Nylon 6,6,

polyethylene, styrene-butadiene rubber and silicones to be manufactured in large tonnages. The company DuPont undertook the controlled preparation of polyesters and polyamides, and subsequently poly(ethylene terphthalate) and polyurethanes were developed.

It was also during this time that the interest in bio-polymers began, with pioneering work by Carothers who derived an aliphatic polyester from lactic acid in 1932. However, the material possessed poor mechanical properties and was later improved and patented by DuPont in 1954 [5]. DuPont were also responsible in later years for the production of synthetic fibres stronger than steel, such as Kevlar discovered by Stephanie Kwoleck [6]. The research into bio-polymers was discontinued as a result of their susceptibility to degradation. In 1972, Ethicon introduced high-strength biocompatible fibres for medical resorbable sutures and the focus for these polymers remained within the medical field. The more attractive cost structure of bio-polymers in recent years has consequently seen a renewed interest and therefore a broadening of applications outside of the medical industry [5].

1.1.1 Polymer microstructure

With a wider range of applications and demands for diversity in polymer properties, the need to improve and develop these materials has remained, although the increased cost of raw materials has placed constraints on what polymer materials are commercially viable. Polymer science is still expanding with new materials, challenges and concepts that are constantly being tackled, a few of which are demonstrated and undertaken in this thesis.

In order to explain the material properties of a polymer, understanding it on a molecular level and defining the morphology of a polymer helps to distinguish its properties and determine its applications. A polymer is composed of molecules constructed from many smaller structural units called monomers, linked to each other by interatomic covalent bonds. Polymerisation is the formation of a polymer by linking together monomer molecules through chemical reactions. For the majority of polymers, these molecules are in the form of long and flexible chains. The backbone of each chain is usually a string of carbon atoms. For example, the polymerisation of ethylene produces polyethylene, a chain typically containing 10,000 carbon atoms linked together [1]. Polymers such as these, are derived from one species of monomer and are termed homopolymers. Heteropolymers exist when there are several monomers present, an example being a copolymer. Copolymers exist in many forms; random, alternating, block and graft copolymers. The repetition of monomer units can be linear, branched (containing side chains) or interconnected (possessing a three-dimensional network) [4].

1.1.1.1 Polymer tacticity

Different arrangements and chemical composition of polymers have large influences on their properties. Stereochemistry may largely influence the polymer morphology and is described by three different forms of spatial arrangement; isotactic, syndiotactic and atactic [7]. Examples are shown in Figure 1.1, which demonstrates the tacticity of polystyrene. Isotactic arrangements have pendant groups all situated on the same side of the chain, while in syndiotactic the pendant groups are arranged in a regular, alternating manner with respect to the chain.

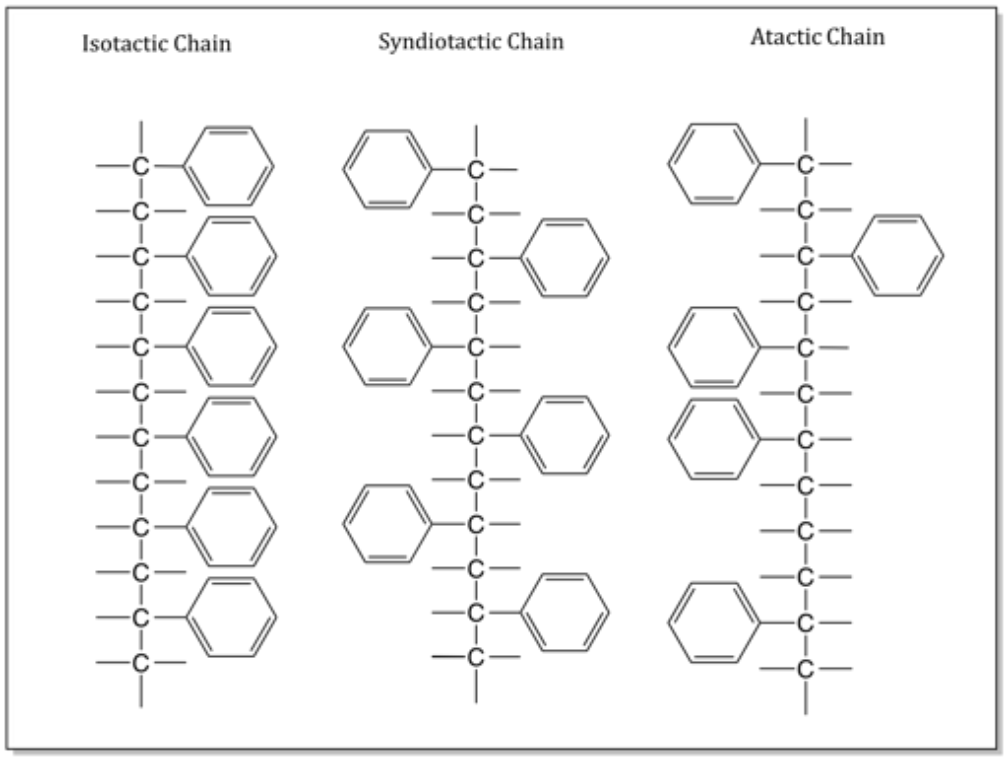

Figure 1.1. Tacticity of polystyrene, illustrating the three forms of spatial arrangement; isotactic, syndiotactic and atactic.

Atactic polymers display a completely irregular arrangement of pendant groups along the chain. These subtle variations in chain tacticity of polystyrene may yield significantly different properties and polymer structure, such as mechanical strength, thermal stability and crystallisation [8]. The irregular nature of the atactic structure produces an amorphous form of this polymer. Both stereoregular isotactic and syndiotactic forms of polystyrene can crystallise. Another similar example is polypropylene, isotactic polypropylene (iPP) is crystalline, whereas atactic is amorphous [9].

1.1.1.2 Partially crystalline polymers

Polymers are considered to be either amorphous or crystalline, although no engineering polymer can be completely crystalline, but in reality are more correctly labelled as partially crystalline. Bulk crystallised polymers have amorphous areas contained between the crystalline regions. These crystalline regions consist of branched lamellar crystals, which are organised into a spherical particle, or spherulite with amorphous regions between the lamellae. Figure 1.2 illustrates a typical example of polymer spherulites, which have been grown by cooling from the melt and observed by hot-stage microscopy.

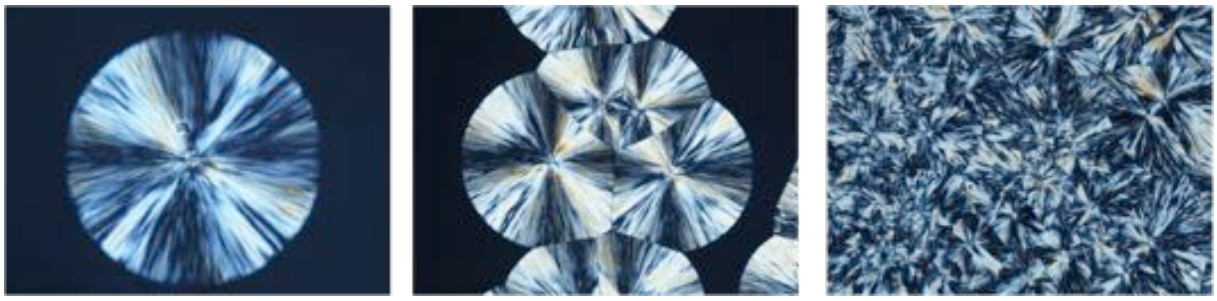

Figure 1.2. A typical example of polymer spherulites across the different stages of growth and impingement. Micrographs of PLA 3051D observed after 60, 90 and 120 minutes at 118 ˚C.

The single spherulite in this particular example is approximately 100 μm in diameter. The spherulite is initiated from a central nucleus, most likely a lamellar crystal which, by repeated branching, produces a spherical contour and grows radially at a linear growth rate. Spherulites will continue to grow until they impinge with neighbouring spherulites and stop growing. The linear boundaries between spherulites are evident in Figure 1.2. A spherulite consists of many chain-folded lamellae formed into plate-shaped polymer

crystallites, approximately 10 nm in thickness [10] (in addition to some amorphous content) that radiate from the centre outwards (Figure 1.3). The chains leaving the surface of the lamallae may re-enter randomly or by regular adjacent re-entry. In addition, tie molecules link the lamellae to one another, strengthening the interface between the crystalline and amorphous content.

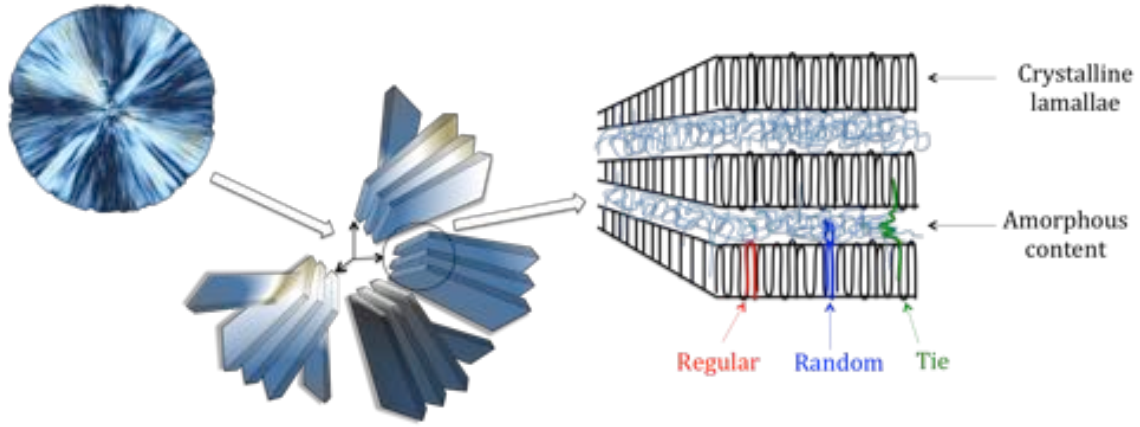

Figure 1.3. Schematic of the structure of a polymer spherulite, composed of plate-shaped crystallites. These crystallites consist of chain-folded lamellae. Contained between each polymer crystallite is unordered amorphous material.

The amorphous regions of a partially crystalline polymer exhibit a glass transition, which occurs at the glass transition temperature (T_g) and at a higher temperature a melting transition (T_m), corresponding to melting of the crystalline components discussed above. Once in the melt, the chains that were aligned and highly ordered in the crystalline regions become random and disordered; the polymer is now a viscous liquid. On cooling the melted polymer may undergo a further transition and re-crystallise at the crystallisation temperature (T_c). This transition is subject to a number of factors such as

the thermal history of a sample, cooling rate and the temperature at which the sample is crystallised. These influence the thickness of the chain-folded lamellae, being thicker as the crystallisation temperature increases. Thicker lamellae have a higher melting temperature. However, the behaviour of all transitions are also a function of the heating and cooling rates applied to the polymer.

1.1.1.3 Amorphous polymers

Amorphous polymers exhibit only a glass transition temperature. This is the temperature at which the polymer transforms from the glassy, brittle state into a more rubbery, flexible one. Above the glass transition, the chains have a significant increase in molecular mobility. The molecular structure of a polymer largely influences the temperature at which the glass transition occurs. A number of factors such as chain flexibility, branching and cross linking all affect the rotation about the polymer chain. Polar groups and large, bulky pendant groups with high molar volume provide a steric hindrance of the chain, and thereby cause restricted motion and the requirement of more thermal energy to set the chains in motion [11].

1.2 Biodegradable polymers

Biodegradable polymers are macromolecules that undergo a significant change in chemical structure under specific environmental conditions, resulting in bond scission of the chain backbone and consequently polymer disintegration [12]. It was initially used in the medical field in 1969 when the first biodegradable polymer, poly(glycolic acid) was developed to be the first degradable suture, previously the intestines of animals was used for this purpose [13]. The investigations and developments of other biodegradable polymers soon followed.

Since most commercial polymers are produced using petrochemicals (non-renewable feedstocks), and many are used for short duration applications, more recently, there has been some concern regarding sustainability [14].

The use of biodegradable polymers is becoming increasingly widespread as their applications broaden both into the biomedical [13] and food packaging industries [15]. Persistent rapid growth in the consumption of biodegradable plastics is forecast for the foreseeable future [16]. Europe continues to be the largest consumer of biodegradable polymers (particularly in the food packaging market), contributing to over half the global total [16].

Some examples of biodegradable polymers are poly(hydroxyalkanoates) (PHAs), these are naturally produced by bacteria, such as poly(3-hydroxybutyrate) (PHB) [17]. Others are produced using renewable resources such as poly(lactic acid) (PLA) (from corn starch) [18] and some are derived via a synthetic route such as poly(butylene succinate) (PBS) and poly(ε-caprolactone) (PCL) [19].

1.2.1 Poly(lactic acid)

Among biopolymers, poly(lactic acid) (PLA) is the most prevalent in the market place, due to availability and having the most attractive cost structure [20]. It is extensively used in various medical applications, such as drug delivery [21] and scaffolds in tissue engineering [22]. Additionally, there is a growing interest in the use of PLA as food packaging because PLA is derived from natural sustainable resources and it does not persist in landfill as it is biodegradable.

PLA is derived from 100% renewable resources such as corn and sugarcane, which are biocompatible, biodegradable and compostable [23, 24]. It has therefore attracted attention as an alternative to synthetic non-biodegradable polymers. Recently, companies such as NatureWorks LLC have developed a large-scale economic production of PLA. With its excellent shaping and moulding properties, PLA is a good candidate for packaging materials. In addition, it has a clarity and rigidity similar to poly(ethylene terephthalate) (PET) and polystyrene (PS) [20]. However, it has been reported that PLA is relatively brittle [25] and this has limited its range of applications.

Lactic acid is derived from the fermentation of sugars derived from corn, sugarcane and tapioca. PLA is produced directly from its basic building block, lactic acid, by condensation polymerisation. However, the commercial production of PLA is from the ring-opening polymerisation (ROP) of the cyclic dimer of lactic acid. This method enables the production of higher molecular weight polymer with lower racemisation and improved mechanical properties. It allows more accurate control of the resulting polymer properties and therefore it is more suitable for large scale production [26]. Figure 1.4 shows the chemical structure of poly(lactic acid).

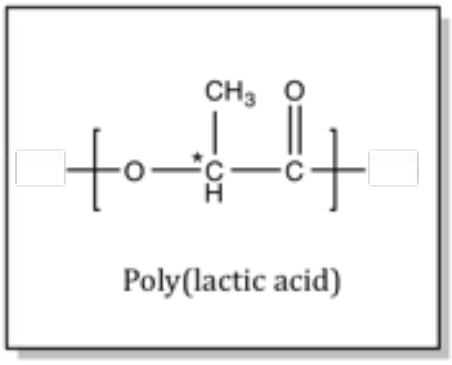

Figure 1.4. Chemical structure of poly(lactic acid) showing the asymmetric carbon atom.

Poly(lactic acid) (PLA) is a linear aliphatic polyester, consisting of lactic acid (2-hydroxy propionic acid) as the building blocks. The cyclic dimer of PLA possesses two asymmetric carbon atoms and consequently exists in three different forms (Figure 1.5). This building block can exist in optically active enantiomers: D-lactide, in which both asymmetric carbon atoms possess the D configuration or L-lactide, where both asymmetric carbon atoms exhibit the L configuration. The third form, *meso*-lactide, has one asymmetric carbon atom with the L configuration and the other with the D configuration as shown in Figure 1.5 [27]. The difference between the optically active D and L form and their effect on polarised light, is that with L-lactic acid the plane is rotated in the clockwise direction and D-lactic acid rotates light in the anti-clockwise direction [5]. In contrast, the *meso*-lactide form is optically inactive [28]. It is well established that depending upon the content of enantiomers and the ratio between L-lactide and D-lactide in a polymer, variable properties can be achieved, from partially crystalline to amorphous [29].

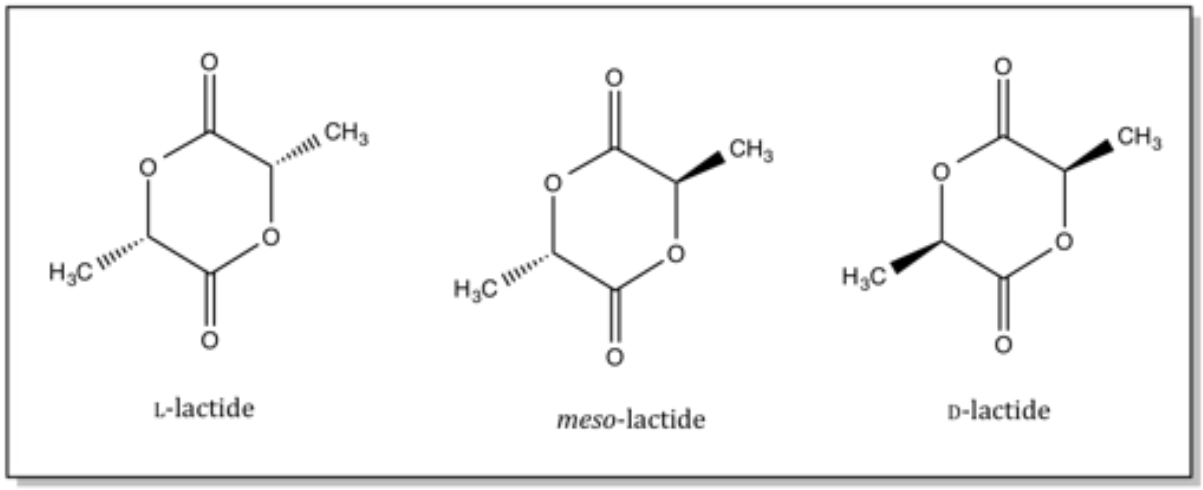

Figure 1.5. The chiral optical isomers of poly(lactic acid): L-lactide, *meso*-lactide and D-lactide.

Homopolymers synthesised entirely from either D or L-lactide produce partially crystalline polymers with a melting point around 180 ˚C [30]. When PLA polymers are produced with L-content greater than approximately 90% they are partially crystalline, however, those with lower stereoregularity are amorphous and exhibit a glass transition temperature around 50-57 ˚C [30, 31]. The majority of lactic acid obtained from biological sources exists as L-lactic acid [32]. The crystallinity of PLA produced from pure L-lactide reaches levels of around 45% [33]. Research into the addition of small amounts of D-lactide into random copolymers containing predominantly L-lactide has been investigated. It was reported that the crystallinity, spherulite growth rate and lamella thickness decreased substantially on increasing D-content of the copolymers [34].

The influence of *meso*-lactide on properties of PLA has also been studied, showing that for every 1% *meso*-lactide introduced into PLA, there is a melting point depression of 3 ˚C corresponding with a significant reduction in crystallisation rate [35]. The reduction in crystallinity caused by both *meso*-lactide and D-lactide is a consequence of the

introduction of macromolecular imperfections into the stereoregular architecture of PLA. These imperfections are seen in the form of twists in the linear chain which may hinder close chain packing to an extent (depending on the amount of D or *meso*-lactide present) that either reduces the crystallinity of PLA or prevents it completely [19].

The formation of *meso*-lactide by racemisation is unavoidable during the polymerisation of PLA. For partially crystalline PLA grades, it is desirable to reduce the content of *meso*-lactide present by purification in order to produce the highest possible stereochemical purity prior to polymerisation. Starting with monomers of a higher purity consequently results in a superior quality PLA, however purification must be deemed technically and economically feasible [20]. Controlling the stereochemical purity and content of the lactide stereoisomers during PLA fabrication enables the tailoring of the obtained properties of the polymer such as crystallinity, melting point, degradation and mechanical strength [36, 37].

1.2.2 Poly(ε-caprolactone)

Poly(ε-caprolactone) (PCL) is a partially crystalline linear aliphatic polyester [38] first synthesised in the 1930s [39]. In contrast to PLA, PCL is a polymer derived from the by-products of crude oil distillation and although not produced from renewable raw materials, it is fully biodegradable. The chemical structure of poly(ε-caprolactone) is shown in Figure 1.6. As a well characterised polymer it is receiving much attention having many useful applications, being both biocompatible and biodegradable.

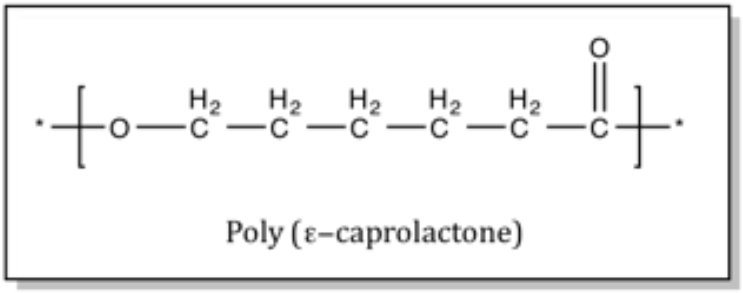

Figure 1.6. The chemical structure of poly(ε-caprolactone).

PCL possesses a degree of crystallinity of approximately 50% [40], which has been seen to decrease with increasing molecular weight [41]. It exhibits a glass transition temperature of -60 ˚C and a melting point of 59-64 ˚C [42].

Two main pathways to produce poly(ε-caprolactone) have been described in the literature; the polycondensation of a hydroxycarboxylic acid (6-hydroxyhexanoic acid) and the ring-opening polymerisation (ROP) of a lactone (ε-caprolactone) [43]. Similar to PLA, the preferred route is ring-opening polymerisation (ROP) because it produces a polymer with a higher molecular weight and a lower polydispersity.

PCL initially became commercially available as a biodegradable packaging material after observing its degradability by microorganisms. However, it is also degraded by hydrolysis in physiological conditions and due to its slow degradation rate it became an

attractive material for applications in the human body, where it could remain for 1-2 years [12]. The slow degradation rate is a result of its crystallinity and low fluid ingress into these regions. It is now one of several degradable polymers approved for use in the human body as a drug delivery device, as a result of its high permeability to various agents [44, 45]. It was initially investigated as a long term delivery vehicle for the contraceptive device Capronor® [46] however, it also acts as a controlled release device for bioactive molecules such as steroids, growth factors, hormones and vaccines [47]. In addition, PCL has also been utilised in the form of sutures and staples [48, 49] and is being extensively investigated as a biomaterial for tissue repair and regeneration [50, 51]. Various tissue scaffolds using poly(ε-caprolactone) have been prepared using a variety of different techniques. These range from selective laser sintering (SLS) (a rapid prototype technique utilising a CAD model) [52], to a more classical method exploiting the textile industry to produce woven, knitted scaffolds for regeneration of the aortic valve [53].

In order to broaden the applications of poly(ε-caprolactone), it has often been blended and copolymerised with other polymers in order to tailor properties such as degradation and improve its mechanical strength [42, 47, 54].

1.3 Polymer blending

Blending is a technique involving the mixing of two or more polymers with different physical properties in order to enhance the overall properties of the resultant system [55]. In comparison to copolymerisation, physical blending is deemed to be a more economical approach to tailoring polymer properties [56]. By controlling and finely adjusting the relative compositions of each polymer in the blend, it can provide an accurate control of the properties and extend the potential applications. In some instances it is used as a technique to produce more cost-effective materials by 'diluting' more expensive polymers with cheaper ones [57]. A successful example often used in polymer science and engineering is one that looks to improve and toughen the properties of a brittle polymer. This is achieved when a second elastomeric component is incorporated into the brittle microstructure, enabling ductile yield mechanisms by acting as a stress concentrator and consequently preventing brittle fracture [58].

Polymer blends may be characterised as miscible, partially miscible or immiscible systems. A miscible polymer system is homogeneous at a molecular level [59], whereas an immiscible blend is heterogeneous, indicated by one discrete phase dispersed in another. A partially miscible blend exhibits a 'window' of miscibility, occurring at specific conditions such as temperature and composition [60].

It is not always desirable or necessarily a requirement to produce a miscible polymer blend, for example rubbery impact modifiers rely upon an immiscible system in order for the rubber toughening mechanism to take effect [61].

Most polymer pairs are immiscible thermodynamically because of their unfavourable interactions and therefore result in a heterogeneous system consisting of a multiphase morphology [62]. This is dictated by the Gibbs free energy of mixing [63];

$$\Delta G_{mix} = \Delta H_{mix} - T\Delta S_{mix} < 0 \qquad \text{Equation 1.1}$$

where ΔG_{mix} is the free energy of mixing, ΔH_{mix} is the enthalpy of mixing and ΔS_{mix} is the entropy of mixing. The expression determines that in order for mixing to occur ΔG_{mix} must be negative and thereby resulting in miscibility. In summary, a miscible polymer system is thermodynamically associated with a negative value of the free energy of mixing while an immiscible polymer blend possesses a positive value [59].

Polymers possessing high molecular weights will have an entropy of mixing that is too small and deemed negligible in contributing to the necessary negative free energy. It is also thought, for high molecular weight polymers, the solubility parameters would have to be almost identical for mixing to take place [64]. Therefore a negative enthalpy value is required in order for miscibility to occur, however it is generally thought that for nonpolar systems the enthalpy of mixing is positive [61]. In contrast, for systems containing polar groups, the enthalpy of mixing may approach a negative value as a result of interactions between these polar groups. Despite the small entropy change, the negative enthalpy contributes to a negative value for the free energy of mixing and as a consequence miscibility is able to occur [65]. It should be noted that there must be a sufficient number of interactions between both polymers to outweigh any van der Waals forces remaining within the homopolymers. Additionally, in order for an interaction to occur, the polymers must be spatially articulated in a favourable manner [61]. For

example, the tacticity of PMMA with its constituent blends indicates a greater miscibility with the syndiotactic or atactic form of PMMA compared to its isotactic one [66, 67].

In a binary immiscible polymer blend, the microstructure is characterised by a dispersion of droplets in a matrix when there is a lower concentration of the dispersed phase. A phase inversion point exists when the concentration of the minor component is increased and the phase that was previously dispersed now becomes the matrix [62]. It is possible for a co-continuous morphology to be exhibited near the phase inversion point where both phases form single continuous inter-penetrating structures [68]. An example of both phase dispersion and a co-continuous morphology can be seen in Figure 1.7. This figure also presents a fine example of adhesion between the dispersed phase (droplet) and the matrix, as demonstrated by the bridging of phases through transcrystallinity. The effect of adhesion and transcrystallinity on polymer blends have been shown to improve important characteristics, such as mechanical properties [69, 70].

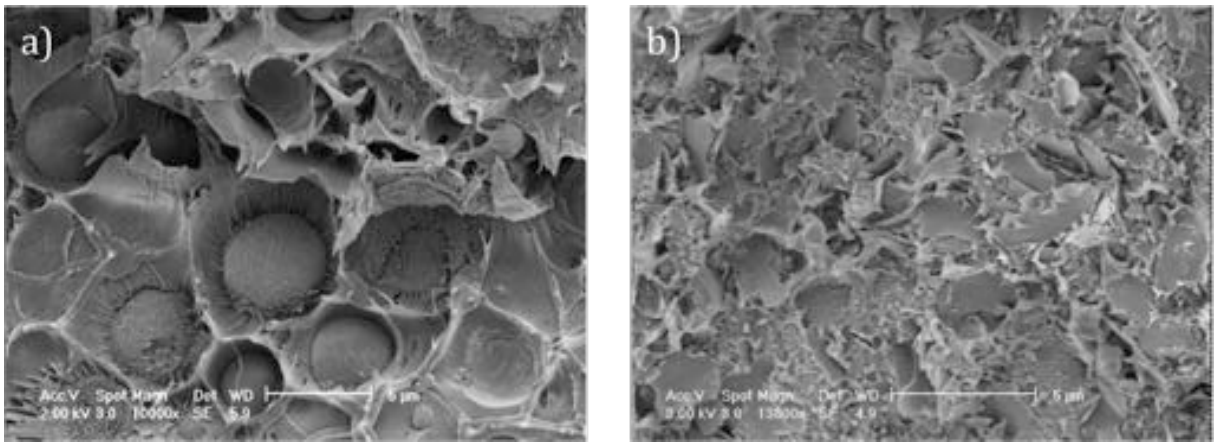

Figure 1.7. Images captured using a scanning electron microscope (SEM) demonstrating blend morphology of PLA 3801X and PCL 6800. a) 25/75 PLA/PCL: exhibits a dispersed (droplet) phase within a matrix and b) 50/50 PLA/PCL: illustrates a co-continuous morphology.

Unfortunately in some instances, the macrophase separation and the poor interfacial adhesion in these immiscible blends, highly restrict property combinations [55, 62].

A polymer blend consisting of two polymers possessing high molecular weights will typically produce a lower critical solution temperature (LCST) [71]. This means that these polymer blends may exhibit miscibility at lower temperatures, however will phase separate at higher temperatures. In contrast, an upper critical solution temperature (UCST) is determined when a polymer blend phase-separates by lowering the temperature. This demonstrates the very small change in entropy of mixing of two polymers, consequently the driving force for chemical change is therefore dictated by the enthalpy of mixing the two polymers in the system [59]. The enthalpy of mixing is derived from the strong intermolecular interactions between the two components, as mentioned previously. An example of a phase diagram depicting the LCST and UCST of a polymer blend is shown in Figure 1.8.

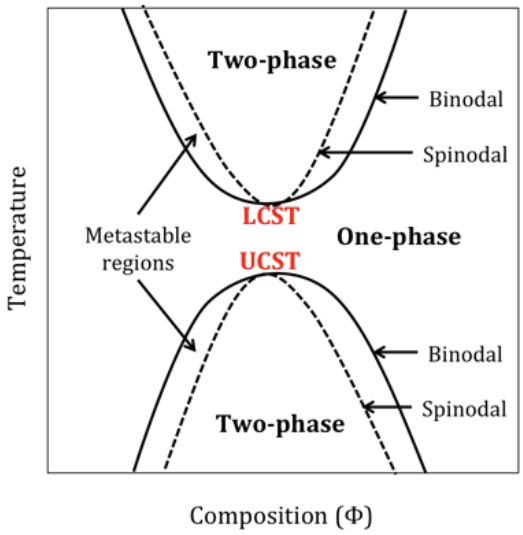

Figure 1.8. A phase diagram for a typical polymer blend system indicating the lower critical solution temperature (LCST) and the upper critical solution temperature (UCST). Adapted from Young and Lovell [72].

A single-phase region is present between the two binodals. Beyond these boundaries the blend exists as a two-phase system. The area between the binodal and spinodal is a metastable region. Here, if the energy barrier can be overcome, phase-separation of the blend takes place via a spontaneous process called spinodal decomposition. Within the unstable spinodal region phase-separation takes place by a nucleation and growth mechanism [72].

Some experimental methods to determine miscibility of polymers are: microscopy (for example scanning electron microscopy), differential scanning calorimetry, dynamic mechanical thermal analysis and Fourier Transform Infrared Spectroscopy. For example, in calorimetry, miscibility is distinguishable by a single glass transition temperature that has shifted from its constituent homopolymer T_g values [56].

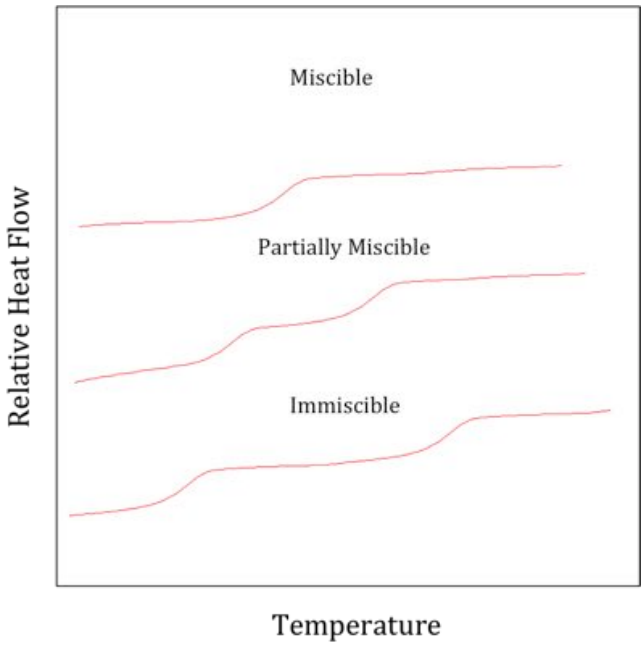

Figure 1.9. Illustration of the glass transitions for miscible, partially miscible and immiscible binary polymer blends.

An example of miscibility, partial miscibility and immiscibility in a binary polymer blend is illustrated in Figure 1.9. An immiscible system exhibits no change in the original T_g values, whereas partial miscibility is characterised by the presence of both T_gs, however the values are shifted towards one another.

The glass transition temperature of a miscible polymer blend depends on the composition and obeys the Fox equation (Equation 1.2):

$$\frac{1}{T_{gblend}} = \frac{w_1}{T_{g1}} + \frac{w_2}{T_{g2}} \qquad \text{Equation 1.2}$$

where w and T_g represent the weight fractions and glass transition temperatures of each blend component respectively. The component with the lower T_g is donated as T_{g1} and the higher as T_{g2} [73].

Surface tension, known as interfacial tension between the different phases in a polymer blend, can largely contribute to the immiscibility between two polymers [74]. Additives and compatibilisers, possessing lower surface tensions and good interfacial adhesion with both phases, can be added as a third component into a polymer blend [72]. These additives migrate to the interface between the polymer phases. Consequently, they reduce the interfacial tension, stabilise the blend morphology (by preventing coalescence of the dispersed phase) and subsequently producing a finer dispersion of the minor phase [59]. Additionally, the compatibilisers also improve the interfacial adhesion facilitating efficient stress transfer across the interface between both phases.

1.3.1 Blending poly(lactic acid) and poly(ε-caprolactone)

Despite the differences in structure of PLA, all forms are found to display brittle, glassy behaviour at room temperature due to a glass transition temperature around 60 °C [75]. At a molecular level it means that rigid chains will be present in the structure rendering the material unsuitable for applications needing flexibility and ductility. Accordingly, there have been a number of attempts to improve the mechanical properties of PLA through blending with other biodegradable (and less brittle) polymers and inclusion of a soft elastomeric second polymer into the microstructure has been identified as a method to improve the original mechanical properties of PLA [56].

Poly(ε-caprolactone) (PCL) is a partially crystalline, biodegradable aliphatic polyester with a low T_g at -60 °C that makes it a viable blend component for PLA as the introduction of PCL into PLA should result in an increase in flexibility and toughness. This is due to PCL having a high elongation at break and low tensile modulus [58]. Poly(lactic acid) and poly(ε-caprolactone) are polymers both possessing polar groups, Figure 1.10 illustrates the potential interactions that can occur between these polymers. The polar nature of the carbonyl group presents a possible interaction between the electronegative oxygen and positive carbon atom between both polymers. Another possibility is the formation of an intramolecular hydrogen bond, as illustrated in the image on the right of Figure 1.10 [76].

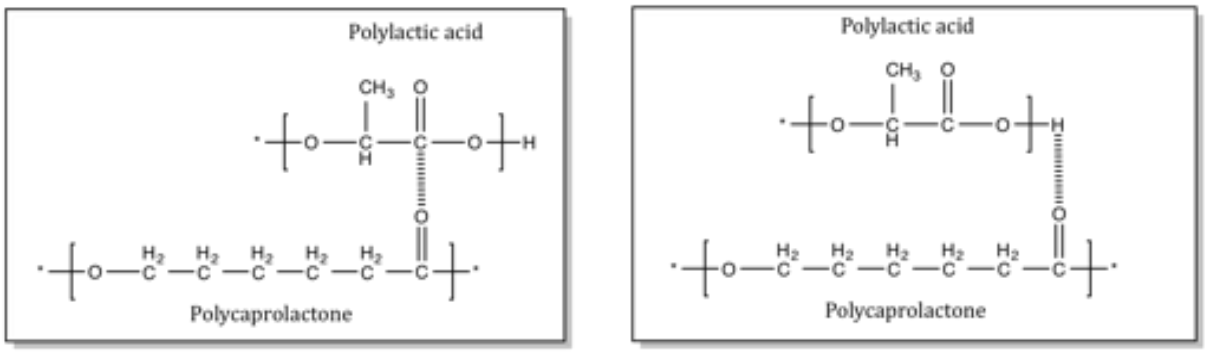

Figure 1.10. Potential interactions between poly(lactic acid) and poly(ε-caprolactone).

As mentioned earlier, the closer the values of the solubility parameters and the greater number and strength of interactions between the components in the polymer blend, the greater the likelihood of miscibility [77]. It has been reported that the differences in the solubility parameters for PLA and PCL is not large; 10.1 $(\text{cal cm}^{-3})^{1/2}$ compared to 9.2 $(\text{cal cm}^{-3})^{1/2}$, respectively [56]. However, many previous studies [25, 56, 78, 79] report findings of immiscibility with little or no interactions occurring.

Blends of PLA and PCL have attracted some attention in investigation of mechanical properties and the rates of biodegradation. In 2002, Choi *et al.* [80] studied the degradation rates of PLA/PCL blends for drug delivery. These authors selected polymers with higher molecular weights than those adopted in this thesis and limited their blend compositions to 70/30 PLA/PCL. Blends were produced by solution casting from chloroform. DSC and SEM analysis indicated that the polymers were clearly immiscible as determined by the absence of shifts in thermal transitions in addition to the observation of large PCL domains within a PLA matrix. However, the blend compatibility was enhanced by introducing a copolymer into the system. This was recognised by a reduction in size of the dispersed PCL domains.

Broz *et al.* (2003) [78] produced PLA/PCL blends by solution casting from methylene chloride. They chose to investigate the mechanical properties of varying mass fractions of PLA (0, 0.2, 0.4, 0.6, 0.8 and 1) with polymers possessing significantly lower molecular weights compared to this research. SEM showed poor adhesion at the interface between the blend components with inconclusive DSC results. However, confirmation of immiscibility and phase separation was made with NMR spectroscopy.

Previous research [58] has shown PLA/PCL blends to have a lower critical solution temperature (LCST) of 86 °C with a critical concentration mass fraction of 36% PCL. Using these findings, Broz *et al.* hypothesised that to improve the mechanical properties of the blends they should be annealed in the single-phase region (denoted by the LCST phase diagram). By treating the blends in this region, they thought to enhance the interfacial adhesion between the two blend components. Conversely, from their experimental data, Broz *et al.* conclude that interfacial adhesion may occur when the majority phase is PCL and not PLA. Analysing the mechanical properties of the blends, the authors suggest that when PLA is the major component, PCL simply dilutes the PLA matrix, reducing the total stress required to fracture.

Similar research [56] was conducted on a range of compositions (0/100, 20/80, 40/60, 60/40, 80/20 and 100/0) on both solution cast films (from chloroform) and melt blended samples. Phase separation was also confirmed using DSC and SEM. An annealing process above the LCST was again employed and the degree of crystallinity for the blends was measured before and after annealing. However, this study utilised two methods of blending for two different types of PLA and it is unclear as to why they employed different methodology. It is therefore difficult to establish if differences were due to the blending technique or type of PLA. Additionally, samples that were melt-

blended were further processed by hot-pressing into plaques. Despite it contributing to the degradation (shown by a reduction in molecular weight), it also altered the morphology and interactions that may have resulted through the mixing process. Therefore, measurements on these blends were a result of the hot-pressing technique and not melt-mixing.

Todo *et al.* [25] in 2007, selected PLA (M_w 200,000 g mol^{-1}) and PCL (M_w 120,000 g mol^{-1}) preparing blends in limited compositions of 5, 10 and 15% of PCL. Blends were prepared using a conventional melt-mixer and subsequently reprocessed by hot-pressing (changes in molecular weight were not specified). These authors investigated the mechanical properties of PLA/PCL blends and found a significant improvement in fracture toughness from adding as little as 5% PCL to brittle PLA. The improvement is a result of multiple craze formation, nucleated by debonding of spherulite interfaces of the PCL domains in a PLA matrix. However, phase separation is still prominent in these blends.

It is commonly reported that PLA/PCL blends have been produced through solution casting using a variety of solvents (chloroform, methylene chloride and dichloromethane). In addition to solution casting, research has also been undertaken on the production of blends using a laboratory mixer, including even fewer studies reporting the production of blends by extrusion. Simoes *et al.* [79] in 2009 employed the preparation of PLA/PCL blends in a twin-screw extruder. Similar to some of the previous studies, the blends were reprocessed and injection moulded into tensile and impact test specimens for mechanical testing. Following the common theme throughout previous research on these blends, PCL decreases the brittleness of PLA determined by an increase in strain at break. However, it also exhibits a decrease in the stress at break.

Using SEM and DSC, Simoes *et al.* confirmed that the preparation of these blends by extrusion also produced a phase-separated system, although some degree of adhesion was present between the two phases.

More recent investigations on these blends [81, 82] showed that PLA/PCL exhibited immiscibility and in a study in 2013 [83], the authors investigate grade PLA 2002D with PCL grade 6500. These blends were produced by solution casting from chloroform at 30/70 and 50/50 PLA/PCL compositions, focusing on evaluating the blends for scaffold fabrication. Their results correspond with all previous works, adding that good thermal stability is seen over 3600 seconds, a property important for polymer processing and extrusion.

In summary, despite the small solubility differences and the potential for interactions through the presence of polar groups, PLA and PCL blends have generally been found to be immiscible. Many researchers have accepted this morphology and in turn looked to improve the adhesion and interfacial tensions using additives such as compatibilisers. These compatibilisers, in the form of copolymers (such as diblock PLA-*b*-PCL and triblock PLA-PCL-PLA) have been introduced as a third component to PLA/PCL blends. The presence of these copolymers reduces the interfacial tension and consequently enhances the mechanical strength of the blends [84]. The persistence and continued research of these authors to improve the properties of PLA/PCL blends is evident from the literature [55, 84-86] as they have utilised different approaches to enhance the blend morphology.

1.4 Polymer processing with supercritical carbon dioxide

Carbon dioxide becomes a supercritical fluid above its critical point of 31.1 ˚C and 73.8 bar [87]. Figure 1.11 shows the phase diagram for supercritical carbon dioxide and defines the conditions under which it is a supercritical fluid ($scCO_2$). Above its critical values supercritical carbon dioxide possesses a special combination of gas-like viscosity and diffusivity with a liquid-like density. These unique properties can be finely tuned by small adjustments within the supercritical region [88], enabling $scCO_2$ to readily penetrate porous solids and evaporate from fragile structures without disrupting them [89].

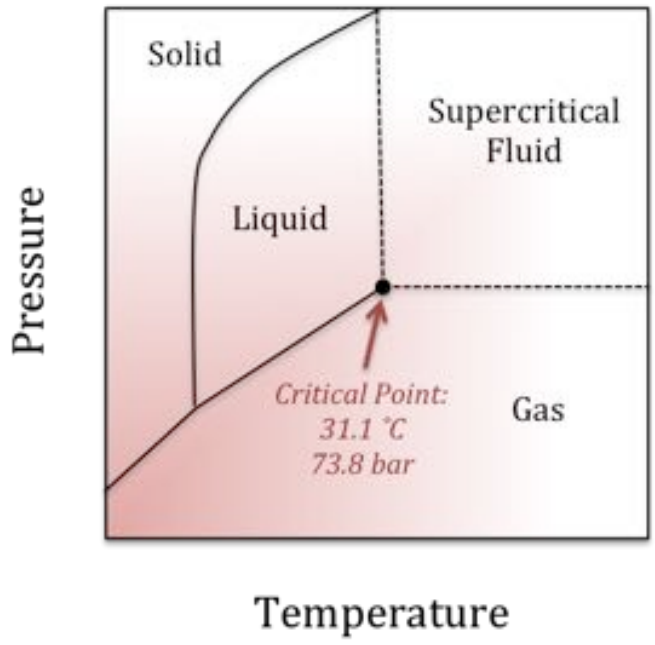

Figure 1.11. Phase diagram of supercritical CO_2.

Supercritical carbon dioxide is commonly employed in fluid extraction processes and is widely used in the food and beverage industry for the decaffeination of tea and coffee, in addition to extracting essential oils and flavours from herbs, spices and hops [89, 90].

The desire to pursue sustainable polymer processes has been governed by the chemical industry with research and development occurring in both academia and industry. The inexpensive, nontoxic and non-flammable nature of supercritical carbon dioxide, in comparison to the more environmentally hazardous volatile organic solvents (VOCs), make $scCO_2$ an appealing alternative in the polymer processing industry [91]. In contrast to these organic solvents, supercritical carbon dioxide can easily be removed as a result of its low critical temperature (31.1 ˚C) simply by depressurising the system once the desired morphology change has been achieved [92]. As a result, there is an elimination of solvent residues within products in addition to a reduction in atmospheric pollution. Therefore, the interest in polymer processing with supercritical fluids has rapidly grown in recent years, with a wealth of research into this subject area. The applications of $scCO_2$ in polymer processing include; polymerisation [93, 94], polymer foaming [95, 96], production of tissue scaffolds [97], preparation of systems for drug delivery [98] and induction of crystallisation in slow crystallising polymers [33, 99, 100]. Polymer blending in the presence of supercritical carbon dioxide is another potential research area, but it is one lacking significant documentation and will be discussed in more detail later in this section.

Not all polymers are soluble in carbon dioxide. CO_2 is a good solvent for mainly non-polar, low molecular weight molecules, however it is a very poor solvent for many high molecular weight polymers [94]. Those exhibiting solubility are characterised by; a flexible backbone, weak interactions between polymer segments, a high free volume (with a low glass transition temperature) and interaction sites such as carbonyl groups [87]. Examples of such polymers are amorphous fluoropolymers and silicones [94]. Processing routes utilising the dissolution of a polymer in $scCO_2$ include the synthesis of

previously mentioned soluble polymers [94] and removal of low molecular weight material in order to improve their properties [101]. In contrast, the solubility of carbon dioxide in polymers is much more extensive [91]. The importance of the presence and accessibility of polar groups on the solubility of CO_2 has long been recognised. The solubility of CO_2 in polymers is largely attributed to its ability to weakly interact with polar groups [102]. Processing routes utilising the dissolution of $scCO_2$ in a polymer include polymer foaming and blending. The effects associated from processing with carbon dioxide on a polymer system are characterised by; a reduction in the glass transition (plasticisation), an increase in the relative crystallinity and a reduction in the viscosity [101, 103]. These are more pronounced in amorphous than in partially crystalline polymers [101, 104] where it is assumed that the gas molecules preferentially penetrate the amorphous regions of the polymer [103]. In order for these effects to take place, carbon dioxide must first enter a polymer system (described below).

The gaseous properties of $scCO_2$ enable its diffusion into the free volume of a polymer, between the individual chains. Once inside, CO_2 forms Lewis acid-base interactions with the carbonyl groups. This disrupts the inter/intra molecular interactions, decreasing the number of chain entanglements within the polymers, consequently reducing their melting point and viscosity [105]. This is contradictory to the Barus equation [106] (Equation 1.3), which is commonly used to express the relationship between pressure and viscosity:

$$\eta_p = \eta_0(1 + \alpha p) \qquad \text{Equation 1.3}$$

where η_p is the viscosity at a given pressure, η_0 is the viscosity at atmospheric pressure, α is the pressure-viscosity coefficient and p is the experimental pressure. Raising the pressure consequently increases the viscosity of a polymer. Carbon dioxide facilitates processing by reducing the intermolecular interactions, increasing the chain separation thereby enhancing the mobility of the polymer [107]. In summary, supercritical carbon dioxide performs as a molecular lubricant.

The plasticised chain segments are able to adopt a crystalline form because of the increased mobility caused by CO_2 [101]. Therefore, $scCO_2$ is also able to induce crystallisation and cause it to occur prematurely [99, 100, 108].

The assistance of carbon dioxide in the blending of polymers can either be utilised to facilitate polymerisation or act as a viscosity reducing agent to enhance mixing [102]. This approach to polymer blending reveals positive findings reported in the literature [109-112]. High pressure and supercritical carbon dioxide assisted blending has been exploited in the production of numerous blend systems. The creation of additional free volume, resulting in a decrease in chain entanglements and characterised by a reduction in viscosity, may allow more effective blending to occur.

Phase dispersion and size within a polymer blend is largely governed by the interfacial tension and viscosity ratio between both components. It has been reported in a number of instances that the presence of $scCO_2$ significantly reduces the interfacial tension between polymers in a blend [113]. The absence of surface tension in $scCO_2$ helps to reduce the interfacial tension and in essence plays the role of a compatibiliser [114]. In PMMA/PS blends, Elkovitch and colleagues established a decrease in the melt viscosity together with a reduction in the viscosity ratio between the two components [115-117]. The size of the dispersed phase (droplets) is kept at a minimum when the viscosity ratio

is close to 1.0 and subsequently increases as the viscosity ratio increases [118]. The viscosity ratio is calculated by:

$$\lambda = \frac{\eta_{disperse}}{\eta_{matrix}} \qquad \text{Equation 1.4}$$

where the viscosity of the dispersed phase (droplets) is divided by the viscosity of the matrix. The viscosity ratio can be manipulated if there is a greater affinity towards carbon dioxide for the phase with the higher viscosity, bringing the value closer to 1.0. Similar findings were also presented by Lee *et al.* in PE/PS blend systems [109, 110]. These blends showed a significant decrease in the size of the dispersed phase from a few microns to submicron by injecting CO_2. Studies by both Elkovitch and Lee produced their blends in various extruder configurations using both twin and single screw extruders. In some instances, the introduction of CO_2 into the melt has been seen to promote miscibility in both PCL/PHB [111] and PLA/PEG blends [112] in certain composition windows. Both blend systems were deemed immiscible prior to the addition of carbon dioxide.

In summary, the introduction of CO_2 into a blend reduces the viscosity and also the interfacial tension between two polymers. As a result, carbon dioxide is able to influence the phase size and dispersion of an immiscible polymer blend, or even change the path of morphology development to become miscible.

It can be seen from previous research that the blending of PCL and PLA has been found to be immiscible when prepared through solution and mechanical blending. The presence of CO_2 on influencing the blending between PLA and PCL has not been reported. However, the solubility of carbon dioxide is described in both PLA and PCL [107, 119].

1.5 Project aims

PLA is a biodegradable polymer that is most prevalent in the market place and used extensively in various medical applications and food packaging. The growing interest in the use of PLA is because it is derived from natural sustainable resources. However, it has been reported that PLA is relatively brittle [25] and this has limited its range of applications. In most recent years there has been some initial research into blending PLA with other biodegradable polymers, in order to enhance its mechanical properties and potential applications.

This thesis aims to investigate whether any level of miscibility occurs in blends comprising of two different grades of PLA with PCL. The research investigates the two blend systems using a variety of blending techniques; solution casting, melt blending and CO_2 assisted blending. Blending in the presence of carbon dioxide has successfully produced miscibility for alternative polymer blends such as PCL/PHB, PE/PS and PLA/PEG [109, 111, 112]. PLA and PCL have previously been blended using conventional methods [56, 78, 79] (although with different grades) and are reported to be immiscible. However, CO_2 assisted blending of these polymers has not been reported.

The PLA/PCL blends are characterised and compared across the different preparation techniques. Chapter 3 will examine the results of the blends produced by conventional blending techniques (solution casting and melt blending). SEM provides an insight into blend morphology, whilst DSC and FTIR are employed to determine miscibility and establish interactions between the blend components. Mechanical testing enables the blend properties to be compared.

Chapter 4 will introduce and analyse the influence of carbon dioxide on both PLA and PCL. Here, the use of rheological studies to determine the reptation time and the use of FTIR to establish the influence and interaction of carbon dioxide will be presented. Blends prepared in the presence of carbon dioxide are characterised and compared with the conventional preparation methods. Viscosity ratios are determined using rheology and SEC is utilised to analyse the molecular weight across blending techniques.

Finally, in chapter 5, a relatively new and unique thermal analysis technique will be presented. This chapter will address the machine capabilities and provide some initial experimental measurements that are otherwise unachievable by conventional methods.

1.6 References

[1] R. J. Young and P. A. Lovell, *Introduction to Polymers* 2nd ed. London: Chapman & Hall, 1991.

[2] W. D. J. Callister, *Materials Science and Engineering An Introduction*, 6th ed. USA: John Wiley & Sonds, Inc., 2003.

[3] IUPAC. (2013). Available: http://iupac.org/polyedu/page33/page33.html

[4] L. C. Sawyer and D. T. Grubb, *Polymer Microscopy*, 2nd ed. London: Chapman & Hall, 1996.

[5] J. Lunt, "Large-scale production, properties and commercial applications of polylactic acid polymers," *Polymer Degradation and Stability,* vol. 59, pp. 145-152, 1/3/ 1998.

[6] DuPont. (2013). Available: http://www.dupont.co.uk

[7] G. W. Ehrenstein, *Polymeric Materials : Structure-Properties-Applications*. Munich: Hanser, 2001.

[8] C.-L. Huang, Y.-C. Chen, T.-J. Hsiao, J.-C. Tsai, and C. Wang, "Effect of Tacticity on Viscoelastic Properties of Polystyrene," *Macromolecules,* vol. 44, pp. 6155-6161, 2011/08/09 2011.

[9] R. A. Phillips, "Macromorphology of polypropylene homopolymer tacticity mixtures," *Journal of Polymer Science Part B: Polymer Physics,* vol. 38, pp. 1947-1964, 2000.

[10] M. Muthukumar, "Nucleation in polymer crystallization," in *Advances in Chemical Physics*, S. A. Rice, Ed., ed New Jersey: Wiley, 2004.

[11] J. M. G. Cowie and V. Arrighi, "The Glassy State and Glass Transition," in *Polymers: chemistry and physics of modern materials*, ed Florida: CRC Press Taylor & Francis Group, 2008.

[12] R. Chandra and R. Rustgi, "Biodegradable polymers," *Progress in Polymer Science,* vol. 23, pp. 1273-1335, 11// 1998.

[13] Z. Zhang, O. Ortiz, R. Goyal, and J. Kohn, "Biodegradable Polymers," in *Handbook of Polymer Applications in Medicine and Medical Devices*, K. Modjarrad and S. Ebnesajjad, Eds., ed Oxford: William Andrew Publishing, 2014, pp. 303-335.

[14] G. Scott, "Why Biodegradable Polymers?," in *Degradable Polymers: Principles and Applications*, G. Scott, Ed., ed Netherlands: Kluwer Academic Publishers, 2002.

[15] M. Bhattacharya, R. L. Reis, V. Correlo, and L. Boesel, "Material properties of biodegradable polymers," in *Biodegradable polymers for industrial applications*, R. Smith, Ed., ed Cambridge: Woodhead Publishing Limited, 2005.

[16] IHS. (2012). *Biodegradable Polymers*. Available: http://www.ihs.com/products/chemical/planning/ceh/biodegradable-polymers.aspx

[17] G. Braunegg, "Sustainable Poly(hydroxyalkanoate) (PHA) Production," in *Degradable Polymers: Principles and Applications*, G. Scott, Ed., ed Netherlands: Kluwer Academic Publishers, 2002.

[18] J.-F. Zhang and X. Sun, "Poly(lactic acid) based bioplastics," in *Biodegradable Polymers for Industrial Applications*, R. Smith, Ed., ed Cambridge: Woodhead Publishing Limited, 2005.

[19] L. Averous and E. Pollet, "Biodegradable Polymers," in *Environmental Silicate Nano-Biocomposites*, L. Averous and E. Pollet, Eds., ed London: Springer, 2012.
[20] W. Groot, J. V. Krieken, O. Sliekersl, and S. De Vos, "Production and Purification of Lactic Acid and Lactide," in *Poly(lactic acid) Synthesis, Structures, Properties, Processing, and Applications*, R. Auras, L.-T. Lim, S. E. M. Selke, and H. Tsuji, Eds., ed New Jersey: Wiley, 2010.
[21] K. S. Soppimath, T. M. Aminabhavi, A. R. Kulkarni, and W. E. Rudzinski, "Biodegradable polymeric nanoparticles as drug delivery devices," *Journal of Controlled Release,* vol. 70, pp. 1-20, 1/29/ 2001.
[22] V. Guarino, F. Causa, P. Taddei, M. di Foggia, G. Ciapetti, D. Martini*, et al.*, "Polylactic acid fibre-reinforced polycaprolactone scaffolds for bone tissue engineering," *Biomaterials,* vol. 29, pp. 3662-3670, 9// 2008.
[23] D. Garlotta, "A Literature Review of Poly(Lactic Acid)," *Journal of Polymers and the Environment,* vol. 9, pp. 63-84, 2001.
[24] NatureWorksLLC. (2013). *How Ingeo Is Made*. Available: http://www.natureworksllc.com/The-Ingeo-Journey/Eco-Profile-and-LCA/How-Ingeo-is-Made
[25] M. Todo, S. D. Park, T. Takayama, and K. Arakawa, "Fracture micromechanisms of bioabsorbable PLLA/PCL polymer blends," *Engineering Fracture Mechanics,* vol. 74, pp. 1872-1883, 2007.
[26] A. Sodergard and M. Stolt, "Industrial Production of High Molecular Weight Poly(lactic acid)," in *Poly(lactic acid): Synthesis, Structures, Properties, Processing and Applications*, R. Auras, L.-T. Lim, S. E. M. Selke, and H. Tsuji, Eds., ed New Jersey: Wiley, 2010.
[27] Z. Jin, Y. Tian, and J. Wang, "Chemistry and thermodynamic properties of lactic acid and lactide and solvent miscibility," in *Poly(lactic acid) Synthesis, Structures, Properties, Processing, and Applications*, R. Auras, L.-T. Lim, and S. E. M. Selke, Eds., ed New Jersey: Wiley, 2010.
[28] D. W. Farrington, J. Lunt, S. Davies, and R. S. Blackburn, "Poly(lactic acid) fibers," in *Biodegradable and sustainable fibres*, R. S. Blackburn, Ed., ed Cambridge: Woodhead Publishing, 2005.
[29] V. Siracusa, P. Rocculi, S. Romani, and M. D. Rosa, "Biodegradable polymers for food packaging: a review," *Trends in Food Science & Technology,* vol. 19, pp. 634-643, 2008.
[30] J. Ahmed, J.-X. Zhang, Z. Song, and S. K. Varshnet, "Thermal Properites of Polylactides: Effect of molecular mass and nature of lactide isomer," *Journal of Thermal Analysis and Calorimetry,* vol. 95, pp. 957-964, 2009.
[31] L. T. Lim, R. Auras, and M. Rubino, "Processing technologies for poly(lactic acid)," *Progress in Polymer Science,* vol. 33, pp. 820-852, 2008.
[32] X. Jiang, Y. Luo, X. Tian, D. Huang, N. Reddy, and Y. Yang, "Chemical Structure of Poly(lactic acid)," in *Poly(lactic acid): Synthesis, Structures, Properties, Processing and Applications*, R. Auras, L.-T. Lim, S. E. M. Selke, and H. Tsuji, Eds., ed New Jersey: Wiley, 2010.
[33] M. Mihai, M. A. Huneault, and B. D. Favis, "Crystallinity development in cellular poly(lactic acid) in the presence of supercritical carbon dioxide," *Journal of Applied Polymer Science,* vol. 113, pp. 2920-2932, 2009.

[34] S. Baratian, E. S. Hall, J. S. Lin, R. Xu, and J. Runt, "Crystallization and Solid-State Structure of Random Polylactide Copolymers:‚Äâ Poly(l-lactide-co-d-lactide)s," *Macromolecules,* vol. 34, pp. 4857-4864, 2001.

[35] J. J. Kolstad, "Crystallization kinetics of poly(L-lactide-co-meso-lactide)," *Journal of Applied Polymer Science,* vol. 62, pp. 1079-1091, 1996.

[36] O. Martin and L. Avérous, "Poly(lactic acid): plasticization and properties of biodegradable multiphase systems," *Polymer,* vol. 42, pp. 6209-6219, 6// 2001.

[37] R. T. MacDonald, S. P. McCarthy, and R. A. Gross, "Enzymatic Degradability of Poly(lactide): Effects of Chain Stereochemistry and Material Crystallinity," *Macromolecules,* vol. 29, pp. 7356-7361, 1996/01/01 1996.

[38] T. Elzein, M. Nasser-Eddine, C. Delaite, S. Bistac, and P. Dumas, "FTIR study of polycaprolactone chain organization at interfaces," *Journal of Colloid and Interface Science,* vol. 273, pp. 381-387, 2004.

[39] F. J. v. Natta, J. W. Hill, and W. H. Carothers, "Studies of Polymerization and Ring Formation. XXIII.1 ε-Caprolactone and its Polymers," *Journal of the American Chemical Society,* vol. 56, pp. 455-457, 1934/02/01 1934.

[40] M. A. T. Duarte, R. G. Hugen, E. S. A. Martins, A. P. T. Pezzin, and S. H. Pezzin, "Thermal and mechanical behavior of injection molded Poly(3-hydroxybutyrate)/Poly(e-caprolactone) blends," *Materials Research,* vol. 9, pp. 25-28, 2006.

[41] M. J. Jenkins and K. L. Harrison, "The effect of molecular weight on the crystallization kinetics of polycaprolactone," *Polymers for Advanced Technologies,* vol. 17, pp. 474-478, 2006.

[42] S. Agarwal and C. Speyerer, "Degradable blends of semi-crystalline and amorphous branched poly(caprolactone): Effect of microstructure on blend properties," *Polymer,* vol. 51, pp. 1024-1032, 3/2/ 2010.

[43] M. Labet and W. Thielemans, "Synthesis of polycaprolactone: a review," *Chemical Society Reviews,* vol. 38, pp. 3484-3504, 2009.

[44] V. R. Sinha, K. Bansal, R. Kaushik, R. Kumria, and A. Trehan, "Poly-ϵ-caprolactone microspheres and nanospheres: an overview," *International Journal of Pharmaceutics,* vol. 278, pp. 1-23, 6/18/ 2004.

[45] E. Piskin, "Biodegradable polymers as biomaterials," *Journal of Biomaterials Science, Polymer Edition,* vol. 6, pp. 775-795, 1995/01/01 1995.

[46] J. Tsung and D. J. Burgess, "Biodegradable Polymers in Drug Delivery Systems," in *Fundamentals and Applications of Controlled Release Drug Delivery*, J. Siepmann, R. A. Siegel, and M. J. Rathbone, Eds., ed London: Springer, 2012, pp. 107-127.

[47] A. G. A. Coombes, S. C. Rizzi, M. Williamson, J. E. Barralet, S. Downes, and W. A. Wallace, "Precipitation casting of polycaprolactone for applications in tissue engineering and drug delivery," *Biomaterials,* vol. 25, pp. 315-325, 2004.

[48] J.-Z. Hu, Y.-C. Zhou, L.-H. Huang, and H.-B. Lu, "Development of biodegradable polycaprolactone film as an internal fixation material to enhance tendon repair: an in vitro study," *BMC Musculoskeletal Disorders,* vol. 14, p. 246, 2013.

[49] F. A. Barber and J. N. Click, "The effect of inflammatory synovial fluid on the breaking strength of new “long lasting” absorbable sutures," *Arthroscopy: The Journal of Arthroscopic & Related Surgery,* vol. 8, pp. 437-441, 12// 1992.

[50] G. Zhu, Q. Xu, R. Qin, H. Yan, and G. Liang, "Effect of [gamma]-radiation on crystallization of polycaprolactone," *Radiation Physics and Chemistry,* vol. 74, pp. 42-50, 2005.

[51] M. Sun, P. J. Kingham, A. J. Reid, S. J. Armstrong, G. Terenghi, and S. Downes, "In vitro and in vivo testing of novel ultrathin PCL and PCL/PLA blend films as peripheral nerve conduit," *Journal of Biomedical Materials Research Part A,* vol. 93A, pp. 1470-1481, 2010.

[52] M. A. Woodruff and D. W. Hutmacher, "The return of a forgotten polymer—Polycaprolactone in the 21st century," *Progress in Polymer Science,* vol. 35, pp. 1217-1256, 10// 2010.

[53] M. Van Lieshout, G. Peters, M. Rutten, and F. Baaijens, "A knitted, fibrin-covered polycaprolactone scaffold for tissue engineering of the aortic valve," *Tissue Eng,* vol. 12, pp. 481-7, Mar 2006.

[54] R. A. Gross and B. Kalra, "Biodegradable Polymers for the Environment," *Science,* vol. 297, pp. 803-807, August 2, 2002 2002.

[55] D. Wu, D. Lin, J. Zhang, W. Zhou, M. Zhang, Y. Zhang*, et al.*, "Selective Localization of Nanofillers: Effect on Morphology and Crystallization of PLA/PCL Blends," *Macromolecular Chemistry and Physics,* vol. 212, pp. 613-626, 2011.

[56] N. López-Rodríguez, A. López-Arraiza, E. Meaurio, and J. R. Sarasua, "Crystallization, morphology, and mechanical behavior of polylactide/poly(ε-caprolactone) blends," *Polymer Engineering & Science,* vol. 46, pp. 1299-1308, 2006.

[57] R. U. Rao, K. N. S. Suman, V. V. S. Rao, and K. Bhanukiran, "Study of Rheological and Mechanical Properties of Biodegradable Polylactide and Polycaprolactone Blends," *International Journal of Engineering Science and Technology,* vol. 3, pp. 6259-6265, 2011.

[58] J. C. Meredith and E. J. Amis, "LCST phase separation in biodegradable polymer blends: poly(D,L-lactide) and poly(ϵ-caprolactone)," *Macromolecular Chemistry and Physics,* vol. 201, pp. 733-739, 2000.

[59] C. Vasile, A. K. Kulshereshtha, and G. G. Bumbu, "Terminology," in *Handbook of Polymer Blends and Composites*. vol. 3A, C. Vasile and A. K. Kulshereshtha, Eds., ed Shropshire: Rapra Technology Limited, 2003.

[60] W. Soontaranum, J. S. Higgins, and T. D. Papathanasiou, "Rheology and thermodynamics in partially miscible polymer blends," *Journal of Non-Newtonian Fluid Mechanics,* vol. 67, pp. 191-212, 11// 1996.

[61] D. R. Paul, "Background and Perspective," in *Polymer Blends*. vol. 1, D. R. Paul and S. Newman, Eds., ed London: Academic Press, 1978.

[62] P. Sarazin, X. Roy, and B. D. Favis, "Controlled preparation and properties of porous poly(l-lactide) obtained from a co-continuous blend of two biodegradable polymers," *Biomaterials,* vol. 25, pp. 5965-5978, 12// 2004.

[63] U. W. Gedde, *Polymer Physics*. London: Chapman & Hall, 1995.

[64] J. M. G. Cowie and V. Arrighi, "Polymers in Solution," in *Polymers: chemistry and physics of modern materials*, ed Florida: CRC Press, 2008.

[65] E. Fekete, E. Földes, and B. Pukánszky, "Effect of molecular interactions on the miscibility and structure of polymer blends," *European Polymer Journal,* vol. 41, pp. 727-736, 4// 2005.

[66] E. J. Vorenkamp, G. ten Brinke, J. G. Meijer, H. Jager, and G. Challa, "Influence of the tacticity of poly(methyl methacrylate) on the miscibility with poly(vinyl chloride)," *Polymer,* vol. 26, pp. 1725-1732, 10// 1985.
[67] G. Beaucage, R. S. Stein, T. Hashimoto, and H. Hasegawa, "Tacticity effects on polymer blend miscibility," *Macromolecules,* vol. 24, pp. 3443-3448, 1991/05/01 1991.
[68] R. C. Willemse, "Co-continuous morphologies in polymer blends: stability," *Polymer,* vol. 40, pp. 2175-2178, 4// 1999.
[69] H. Quan, Z.-M. Li, M.-B. Yang, and R. Huang, "Review On transcrystallinity in semi-crystalline polymer composites," *Composites Science and Technology,* vol. 65, pp. 999-1021, 2005.
[70] M. Zhang, J. Xu, Z. Zhang, H. Zeng, and X. Xiong, "Effect of transcrystallinity on tensile behaviour of discontinuous carbon fibre reinforced semicrystalline thermoplastic composites," *Polymer,* vol. 37, pp. 5151-5158, 11// 1996.
[71] P. J. Halley and G. A. George, "Chemorheology of Polymers - From Fundamental Principles to Reactive Processing," ed: Cambridge University Press, 2009.
[72] R. J. Young and P. A. Lovell, *Introduction to Polymers*, 3rd ed. London: CRC Press, 2011.
[73] H. A. Schneider, "Glass Transition in Polymer Blends," in *Handbook of Polymer Blends and Composites*. vol. 3B, C. Vasile and A. K. Kulshereshtha, Eds., ed Shropshire: Rapra Technology Limited, 2003.
[74] D. R. Paul, "Interfacial Agents ("Compatibilizers") for Polymer Blends," in *Polymer Blends*. vol. 2, D. R. Paul and S. Newman, Eds., ed London: Academic Press, 1978.
[75] G. Perego and G. D. Cella, "Mechanical Properties," in *Poly(lactic acid) Synthesis, Structures, Properties, Processing and Applications*, R. Auras, L.-T. Lim, S. E. M. Selke, and H. Tsuji, Eds., ed New Jersey: Wiley, 2010.
[76] W. H. Hoidy, M. B. Ahmad, E. A. Jaffar Al-Mulla, and N. A. B. Ibrahim, "Preparation and Characterization of Polylactic Acid/Polycaprolactone Clay Nanocomposites. ," *Journal of Applied Sciences,* vol. 10, pp. 97-106, 2010.
[77] M. M. Coleman, C. J. Serman, D. E. Bhagwagar, and P. C. Painter, "A practical guide to polymer miscibility," *Polymer,* vol. 31, pp. 1187-1203, 7// 1990.
[78] M. E. Broz, D. L. VanderHart, and N. R. Washburn, "Structure and mechanical properties of poly(,-lactic acid)/poly([var epsilon]-caprolactone) blends," *Biomaterials,* vol. 24, pp. 4181-4190, 2003.
[79] C. L. Simões, J. C. Viana, and A. M. Cunha, "Mechanical properties of poly(ε-caprolactone) and poly(lactic acid) blends," *Journal of Applied Polymer Science,* vol. 112, pp. 345-352, 2009.
[80] N.-S. Choi, C.-H. Kim, K. Y. Cho, and J.-K. Park, "Morphology and hydrolysis of PCL/PLLA blends compatibilized with P(LLA-co-ϵCL) or P(LLA-b-ϵCL)," *Journal of Applied Polymer Science,* vol. 86, pp. 1892-1898, 2002.
[81] N. Noroozi, L. L. Schafer, and S. G. Hatzikiriakos, "Thermorheological properties of poly (ε-caprolactone)/polylactide blends," *Polymer Engineering & Science,* vol. 52, pp. 2348-2359, 2012.
[82] T. Takayama, M. Todo, and H. Tsuji, "Effect of annealing on the mechanical properties of PLA/PCL and PLA/PCL/LTI polymer blends," *Journal of the Mechanical Behavior of Biomedical Materials,* vol. 4, pp. 255-260, 2011.

[83] T. Patrício and P. Bártolo, "Thermal Stability of PCL/PLA Blends Produced by Physical Blending Process," *Procedia Engineering,* vol. 59, pp. 292-297, 2013.
[84] D. Wu, Y. Zhang, L. Yuan, M. Zhang, and W. Zhou, "Viscoelastic interfacial properties of compatibilized poly(ε-caprolactone)/polylactide blend," *Journal of Polymer Science Part B: Polymer Physics,* vol. 48, pp. 756-765, 2010.
[85] D. Wu, Y. Zhang, M. Zhang, and W. Zhou, "Phase behavior and its viscoelastic response of polylactide/poly([epsilon]-caprolactone) blend," *European Polymer Journal,* vol. 44, pp. 2171-2183, 2008.
[86] D. Wu, Y. Zhang, M. Zhang, and W. Yu, "Selective Localization of Multiwalled Carbon Nanotubes in Poly(ε-caprolactone)/Polylactide Blend," *Biomacromolecules,* vol. 10, pp. 417-424, 2009/02/09 2009.
[87] M. F. Kemmere, "Supercritical Carbon Dioxide for Sustainable Polymer Processes," in *Supercritical Carbon Dioxide: in Polymer Reaction Engineering*, M. F. Kemmere and T. Meyer, Eds., ed Germany: WILEY-VCH, 2005.
[88] M. Garcia-Leiner and A. J. Lesser, "CO2-assisted polymer processing: A new alternative for intractable polymers," *Journal of Applied Polymer Science,* vol. 93, pp. 1501-1511, 2004.
[89] T. W. Swaddle, "Inorganic Chemistry - An Industrial and Environmental Perspective," ed. London: Academic Press, 1997.
[90] M. F. Kemmere and T. Meyer, *Supercritical Carbon Dioxide: in Polymer Reaction Engineering*. Germany: WILEY-VCH, 2005.
[91] S. P. Nalawade, F. Picchioni, and L. P. B. M. Janssen, "Supercritical carbon dioxide as a green solvent for processing polymer melts: Processing aspects and applications," *Progress in Polymer Science,* vol. 31, pp. 19-43, 1// 2006.
[92] Z. Zhang and Y. P. Handa, "CO2-Assisted Melting of Semicrystalline Polymers,Ä†," *Macromolecules,* vol. 30, pp. 8505-8507, 1997.
[93] J. L. Kendall, D. A. Canelas, J. L. Young, and J. M. DeSimone, "Polymerizations in supercritical carbon dioxide," *Chemical Reviews,* vol. 99, pp. 543-564, 1999.
[94] A. I. Cooper, "Polymer synthesis and processing using supercritical carbon dioxide," *Journal of Materials Chemistry,* vol. 10, pp. 207-234, 2000.
[95] E. Reverchon and S. Cardea, "Production of controlled polymeric foams by supercritical CO2," *The Journal of Supercritical Fluids,* vol. 40, pp. 144-152, 2// 2007.
[96] Y. Ema, M. Ikeya, and M. Okamoto, "Foam processing and cellular structure of polylactide-based nanocomposites," *Polymer,* vol. 47, pp. 5350-5359, 7/12/ 2006.
[97] E. Reverchon, R. Adami, S. Cardea, and G. D. Porta, "Supercritical fluids processing of polymers for pharmaceutical and medical applications," *The Journal of Supercritical Fluids,* vol. 47, pp. 484-492, 1// 2009.
[98] O. R. Davies, A. L. Lewis, M. J. Whitaker, H. Tai, K. M. Shakesheff, and S. M. Howdle, "Applications of supercritical CO2 in the fabrication of polymer systems for drug delivery and tissue engineering," *Advanced Drug Delivery Reviews,* vol. 60, pp. 373-387, 2/14/ 2008.
[99] W. T. Zhai, Y. Ko, W. L. Zhu, A. S. Wong, and C. B. Park, "A Study of the Crystallization, Melting, and Foaming Behaviors of Polylactic Acid in Compressed CO2," *International Journal of Molecular Sciences,* vol. 10, pp. 5381-5397, Dec 2009.

[100] L. Yu, H. Liu, K. Dean, and L. Chen, "Cold crystallization and postmelting crystallization of PLA plasticized by compressed carbon dioxide," *Journal of Polymer Science Part B: Polymer Physics,* vol. 46, pp. 2630-2636, 2008.
[101] Y.-T. Shieh, J.-H. Su, G. Manivannan, P. H. C. Lee, S. P. Sawan, and W. Dale Spall, "Interaction of supercritical carbon dioxide with polymers. I. Crystalline polymers," *Journal of Applied Polymer Science,* vol. 59, pp. 695-705, 1996.
[102] O. S. Fleming and S. G. Kazarian, "Polymer Processing with Supercritical Fluids," in *Supercritical Carbon Dioxide: in Polymer Reaction Engineering*, M. F. Kemmere and T. Meyer, Eds., ed Germany: WILEY-VCH, 2005.
[103] S. G. Kazarian, "Polymer Processing with Supercritical Fluids," *Polymer Science Series C,* vol. 42, pp. 78-101, 2000.
[104] Y.-T. Shieh, J.-H. Su, G. Manivannan, P. H. C. Lee, S. P. Sawan, and W. Dale Spall, "Interaction of supercritical carbon dioxide with polymers. II. Amorphous polymers," *Journal of Applied Polymer Science,* vol. 59, pp. 707-717, 1996.
[105] Z. Shen, M. A. McHugh, J. Xu, J. Belardi, S. Kilic, A. Mesiano*, et al.*, "CO2-solubility of oligomers and polymers that contain the carbonyl group," *Polymer,* vol. 44, pp. 1491-1498, 2003.
[106] G. W. Stachowiak and A. W. Batchelor, *Engineering Tribology*, 3rd ed. London: Elsevier, 2005.
[107] G. A. Leeke, J. Cai, and M. Jenkins, "Solubility of Supercritical Carbon Dioxide in Polycaprolactone (CAPA 6800) at 313 and 333 K," *Journal of Chemical & Engineering Data,* vol. 51, pp. 1877-1879, 2006/09/01 2006.
[108] J. Reignier, J. Tatibouët, and R. Gendron, "Effect of dissolved carbon dioxide on the glass transition and crystallization of poly(lactic acid) as probed by ultrasonic measurements," *Journal of Applied Polymer Science,* vol. 112, pp. 1345-1355, 2009.
[109] M. Lee, C. Tzoganakis, and C. B. Park, "Extrusion of PE/PS blends with supercritical carbon dioxide," *Polymer Engineering & Science,* vol. 38, pp. 1112-1120, 1998.
[110] M. Lee, C. Tzoganakis, and C. B. Park, "Effects of supercritical CO2 on the viscosity and morphology of polymer blends," *Advances in Polymer Technology,* vol. 19, pp. 300-311, 2000.
[111] M. J. Jenkins, Y. Cao, L. Howell, and G. A. Leeke, "Miscibility in blends of poly(3-hydroxybutyrate-co-3-hydroxyvalerate) and poly(ε-caprolactone) induced by melt blending in the presence of supercritical CO2," *Polymer,* vol. 48, pp. 6304-6310, 2007.
[112] C. A. Kelly, A. Naylor, L. Illum, K. M. Shakesheff, and S. M. Howdle, "Supercritical CO2: A Clean and Low Temperature Approach to Blending PDLLA and PEG," *Advanced Functional Materials,* vol. 22, pp. 1684-1691, 2012.
[113] A. Xue, C. Tzoganakis, and P. Chen, "Measurement of interfacial tension in PS/LDPE melts saturated with supercritical CO2," *Polymer Engineering & Science,* vol. 44, pp. 18-27, 2004.
[114] L. P. B. M. Janssen and S. Nalawade, P., "Polymer Extrusion with Supercritical Carbon Dioxide," in *Supercritical Carbon Dioxide: in Polymer Reaction Engineering*, M. F. Kemmere and T. Meyer, Eds., ed Germany: WILEY-VCH, 2005.

[115] M. D. Elkovitch, D. L. Tomasko, and L. J. Lee, "Supercritical carbon dioxide assisted blending of polystyrene and poly(methyl methyacrylate)," *Polymer Engineering & Science,* vol. 39, pp. 2075-2084, 1999.
[116] M. D. Elkovitch, L. J. Lee, and D. L. Tomasko, "Effect of supercritical carbon dioxide on PMMA/rubber and polystyrene/rubber blending: Visosity ratio and phase inversion," *Polymer Engineering & Science,* vol. 41, pp. 2108-2125, 2001.
[117] M. D. Elkovitch and D. L. Tomasko, "Effect of supercritical carbon dioxide on morphology development during polymer blending," *Polymer Engineering & Science,* vol. 40, pp. 1850-1861, 2000.
[118] B. D. Favis and J. P. Chalifoux, "The effect of viscosity ratio on the morphology of polypropylene/polycarbonate blends during processing," *Polymer Engineering & Science,* vol. 27, pp. 1591-1600, 1987.
[119] S. P. Nalawade, F. Picchioni, L. P. B. M. Janssen, D. W. Grijpma, and J. Feijen, "Investigation of the interaction of CO2 with poly (L-lactide), poly(DL-lactide) and poly(ε-caprolactone) using FTIR spectroscopy," *Journal of Applied Polymer Science,* vol. 109, pp. 3376-3381, 2008.

CHAPTER 2 – MATERIALS, EXPERIMENTAL TECHNIQUES AND METHODS

2.1 Materials

2.1.1 Poly(lactic acid)

The repeat unit of PLA together with the chemical structures of the D, L and *meso* stereoisomers are shown in Figure 2.2 and Figure 2.1.

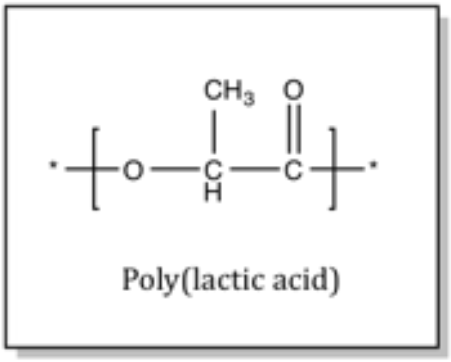

Figure 2.1. Chemical structure of poly(lactic acid) showing asymmetric C atom.

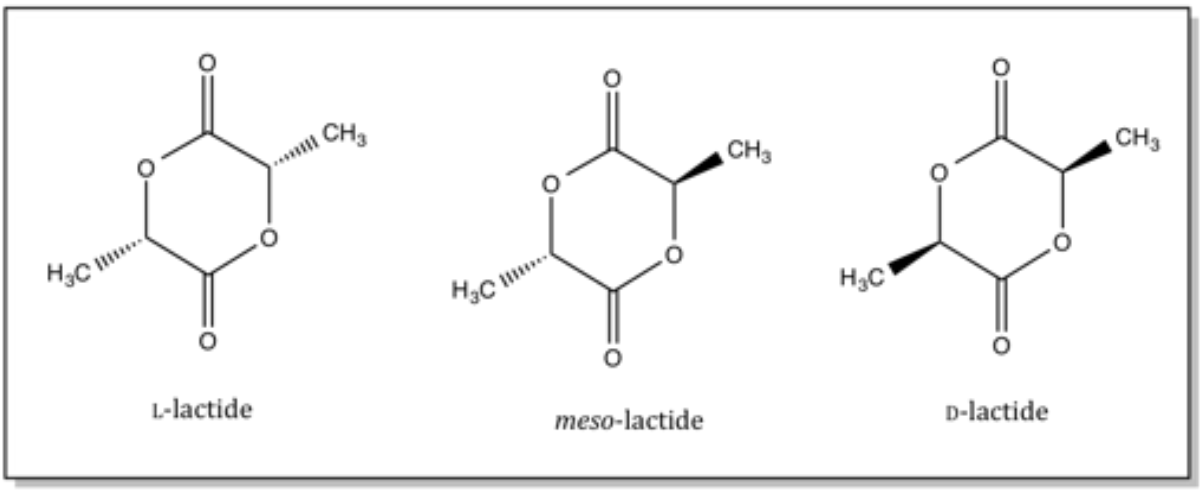

Figure 2.2. L, D and *meso* stereoisomer structures of precursor.

2.1.1.1 Poly(lactic acid) 2002D

PLA 2002D is a partially crystalline grade of PLA supplied in pellet form by NatureWorks LLC (Nebraska, USA). It has a glass transition temperature around 59 ˚C and a melting point of 154 ˚C. PLA 2002D has a molecular weight (M_w) of 194,000 g mol^{-1}.

2.1.1.2 Poly(lactic acid) 4060D

PLA 4060D is an amorphous grade of PLA supplied in the form of pellets by NatureWorks LLC. It possesses a glass transition temperature around 58 °C. PLA 4060D has a molecular weight (M_w) of 181,000 g mol^{-1}.

2.1.2 Poly(ε-caprolactone)

PCL (CAPA6800) was supplied in pellet form by Perstorp UK Ltd (Warrington, UK). The molecular weight (M_w) of CAPA6800 was 212,000 g mol^{-1}, a high molecular weight caprolactone and a degree of crystallinity 49%. The melting region for the CAPA 6800 grade is typically 60 ℃ with a glass transition temperature of - 60 °C. Crystallisation of PCL occurs between the T_g and T_m, around 30 °C. The repeat unit for CAPA 6800 is shown in Figure 2.3.

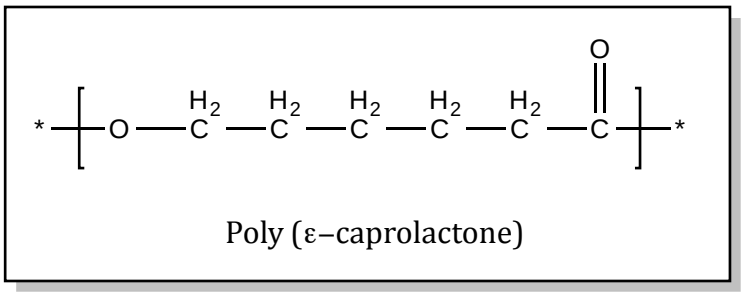

Poly (ε–caprolactone)

Figure 2.3. The repeat unit for poly(ε-caprolactone) (CAPA 6800).

	PLA 2002D	PLA 4060D	PCL 6800
T_g / °C	55	52	-62
T_m / °C	154	-	58
T_c (onset) / °C	-	-	28
Crystallinity / %	37	-	60
M_w / g mol^{-1}	194,000	181,000	212,000
D-lactide content / wt %	4*	11-13**	-
	*[1]	**[2]	

Table 1. Properties of poly(lactic acid) grade 2002D, 4060D and poly(ε-caprolactone) grade 6800.

2.1.3 Dichloromethane

Dichloromethane was used as a solvent for both the PCL and PLA grades described above. It was supplied by Fisher Scientific UK Ltd. (Leicestershire) as laboratory grade material. It was used as received.

2.1.4 Carbon dioxide

CO_2 (purity 99.9% v/v) was obtained from BOC (Birmingham, UK) and used as received.

2.2 Differential Scanning Calorimetry (DSC)

2.2.1 Experimental technique

Differential scanning calorimetry (DSC) is an important thermal analysis technique that can detect thermal transitions in a polymer by changes in heat capacity of the sample. In the case of a polymer, phase transitions such as glass transition (T_g), crystallisation (T_c) and melting point (T_m) can be measured as illustrated in Figure 2.4. In this instance, endothermic processes are represented by an upwards peak, and exothermic, downward. Polymers that exhibit all thermal transitions noted above are said to be partially crystalline whereas those only exhibiting a T_g are amorphous. DSC can be used to measure the degree of miscibility between two polymers, crystallisation kinetics and polymer morphology.

The characteristic feature of all DSCs is that they have both a sample and a reference cell. The sample is commonly placed in an aluminum crucible, consisting of a sealed pan and lid, whilst the reference is an empty pan (and lid). Two types of DSC were used to complete this research. A Perkin Elmer (Massachusetts, USA) differential scanning calorimeter (DSC 7), a power compensation technique, and a Mettler Toledo (Greifensee, Switzerland) DSC1, which operates by a heat flux system. An example of the different sensors used in each instrument can be seen in Figure 2.5.

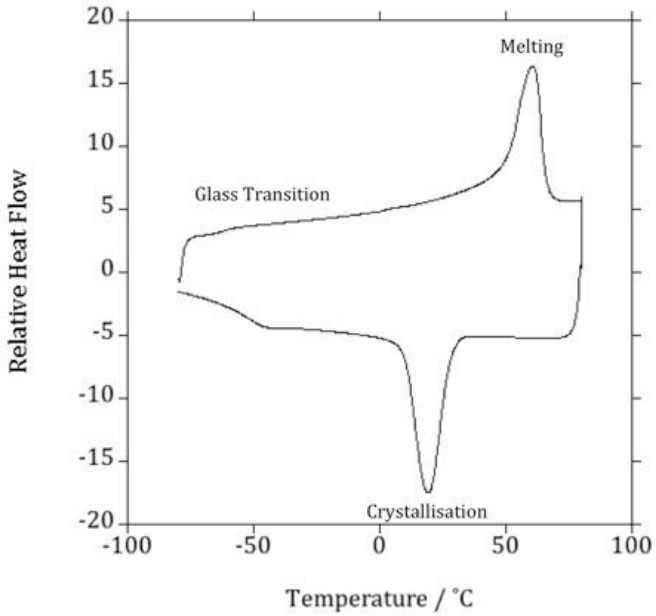

Figure 2.4. DSC trace illustrating the thermal transitions of a partially crystalline polymer on heating and subsequent cooling at 10 ˚C min^{-1}. Endo is up.

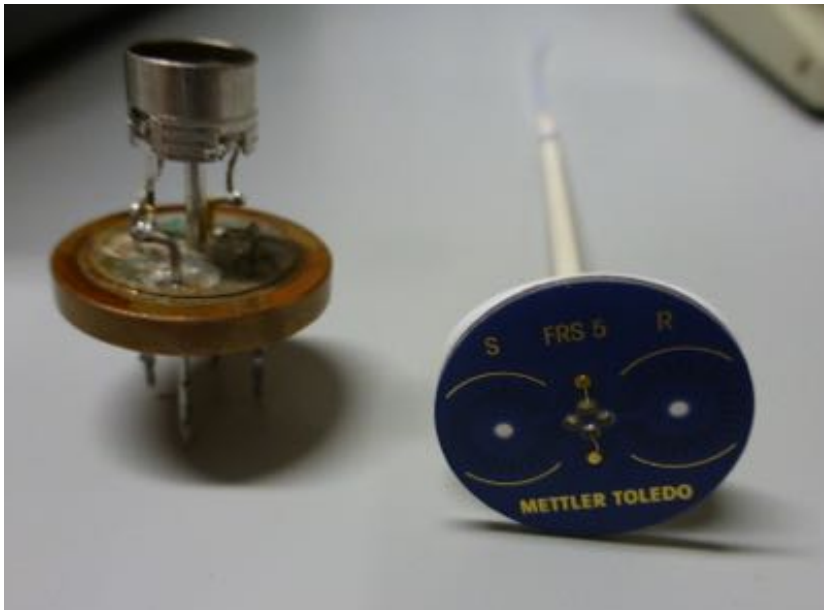

Figure 2.5. Perkin Elmer DSC 7 single cell, one of a pair in the power compensated system (left) compared to the Mettler Toledo DSC 1 sensor containing both sample and reference cells (right).

Power compensation DSCs aim to keep both the sample and reference cells at the same temperature by 'compensating' the heat required (by varying the power input) to maintain the two cells at the same temperature. Each cell is controlled independently. Due to the exo/endothermic thermal transitions occurring in the sample, the sample may require more or less heat (energy) than the reference to maintain them at the same temperature. The differential heating power is measured and plotted as heat flow versus temperature or time.

In contrast to the two furnaces in a power compensated DSC, a heat flux DSC utilises only one. Both sample and reference crucibles are contained in a single furnace, relying upon a good heat-flow path between them. See Figure 2.6 for a schematic of both power compensation and heat flux DSC. The heat flux DSC establishes the heat flow through an indirect approach by converting the temperature differential into energy flow by calibration. Heat flow is measured directly between two independent furnaces in power compensated DSC and provides greater sensitivity and therefore higher accuracy, particularly on cooling. However, results between both machines are comparable within the limits of acceptable experimental error.

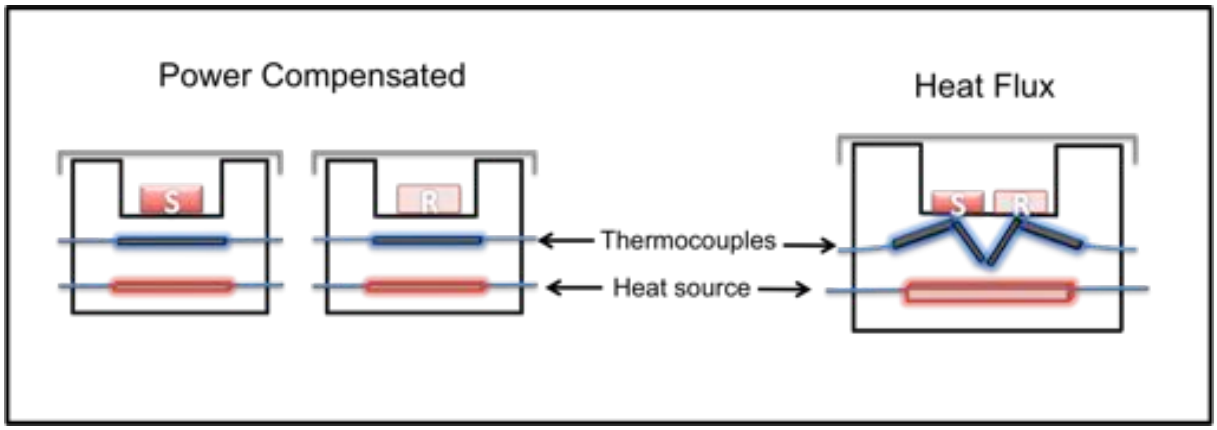

Figure 2.6. Schematic of both power compensation and heat flux DSCs.

2.2.2 Method

The glass transition, melting and crystallisation behaviour of the 'as received' materials were measured using a Perkin Elmer (DSC 7) (Figure 2.7) connected to a cooling system (Grant) which can cool the instrument to 3 ˚C with a control of ± 0.02 ˚C. The DSC 7 is interfaced to a personal computer running the Perkin Elmer Pyris management software.

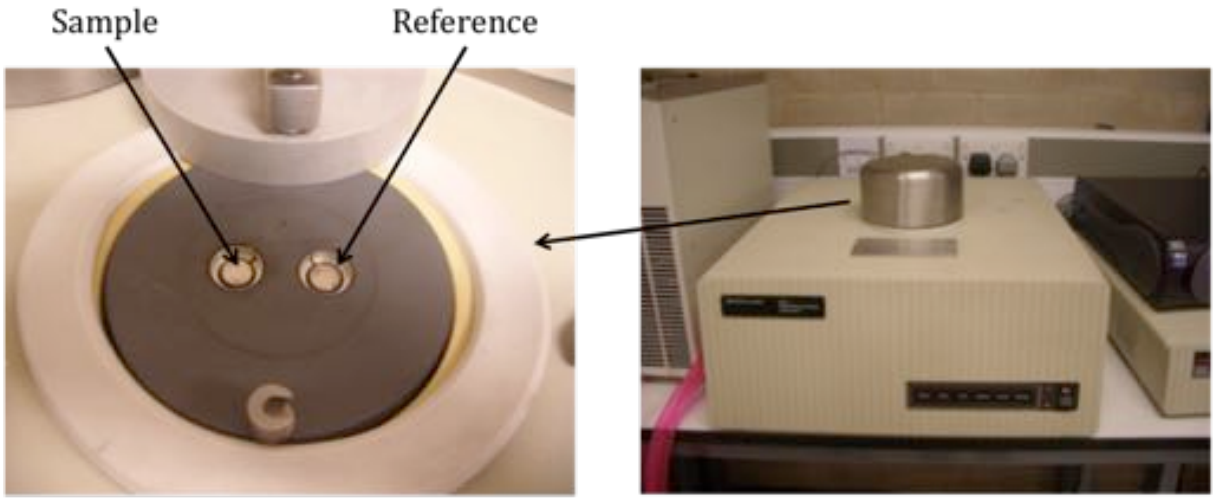

Figure 2.7. Perkin Elmer DSC 7. The left-hand image indicates the sample and reference cells.

'As received' pellets were cut into samples of approximately 6-8 mg in mass to record the thermal transitions specific to each polymer. Samples were heated at 10 °C min^{-1} from 25 °C to a temperature in the melt (selected in accordance with the material under investigation). The samples were then cooled to 25 °C at 10 °C min^{-1}. Analysis was performed on the initial run in order to determine the morphology created during processing.

The Mettler Toledo DSC1 (Figure 2.8) was used to analyse the majority of the blend systems. The instrument was interfaced to a personal computer and controlled using proprietary STARe software (version 11). This DSC was purged with nitrogen at a gas flow rate of 100 mL min^{-1} and also connected to a T100 Intracooler. The Intracooler allowed the DSC to cool to temperatures of -100 ˚C, a requirement for the analysis of the T_g of PCL, which occured around -60 ˚C.

The thermal response of both instruments were calibrated from the enthalpy of fusion of a known mass of indium (99.999% pure). The temperature of the calorimeter was calibrated using the melting point of tin. Samples of around 6-8 mg were contained in aluminium pans with an empty pan used as a reference.

T_g, T_m and the enthalpy of fusion (ΔH_m) of the blends were measured and determined (method described at the end of section 2.2.2) from the initial heating run at 10 ˚C min^{-1}. This was to examine the prior morphological information created during blending.

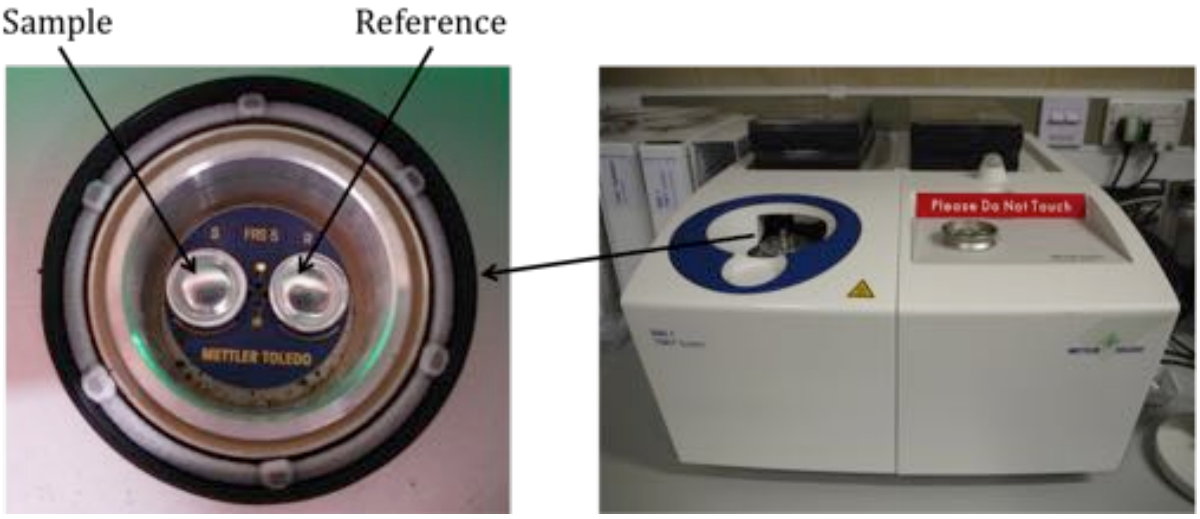

Figure 2.8. Mettler Toledo DSC 1. The sample and reference cells can be seen in the left-hand image, indicated by 'S' and 'R' positioned above the aluminum crucibles.

In some instances, the glass transition temperature was measured according to the method proposed by Richardson [3]. This method is most appropriate for polymers exhibiting an exotherm superimposed on the glass transition. In this case, simply taking the mid-point of the transition can lead to elevated and incorrect values of the T_g. The Richardson method [3] for determining the thermodynamic T_g is shown graphically in Figure 2.9. The T_g follows the path 1234 with a step increment occurring between points 2 and 3. The T_g is located where areas A+B=C.

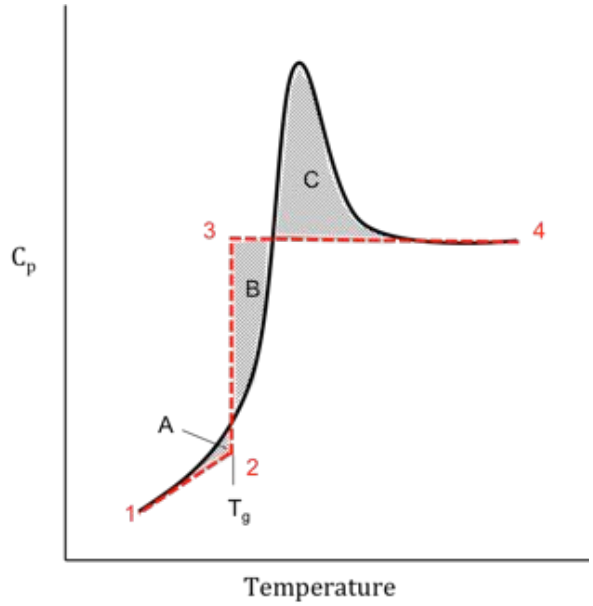

Figure 2.9. Schematic of the Richardson method for determining T_g [3].

The melting point was measured from the DSC trace recorded at 10 °C min^{-1} (figure 2.10). All experiments measuring the melting point were performed with a fixed heating rate of 10 °C min^{-1}.

In order to determine the degree of crystallinity, a linear baseline was drawn from the first onset of melting to the last trace of crystallinity. The enthalpy of fusion was then

calculated from the area under the endotherm (as seen in Figure 2.10, endo assumed as up). The weight fraction degree of crystallinity (Xc) was defined as,

$$\chi_c = \frac{\Delta H_m(T_m)}{\Delta H_m^0(T_m^0)} \times 100 \qquad \text{(Equation 2.1)}$$

where $\Delta H_m(T_m)$ is the enthalpy of fusion measured at the melting point and $\Delta H_m^0(T_m^0)$ is the enthalpy of fusion of the completely crystalline polymer. A literature value of 139.3 J g^{-1} for $\Delta H_m^0(T_m^0)$ was used for PCL [4] and 93 J g^{-1} for PLA [5].

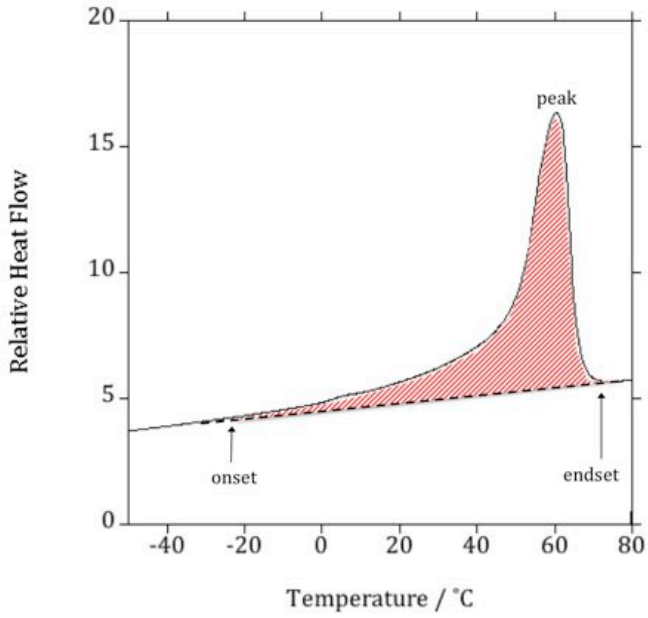

Figure 2.10. Measurement of the enthalpy of fusion, indicating the determination of onset, peak and endset.

2.3 Scanning Electron Microscopy (SEM)

2.3.1 Experimental technique

Scanning electron microscopy (SEM) is a characterisation technique used to study surface topography with a resolution down to nanometers. Operating in high vacuum, an electron beam is scanned across the surface of (a conductive) sample causing the generation of low energy secondary electrons and back-scattered electrons. Some of these secondary electrons escape from the sample surface and yield topological information produced by SEM. The back-scattered electrons are generated from a greater penetration within the sample and are used to distinguish contrasts in chemical composition in a sample. Those elements with a higher atomic number appear brighter in the image than those with a lower atomic number.

2.3.2 Method

Samples were prepared for SEM analysis by cryogenic fracture. The base of the fracture surfaces mounted on an aluminum stub using conductive carbon adhesive discs and coated in gold using a Polaron SC7640 sputter coater. Coating the samples for 3 minutes deposits approximately 10 to 12 nm of gold, which provided sufficient conductivity. A conductive silver solution was additionally painted where sample and stub made contact to promote enhanced conductivity and minimise potential 'charging' of the sample which can reduce the quality of the SEM image. Samples were imaged using a Phillips (XL30 ESEM) scanning electron microscope with 10 kV accelerating voltage. Images were captured at magnifications ranging from 250 to 30,000 x.

2.4 Fourier Transform Infrared (FTIR) Spectroscopy

2.4.1 Experimental technique

Fourier Transform Infrared Spectroscopy (FTIR) is a non-destructive characterisation technique. Changes in polymer crystallinity and chain conformation were characterised through identification of the IR spectral features in intensity, bandwidth and position. An infrared laser beam is directed on to an interferometer where it is immediately split into two paths. One path passes through the sample. The interferometer consists of two mirrors which redirects the beams back together. The recombined beam is directed to a detector enabling the production of an interferogram. When using an ATR accessory to obtain a spectrum, the infrared beam is reflected from the inside surface of the diamond crystal within the ATR accessory (as it has a high refractive index) producing an evanescent wave. It is these evanescent waves that penetrate the sample, and cause certain molecules in the sample to vibrate. The attenuated energy from each evanescent wave is passed back to the infrared beam to the spectrometer detector. A complex, mathematical calculation, a Fast Fourier transform determines the intensity of each frequency received by the detector. This results with the production of a FTIR spectrum. A chemical functional group within a sample will tend to absorb infrared radiation in a specific wave number range, regardless of the structure of the rest of the molecule.

2.4.2 Method

A Jasco FTIR-6300 (Essex, UK) was used with a Specac ATR golden gate attachment (Figure 2.11) to capture the spectra of all samples. Measurements were taken in absorbance with a resolution of 8 cm^{-1} and 64 scans (corresponding to a data interval capture of 1.9 cm^{-1}). These parameters were chosen for the optimal balance between spectrum quality and speed of acquisition. Changes or shifts in peak position or height were determined, with particular interest towards the C=O (carbonyl region). The C=O group is polar and is anticipated that any interactions involving this group would result in a spectral shift in this region. Examples of FTIR spectra for the polymers used in this project are shown in Figure 2.12, Figure 2.13 and Figure 2.14 for the 'as received' polymers, PLA 2002D, PLA 4060D and PCL 6800, respectively. The main spectral assignments in these polymers are indicated in Figure 2.12.

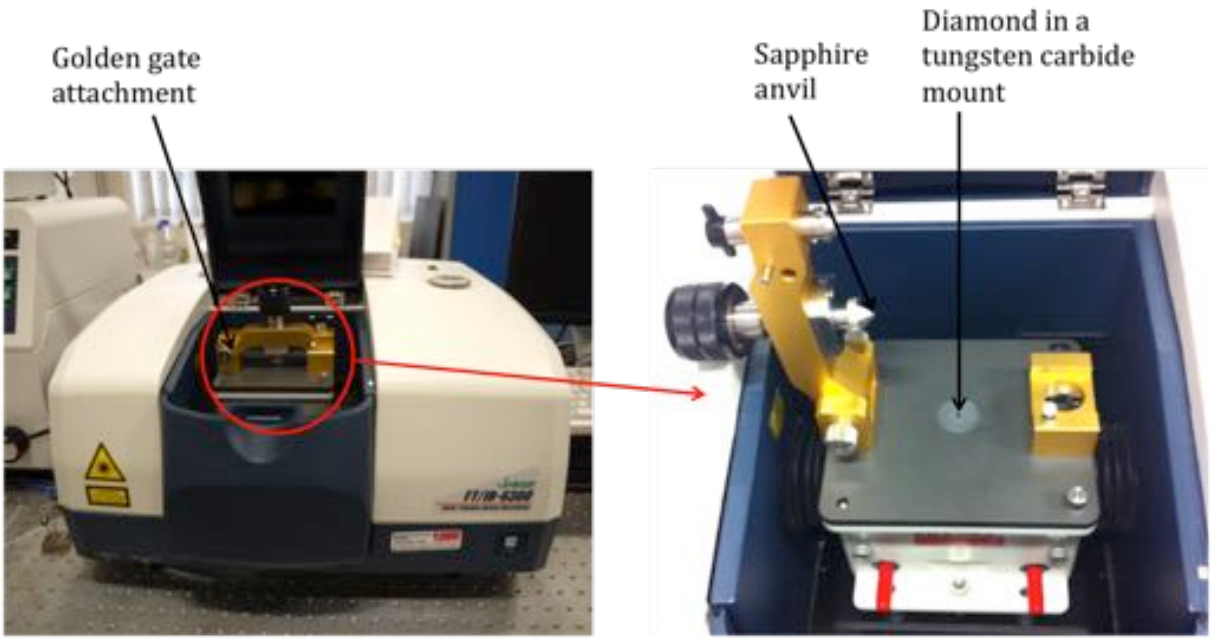

Figure 2.11. Jasco FTIR-6300 with golden gate ATR attachment.

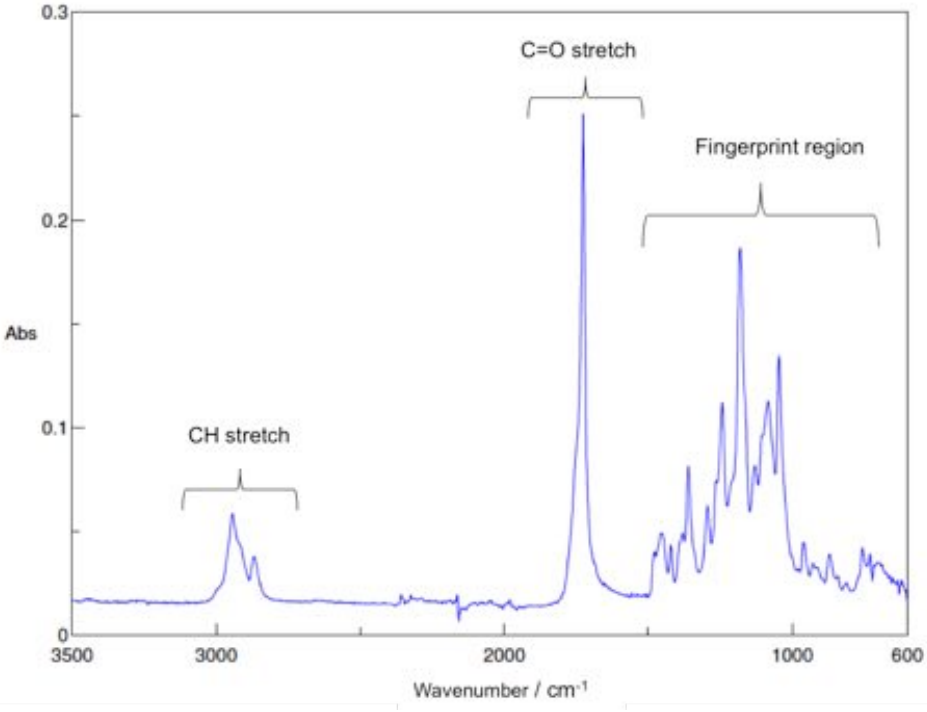

Figure 2.12. The FTIR spectrum of 'as received' poly(lactic acid) (PLA) 2002D indicating the major peak assignments.

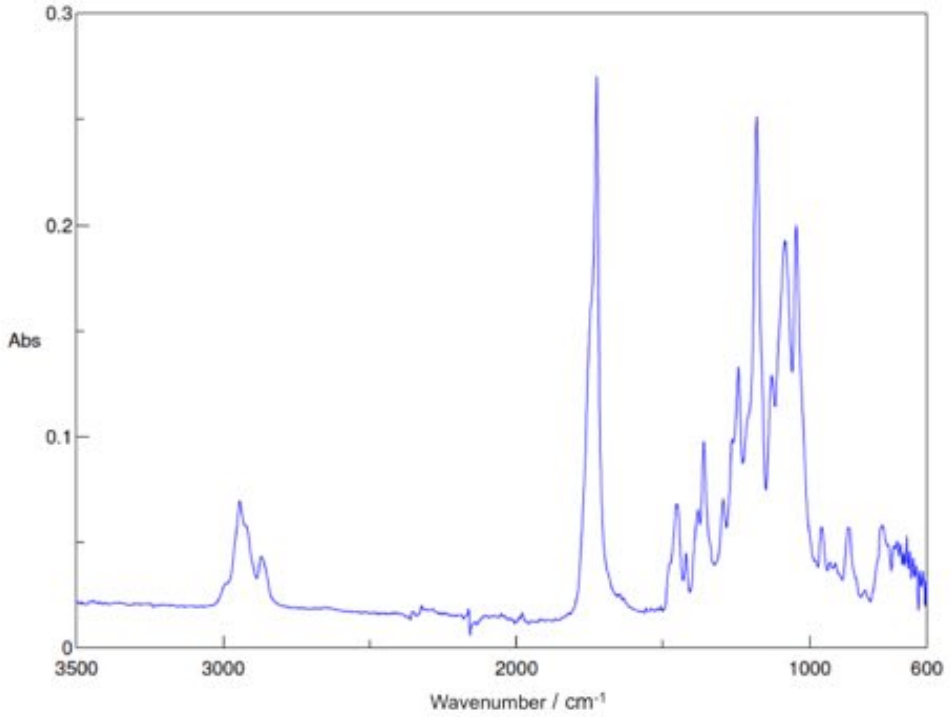

Figure 2.13. Poly(lactic acid) (PLA) 4060D 'as received' FTIR spectrum.

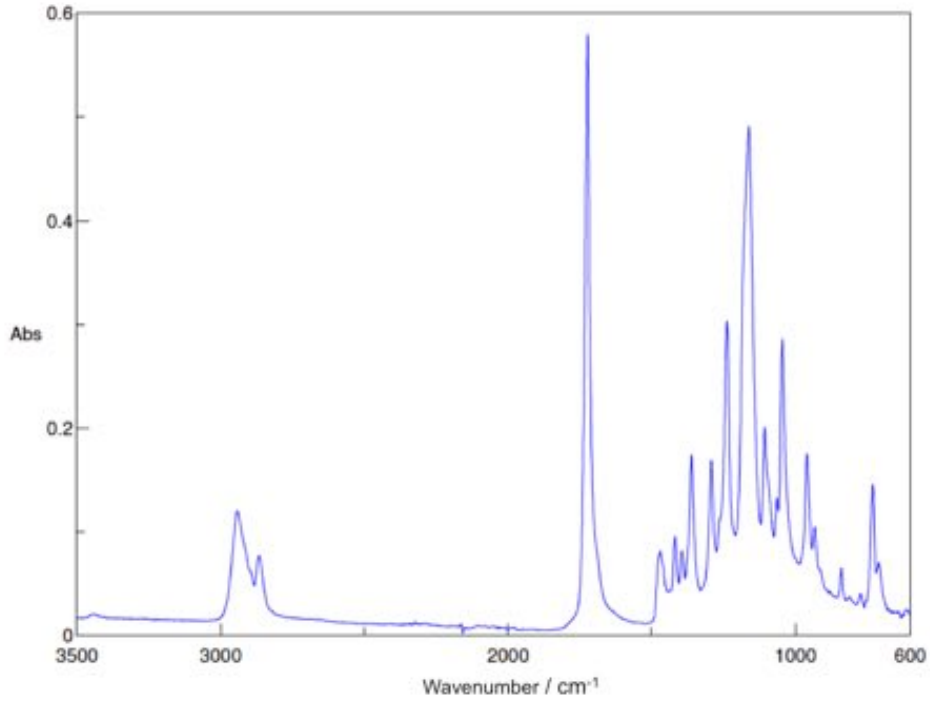

Figure 2.14. Poly(ε-caprolactone) (PCL) 6800 'as received' FTIR spectrum.

2.5 Mechanical testing

2.5.1 Method

Tensile tests were carried out using a mechanical test instrument (Instron 5566, Buckinghamshire, UK) with a 100 kN load cell, interfaced to a PC. The instrument was controlled using proprietary Instron Merlin software. Samples were cut into a standard 25 mm (L_o) 'dog-bone' shape. The width of the narrow central section was 4 mm and the thickness was determined from a three-point average. Mechanical properties of all solvent cast samples were determined at room temperature with a cross-head speed of 2.5 mm min^{-1} due to their extremely brittle nature. A cross-head speed of 10 mm min^{-1} was applied for all mechanical and CO_2 assisted samples. Young's modulus, elongation to break and ultimate tensile strength were determined from the stress-strain curves. A minimum of 5 repeats were performed for each composition within each blend system.

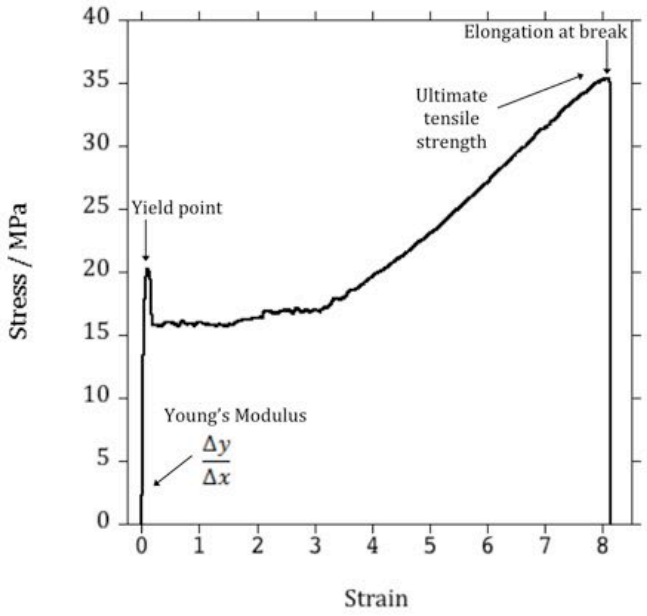

Figure 2.15. A typical stress-strain plot, indicating how the mechanical properties are determined for each experiment.

Figure 2.15 demonstrates how the mechanical properties were determined for all samples. Young's modulus was taken from the initial linear portion of the stress-strain plot and determined from the gradient. The ultimate tensile strength was found from the maximum stress exhibited during the experiment. The elongation at break was taken as the maximum strain prior to sample failure.

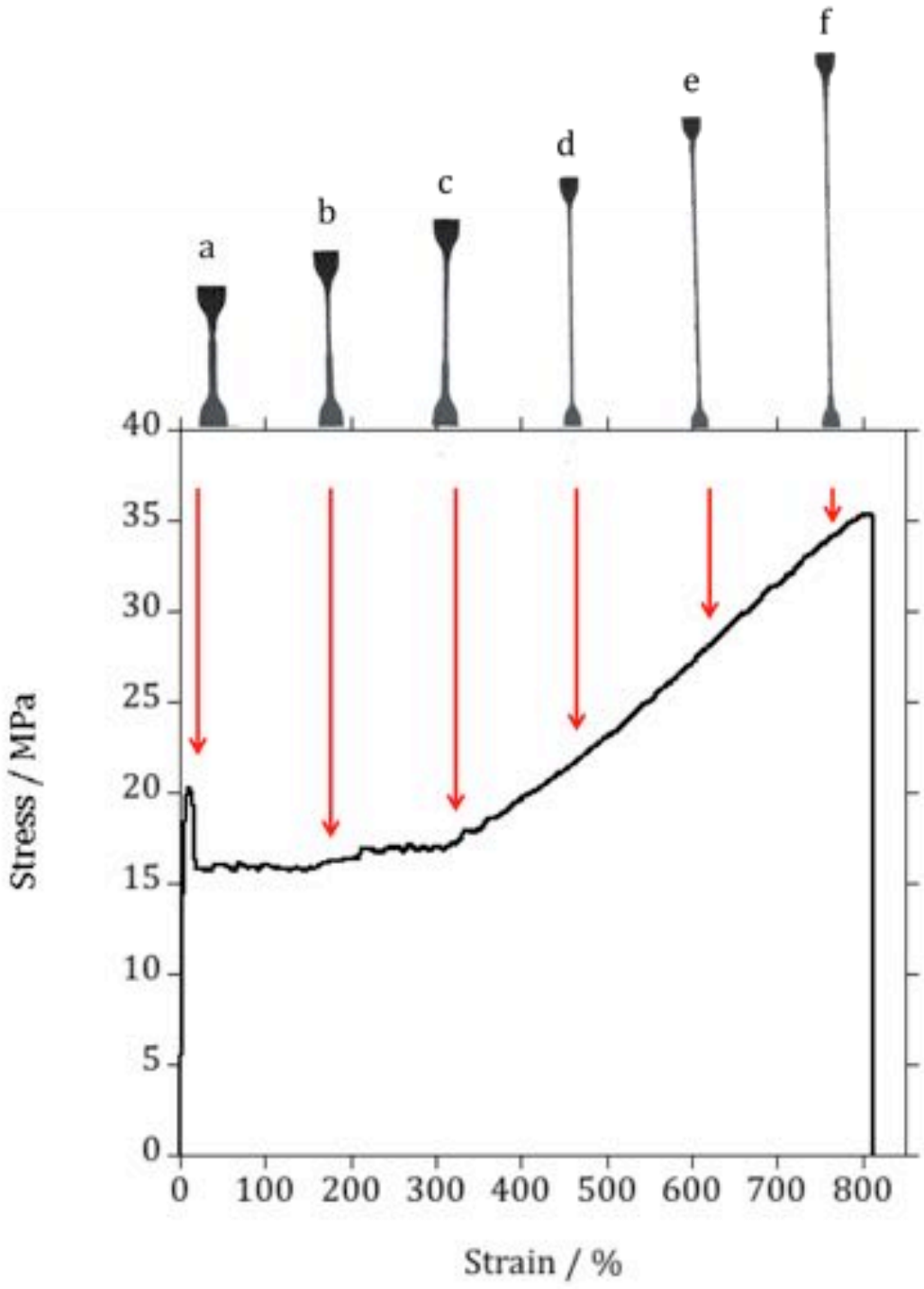

Figure 2.16. Example of the failure of a ductile polymer in tension.

Figure 2.16 illustrates the evolution and failure of a ductile polymer sample over the course of an experiment. Photograph (a) depicts the sample necking corresponding to the yield point exhibited on the stress-strain plot. The sample continues to uniformly

draw (with the necking region growing) throughout photographs (b) and (c). Once drawing within the gauge length portion of the dog-bone is completed, it subsequently takes places from the non-uniform area (the ends) of the specimen, in photographs (d), (e) and (f). This corresponds to an increase in stress (strain hardening) caused by the difficulty to draw from a larger, non-uniform cross–sectional area. This mechanism continues until sample failure takes place. In contrast, Figure 2.17 illustrates a brittle polymer sample after failure. The striations across the sample are known as crazes, formed under tension prior to sample failure. The image shows that crazes have developed homogeneously across the gauge length portion with the absence of necking, this is typical behaviour of a brittle polymer.

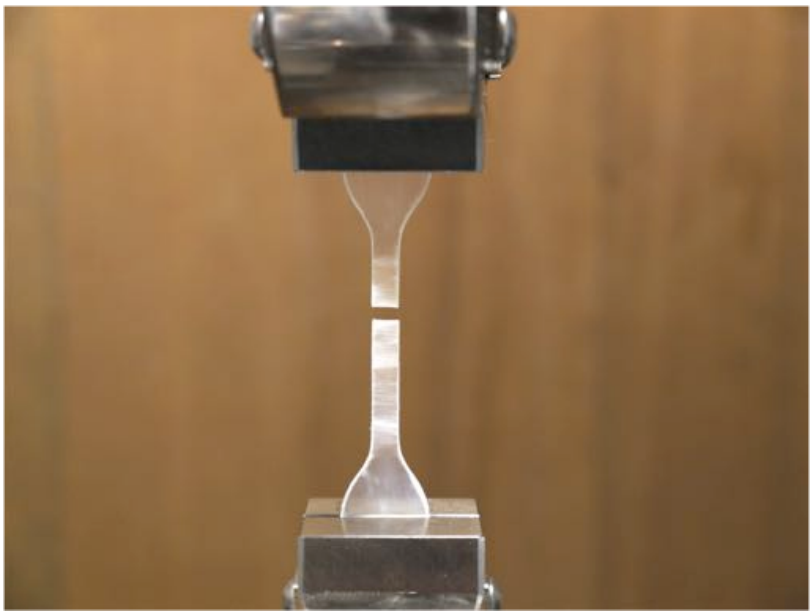

Figure 2.17. Failure of a brittle polymer sample.

2.6 Rheology

2.6.1 Experimental technique

Rheology is the study of deformation and flow of soft matter. The rheological properties of a polymer, for instance its melt viscosity, have important implications on thermal processes such as injection moulding or sheet forming.

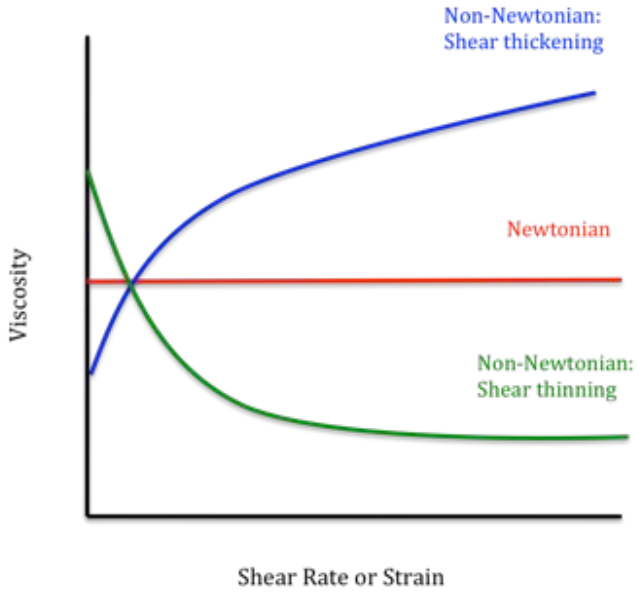

Figure 2.18. Fluid viscosity behaviour with increasing shear rate.

Two common techniques to measure the viscosity of a polymer are rotational and capillary rheometers. Rotational rheometers measure the torque needed to rotate two plates situated on top and bottom of a film sample. A capillary rheometer measures the flow rate of the polymer as it is extruded through a die. Through these experiments, the viscosity of a polymer can be calculated and either classed as Newtonian or non-Newtonian by the way it changes with shear rate or strain (see Figure 2.18). In Newtonian fluids the viscosity is independent of shear rate e.g. oil, whereas a non-

Newtonian fluid may increase or decrease in viscosity through increasing shear rate. This increase and decrease in viscosity is known as shear thickening and shear thinning, respectively.

2.6.2 Method

A Rheometric Scientific (TA, Hertfordshire, UK) 25 mm parallel plate rheometer (Figure 2.19) was used to investigate the viscosity of the homopolymers used in this research.

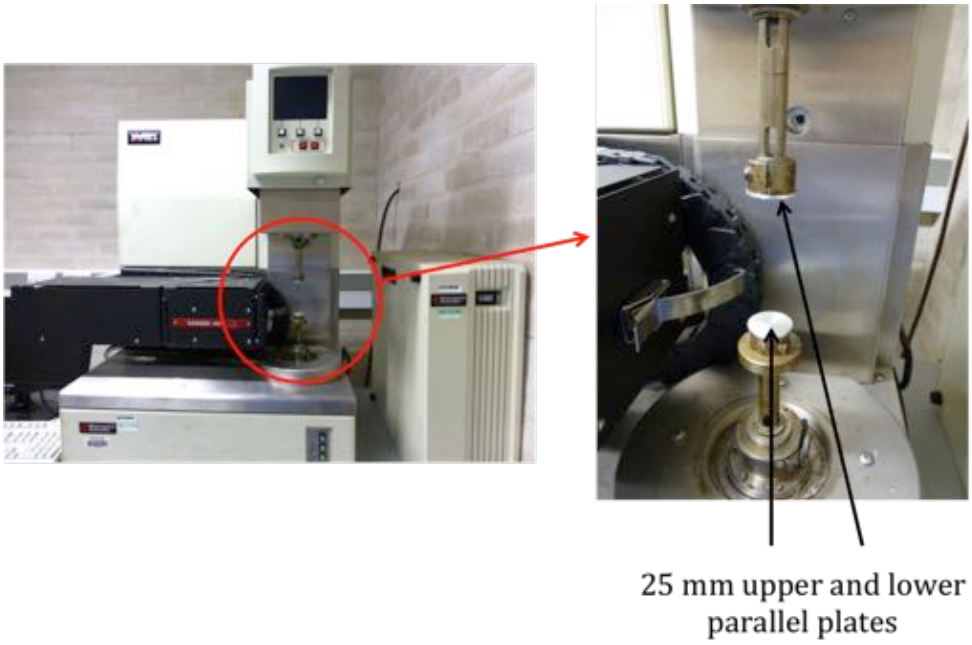

Figure 2.19. Rheometric Scientific 25 mm parallel plate rheometer.

The instrument was connected to a hydrovane compressor (Worcestershire, UK) and experiments were conducted using TA Orchestrator software (version 1 ARES-18A).

Plaques with thicknesses of 1 mm were produced by compression moulding using a Moore E1127 hydraulic hot press (Birmingham, UK). The press was preheated to either 200 ˚C or 150 ˚C (for PLA and PCL respectively) and approximately 30 g of polymer

pellets were placed into a mould (150 x 150 x 1 mm) and subsequently inserted into the hot press. After the mould was provided sufficient time to warm, the plaques were pressed under a load of 10 tonnes for 10 minutes and subsequently removed to cool. Circular samples with a diameter of 25 mm were prepared for rheological analysis.

Samples were inserted into the rheometer and heated to temperatures of either 140 ˚C or 160 ˚C and held for 5 minutes prior to analysis. A dynamic strain sweep was then performed in which the strain was varied logarithmically from 1 to 100% at a frequency of 1.0 Hz.

The effect of temperature and CO_2 pressure on the viscosity of the hot-pressed homopolymers was determined with assistance from Catherine Kelly at Nottingham University using a Physica MCR 301 rheometer (Anton Paar, St. Albans, Figure 2.20) and RheoPlus/32 software (version 3.40). The samples for these measurements were prepared by myself, the instrument was operated by Catherine Kelly and I subsequently analysed all results obtained in order to produce the various plots shown in Chapter 4. The machine was coupled with a high-pressure attachment which mimics a 20 mm parallel plate geometry. Discs, 20 mm in diameter, were cut from the films and inserted into the preheated (140 °C) high pressure cell. The cell was sealed and charged with 80 bar of CO_2 using a 2600D Teledyne syringe pump (California, USA). The samples were then left for 5 minutes to allow the CO_2 to diffuse into the polymer. The shear rate was logarithmically increased from 0.1 to 100 s^{-1} over 2 minutes. Data points were recorded every 5 seconds. The viscosity of each sample was obtained from the linear portion, prior to shear thinning, this represents the linear viscoelastic region of the polymer.

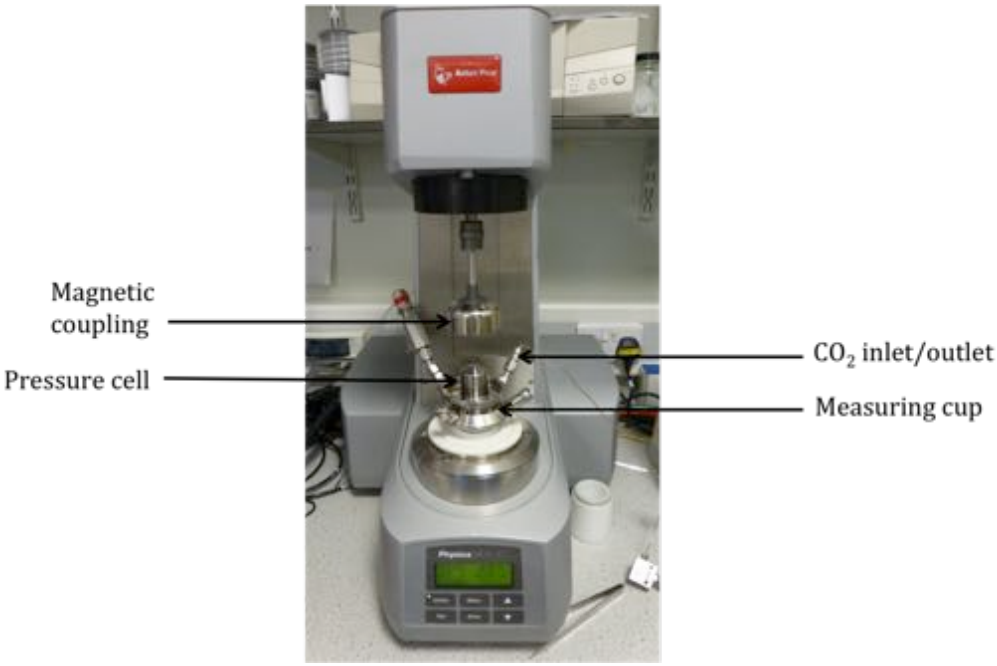

Figure 2.20. Anton Paar Physica MCR 301 high pressure rheometer.

2.7 Size Exclusion Chromatography (SEC)

2.7.1 Experimental technique

Size exclusion chromatography (SEC), also known as gel permeation chromatography, is a technique involving the separation of dissolved molecules by their size or hydrodynamic volume. Separation occurs in a column containing porous beads of a cross linked polymer (the gel) through which the solution passes. Polymer molecules with different molecular weights are excluded from the gel or pass through it depending on their hydrodynamic volume. This varies the time different molecules pass through the columns. Some of the polymer molecules, those with higher molecular weights, will be too large to fit through the smaller pores and therefore will reach the end of the column faster than the lower molecular weight molecules. The time it takes for the molecules to elute through the column determines the size and thereby the molecular weight. The experiment produces a molecular weight- weight distribution but requires calibrating with standard polystyrene or PMMA samples. An approximation of the molecular weights of other polymers can be calculated using the established relationship between hydrodynamic volume and molecular weight of polystyrene or PMMA. However, not all polymers will have the same relationship between hydrodynamic volume and molecular weight, therefore the results obtained are not exact, but are useful for drawing relative comparisons between samples.

2.7.2 Method

The molecular weights of the 'as received' and extruded homopolymers were determined using an Agilent Technologies (Berkshire, UK) LC 390-MDS GPC with analysis performed using Cirrus software. The GPC consisted of one PLgel guard column

(5 μm) and two PLgel MIXED-D (5 μm) with an RI (refractive index) detector. Samples of approximately 1 mg were dissolved in 1 mL of chloroform. The solution was subsequently filtered with a syringe to remove any impurities and placed into the instrument for analysis.

This particular system operated at 30 ˚C with chloroform and 2% triethanolamine (TEA) as the eluent at a flow rate of 1 mL min^{-1}. Using PMMA as a calibration, analysis was performed with the assistance of Kayleigh McEwan at Warwick University, providing values for M_n (number average molecular weight), M_w (weight average molecular weight) and polydispersity index (M_w/M_n).

2.8 References

[1] M. Mihai, M. A. Huneault, and B. D. Favis, "Crystallinity development in cellular poly(lactic acid) in the presence of supercritical carbon dioxide," *Journal of Applied Polymer Science,* vol. 113, pp. 2920-2932, 2009.

[2] P. Krishnamachari, J. Zhang, J. Lou, J. Yan, and L. Uitenham, "Biodegradable Poly(Lactic Acid)/Clay Nanocomposites by Melt Intercalation: A Study of Morphological, Thermal, and Mechanical Properties," *International Journal of Polymer Analysis and Characterization,* vol. 14, pp. 336-350, 2009/05/19 2009.

[3] L. Aras and M. J. Richardson, "The glass transition behaviour and thermodynamic properties of amorphous polystyrene," *Polymer,* vol. 30, pp. 2246-2252, 1989.

[4] M. van der Elst, C. P. Klein, J. M. de Blieck-Hogervorst, P. Patka, and H. J. Haarman, "Bone tissue response to biodegradable polymers used for intra medullary fracture fixation: a long-term in vivo study in sheep femora," *Biomaterials,* vol. 20, pp. 121-8, Jan 1999.

[5] J. Ahmed, J.-X. Zhang, Z. Song, and S. K. Varshnet, "Thermal Properites of Polylactides: Effect of molecular mass and nature of lactide isomer," *Journal of Thermal Analysis and Calorimetry,* vol. 95, pp. 957-964, 2009.

CHAPTER 3 – CONVENTIONAL BLENDING OF POLY(LACTIC ACID) AND POLY(ε-CAPROLACTONE)

3.1 Experimental

3.1.1 Solution casting of poly(lactic acid) and poly(ε-caprolactone) blends

Blends with varying compositions (listed in Table 3.1) were prepared by solution casting. Dichloromethane was selected as a common solvent to dissolve both PLA and PCL. Both polymers (totalling 4 g) were weighed in accordance with each composition and dissolved in dichloromethane (40 mL) to give a 10 wt% solution. The solution was then covered and stirred for 2 hours to ensure complete dissolution of both polymers. Films (approximately 0.5 mm in thickness) were cast into petri dishes, 9 cm in diameter, covered with glass lids and left to evaporate slowly under a fume hood (0.5 m s^{-1} air flow) for approximately 2-3 days. It was important to control and prevent the rapid evaporation of solvent in order to produce improved sample homogeneity. Fast evaporation resulted in larger pores and an uneven surface.

3.1.2 Melt blending of poly(lactic acid) and poly(ε-caprolactone)

Prior to extrusion, the PLA grades were dried to remove any residual moisture. Drying temperatures and times were selected in accordance with the processing data sheets provided by NatureWorks LLC (Nebraska, USA)[1]. Consequently, PLA 4060D was subjected to 4 hours at 45 °C [2] and 2002D for 4 hours at 70 °C [3]. The dried polymer was subsequently stored in desiccators with dry silica gel until required for processing.

The melt blends were produced using a Rondol (Staffordshire, UK) bench top linear 25 mm rotating single-screw extruder with a L/D (length/diameter) ratio of 25:1.

Polymer	**Composition**
PCL CAPA 6800	100
PLA 4060D / PCL CAPA 6800	25/75
PLA 4060D / PCL CAPA 6800	50/50
PLA 4060D / PCL CAPA 6800	75/25
PLA 4060D	100
PLA 2002D / PCL CAPA 6800	25/75
PLA 2002D / PCL CAPA 6800	50/50
PLA 2002D / PCL CAPA 6800	75/25
PLA 2002D	100

Table 3.1. List of polymers and compositions for both solution and melt blending.

The screw possesses a standard purpose profile of 3:1 compression ratio. It was made of high strength carbon steel, heat-treated, polished and removable to enable cleaning. The screw speed was infinitely variable between 0 and 120 rpm. The barrel was also composed of heat-treated high strength carbon steel, fitted with bursting discs for over pressure protection. The temperature was controlled through a series of heaters, one in each zone. The barrel and die temperatures were controlled between 0-300 ˚C and cooled using a tangential water cooling system. A stainless steel two roll take-off unit (with cooling / polishing rolls) placed after the die, cooled the extrudate before passing

onto a conveyor belt.

The polymers, in the form of pellets were added to the hopper of the extruder. Blends were weighed (200 g batches) and physically mixed to ensure an even distribution of pellets prior to extrusion. Barrel and die temperatures were set to 160 °C and 170 °C respectively. The pressure in the screw was monitored using an external pressure transducer. Samples were extruded through a 1 mm slit die and passed through the cooled rollers onto a conveyor belt. A range of screw speeds (10-40 rpm) were used.

Blend extrusions at 10 rpm were discarded as a consequence of the long residence time at the processing temperature and more practical, efficient screw speeds of 20, 30 and 40 rpm were used to produce the blends for subsequent analysis. This range of screw speeds were selected in order to determine the influence of shear rate upon mixing and final properties within the blends. Increasing the screw speed, increases the shear exerted upon the polymers within the barrel. However as a consequence it reduced the residence time, resulting in less time for the polymers to mix in contact with one another and react. Blends were continuously extruded and approximately 10 samples were collected, after 1 m had extruded.

Allowing the machine to 'run dry' for each experimental condition provided an accurate window, indicating where the samples should be collected (thereby determining the residence time for each blend). This approach was limited to an initial trial. Subsequent experiments were conducted using the continual addition and extrusion of blends. In order to preserve the condition of the extruder it was desirable to prevent the machine from 'running dry'. Additionally, consistency needed to be maintained across the two blend preparation extrusion techniques (with and without the presence of carbon dioxide). Extruding in the presence of carbon dioxide needed a continuous flow of

polymer within the barrel in order to maintain a melt seal, which prevents backflow and escape of CO_2 through the hopper. Further details on extrusion with carbon dioxide will be presented in Chapter 4. Prior to this method of determining the residence time an alterative approach was initially employed. One or two pellets containing a polymer dye were introduced into the hopper in addition to the blend. However, this method provided an inaccurate indication of residence time due to the dye lingering for much longer in the extruder than anticipated.

3.2 Results and discussion

3.2.1 Solution casting

Figure 3.1. PCL 6800 solvent cast sample. A smooth, homogeneous surface finish obtained by the slow evaporation of the solvent.

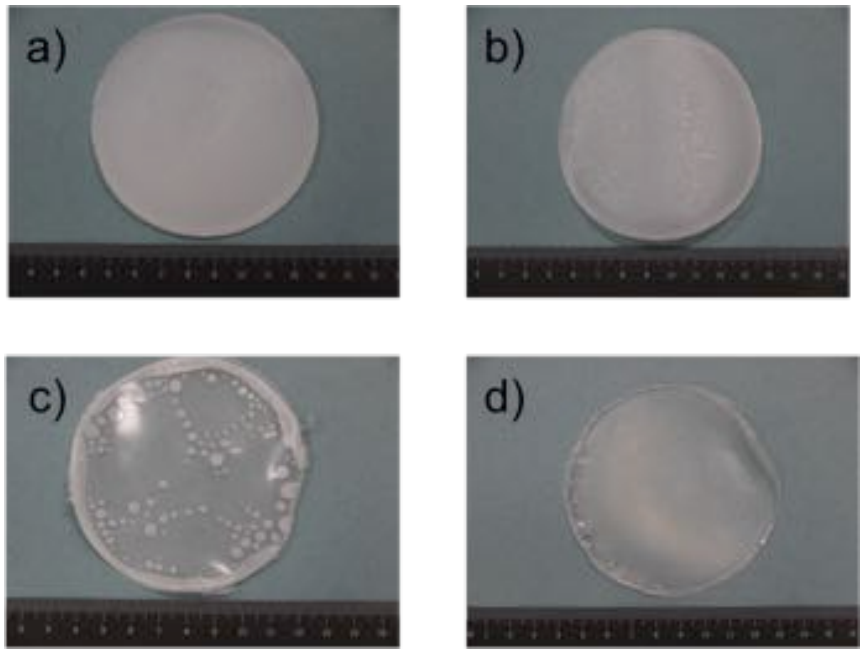

Figure 3.2. PLA 2002D / PCL 6800 solvent cast blends: a) 25/75 PLA/PCL, b) 50/50 PLA/PCL, c) 75/25 PLA/PCL, d) 100 PLA. Large scale phase separation can be observed in image c.

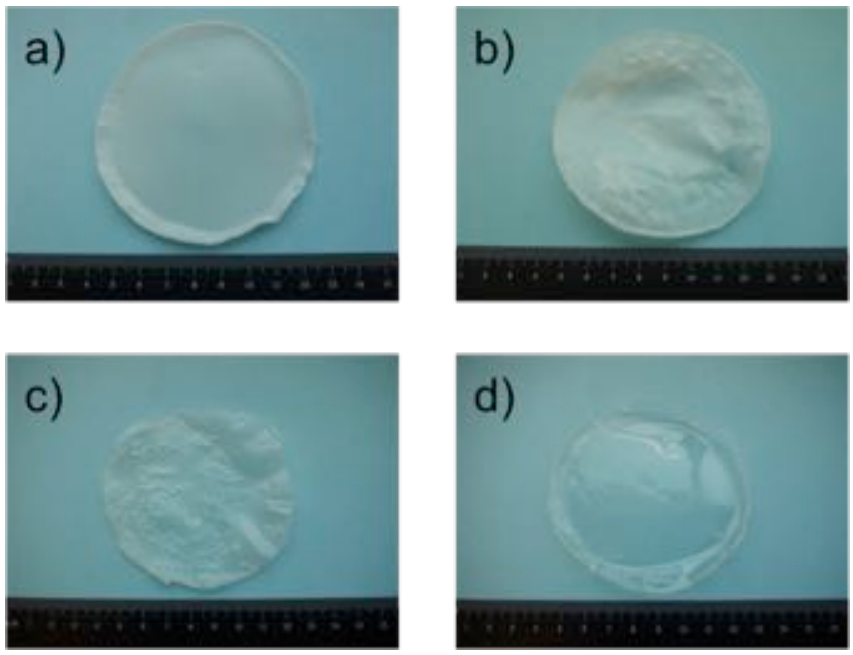

Figure 3.3. PLA 4060D / PCL 6800 solvent cast blends: a) 25/75 PLA/PCL, b) 50/50 PLA/PCL, c) 75/25 PLA/PCL, d) 100 PLA. Large scale phase separation can be observed in image c.

Figure 3.1 to Figure 3.3 display the solvent cast blends and corresponding compositions of homopolymers. In some instances, for example image c) in Figure 3.1 and Figure 3.3 the 75/25 PLA/PCL samples show obvious large scale phase separation.

3.2.2 Scanning Electron Microscopy (SEM)

Figure 3.4 shows the fracture surfaces of the solvent cast homopolymers. Both PLA grades exhibit brittle fracture surfaces in contrast to the more ductile PCL surface. As a result of the low glass transition temperature of PCL (-60 ˚C), it was difficult to produce a satisfactory fracture surface from samples with high contents of this polymer. To ensure a brittle fracture, samples were immersed in liquid nitrogen for a minimum time of 20 minutes. For immersion times less than 20 minutes, ductility was readily observed. Figure 3.5 shows the fracture surfaces of solvent cast PLA 2002D and PCL blends. At all compositions the blends were immiscible and phase separation was present as indicated by the formation of droplets dispersed throughout the matrix. Pores or voids were also present (Figure 3.5b) where droplets had been 'pulled-out' on the fracture, indicating that there was little or no adhesion between the two phases present. This is also confirmed by the separation of both phases by the presence of cavities between the droplet and matrix.

The morphology of the blends was assumed to change with the composition, for example the dominant component makes up the matrix in which the minor component was dispersed. For example, Figure 3.5a) (25/75 PLA2002D/PCL) the matrix was assumed to be PCL dispersed with PLA droplets. Typically, by increasing the content of the dispersed phase, the size of the droplets increase due to coalescence of the relative

increase in volume [4, 5]. This is evident throughout alternative compositions studied in these blend systems, however is not presented in these results (see Appendix 1).

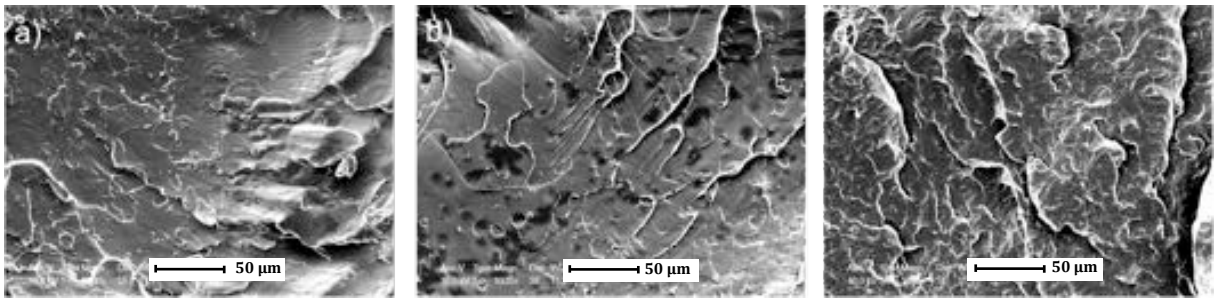

Figure 3.4. Fracture surfaces of the solvent cast homopolymers. Image a) poly(lactic acid) 2002D, b) poly(lactic acid) 4060D and c) poly(ε-caprolactone).

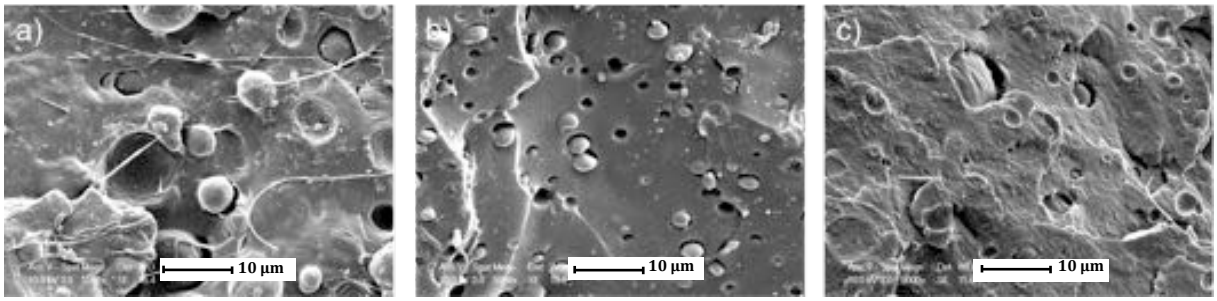

Figure 3.5. Fracture surfaces of solvent cast poly(lactic acid) 2002D blends. Image a) 25/75 PLA2002D/PCL, b) 50/50 PLA2002D/PCL and c) 75/25 PLA2002D/PCL.

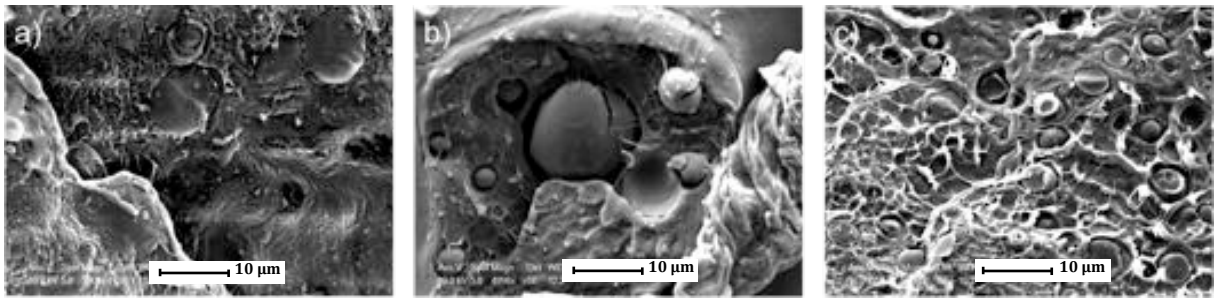

Figure 3.6. Fracture surfaces of solvent cast poly(lactic acid) 4060D blends. Image a) 25/75 PLA4060D/PCL, b) 50/50 PLA4060D/PCL and c) 75/25 PLA4060D/PCL.

The dispersed PLA phase in the 25/75 PLA/PCL blends has a larger diameter than the dispersed PCL in the 75/25 blends (Table 3.3 and Table 3.4). This is thought to be attributed to the different viscosities of the two materials [6].

The solvent cast PLA 4060D and PCL blends (Figure 3.6) present very similar results to those displayed in the PLA 2002D blend system (Figure 3.5). Relatively large droplets (up to 10 μm) are obviously apparent at all compositions. This observation is in accordance with other reports in the literature in which phase separation was present, although it should be noted that these observations were made in blends produced from different grades of PLA and PCL. It is clear that both blend systems in this research, created by solvent casting from dichloromethane, can be considered to be immiscible from gross phase separation. Although there is no evidence as yet that the phases are composed of each homopolymers alone and there is some limited partial miscibility.

Solvent casting in dichloromethane dissolves both polymers allowing any polar groups (in this case, the carbonyl groups) in the polymer chains to interact with one another. However, slow evaporation of the solvent allows time for the polymers to phase separate and encourages crystallinity to develop causing further phase separation to occur. The observation of phase separation in previous PLA/PCL solution-cast blends was attributed to crystallisation of PCL and expulsion of PLA in these crystalline regions through spherulitic growth [7]. It was noted that phase separation may also be induced by the presence of a third component, the solvent. Solution-casting these blends promotes phase separation and may not reflect the true morphology of the two component systems.

The application of heat (160 °C which is above the melting point) combined with the shear forces of mechanical mixing during melt blending, creates a higher level of

interaction allowing the blends to transform from the two phase into the one phase region of the LCST curve [8]. When producing immiscible blends, the minor phase (polymer 1) is dispersed as droplets within the major phase (polymer 2), as demonstrated in these blends by SEM.

Final blend morphology is determined by droplet break-up and coalescence. These are competing mechanisms that are influenced by interfacial tension [9]. Taylor studied the breakup of a single Newtonian drop in a simple shear field [10, 11]. According to Taylor's theory, the deformation of a Newtonian drop in a Newtonian matrix depends on two parameters; the viscosity ratio, $\lambda = \eta_d/\eta_m$ and capillary number, κ (the ratio of the local shear stress and drop diameter to the interfacial tension)[12]:

$$\kappa = \eta_m \dot{\gamma} d/\nu \qquad \text{Equation 3.1}$$

where η_m is the viscosity of the matrix, $\dot{\gamma}$ is the shear rate, d is the diameter of the droplet and ν is the interfacial tension. Therefore, the deformation of a droplet is encouraged by a high matrix viscosity, large shear rates, large droplet size and small interfacial tension. This means by introducing shear rates into the blend system through processing using an extruder, deformation of a droplet is more likely to occur in comparison to solvent casting. Taylor balanced the shear and interfacial forces to give an expression for the maximum droplet size that would be stable:

$$d = \frac{4\nu(\lambda + 1)}{\dot{\gamma}\eta_m\left(\frac{19}{4}\lambda + 4\right)} \qquad \lambda < 2.5 \qquad \text{Equation 3.2}$$

Taylor predicted that no breakup of droplets would occur when $\lambda < 2.5$. Equation 3.2 implies that droplet size will be reduced through increasing the shear rate. However, this relation is valid for *small* deformations in Newtonian fluids [13]. There are limitations to Taylor's theory when applied to polymer blends and to viscoelastic systems. The individual components in polymer blends exhibit large normal stresses in flow. In addition, the process of coalescence is not taken into consideration [14]. Therefore, Wu established a correlation relating capillary number to viscosity ratio for extruded polymer blends. He expresses the droplet diameter as:

$$d = \frac{4\nu\lambda^{\pm 0.84}}{\dot{\gamma}\eta_m} \qquad \text{Equation 3.3}$$

where the plus (+) sign is applied when $\lambda > 1$ and the minus (-) sign is applied when $\lambda < 1$. He suggests that the droplet diameter is a minimum when the viscosities of both polymers are close to unity and the interfacial tension is low [15]. Therefore, the viscosity ratios of both blend systems and interfacial tensions will be analysed later in this chapter.

Figure 3.7 to 3.9 display the SEM images for the PLA 2002D and PCL blends extruded at 40, 30 and 20 rpm. In contrast to the blends produced by solvent casting, these blends exhibit greatly reduced droplet size and better dispersion. Low interfacial tension, high shear rates and similar viscosities of both polymers contribute to the size and homogeneity of the dispersed phase and final sample morphology [16].

The total surface energy of a solid is the summation of the polar and the dispersive surface energy components (Equation 3.4), measured from the contact angle of probe

liquids during a contact angle experiment [17]. These probe liquids have pre-determined values for the total, polar and dispersive surface energy components.

$$\gamma_S^{Total} = \gamma_s^d + \gamma_s^p \quad \text{Equation 3.4}$$

The surface energies of PLA and PCL 6800 have previously been determined in the literature via means of contact angle experiments [17]. These are displayed in Table 3.2.

	γ (mN m^{-1})	γ_d (mN m^{-1})	γ_p (mN m^{-1})
PLA	49 ± 2	37 ± 2	11 ± 2
PCL	52 ± 2	41 ± 2	11 ± 2

Table 3.2. Surface energy parameters for PLA and PCL [17].

Similar values were also reported for PLA 2002D and PCL 6500 [18]. The interfacial tension (γ_{12}) was determined using the following equation by Wu [19]:

$$\gamma_{12} = \gamma_1 + \gamma_2 - \frac{4\gamma_1^d \gamma_2^d}{\gamma_1^d + \gamma_2^d} - \frac{4\gamma_1^p \gamma_2^p}{\gamma_1^p + \gamma_2^p} \quad \text{Equation 3.5}$$

The interfacial tension between PLA and PCL was calculated to be 1.21 mN m^{-1} from Equation 3.5. The magnitude of the interfacial tension between the two components determines their compatibility and miscibility with one another. As mentioned previously, if the value of interfacial tension tends to zero, miscibility is assumed. In

contrast, as interfacial tension increases so does the immiscibility between both components. Large differences in polarity between both polymers increase the interfacial tension [20]. Interfacial tension values of 10.0 and 4.4 mN m^{-1} are given for blends PE/PMMA and PE/PS respectively [21]. It is reported that interfacial tension in a polymer blend is seen to decrease linearly with increasing temperature [22-24]. The interfacial tension of PLA/PCL blends at 180 ˚C has been measured to be 0.33 mN m^{-1}, indicating enhanced compatibility between both components at this temperature [25]. This study further confirmed compatibility, with evidence of mechanical properties following the rule of mixtures theory. Increasing molecular weight correspondingly increases the interfacial tension in other polymer blends. However, the interfacial tension is seen to plateau above the entanglement chain length [24, 26]. Additionally it has been found that interfacial tension decreases with increasing polydispersity. This may be attributed to the migration of the short chains to the interface which performs as a surfactant thus lowering the interfacial tension between both polymers [22, 27].

Figure 3.7 to Figure 3.9 show that screw speed in these experiments has little influence on the microstructure of the blends. However, the most improved microstructure appears in the 75/25 PLA/PCL blends. The largest domains and the most dispersed phase is observed in the 50/50 blends. This trend is also present in the PLA 4060D and PCL system as illustrated in Figure 3.10 to 3.12. The typical appearance in the majority of the blends of a clean interface between the spherical inclusions and the matrix suggests there is little adhesion between the two phases. However, an indication of slight adhesion by the absence of voids and obvious boundaries between the dispersed phase and the matrix may be seen in Figure 3.12 (b). None of these blends exhibit any evidence of transcrystallinity or a co-continuous microstructure.

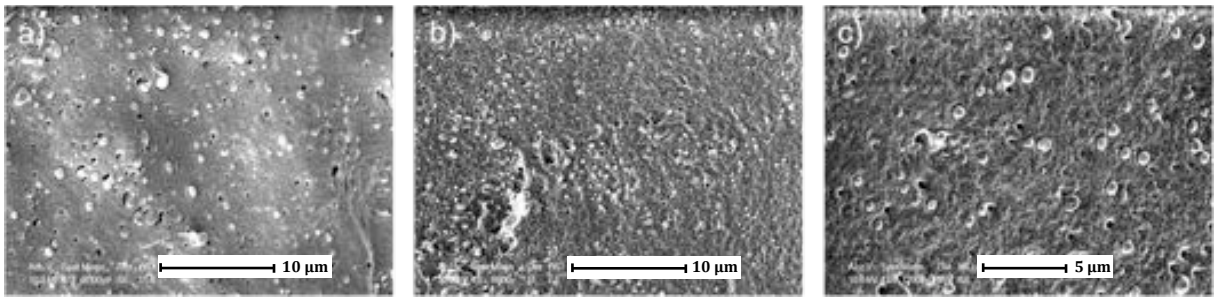

Figure 3.7. Fracture surfaces of melt blended 25/75 PLA2002D/PCL. Image a) extruded at 40 rpm, b) at 30 rpm and c) at 20 rpm.

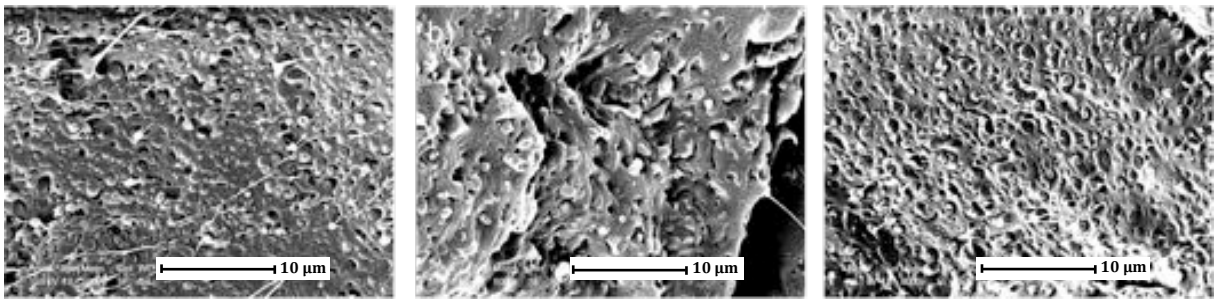

Figure 3.8. Fracture surfaces of melt blended 50/50 PLA2002D/PCL. Image a) extruded at 40 rpm, b) at 30 rpm and c) at 20 rpm.

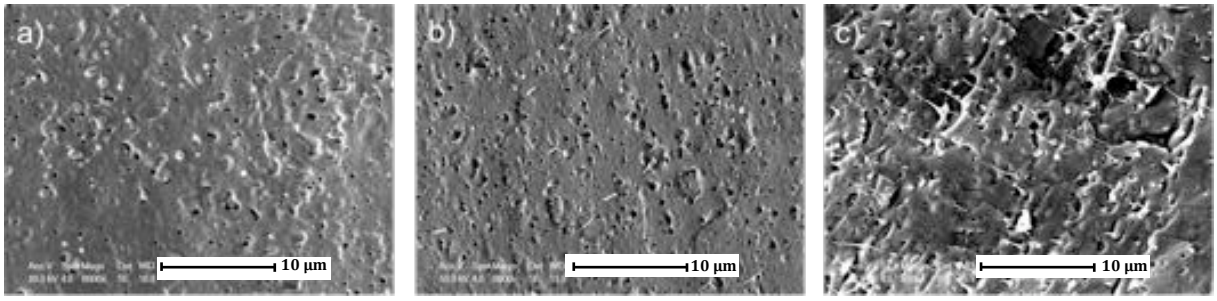

Figure 3.9. Fracture surfaces of melt blended 75/25 PLA2002D/PCL. Image a) extruded at 40 rpm, b) at 30 rpm and c) at 20 rpm.

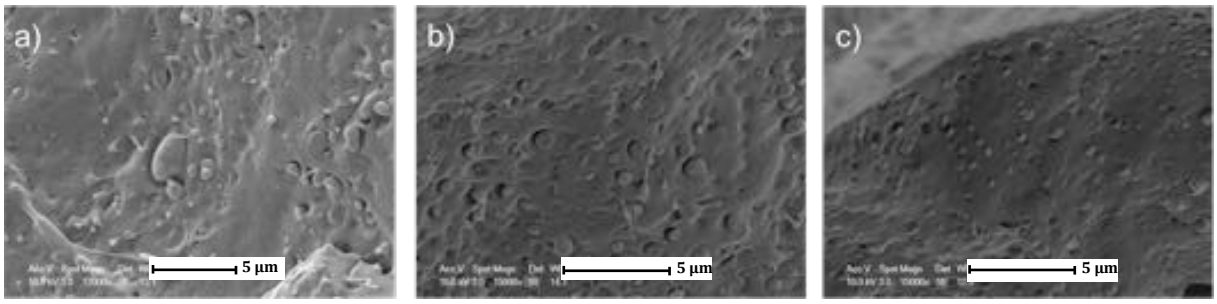

Figure 3.10. Fracture surfaces of melt blended 25/75 PLA4060D/PCL. Image a) extruded at 40 rpm, b) at 30 rpm and c) at 20 rpm.

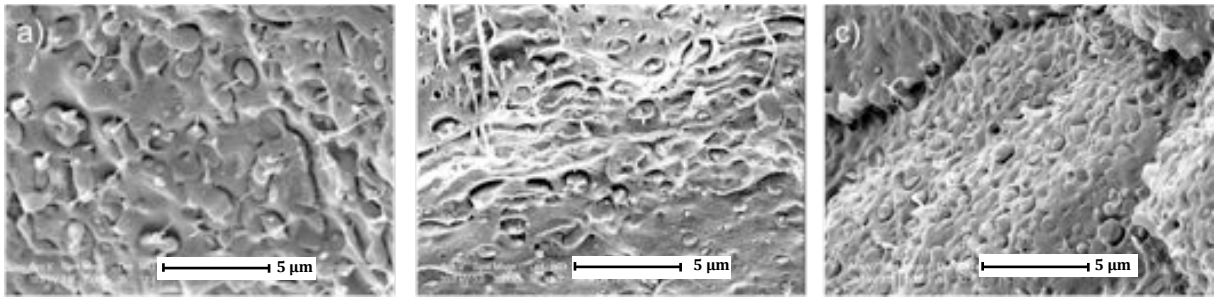

Figure 3.11. Fracture surfaces of melt blended 50/50 PLA4060D/PCL. Image a) extruded at 40 rpm, b) at 30 rpm and c) at 20 rpm.

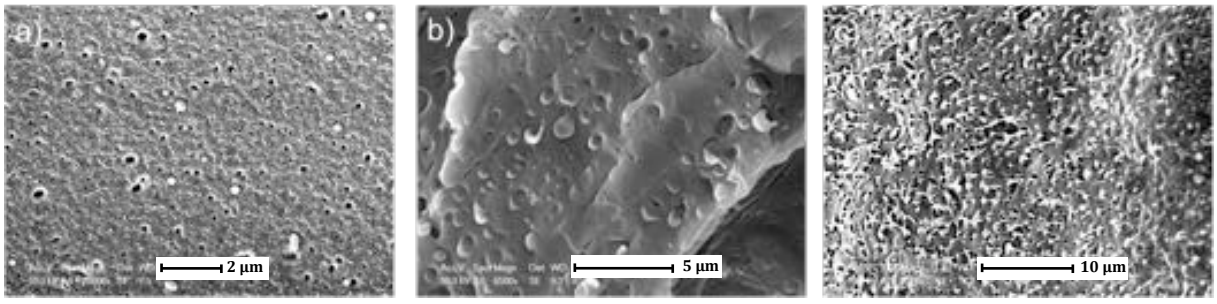

Figure 3.12. Fracture surfaces of melt blended 75/25 PLA4060D/PCL. Image a) extruded at 40 rpm, b) at 30 rpm and c) at 20 rpm.

Further analysis, presented in section 3.2.3, e.g. mechanical testing was carried out to give further insight into the interactions between both phases in the blend, particularly on the influence of screw speed. The presence of adhesion should result in an improvement in mechanical properties.

Some porosity was present see Figure 3.7 (a), Figure 3.9 (a) & (b) and Figure 3.12 (a) predominantly in samples produced at a screw rate of 40 rpm. The faster screw speed accounts for this porosity since increasing the screw speed entraps air into the polymer melt [28]. Additionally, a reduction of residence and consequently melt time reduces the capacity for air removal from between the pellets in the compression zone of the extruder [29, 30]. The efficiency of blending PLA and PCL in a twin-screw extruder, in comparison to a single-screw, has been demonstrated by Dell'Erba *et al.* [9]. Utilising a twin-screw extruder when blending polymers enables a more significant 'break-up' of the dispersed phase due to the high shear deformations and stresses on the melt. Dell'Erba presents evidence of how low shear forces applied to the melt lead to a very coarse final blend morphology. Blends produced via single screw extrusion possessed dispersed phase dimensions one order of magnitude higher than those obtained in the case of the twin extruder [9].

Numerous attempts have been made in the literature to quantitatively analyse droplet dispersion from the SEM images [4, 13, 31, 32]. Equation 3.6 and Equation 3.7 are the number and weight average equations for calculating the average diameters of the droplets in the blends. These equations were used to determine the average droplet diameter across the solvent cast and melt blends. Five different SEM images were evaluated for each composition where the droplet diameters and associated cavities were measured from the scale bar of each image. Cavities and pores that were assumed

to be a consequence of porosity were discarded from this analysis. A consistency in the precision of the measurements around ± 0.4 μm for the solvent cast and ± 0.2 μm for the melt blends was considered to be appropriate.

$$d_n = \frac{\Sigma n_i d_i}{\Sigma n_i} \qquad \text{Equation 3.6}$$

$$d_w = \frac{\Sigma n_i d_i^2}{\Sigma n_i d_i} \qquad \text{Equation 3.7}$$

Where n_i is the number of particles with a diameter d_i. The d_n and d_w values for the PLA2002D/PCL and PLA4060D/PCL blends are presented in Table 3.3 and Table 3.4 respectively. The d_w data is also presented in Figure 3.13.

	PLA2002D/PCL 25/75		**PLA2002D/PCL 50/50**		**PLA2002D/PCL 75/25**	
	Solvent	**Melt**	**Solvent**	**Melt**	**Solvent**	**Melt**
d_n / μm	5.20 ± 2.52	0.57 ± 0.43	2.24 ± 0.67	0.92 ± 0.77	3.31 ± 2.00	0.34 ± 0.54
d_w /μm	6.31 ± 2.52	0.66 ± 0.43	2.45 ± 0.67	1.75 ± 0.77	4.41 ± 2.00	0.43 ± 0.54

Table 3.3. Number and weight average droplet diameter and standard deviations. PLA2002D/PCL solvent cast and melt blends (30 rpm).

	PLA4060D/PCL 25/75		PLA4060D/PCL 50/50		PLA4060D/PCL 75/25	
	Solvent	**Melt**	**Solvent**	**Melt**	**Solvent**	**Melt**
d_n / µm	5.32 ± 2.88	0.76 ± 0.24	5.14 ± 4.28	0.78 ± 0.40	3.33 ± 1.1	0.50 ± 0.18
d_w / µm	6.65 ± 2.88	0.82 ± 0.24	8.91 ±4.28	0.96 ± 0.40	2.78 ± 1.1	0.63 ± 0.18

Table 3.4. Number and weight average droplet diameter and standard deviation. PLA4060D/PCL solvent cast and melt blends (30 rpm).

Additionally, the average diameter volume may also be calculated using Equation 3.8:

$$d_v = \frac{\Sigma n_i d_i^4}{\Sigma n_i d_i^3}$$ Equation 3.8

Previous studies [13, 31] have measured the cross-sectional area (A_i) of each individual droplet (i) and converted this into an equivalent diameter of a sphere using Equation 3.9:

$$D_i = 2(A_i|\pi)^{1/2}$$ Equation 3.9

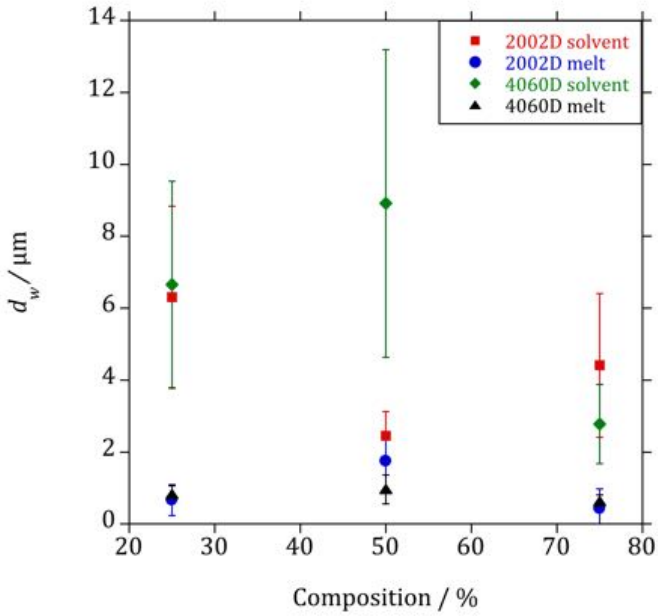

Figure 3.13. The d_w values for PLA2002D/PCL and PLA4060D/PCL solvent cast and melt blends.

In summary, melt blending with a single screw extruder was also found to yield phase-separated blends at all compositions and extrusion speeds investigated. However, an improvement in dispersion and droplet size, e.g. a reduction from 9 µm produced by solvent casting to around 1 µm by melt blending, was observed in the 50/50 PLA4060D/PCL system.

3.2.3 Mechanical testing

Figure 3.14, Figure 3.15 and Figure 3.16 show the elongation at break, yield stress and Young's modulus for the solvent cast PLA 2002D and PCL blends respectively. Elongation at break is typically greatest in the homopolymers, with the lowest value observed for the 25/75 PLA2002D/PCL blend. The greatest elongation at break within the blends is for the 75/25 PLA2002D/PCL composition. However, as demonstrated in SEM, all blends have exhibited gross immiscibility by large droplets and phase separation. Droplets act as stress initiation sites and severely hinder the mechanical properties within the sample. Stress concentration usually takes place in the vicinity of the dispersed phase and initiates localised micro-damages in this region. It results from the difference of elastic modulus between the dispersed phases and the surrounding matrix. Consequently there is a reduction in the mechanical properties such as strength and toughness in comparison to miscible polymer blends [5]. Larger dispersed phases induce greater stress concentrations and subsequently show a greater reduction in mechanical properties. This corresponds with a study by Rao and colleagues, who noticed that larger voids caused by large droplets of PCL resulted in local stress concentrations, contributing to a faster fracture of the samples [33].

Subject to the droplet size, dispersion and porosity within the samples caused by evaporation of the solvent, there was extreme variation in mechanical properties. This can be seen by the large error within the majority of the compositions. The error within the experiments is consistent across all measured mechanical properties for both blend systems.

Results for yield stress (Figure 3.15) for the 2002D blend system follow a U-shaped trend, with the 50/50 PLA2002D/PCL blend possessing the lowest value. Young's modulus, as depicted in Figure 3.16, shows an initial increase when PLA is introduced to PCL. Following this, the error bars denoted by standard deviation over multiple experiments are much larger. This indicates that phase separation (and disparity in the size of the dispersed phase) in addition to the absence of adhesion within the blends are contributing to the large variation in results. The interfacial adhesion at the microphase boundaries is vital to the mechanical strength of a sample [8].

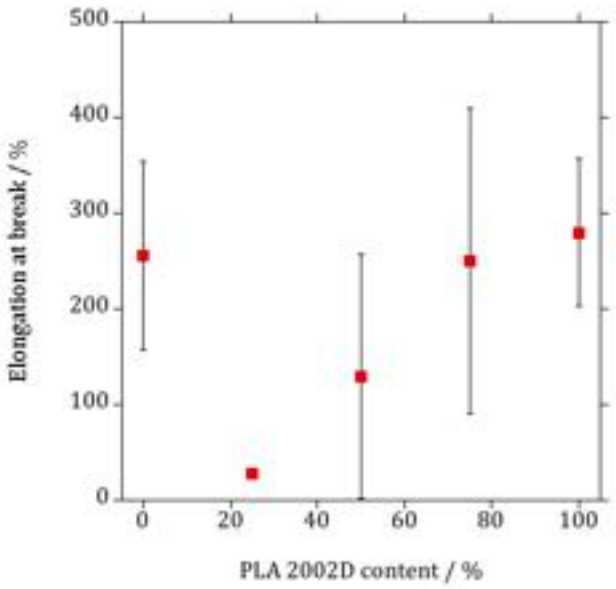

Figure 3.14. Elongation at break for the solvent cast PLA 2002D/ PCL blends. Error bars represent the standard deviation averaged over multiple experiments.

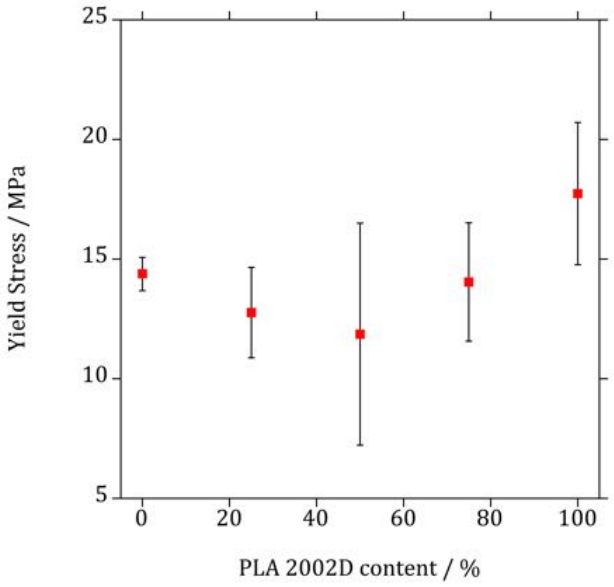

Figure 3.15. Yield stress for the PLA 2002D / PCL blends. Error bars represent the standard deviation averaged over multiple experiments.

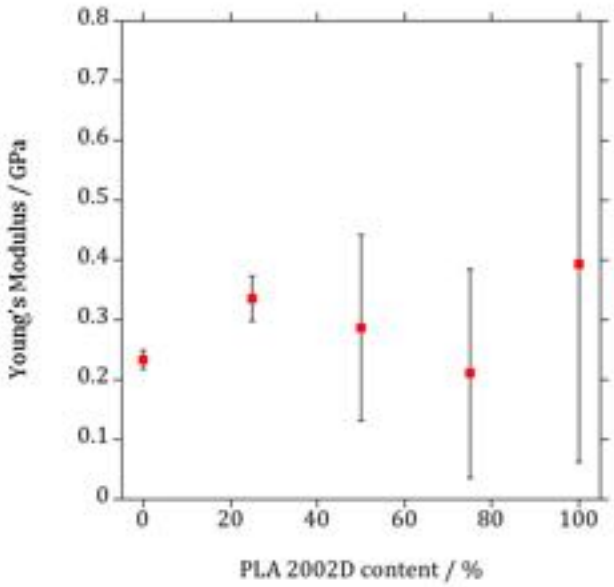

Figure 3.16. Young's modulus for the PLA 2002D / PCL blends. Error bars represent the standard deviation averaged over multiple experiments.

Figure 3.17 to Figure 3.19 display the mechanical results for the PLA 4060D and PCL blends. Figure 3.17 shows the effect of blend composition on elongation at break. As with the 2002D blend system, the lowest value is exhibited by the 25/75 PLA4060D/PCL composition and the highest with the 75/25 PLA4060D/PCL blend. Both systems exhibit similar trends in elongation at break and Young's modulus, however the variation in yield stress is not comparable.

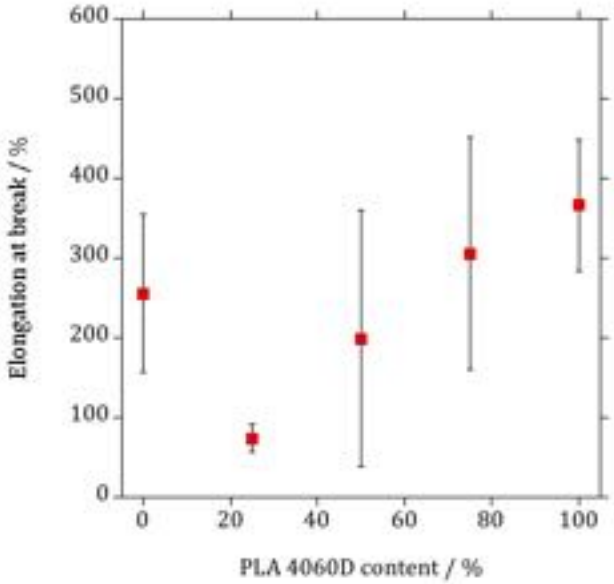

Figure 3.17. Elongation at break for the solvent cast PLA 4060D/ PCL blends. Error bars represent the standard deviation averaged over multiple experiments.

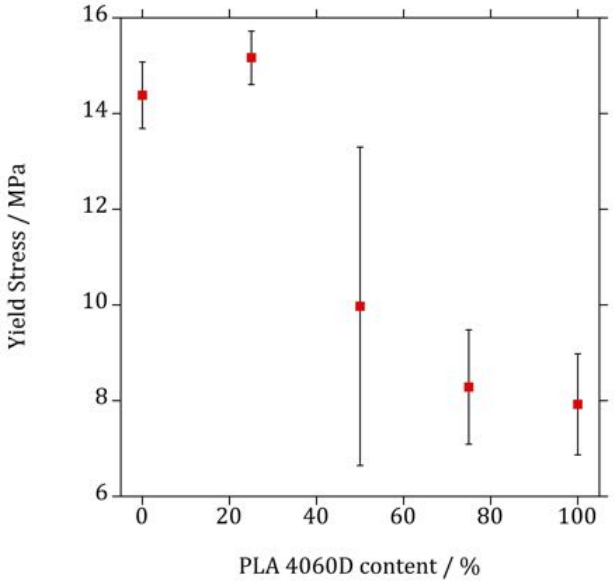

Figure 3.18. Yield stress for the PLA 4060D / PCL blends. Error bars represent the standard deviation averaged over multiple experiments.

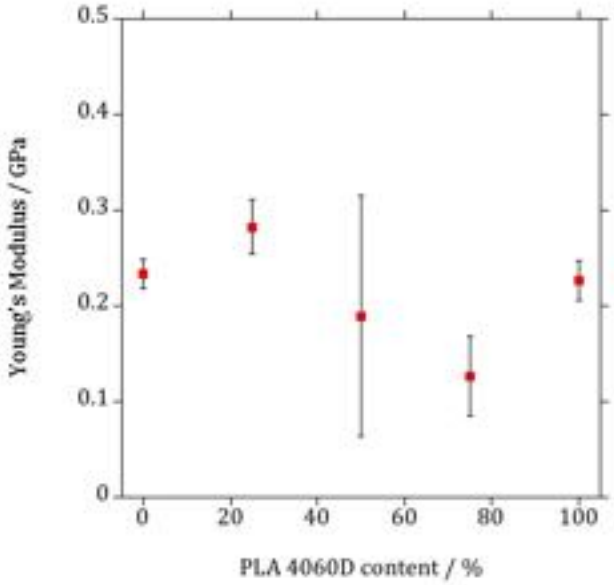

Figure 3.19. Young's modulus for the PLA 4060D / PCL blends. Error bars represent the standard deviation averaged over multiple experiments.

Figure 3.20 and Figure 3.21 show the representative examples of the engineering stress-strain curves for all compositions of PLA2002D/PCL and PLA4060D/PCL produced by melt blending. The curve for 100% PLA is indistinguishable because of the dramatic change in strain across composition, therefore an additional inset of this result is presented within the graphs. It is clear that with increasing PCL content in the blend, the tensile behaviour of the blend system changed dramatically. A reduction in yield stress was compensated by a significant increase in elongation at break.

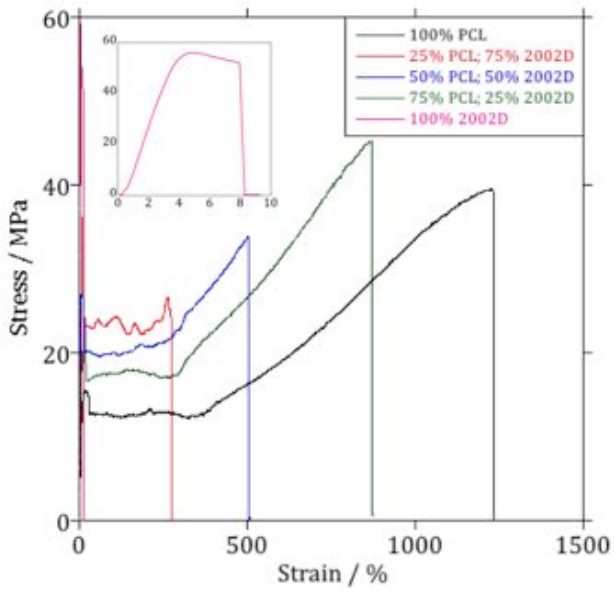

Figure 3.20. Examples of the engineering stress-strain curves for the melt blended PLA2002D/PCL blend system. Inset is the result for 100% PLA.

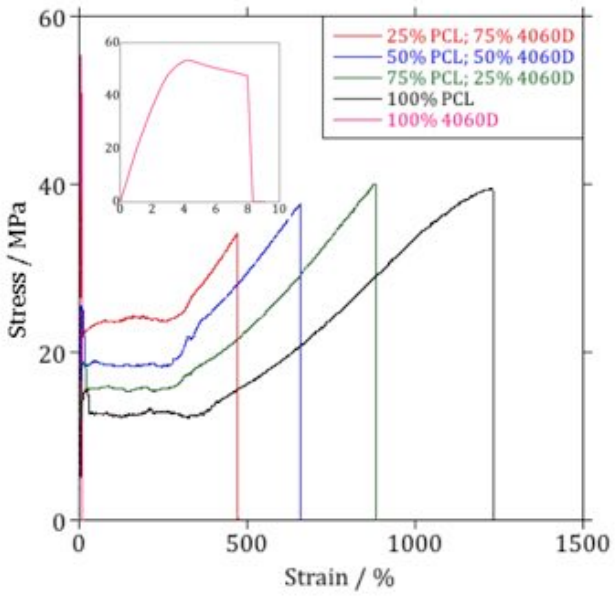

Figure 3.21. Examples of the engineering stress-strain curves for the melt blended PLA4060D/PCL blend system. Inset is the result for 100% PLA.

The yield stress is defined as the maximum stress in the stress/strain curve and is a result of plastic deformation, i.e. non-reversible deformation of the sample. In PCL homopolymers and blends, the drop in stress corresponds to neck formation or localised yielding of the material with a reduction in cross sectional area as strain increases. This is followed by extension of the neck through the specimen until it reaches the end profile, which accounts for the increase in stress after 400 % extension. The increase in length corresponds to the polymer chains aligning along the direction of the load characterised by the material drawing.

PLA appears to form a more diffuse neck in which a greater volume of material is involved in the neck formation or to uniformly draw but since it breaks at the onset of yielding it is not possible to separate the two mechanisms.

Shark skin is a regular ridged surface distortion, exhibiting ridges that run perpendicular to the direction of extrusion [34]. The manifestation of the shark skin surface defect amongst many of the extrudates, particularly in the samples containing higher concentrations of PLA, may be a contributing factor to variation seen in mechanical properties. An example of the evolution in surface appearance can be seen in Figure 3.22. The appearance of a matte surface finish, in contrast to a glossy one, also represents the presence of shark skin in a less severe form. It is assumed that shark skin is formed and caused by tensile stresses within or at the exit of the die and can be reduced by decreasing the screw speed or increasing the temperature of the die [30]. Increasing the temperature of the die will help thermally relax the stresses and lower the viscosity [29]. Polymers with high viscosities, high modulus, low elongation and narrow molecular weight distributions are more susceptible to shark skin [35]. Therefore, it is not surprising that this phenomenon occurred in the extrudates containing higher concentrations of PLA and at the faster screw speeds.

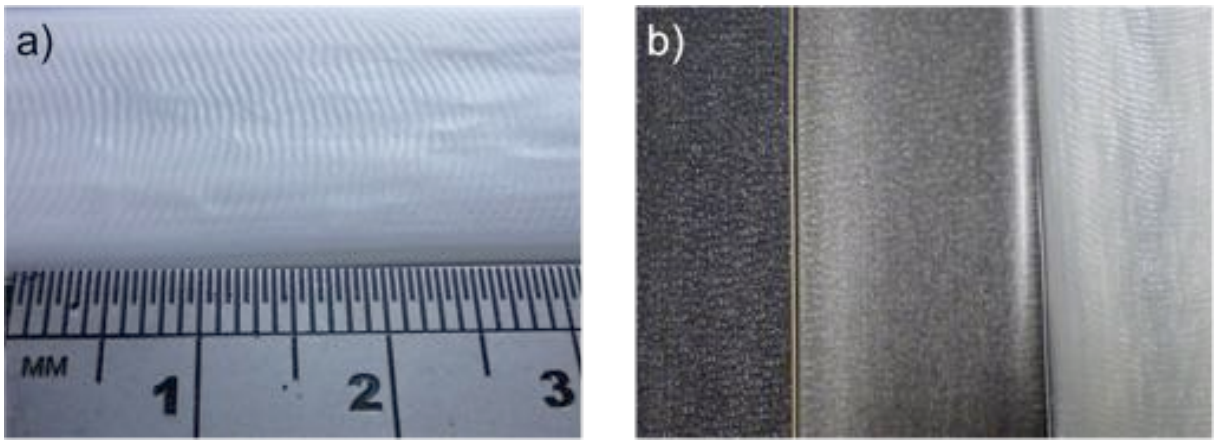

Figure 3.22. a) Shark skin surface defect in PLA2002D/PCL 75/25 40 rpm. b) illustrates the evolution of surface finish; glossy, matt and shark skin from left to right.

Figure 3.23 shows the variation of elongation at break on blends produced at different rpms for the PLA2002D/PCL blends and indicates that elongation increases with increasing PCL content in the blend and decreasing the rpms has a small but positive effect. Error bars are typically smaller for these experiments, contrasting to those seen for the solution casting samples. This indicates sample quality has improved, with perhaps a more homogeneous morphology. SEM confirms that droplet size is significantly reduced, with a more even dispersion. Elongation is significantly increased using this method of blending, for example, the solution cast 50/50 blend exhibited an elongation at break around 150%, and extruded blends show an improvement to around 500%. These results are in concurrence with a previous report in the literature that also notes improvements in mechanical properties from solution casting to melt blending [36].

The 75/25 PLA2002D/PCL blend shows a larger variation in elongation with rpm than the other compositions. There is little evidence using SEM to distinguish the reason for this result, as these samples exhibited superior microstructure, with smaller and more finely dispersed domains of PCL.

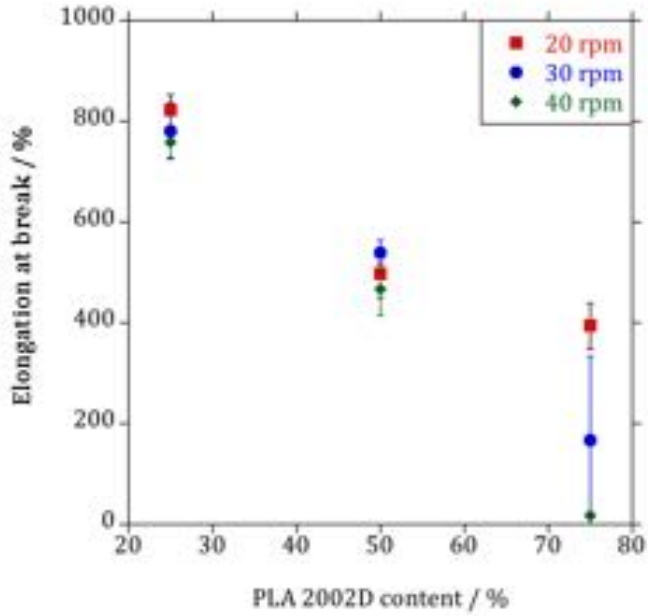

Figure 3.23. A comparison of elongation at break for PLA 2002D / PCL blends with varying rpm. The standard uncertainty is denoted by error bars averaged over multiple experiments.

As expected, the reduction of PCL in the 75/25 PLA/PCL blend promotes a decrease in elongation at break compared to other compositions. Perhaps the variation with rpm for the 75/25 blend can be attributed to an increased adhesion between phases, corresponding to an increase in residence time. Another possibility is the influence of porosity within some samples, particularly evident in the 40 rpm blends. These results demonstrate that PCL possesses the ability to influence the mechanical properties of PLA, albeit with an absence of miscibility within the system. Figure 3.24 shows the yield stress for the PLA2002D/PCL melt blended system. Here, tensile strength of the blends are improved with increasing content of PLA.

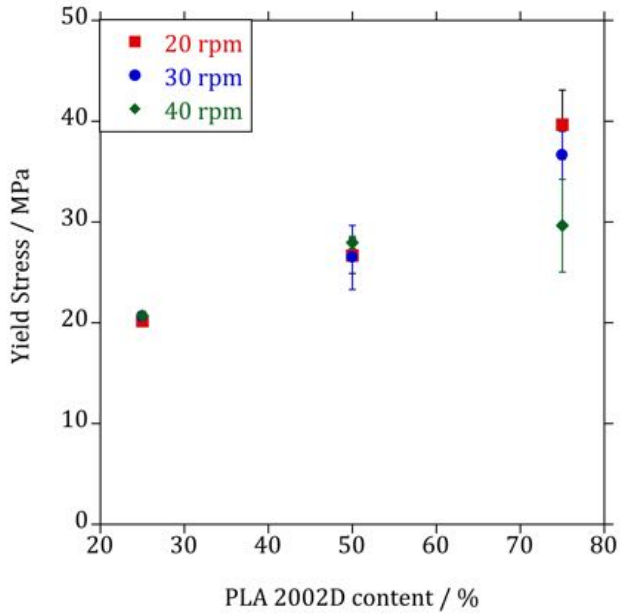

Figure 3.24. A comparison of yield stress for PLA 2002D / PCL blends prepared with varying rpm. The standard uncertainty is denoted by error bars, averaged over multiple experiments.

There is a greater variation with screw speed in the 75/25 PLA/PCL blend as also observed in the elongation at break for this system. As mentioned previously, this variation may be a result of disparity in adhesion and porosity between phases.

The Young's modulus (see Figure 3.25) also showed an improvement with increasing concentrations of PLA, with a similar (less significant) variation in the 75/25 blends with rpm. Across all properties within this blend system for the 75/25 composition, 20 rpm exhibits the greatest improvement with the poorest properties observed for the 40 rpm samples.

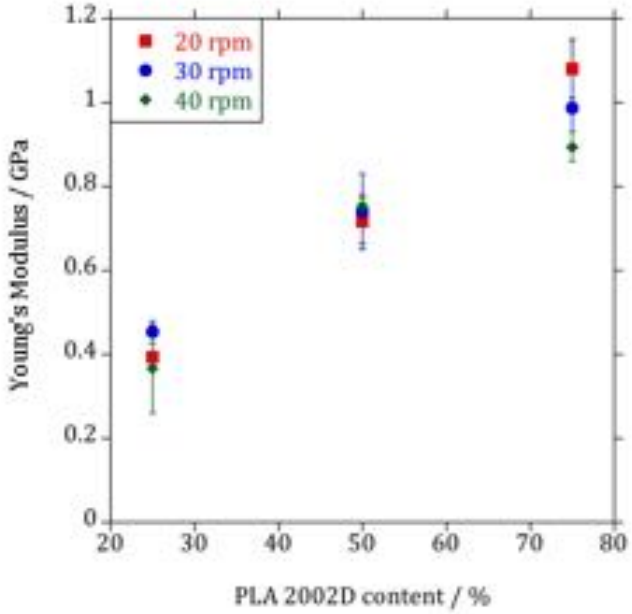

Figure 3.25. A comparison of the Young's modulus for PLA 2002D / PCL blends with varying rpm. The standard uncertainty is denoted by error bars, averaged over multiple experiments.

Figure 3.26 to Figure 3.28 display the mechanical properties of the PLA4060D/PCL melt blends. There was little influence of rpm on mechanical properties of both 25/75 and 50/50 blend compositions. This corresponds to the trends previously discussed in the PLA2002D/PCL blends (such as improvements in elongation with greater PCL content, and a deterioration in yield stress and Young's modulus). However, the 75/25 blends (noted previously) also demonstrate an influence of the screw speed on the mechanical behaviour. In particular, it is evident that blends produced at 40 rpm consistently exhibited inferior properties at this composition.

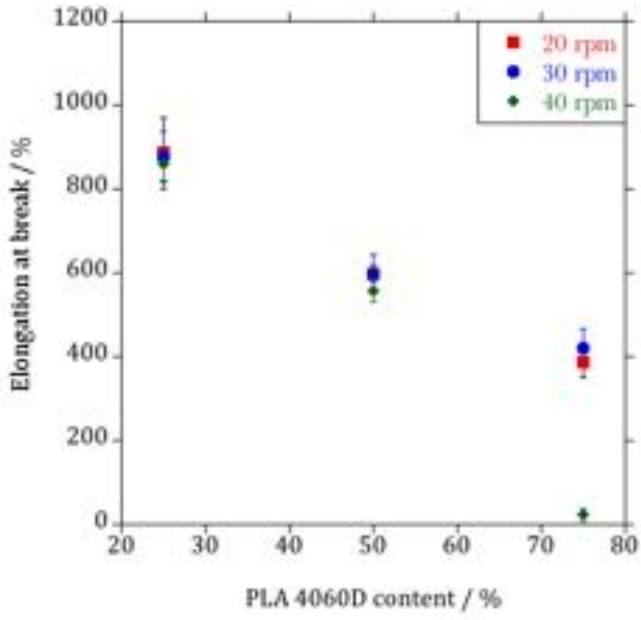

Figure 3.26. A comparison of elongation at break for PLA 4060D / PCL blends with varying rpm. The standard uncertainty is denoted by error bars, averaged over multiple experiments.

There were no significant differences between 20 and 30 rpm over the mechanical properties for both blend systems. Therefore, it was concluded that blends produced in

the presence of carbon dioxide would be limited to 20 and 30 rpm. Further analysis and discussions on the mechanical properties of these blends will be presented in Chapter 4.

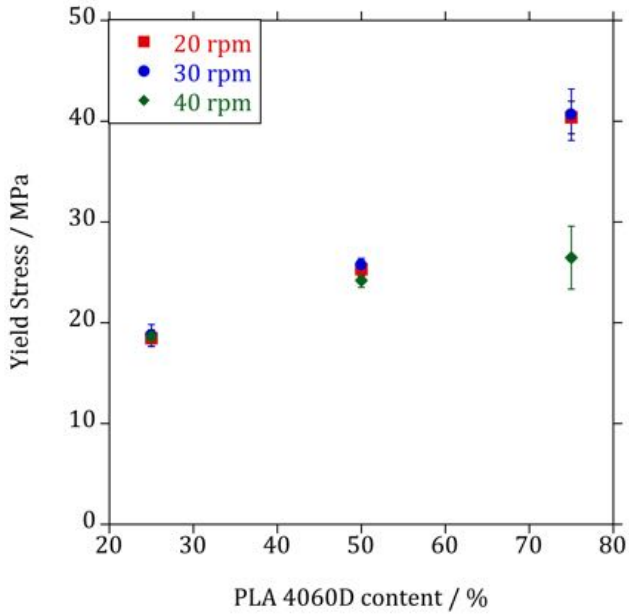

Figure 3.27. A comparison of yield stress for PLA 4060D / PCL blends with varying rpm. The standard uncertainty is denoted by error bars, averaged over multiple experiments.

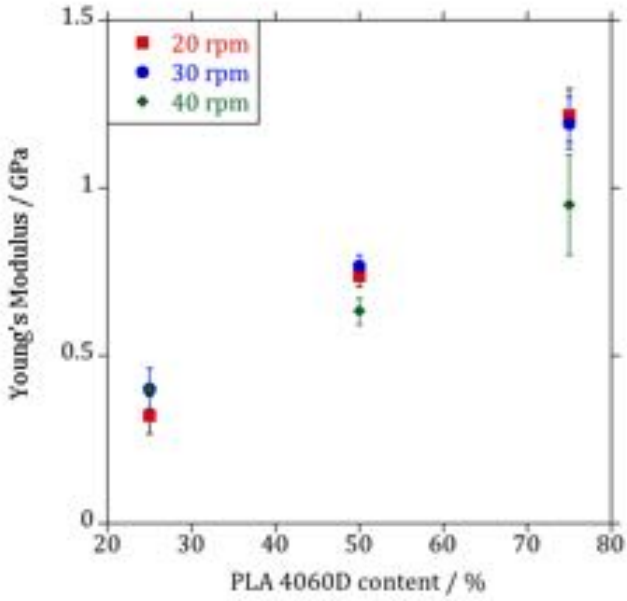

Figure 3.28. A comparison of the Young's modulus for PLA 4060D / PCL blends with varying rpm. The standard uncertainty is denoted by error bars, averaged over multiple experiments.

3.2.4 Fourier Transform Infrared (FTIR) Spectroscopy

Fourier Transform Infrared (FTIR) Spectroscopy is a useful technique to study the specific interactions in polymer blends. As mentioned previously in Chapter 2, the FTIR spectra of the blends were recorded, with particular interest in the carbonyl band. Spectral shifts and changes in this region were expected to occur with any corresponding interaction in the blend.

Figure 3.29 and Figure 3.30 show the carbonyl absorption band of solvent cast PLA2002D/PCL and 4060D/PCL blends respectively. The carbonyl band for solvent cast PCL absorbs with a peak maximum at 1721 cm^{-1}, PLA 2002D at 1748 cm^{-1} and PLA 4060D at 1747 cm^{-1}. The blends unfortunately show no compositional changes, assumed to be attributed to the gross phase separation and solubility differences between the constituent homopolymers and solvent, resulting in a phase layered composition (Figure 3.31).

ATR-FTIR is a surface characterisation technique, relying upon the depth of penetration of the IR beam into a sample. The penetration depth is dependent upon the refractive indices of the ATR crystal and sample, in addition to the wavelength of the incident beam (photons with higher wavenumber penetrate the sample less than photons with lower wavenumber). Depending on these experimental conditions, depth of penetration can range between 0.5 to 5 microns [37]. For a diamond ATR the penetration depth at 1000 cm^{-1} is typically 1 to 2 microns [38]. Therefore, the ATR-FTIR spectra obtained were representative of the surface composition and not the bulk. Ideally for these samples a FTIR experiment in transmission should be considered, however the solvent

cast blends produced were far in excess of the thickness needed to perform this experiment.

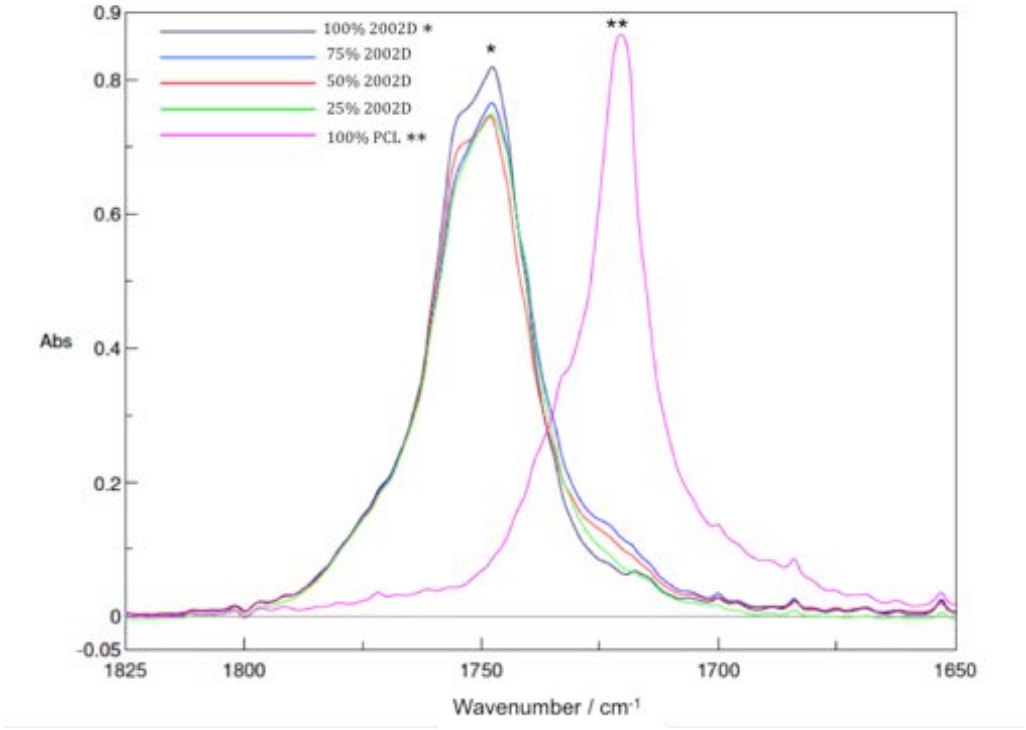

Figure 3.29. FTIR spectra of the PLA 2002D / PCL solvent cast blends carbonyl peak.

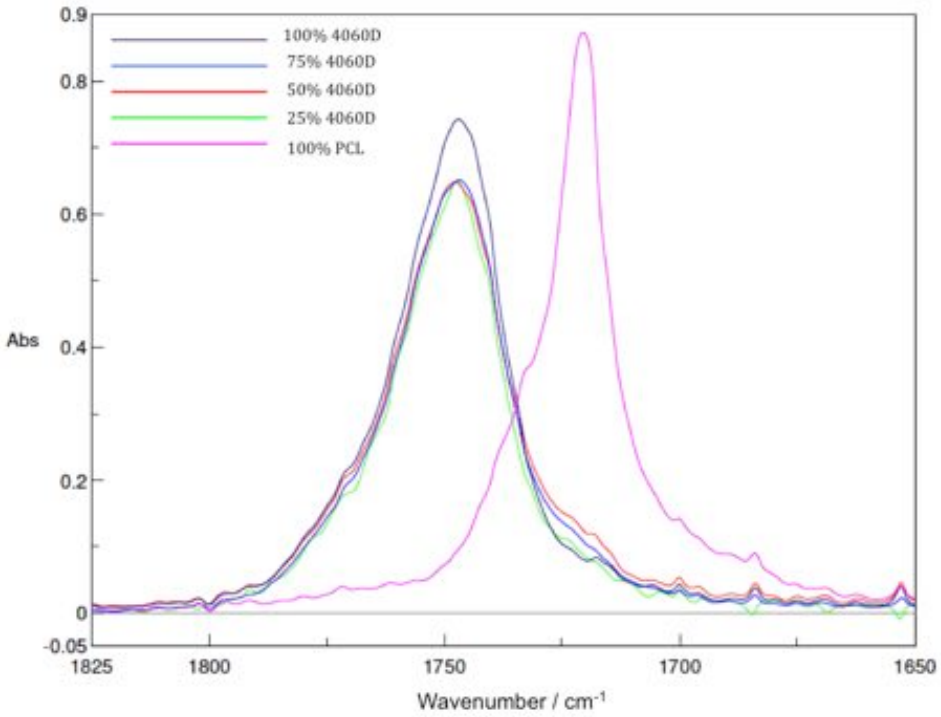

Figure 3.30. FTIR spectra of the PLA 4060D / PCL solvent cast blends carbonyl peak.

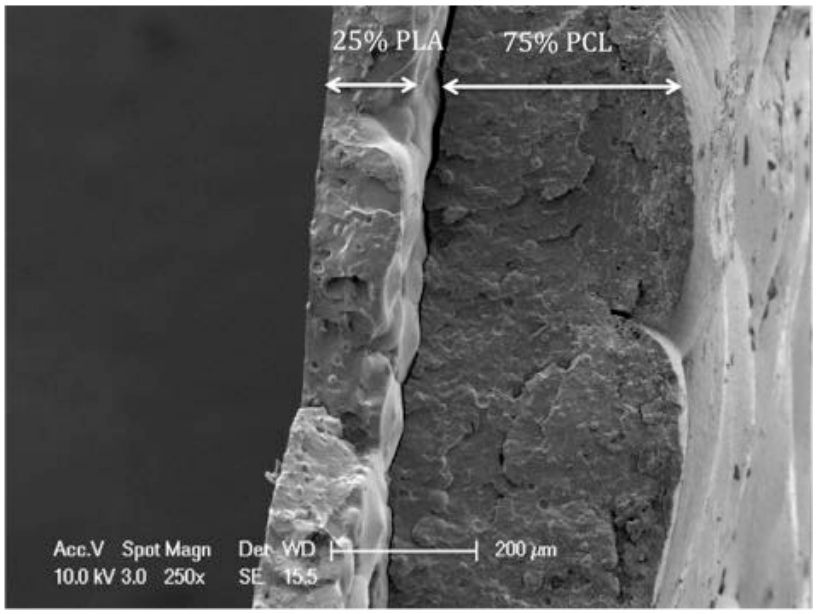

Figure 3.31. SEM image of solvent cast 25/75 PLA2002D/PCL illustrating gross phase separation.

Figure 3.32 and Figure 3.33 show the FTIR absorption band of carbonyl groups in the melt blended PLA2002D/PCL and PLA4060D/PCL blends at 30 rpm, respectively. In general the results showed no variation in peak position with screw speed. Therefore, the 30 rpm sample is presented as a representative example of the melt blends. These blends exhibit absorbances of the carbonyl band (absent in the solvent cast spectra) which depend on composition. Pure PCL is represented by the spectrum (**), exhibits a C=O peak at 1721 cm^{-1} and PLA 2002D (*) at 1747 cm^{-1}. The 75/25 PLA2002D/PCL blend exhibits both the homopolymers bands, with a greater absorbance in the major component. This behaviour is also apparent in the other blend compositions, 50/50 displaying two peaks of equal height and 25/75 displaying a smaller and larger peak corresponding to the lesser and greater component. Analysis of carbonyl peak position indicates that as the content of both PLA and PCL decreases, their peak position is correspondingly shifted to a higher wavenumber (Table 3.5). This trend is also exhibited by the PLA4060D/PCL blend (Table 3.6), however the shifts are less significant than those displayed by the PLA2002D system. Both grades of blended PLA demonstrate a greater change from their 100% values compared to PCL. According to the literature, carbonyl band shifts to higher wavenumbers are associated with hydrogen bonding within blends [39, 40].

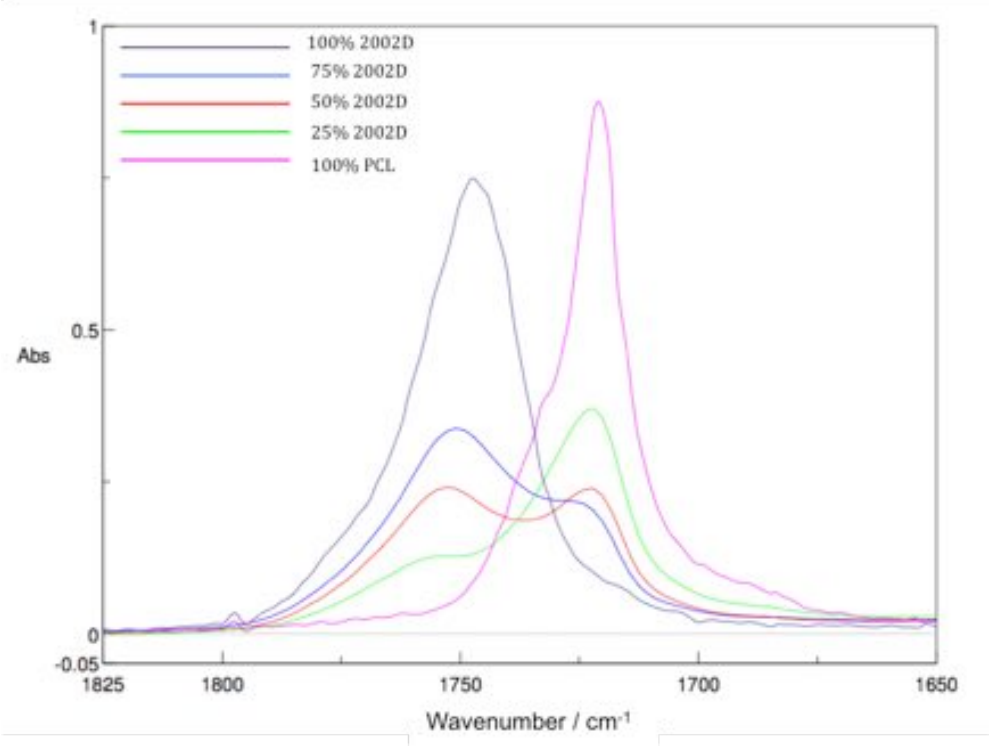

Figure 3.32. FTIR spectra of the melt blended PLA 2002D / PCL carbonyl band in the 30 rpm blends.

PLA/PCL	PLA 2002D / cm $^{-1}$	PCL / cm $^{-1}$
0/100	-	1721
25/75	1755	1722
50/50	1753	1722
75/25	1751	1726
100/0	1747	-

Table 3.5. The variance of PLA 2002D and PCL maximum peak position of the carbonyl band with composition.

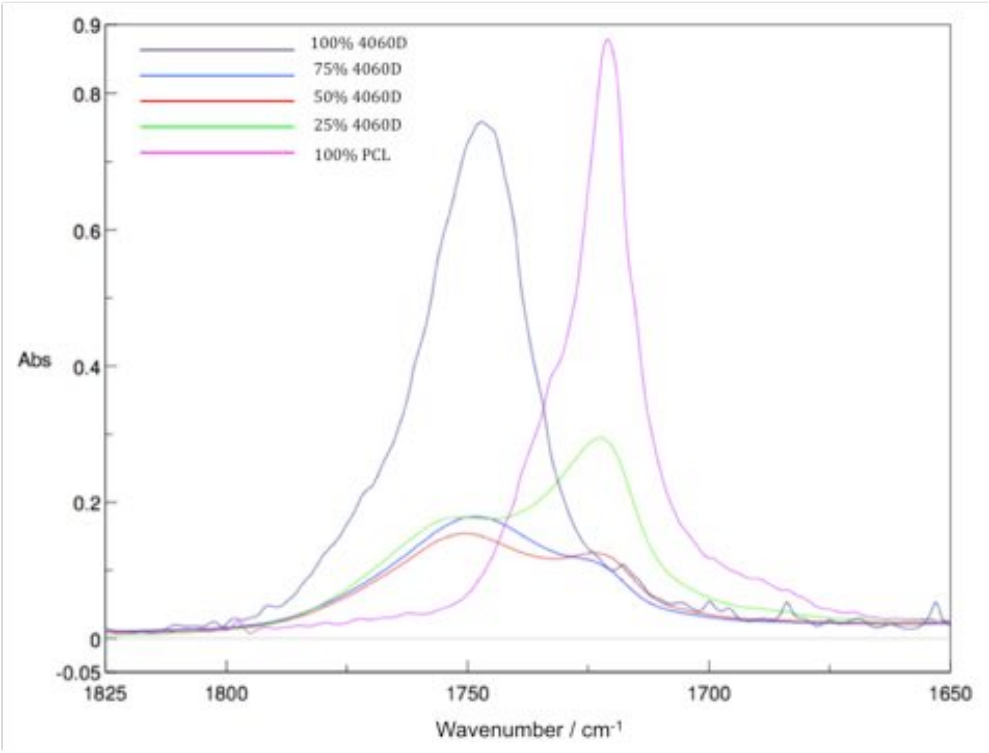

Figure 3.33. FTIR spectra of the melt blended PLA 4060D/ PCL carbonyl band in the 30 rpm blends.

PLA/PCL	PLA 4060D / cm $^{-1}$	PCL / cm $^{-1}$
0/100	-	1721
25/75	1753	1722
50/50	1751	1722
75/25	1749	1724
100/0	1747	-

Table 3.6. The variance of PLA 4060D and PCL maximum peak position of the carbonyl with composition.

3.2.5 Rheology

The effect of shear on a polymer involves the breaking down of molecular interactions arising from chain entanglement. Chain entanglement is a function of both size and number of molecules, therefore viscosity is influenced by the molecular weight and molecular weight distribution of polymeric materials [41]. The shear thinning behaviour of molten polymers is of great importance in plastic processing operations such as extrusion. The melt rheology of PLA is distinct from other commercial plastics due to it possessing a low thermal stability [42]. Therefore rheological measurements on PLA are particularly beneficial when determining the effectiveness of drying procedures (a preventative measure for hydrolytic degradation) and chemical stabilisation (preventing thermal degradation) [43]. It has been previously reported that both PLA and PCL behave as a non-Newtonian fluids and undergo shear thinning [44].

When considering polymer blends, rheological behaviours are strongly influenced by their structures and interfacial characteristics. The studies of melt rheological properties are also helpful to find out the structure–property relationship in blends. It is frequently discussed in the literature that an important parameter influencing polymer blending is their viscosity ratio:

$$\lambda = \frac{\eta_{disperse}}{\eta_{matrix}} \qquad \text{Equation 3.10}$$

It is believed that the differences in viscosities between the two polymers can influence the blend compositional morphology. As mentioned previously, the viscosity ratio should be as small as possible with the major phase possessing the highest viscosity

[16]. Figure 3.34 exhibits the Newtonian region of the homopolymers at 160 ˚C (processing temperature of the extruder). At this temperature PCL possesses the highest viscosity, followed by PLA 4060D and 2002D. This would suggest the 25/75 PLA/PCL blends would exhibit superior morphology.

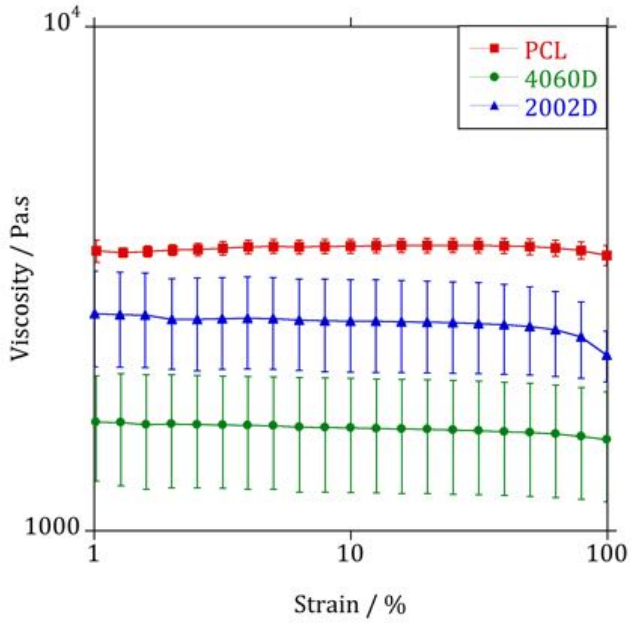

Figure 3.34. The viscosity (Newtonian region) of the hotpressed homopolymers at 160 ˚C.

At a strain of 1% the average viscosity ratio for both blend systems is tabulated below:

PLA/PCL	PLA 2002D / PCL	PLA 4060D / PCL
25/75	0.75	0.46
75/25	1.33	2.19

Table 3.7. The viscosity ratio (at 1% strain) for compositions 25/75 and 75/25 PLA 2002D/PCL and PLA 4060D/PCL at 160 ˚C.

The viscosity ratio values in Table 3.7 confirm that the 25/75 PLA/PCL blends have the smaller viscosity ratios. The 75/25 PLA/PCL ratio is significantly greater in the 4060D blend system in comparison to 2002D. However, the 75/25 2002DPLA/PCL blend has only a slightly larger ratio than the 25/75 blend. It is evident that these results do not correspond with the calculations of the weight average droplet diameter for the melt blended samples, which indicated a better morphology for the 75/25 PLA/PCL blends. Viscosity measurements were performed using a rotational rheometer using parallel plates, however the use of a capillary rheometer may have provided more of an accurate representation of the extrusion process. Therefore, there may be some discrepancies between isolated viscosity measurements and extruded sample morphology. Additionally, the viscosity ratio is only one out of many contributing factors that influence the final blend morphology.

The dependence of steady shear viscosity on shear rate for alternative grades of PLA and PCL homopolymers and their blends has been previously reported [33]. In this study, the authors presented rheology data that indicated higher viscosity of PCL than PLA at 200 ˚C. However, they noted that the addition of PCL was found to increase the processability of PLA in extrusion. The shear stress of the blends increased with increase in PCL content, indicating a higher elasticity.

3.2.6 Differential Scanning Calorimetry (DSC)

DSC is commonly used to determine miscibility within a polymer blend. If a blend is deemed to be miscible, only a single T_g is exhibited in the DSC trace. Partial miscibility is present in the blend when the both glass transition of separated phases are compositionally dependent and lie between the glass transitions of the two components. The Fox equation (Equation 3.11) can be used to predict the glass transition temperature for a miscible polymer blend for a given composition;

$$\frac{1}{T_{gblend}} = \frac{w_1}{T_{g1}} + \frac{w_2}{T_{g2}} \qquad \text{Equation 3.11}$$

where w and T_g represent the weight fractions and glass transition temperatures of each blend component respectively. The component with the lower T_g is donated as T_{g1} and the higher T_g as T_{g2} [45]. The calculated T_gs for blends of PLA 2002D and PLA 4060D with PCL can be seen in Table 3.8.

Composition PLA/PCL	PLA 2002D/PCL blend ˚C	PLA 4060D/PCL blend ˚C
100/0	55	52
75/25	15.07	13.33
50/50	-16.20	-17.12
25/75	-41.34	-41.72
0/100	-62	-62

Table 3.8. The glass transition temperatures of PLA2002D/PCL and PLA4060D/PCL blends calculated by the Fox equation.

It is frequently reported in the literature that there are difficulties when using DSC to detect shifts in T_g of these blends. This issue is attributed to overlapping thermal transitions between the T_g of PLA and the T_m of PCL, both occurring in similar temperature regions [46-49]. Attempts to observe the glass transition temperature for PCL was undertaken using a DSC connected to an intracooler (-100 ˚C), however in the majority of blends (particularly for low PCL compositions), the T_g transition was too small to detect. Therefore, the melting peaks of both PCL and when possible PLA, were analysed to detect any physical depression corresponding with partial miscibility or adhesion. Examples of DSC traces for the solvent cast blends can be seen in Figure 3.35 and Figure 3.36.

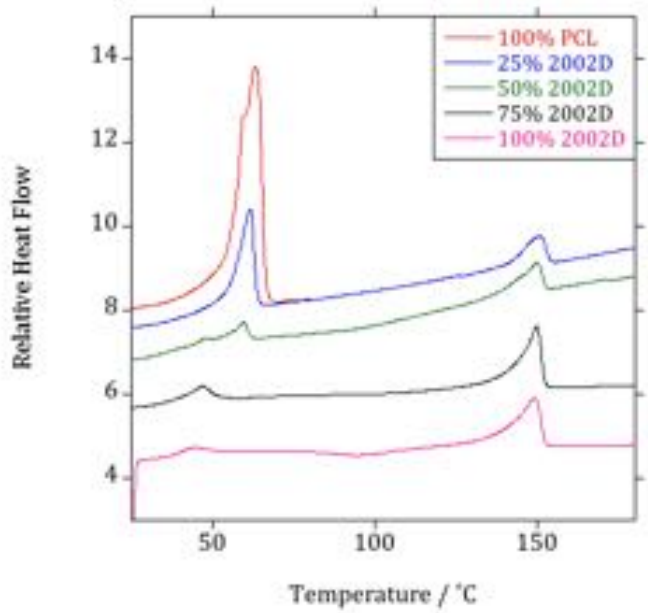

Figure 3.35. DSC traces of solvent cast PLA2002D/PCL blends and homopolymers.

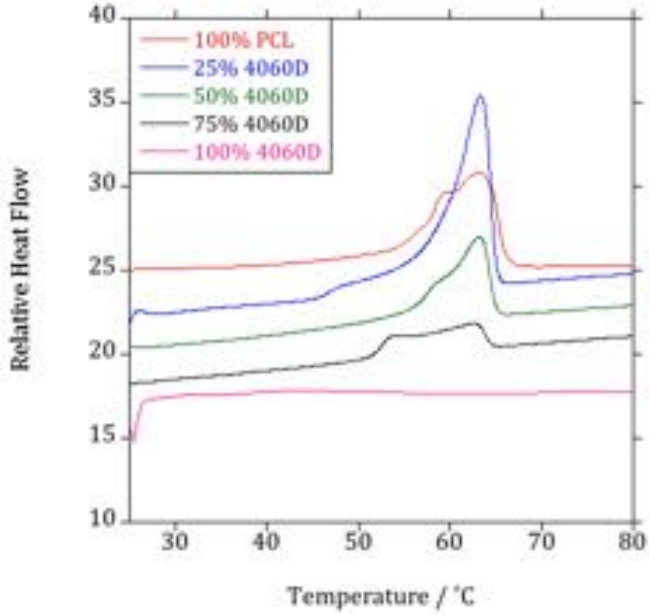

Figure 3.36. DSC traces of solvent cast PLA4060D/PCL blends and homopolymers.

Given the evidence of gross phase separation for the solvent cast blends as seen by SEM and large variance in the results obtained from mechanical testing and FTIR spectroscopic analysis, the DSC results were considered not to be representative and therefore will not be considered in any detail. However, it should be noted that on solvent casting, the constituent homopolymers were crystalline, approximately 67% and 30% for PCL and PLA 2002D respectively. These values are greater than those obtained for the extruded samples, e.g. PCL and PLA 2002D extruded at 30 rpm were 45% and 1.4% crystalline, respectively. For blends exhibiting a cold crystallisation peak for the PLA component, the % crystallisation of PLA was calculated from the equation:

$$\chi_c = \frac{\Delta H_m - \Delta H_c}{w\Delta H^0{}_m} \times 100 \qquad \text{Equation 3.12}$$

where ΔH_m and ΔH_c are the experimental melting and cold crystallisation enthalpy, respectively. w represents the weight fraction of PLA in the blend and $\Delta H^0{}_m$ is the reported 100% crystalline value of 93 J g^{-1} [50]. The calculated values of crystallinity correspond to normalised values, weighted to the actual content of PLA or PCL present in the blend.

Examples of homopolymer samples extruded at 30 rpm can be seen in Figure 3.37 to Figure 3.39. The introduction of 25% PCL into PLA 2002D (at 30 rpm) shows a slight increase in PLA crystallinity from 1.4% to 4%. This was also observed in previous studies [4, 6, 9, 49] where they attribute the increase in PLA crystallinity in the presence of PCL to the influence of the interface acting as a nucleating region. In contrast, PLA addition does not have a significant effect on PCL crystallinity.

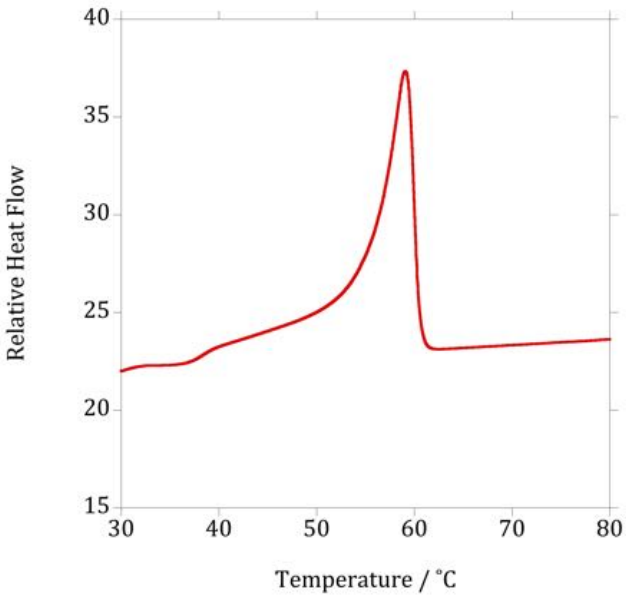

Figure 3.37. DSC trace of PCL extruded at 30 rpm.

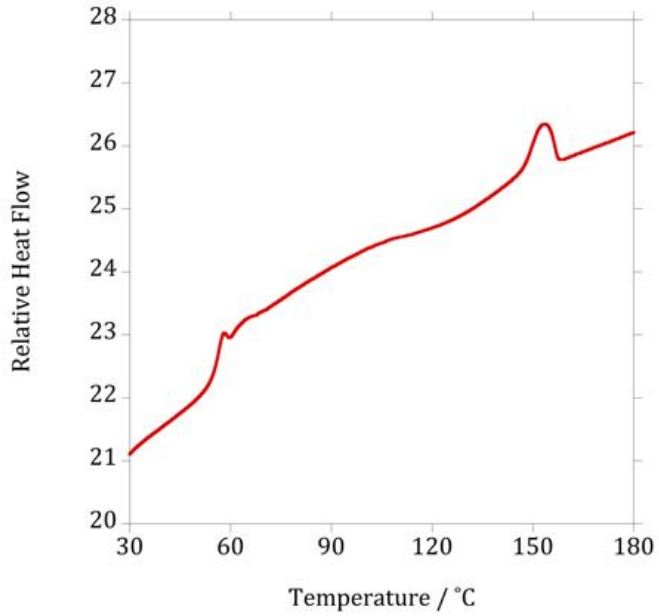

Figure 3.38. DSC trace of PLA 2002D extruded at 30 rpm.

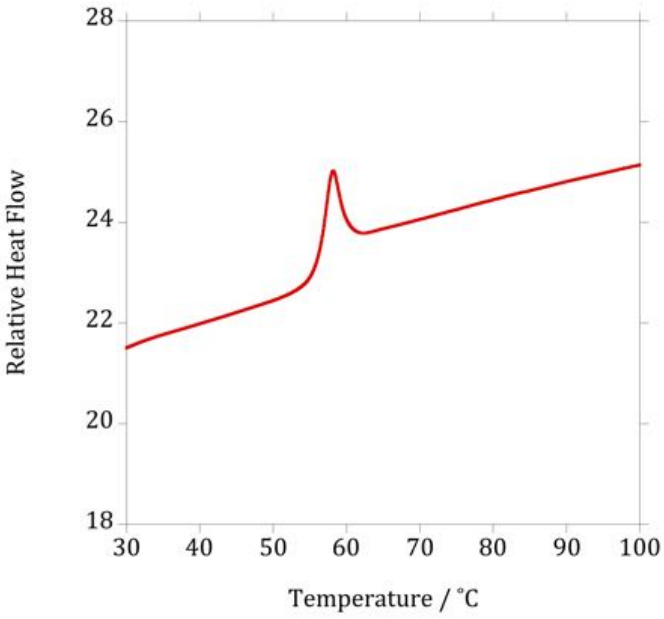

Figure 3.39. DSC trace of PLA 4060D extruded at 30 rpm.

Figure 3.40 to Figure 3.45 show the DSC analysis of the melt blends prepared with different screw speeds. Previous DSC analysis of PLA/PCL blends also exhibited cold crystallisation of the PLA component with no evidence for the cold crystallisation of PCL [9]. They showed that the cold crystallisation of PLA alone was shifted from 115 to 100 ˚C by introducing PCL. A similar shift was observed in the present results but the shift is 125 to 110 ˚C. PCL is in the melt at the cold crystallisation temperature of PLA. The reduction of the cold crystallisation temperature in the blends compared to neat PLA indicates that the presence of PCL encourages crystallisation of PLA [4, 18]. All blends show a reduction in PCL crystallinity corresponding with a decrease in PCL content in the blend as a result of dilution [51], with the exception of Figure 3.45 (a) (PLA4060D/PCL at 20 rpm). Here, a reduction in PCL crystallinity is observed with increasing PCL content. There is fine dispersion of PLA droplets in the PLA4060D/PCL 25/75 20 rpm blend as demonstrated by SEM. Any interaction or adhesion present between the droplets and matrix may decrease the mobility of the PCL chains, thereby reducing reorganisation and crystallisation [51]. The corresponding FTIR carbonyl absorption band for the PLA component in the 20 rpm blend displays a 2 cm^{-1} greater shift to higher wavenumbers than at 30 and 40 rpm. This also indicates an increased interaction between components in this blend.

There is no significant change to PCL melting point across composition, a slight increase is observed in a number of instances for the 50/50 blends. This may indicate a reduction in adhesion between both phases for this composition which corresponds to the poor morphology observed in these blends by SEM.

The variations in crystallinity and melting point of PLA are typically less significant than those observed for PCL. In general, there are no significant changes in the blends observed by DSC, also presented in previous studies [7]. This confirms the presence of immiscibility.

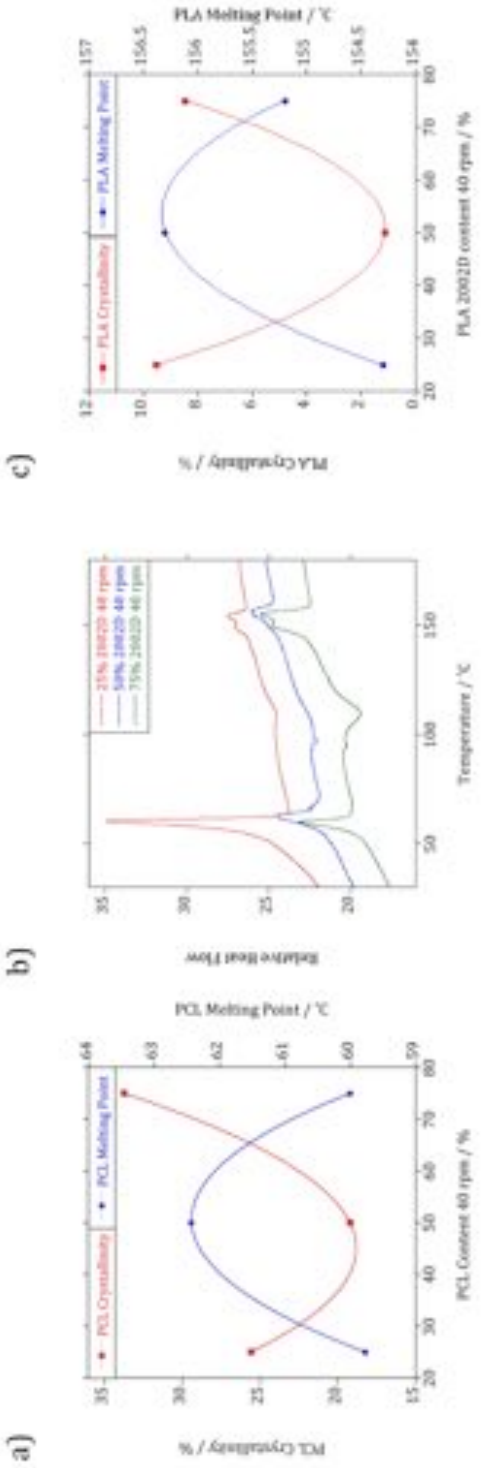

Figure 4.30. DSC analysis of PLA2002D/PCL melt blends at 40 rpm.

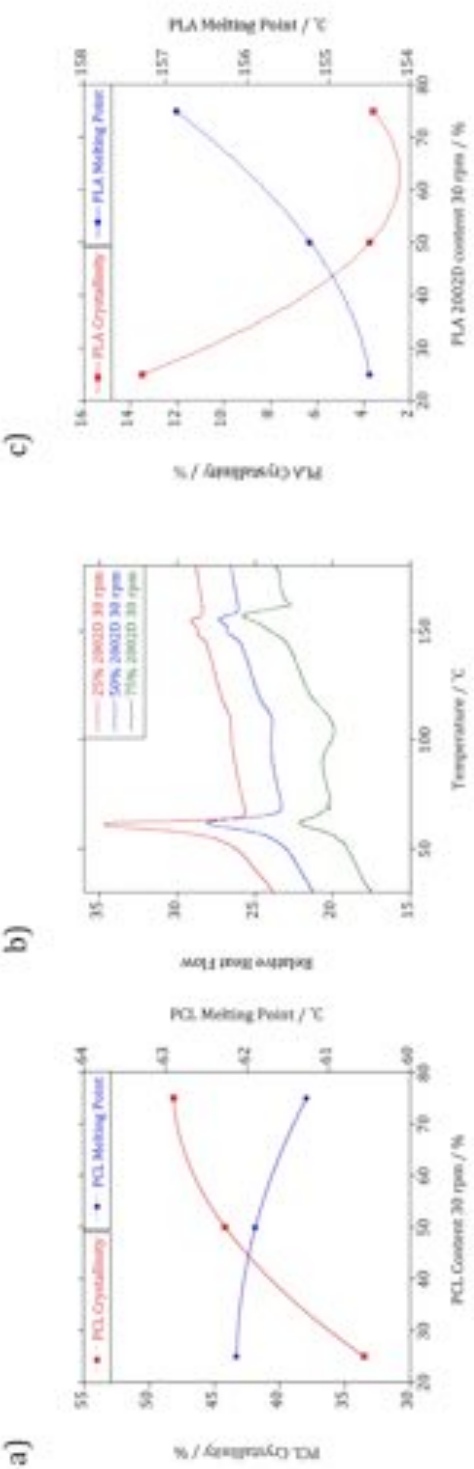

Figure 4.31. DSC analysis of PLA2002D/PCL melt blends at 30 rpm.

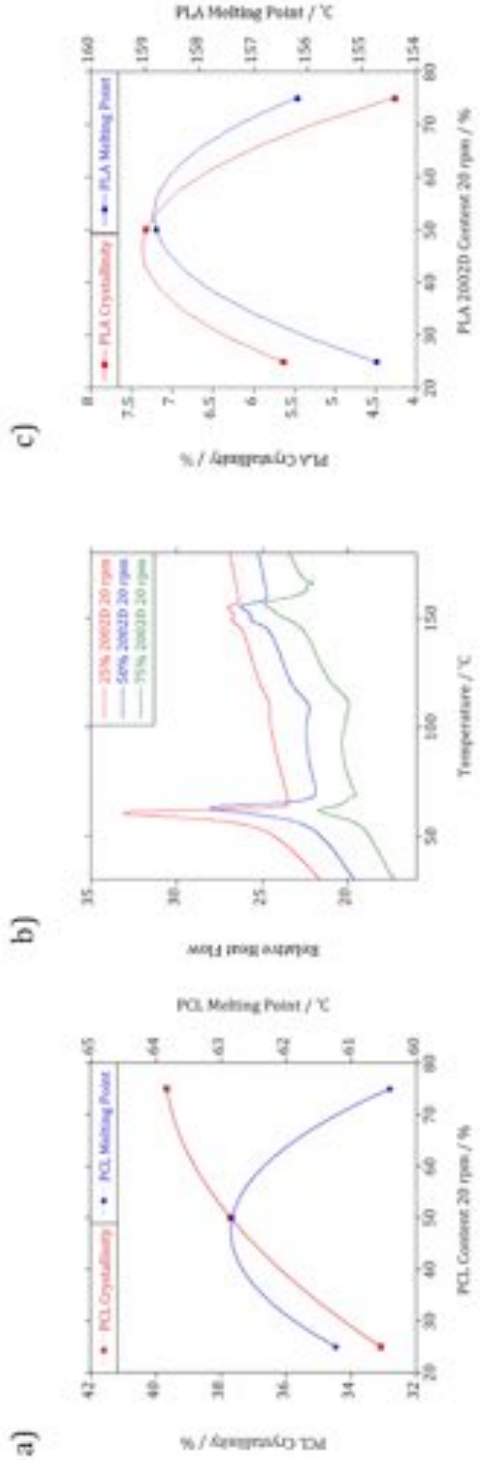

Figure 3.42. DSC analysis of PLA2002D/PCL melt blends at 20 rpm.

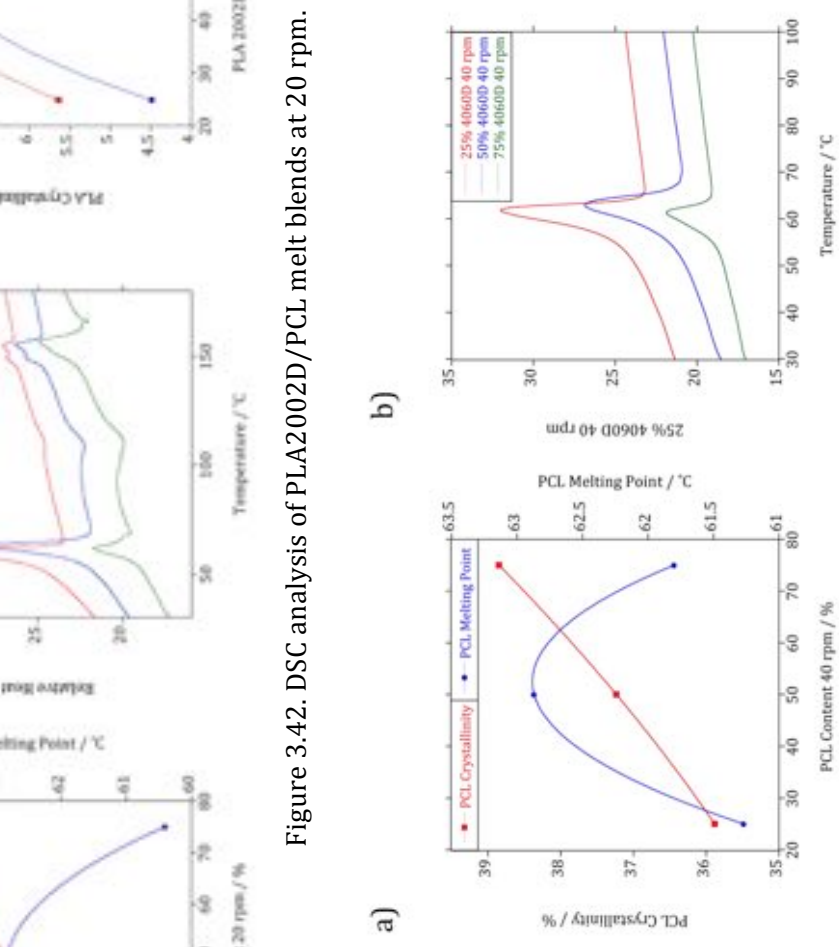

Figure 3.43. DSC analysis of PLA4060D/PCL melt blends at 40 rpm.

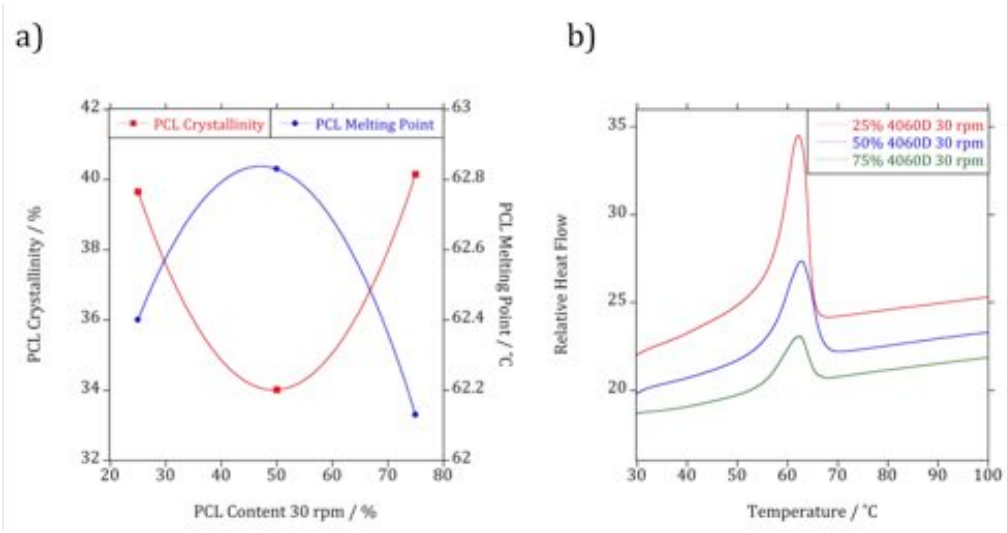

Figure 3.44. DSC analysis of PLA4060D/PCL melt blends at 30 rpm.

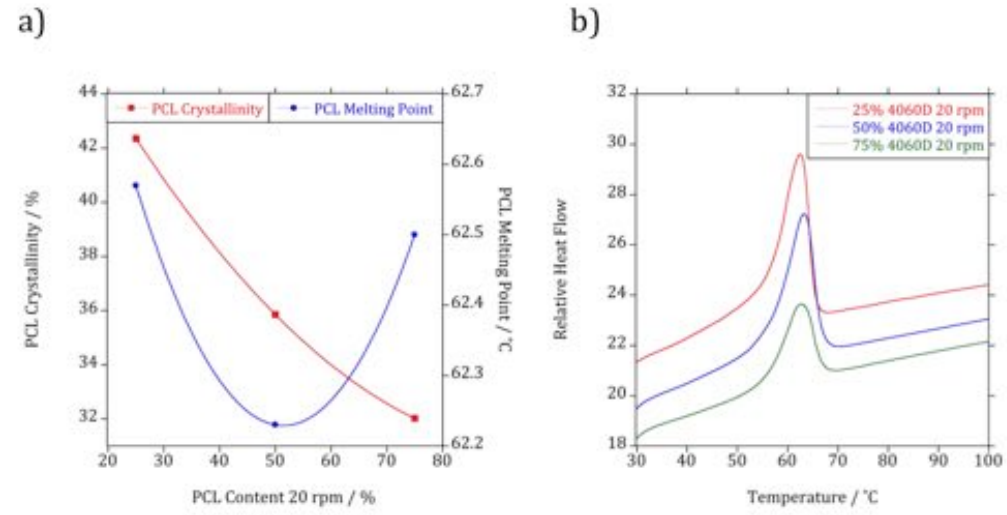

Figure 3.45. DSC analysis of PLA4060D/PCL melt blends at 20 rpm.

3.3 Conclusions

Blends produced by solution casting and melt blending were immiscible under all processing conditions and compositions. SEM analysis indicated that an improved microstructure (smaller and more finely dispersed) was obtained with the 75/25 PLA/PCL melt blends, with the favoured processing conditions dictated by mechanical testing, at 20 and 30 rpm for this composition. Analysis by FTIR spectroscopy confirmed gross phase separation in the solvent cast blends through lack of any compositional dependencies. The samples produced through melt blending however, exhibited clear changes in carbonyl band absorbance with composition. Additionally, the carbonyl bands assigned to both PLA and PCL were seen to shift to higher wavenumbers corresponding to decreasing content of each component. Shifting of the carbonyl peak is associated with an interaction between the polymers.

Rheological analysis of the homopolymers illustrated a higher viscosity for PCL than PLA, signifying mixing will be preferred in the 25/75 PLA/PCL blends (where the matrix possesses the higher viscosity). The average viscosity ratios calculated at 1% strain confirmed the lowest ratios were for the 25/75 PLA/PCL blend for both systems. These results contradict the weight average droplet diameter calculations from SEM images, indicating discrepancies between processing and isolated viscosity measurements. However, 75/25 PLA2002D/PCL also exhibited a relatively low viscosity ratio.

DSC analysis confirmed immiscibility and showed an increase in PLA 2002D crystallinity by introducing PCL, indicating PCL is behaving as a nucleating agent. It was determined that blending investigations with carbon dioxide would proceed without the inclusion of 40 rpm as a result of the comparatively inferior mechanical properties.

3.4 References

[1] NatureWorksLLC. *Crystallizing and Drying Ingeo Biopolymer*. Available: http://www.natureworksllc.com/~/media/Technical_Resources/Processing_Guides/ProcessingGuide_Crystallizing-and-Drying_pdf.pdf

[2] NatureWorksLLC. *Ingeo Biopolymer 4060D Technical Data Sheet*. Available: http://www.natureworksllc.com/~/media/Technical_Resources/Technical_Data_Sheets/TechnicalDataSheet_4060D_films_pdf.pdf

[3] NatureWorksLLC. *NatureWorks PLA Polymer 2002D*. Available: http://www.unicgroup.com/upfiles/file01170656495.pdf

[4] N. Noroozi, L. L. Schafer, and S. G. Hatzikiriakos, "Thermorheological properties of poly (ε-caprolactone)/polylactide blends," *Polymer Engineering & Science,* vol. 52, pp. 2348-2359, 2012.

[5] M. Todo, S. D. Park, T. Takayama, and K. Arakawa, "Fracture micromechanisms of bioabsorbable PLLA/PCL polymer blends," *Engineering Fracture Mechanics,* vol. 74, pp. 1872-1883, 2007.

[6] C. L. Simões, J. C. Viana, and A. M. Cunha, "Mechanical properties of poly(ε-caprolactone) and poly(lactic acid) blends," *Journal of Applied Polymer Science,* vol. 112, pp. 345-352, 2009.

[7] H. Tsuji and Y. Ikada, "Blends of aliphatic polyesters. I. Physical properties and morphologies of solution-cast blends from poly(DL-lactide) and poly(ε-caprolactone)," *Journal of Applied Polymer Science,* vol. 60, pp. 2367-2375, 1996.

[8] J. C. Meredith and E. J. Amis, "LCST phase separation in biodegradable polymer blends: poly(D,L-lactide) and poly(ϵ-caprolactone)," *Macromolecular Chemistry and Physics,* vol. 201, pp. 733-739, 2000.

[9] R. Dell'Erba, G. Groeninckx, G. Maglio, M. Malinconico, and A. Migliozzi, "Immiscible polymer blends of semicrystalline biocompatible components: thermal properties and phase morphology analysis of PLLA/PCL blends," *Polymer,* vol. 42, pp. 7831-7840, 8// 2001.

[10] G. Taylor, "The formation of emulsions in definable fields of flow," *Proceedings of the Royal Society of London. Series A,* vol. 146, pp. 501-523, 1934.

[11] G. I. Taylor, "The Viscosity of a Fluid Containing Small Drops of Another Fluid," *Proceedings of the Royal Society of London. Series A,* vol. 138, pp. 41-48, October 1, 1932 1932.

[12] J. Lyngaae-Jørgensen, "Polymer Blends and Alloys," in *Rheology of Polymer Blends*, M. J. Folkes and P. S. Hope, Eds., ed London: Chapman & Hall, 1993.

[13] U. Sundararaj and C. Macosko, "Drop breakup and coalescence in polymer blends: the effects of concentration and compatibilization," *Macromolecules,* vol. 28, pp. 2647-2657, 1995.

[14] G. Groeninckx, C. Harrats, and S. Thomas, "Reactive Blending with Immiscible Functional Polymers: Molecular, Morphological, and Interfacial Aspects," in *Reactive Polymer Blending*, W. E. Baker, C. E. Scott, and G.-H. Hu, Eds., ed USA: Hanser, 1991.

[15] S. Wu, "Formation of dispersed phase in incompatible polymer blends: Interfacial and rheological effects," *Polymer Engineering & Science,* vol. 27, pp. 335-343, 1987.
[16] L. P. B. M. Janssen and S. Nalawade, P., "Polymer Extrusion with Supercritical Carbon Dioxide," in *Supercritical Carbon Dioxide: in Polymer Reaction Engineering*, M. F. Kemmere and T. Meyer, Eds., ed Germany: WILEY-VCH, 2005.
[17] E. Schwach and L. Avérous, "Starch-based biodegradable blends: morphology and interface properties," *Polymer International,* vol. 53, pp. 2115-2124, 2004.
[18] D. Wu, D. Lin, J. Zhang, W. Zhou, M. Zhang, Y. Zhang*, et al.*, "Selective Localization of Nanofillers: Effect on Morphology and Crystallization of PLA/PCL Blends," *Macromolecular Chemistry and Physics,* vol. 212, pp. 613-626, 2011.
[19] S. Wu, "Calculation of interfacial tension in polymer systems," *Journal of Polymer Science Part C: Polymer Symposia,* vol. 34, pp. 19-30, 1971.
[20] E.K. Kim and J. L. White, "Manufacturing of Polymer Blends Using Polymeric and Low Molecular Weight Reactive Compatibilizers," in *Encyclopedia of Polymer Blends*. vol. 2: processing, A. I. Isayev, Ed., ed Germany: Wiley-VCH, 2011.
[21] L. A. Utracki, *Polymer Alloys and Blends Thermodynamics and Rheology*. New York: Hanser Publishers, 1989.
[22] E. Y. Arashiro and N. R. Demarquette, "Influence of temperature, molecular weight, and polydispersity of polystyrene on interfacial tension between low-density polyethylene and polystyrene," *Journal of Applied Polymer Science,* vol. 74, pp. 2423-2431, 1999.
[23] A. Xue, C. Tzoganakis, and P. Chen, "Measurement of interfacial tension in PS/LDPE melts saturated with supercritical CO2," *Polymer Engineering & Science,* vol. 44, pp. 18-27, 2004.
[24] P. C. Ellingson, D. A. Strand, A. Cohen, R. L. Sammler, and C. J. Carriere, "Molecular Weight Dependence of Polystyrene/Poly(methyl methacrylate) Interfacial Tension Probed by Imbedded-Fiber Retraction," *Macromolecules,* vol. 27, pp. 1643-1647, 1994/03/01 1994.
[25] T. Semba, K. Kitagawa, U. S. Ishiaku, and H. Hamada, "The effect of crosslinking on the mechanical properties of polylactic acid/polycaprolactone blends," *Journal of Applied Polymer Science,* vol. 101, pp. 1816-1825, 2006.
[26] M. R. Kamal, R. Lai-Fook, and N. R. Demarquette, "Interfacial tension in polymer melts. Part II: Effects of temperature and molecular weight on interfacial tension," *Polymer Engineering & Science,* vol. 34, pp. 1834-1839, 1994.
[27] A. Luciani, M. F. Champagne, and L. A. Utracki, "Interfacial tension in polymer blends," *Macromolecular Symposia,* vol. 126, pp. 307-321, 1998.
[28] B. Siaotong, L. Tabil, S. Panigrahi, and W. Crerar, "Effect of Extrusion Parameters on the Physical Characteristics of Extruded Flax Fiber-Reinforced Polyethylene Composites," 2005.
[29] D. H. Morton-Jones, *Polymer Processing*. London: Chapman & Hall, 1989.
[30] C. Rauwendaal, *Polymer Extrusion*, Third ed. New York: Hanser 1994.
[31] H. Liu, W. Song, F. Chen, L. Guo, and J. Zhang, "Interaction of Microstructure and Interfacial Adhesion on Impact Performance of Polylactide (PLA) Ternary Blends," *Macromolecules,* vol. 44, pp. 1513-1522, 2011/03/22 2011.

[32] D. Wu, Y. Zhang, L. Yuan, M. Zhang, and W. Zhou, "Viscoelastic interfacial properties of compatibilized poly(ε-caprolactone)/polylactide blend," *Journal of Polymer Science Part B: Polymer Physics,* vol. 48, pp. 756-765, 2010.

[33] R. U. Rao, K. N. S. Suman, V. V. S. Rao, and K. Bhanukiran, "Study of Rheological and Mechanical Properties of Biodegradable Polylactide and Polycaprolactone Blends," *International Journal of Engineering Science and Technology,* vol. 3, pp. 6259-6265, 2011.

[34] J. A. Brydson, *Flow Properties of Polymer Melts*, 2nd ed. London: George Godwin Limited, 1981.

[35] F. N. Cogswell, *Polymer Melt Rheology A Guide For Industrial Practice*. London: George Godwin Limited, 1981.

[36] W. H. Hoidy, M. B. Ahmad, E. A. Jaffar Al-Mulla, and N. A. B. Ibrahim, "Preparation and Characterization of Polylactic Acid/Polycaprolactone Clay Nanocomposites. ," *Journal of Applied Sciences,* vol. 10, pp. 97-106, 2010.

[37] P. technologies. (2011). Available: http://www.piketech.com/files/pdfs/ATRAN611.pdf

[38] PerkinElmer. Available: http://www.perkinelmer.co.uk/CMSResources/Images/44-135840TCH_010127_01_ATR.pdf

[39] P. W. Labuschagne, S. G. Kazarian, and R. E. Sadiku, "In situ FTIR spectroscopic study of the effect of CO2 sorption on H-bonding in PEG–PVP mixtures," *Spectrochimica Acta Part A: Molecular and Biomolecular Spectroscopy,* vol. 78, pp. 1500-1506, 5// 2011.

[40] E. Yilgör, E. Yurtsever, and I. Yilgör, "Hydrogen bonding and polyurethane morphology. II. Spectroscopic, thermal and crystallization behavior of polyether blends with 1,3-dimethylurea and a model urethane compound," *Polymer,* vol. 43, pp. 6561-6568, 11// 2002.

[41] C. D. Han, *Rheology in Polymer Processing*. London: Academic Press, 1976.

[42] P. Sarazin, G. Li, W. J. Orts, and B. D. Favis, "Binary and ternary blends of polylactide, polycaprolactone and thermoplastic starch," *Polymer,* vol. 49, pp. 599-609, 2008.

[43] R. Auras, L.-T. Lim, S. E. M. Selke, and H. Tsuji, *Poly(lactic acid) Synthesis, Structures, Properties, Processing, and Applications*. New Jersey: Wiley, 2010.

[44] D. H. S. Ramkumar and M. Bhattacharya, "Steady shear and dynamic properties of biodegradable polyesters," *Polymer Engineering & Science,* vol. 38, pp. 1426-1435, 1998.

[45] H. A. Schneider, "Glass Transition in Polymer Blends," in *Handbook of Polymer Blends and Composites*. vol. 3B, C. Vasile and A. K. Kulshereshtha, Eds., ed Shropshire: Rapra Technology Limited, 2003.

[46] M. E. Broz, D. L. VanderHart, and N. R. Washburn, "Structure and mechanical properties of poly(,-lactic acid)/poly([var epsilon]-caprolactone) blends," *Biomaterials,* vol. 24, pp. 4181-4190, 2003.

[47] C.-C. Chen, J.-Y. Chueh, H. Tseng, H.-M. Huang, and S.-Y. Lee, "Preparation and characterization of biodegradable PLA polymeric blends," *Biomaterials,* vol. 24, pp. 1167-1173, 2003.

[48] S. Aslan, L. Calandrelli, P. Laurienzo, M. Malinconico, and C. Migliaresi, "Poly (D,L-lactic acid)/poly (∈-caprolactone) blend membranes: preparation and

morphological characterisation," *Journal of Materials Science,* vol. 35, pp. 1615-1622, 2000.

[49] N. López-Rodríguez, A. López-Arraiza, E. Meaurio, and J. R. Sarasua, "Crystallization, morphology, and mechanical behavior of polylactide/poly(ε-caprolactone) blends," *Polymer Engineering & Science,* vol. 46, pp. 1299-1308, 2006.

[50] J. Ahmed, J.-X. Zhang, Z. Song, and S. K. Varshnet, "Thermal Properites of Polylactides: Effect of molecular mass and nature of lactide isomer," *Journal of Thermal Analysis and Calorimetry,* vol. 95, pp. 957-964, 2009.

[51] H. Tsuji, T. Yamada, M. Suzuki, and S. Itsuno, "Part 7. Effects of poly(L-lactide-co-ϵ-caprolactone) on morphology, structure, crystallization, and physical properties of blends of poly(L-lactide) and poly(ϵ-caprolactone)," *Polymer International,* vol. 52, pp. 269-275, 2003.

CHAPTER 4 – BLENDING POLY(LACTIC ACID) AND POLY(ε-CAPROLACTONE) IN THE PRESENCE OF CARBON DIOXIDE

4.1 Introduction

4.1.1 Macromolecular dynamics

Macromolecular dynamics is an area of polymer science that addresses the motion and mobility of polymer chains. Some elements of this subject have been mentioned in chapter 1 such as polymer crystallisation and the onset of molecular motion at the glass transition. Small molecules in a gas move by translation, colliding with other molecules or containing walls. In a liquid, small molecules also move by translation however, their motion is governed and confined by the molecular dimensions. These random motions are often termed Brownian motion. The motion of polymer chains can occur in two different forms; (i) the chain can alter its overall conformation (such as in relaxation after subjected to strain) or, (ii) the chain can move relative to that of neighbouring and surrounding chains [1]. Induced by thermal activation, these processes occur by Brownian motion and are deemed as types of self-diffusion. The diffusion process concerning polymer chains is largely restricted to their incapability to move sideways caused by obstructing surrounding polymer chains. Therefore, diffusion of polymer chains is only achievable by cooperative motions of these restricting neighbouring chains and is considered an extremely long process [2]. In order to provide a greater

understanding of the motion of polymer chains, numerous theories and models have been developed and some will be presented in this chapter.

4.1.1.1 The Rouse model

In 1953 Rouse [3] developed one of the first theories on the motion of polymer chains. This theory considers that a polymer chain consists of a succession of repeating units obeying the Gaussian distribution function, therefore each chain exists as a random coil [4]. These repeat units can be represented by a series of beads (N) connected by springs behaving as joints along the chain (Figure 4.1). Each bead possesses its own individual friction coefficient ζ. The total friction coefficient of the Rouse chain is the sum of the beads (N):

$$\zeta_R = N\zeta \qquad \text{Equation 4.1}$$

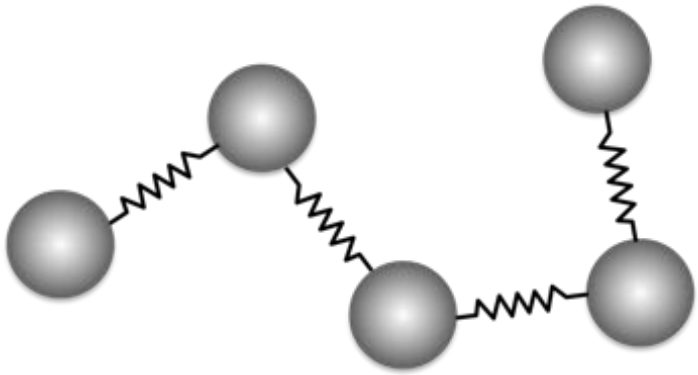

Figure 4.1. A polymer chain represented by the bead and spring model.

There are three different forces influencing the dynamics of polymer chains: (i) a frictional force, proportional to the velocity of the repeat unit in its surrounding medium, (ii) the force between adjoining repeat units along the same chain and (iii) a

random force resulting from collisions with the surrounding medium (Brownian motion). If a polymer chain is left undisturbed and is in a relaxed state, it is assumed to adopt the most favourable conformation; one possessing the lowest energy. The application of an external force to a polymer chain will result in modification of its conformation to a less favourable one. Upon removal of the external force, the polymer chain is able to return / relax to its original conformation in order to lower the energy of the system. There are a number of modes of motion whereby a polymer chain can return to its preferred conformation, each with an associated relaxation time. The first three modes of motion are illustrated in Figure 4.2. The first mode of motion $p = 1$ has the longest relaxation time involving translation of the whole polymer chain (where the maximum number of repeat units / beads are involved). Mode $p = 2$ represents the chain moving in 2 places (at the chain ends in opposite directions). Mode $p = 3$ corresponds with three points of movement (both chain ends moving in the same direction and the centre in the opposite). Modes continue to $p = 4, 5, 6$….etc. corresponding with progressively lower relaxation times [5].

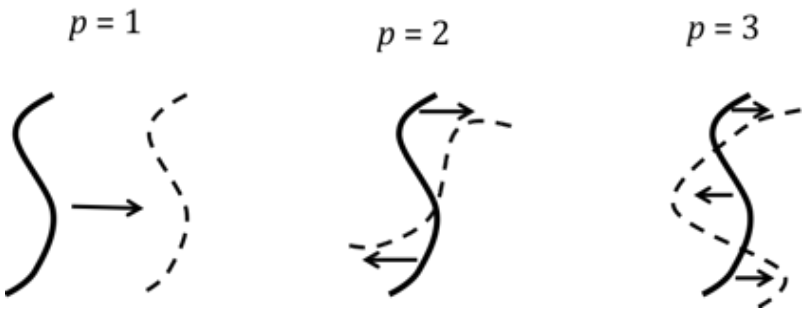

Figure 4.2. An illustration of the first three Rouse relaxation modes.

The diffusion coefficient of the Rouse chain (D_R) (Equation 4.3) is obtained using the Einstein equation (Equation 4.2) and the friction coefficient of the Rouse chain (Equation 4.1). Einstein formulated:

$$D = \frac{kT}{\zeta} \qquad \text{Equation 4.2}$$

where the diffusion of particles D (the diffusion coefficient) is inversely proportional to the friction coefficient ζ between the particle and medium, k is the Boltzmann constant and T is the temperature. This allows the calculation of D_R:

$$D_R = \frac{kT}{N\zeta} \qquad \text{Equation 4.3}$$

The polymer chain is able to diffuse a distance of an order of its radius R, during a characteristic time, Rouse time τ_R:

$$\tau_R \approx \frac{R^2}{D_R} = \frac{\zeta}{kT} NR^2 \qquad \text{Equation 4.4}$$

The size of the polymer chain can be related to the number of monomers N of length b:

$$R = bN^{\frac{1}{2}} \qquad \text{Equation 4.5}$$

By substituting Equation 4.5 into Equation 4.4 the relaxation time of an ideal chain, τ_R now becomes:

$$\tau_R = \frac{\zeta b^2}{6\pi^2 kT} N^2 \qquad \text{Equation 4.6}$$

The full calculation was published by Rouse in 1953 with a coefficient $1/(6\pi^2)$.

4.1.1.2 The reptation model

The Rouse theory was useful for establishing chain motion responsible for relaxation, creep and viscosity, however does not take into account the inability of chains to cross each other. Polymer chains will only form isolated coils in dilute solution, subsequently becoming entangled as the concentration is increased. The theory was therefore valuable for applying to dilute polymer solutions, but less successful for bulk polymer melts resulting in poor quantitative agreement with experimental measurements. However, the Rouse theory is important as it serves as a valuable precursor to the reptation theory proposed by de Gennes in 1971 [6]. In polymer networks consisting of long linear chains, each chain imposes topological constraints (entanglements) on each other because they cannot cross. In order to navigate through this network of chains it is thought that linear chains renew their configurations resulting in translational motion, by a process called reptation. The term 'reptation' is derived from the word reptile and is associated with the chains undertaking a snake-like motion [7]. Therefore de Gennes proposed a theory that accounted for these long chains to translate and diffuse through the polymer network embodied in the 'reptation model'. Here, the chain is assumed to be contained in a hypothetical tube (proposed by Edwards 1977), formed by the surrounding network of entangled polymer chains (Figure 4.3).

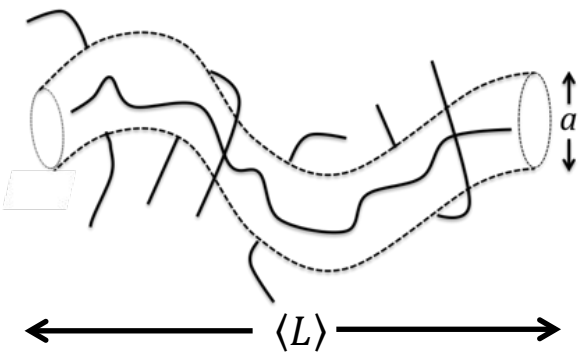

Figure 4.3. Schematic of a polymer chain confined by the hypothetical tube.

The chain within the tube can adopt different conformations without any influence from interactions with surrounding chains, any kinks/bumps move along the chain resulting in translative motion. However, the pathway is restricted by the diameter of the tube a:

$$a \approx bN_e^{\frac{1}{2}} \quad \text{Equation 4.7}$$

where N_e is the number of monomers of size b (equalling that of the tube diameter). The average tube length $\langle L \rangle$ is the product of the average number of entanglements $\frac{N}{N_e}$ of length a.

$$\langle L \rangle \approx a\frac{N}{N_e} \approx \frac{b^2N}{a} \approx \frac{bN}{N_e^{\frac{1}{2}}} \quad \text{Equation 4.8}$$

Reptation time, is the time it takes for a polymer chain to diffuse out of the tube of average length $\langle L \rangle$ and can be calculated using the Rouse diffusion coefficient, D_R mentioned previously (Equation 4.3) and the average tube length (Equation 4.8).

$$\tau_{rep} \approx \frac{\langle L \rangle^2}{D_R} \approx \frac{\zeta b^2}{kT}\frac{N^3}{N_e} = \frac{\zeta b^2}{kT} N_e{}^2 \left(\frac{N}{N_e}\right)^3 \quad \text{Equation 4.9}$$

The reptation time was predicted to be the cube of the molar mass (M), however experimental values determined:

$$\tau_{rep} = M^{3.4} \quad \text{Equation 4.10}$$

A number of physical processes unaccounted for by the reptation theory have since been proposed in order to resolve the discrepancies between the theory and experimental values [8]. The reptation model assumes that entanglements and therefore the confinements of the tube, stay fixed. However, in reality, the network of entanglements are also in motion. The constraint-release mechanism proposes that the tube comprising of the surrounding chains are able to reptate away from their entanglements, releasing themselves and any contribution to the tube [9]. This results in a removal on the constraint of the chain inside, consequently providing an extra degree of freedom. A small portion of the chain is able to bulge out and escape from gaps in the walls of the tube as illustrated in Figure 4.4. In addition, another mechanism termed 'contour-length-fluctuations' indicates that the length of the tube is fluctuating in time whilst the chain inside is reptating [10]. This process is the fluctuation-driven stretching and contractions of the chain along the tube. In other words, the chain within the tube contracts and subsequently stretches back out. During this activity, the ends of the tubes are forgotten/lost resulting in a reduction in the length of the tube. Therefore, upon fluctuating and stretching back out, the chain ends are able to relax outside of the confinements of the tube [11].

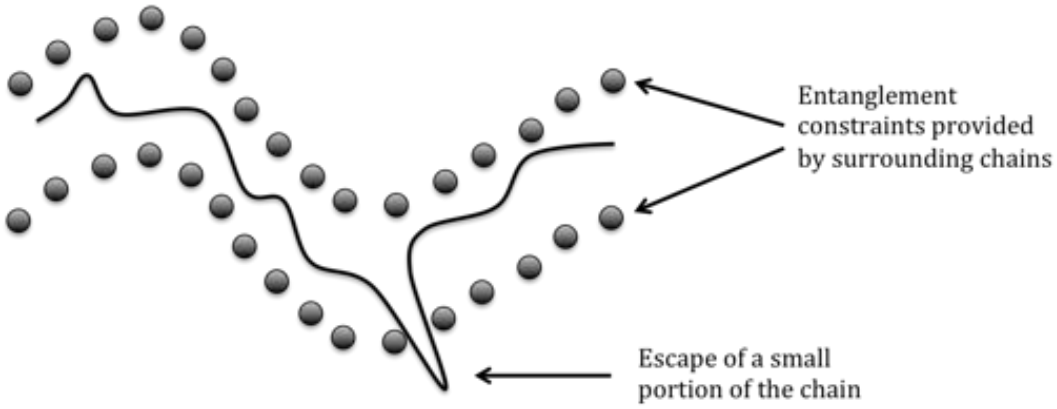

Figure 4.4. Illustration of the constraint-release mechanism whereby a small portion of the chain is able to escape from confinement of the tube.

This section has addressed some theories of macromolecular dynamics; the Rouse model and the Reptation model and their applications and developments in polymer science. Within the results section of this chapter, the Reptation model becomes the main focus of attention for investigations on polymer mobility in the presence of carbon dioxide, where rheological studies are undertaken to determine the reptation time of poly(ε-caprolactone).

The interactions between poly(lactic acid), poly(ε-caprolactone) and carbon dioxide assessed using Fourier Transform Infrared Spectroscopy will also be presented.

The remainder of the chapter will subsequently focus on the influence of carbon dioxide poly(lactic acid) and poly(ε-caprolactone) blends. The blends are characterised and compared to the blends prepared using conventional blending methods.

4.2 Experimental

4.2.1 The influence of carbon dioxide on the reptation of poly(ε-caprolactone)

An Anton Paar Physica MCR301 high pressure rheometer (previously described in chapter 2) was used to probe the influence of carbon dioxide on the reptation time of poly(ε-caprolactone). A PCL polymer disc with a thickness of 1 mm (cut from a hotpressed plaque – see methodology in chapter 2) was added to the lower plate of the preheated rheometer (80, 100 or 120 ˚C). The rheometer was then sealed and charged with the desired pressure of carbon dioxide (atmospheric, 60, 80 or 100 bar). The sample was provided a 5 minute soak time to allow CO_2 to diffuse into the polymer prior to undertaking analysis. Initial viscosity measurements were performed in order to determine the shear rates at which the Newtonian region of PCL occurred. Accordingly, a series of strain sweeps over a range of angular frequencies were then performed to establish the strain required to obtain a shear rate within the Newtonian region. Finally, oscillation measurements were performed and the angular frequency was varied on a log scale over 14 data points between 0.2 to 100 rad s^{-1}. At each angular frequency the torque was allowed to stabilise, resulting in experimental times of typically 14 minutes. Three repeats of each temperature and pressure were performed and the average storage (G') and loss (G") modulus against angular frequency (ω) were plotted with the standard deviation denoted by error bars.

4.2.2 Investigations of interactions of poly(lactic acid) and poly(ε-caprolactone) with carbon dioxide using Fourier Transform Infrared (FTIR) Spectroscopy

FTIR was employed to investigate any potential interaction with both poly(lactic acid), poly(ε-caprolactone) and carbon dioxide. A Jasco FTIR-6300 was used with a Specac supercritical fluid golden gate ATR attachment connected to a Specac temperature controller (Figure 4.5).

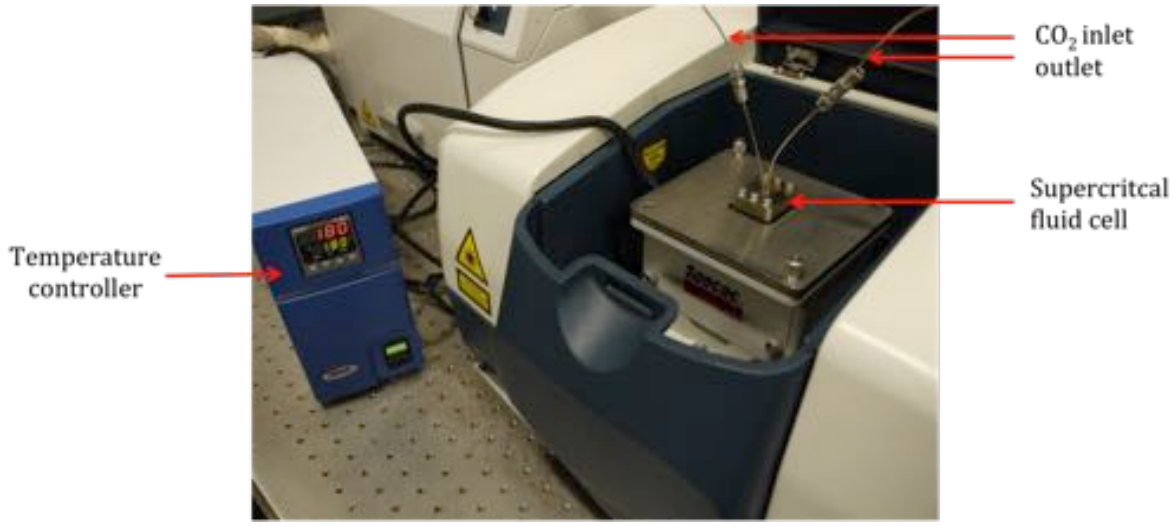

Figure 4.5. Jasco FTIR-6300 with a Specac supercritical fluids golden gate ATR attachment and temperature controller.

A sliced segment of a PLA or PCL pellet was placed over the ATR crystal which was subsequently covered and sealed with the supercritical fluid attachment. This arrangement requires an initial melt contact to be made (in the absence of an applied force) to provide sufficient contact with the crystal in order to acquire spectral measurements.

The cell was then preheated to 150 ˚C (to replicate extrusion conditions) and a spectrum was captured prior to the addition of CO_2. In order to minimise experimental time (and potential thermal degradation) a resolution of 4 cm^{-1} and 100 scans was employed. A

Jasco pump (Model PU-2086 Plus) was used in order to pressurise and control CO_2 in the cell throughout the experiment. A spectrum was captured after a 5 minute soak at pressures from bottle pressure (approximately 60 bar) to 120 bar.

4.2.3 Carbon dioxide assisted extrusion of poly(lactic acid) and poly(ε-caprolactone) blends

It was noted in chapter 3 that blending investigations would proceed without the inclusion of 40 rpm as a result of comparatively inferior mechanical properties to those exhibited for 20 and 30 rpm. Therefore, the methodology detailed in this section will be for screw speeds of 20 and 30 rpm only.

Prior to extrusion, the PLA grades were dried to remove any residual moisture (previously detailed in Chapter 3). The blends produced in the presence of carbon dioxide were produced using the same extruder used for melt blending, however the extruder was modified to allow the injection of CO_2 into the polymer melt. CO_2 was injected into zones 2 and 3 of the barrel via a custom made design, using a Jasco pump (Model PU-2086 Plus) fitted with a chiller head to enable the CO_2 to be pumped in liquid form (see Figure 4.6 for extruder set-up). There are 4 injection ports, 2 on either side of the barrel. The first set of injection ports are situated 28.5 cm along the extruder (zone 2) and the second set are 54.5 cm along (zone 3), 8.5 cm from the die. Interchangeable fittings to run with and without CO_2 can be seen in Figure 4.7. The CO_2 fitting has a 0.5 mm diameter opening at the end to allow carbon dioxide to pass through into the barrel. The head of the CO_2 fitting was connected to a male pressure tube fitting, which was wrapped with PTFE tape to enhance the seal between both components. This allowed the connection of the lines (1/16”) which were connected with a union cross

fitting. Between experiments, all screws and components needed to be removed, separated and cleaned to remove any solidified polymer blocking the CO_2 flow. A pressure relief valve was installed to prevent over pressurisation in the extruder. The pressure in the extruder was monitored using a pressure transducer.

In order to calculate the CO_2 concentration for addition into the extruder, each polymer was extruded at both 20 and 30 rpm and the average of three extruded masses per minute was calculated for each screw speed. The CO_2 flow rate (g min^{-1}) was then calculated as a wt% of the measured polymer mass extruded per minute using Equation 4.11. This enabled the input of a given concentration of CO_2, in relation to the polymer, into the extruder. This calculated value must be converted into ml min^{-1} as CO_2 is injected as liquid. Equation 4.12 shows this conversion. The density of CO_2 was calculated by NIST web-book [12] as 0.91898 g ml^{-1} based on the CO_2 pressure and temperature in the pump (at 4 °C). CO_2 wts% of 1, 5, 10 and 20% were injected for each blend system at 20 and 30 rpm.

$$\boldsymbol{Flow\ rate_{CO2}\ (g\ min^{-1})} = \frac{\boldsymbol{CO_2\ Concentration\ (wt\%)}}{\boldsymbol{100}} \times \boldsymbol{Flow\ rate_{polymer}\ (g\ min^{-1})} \qquad \text{Equation 4.11}$$

$$\boldsymbol{Flow\ rate_{CO2}\ (ml\ min^{-1})} = \frac{\boldsymbol{Flow\ rate_{CO2}\ (g\ min^{-1})}}{\boldsymbol{Density_{CO2}\ (g\ min^{-1})}} \qquad \text{Equation 4.12}$$

Since CO_2 is known to depress the melting point of partially crystalline polymers, it was found that the blend of PLA and PCL could be readily extruded at reduced barrel and die temperatures (150 °C and 160 °C respectively).

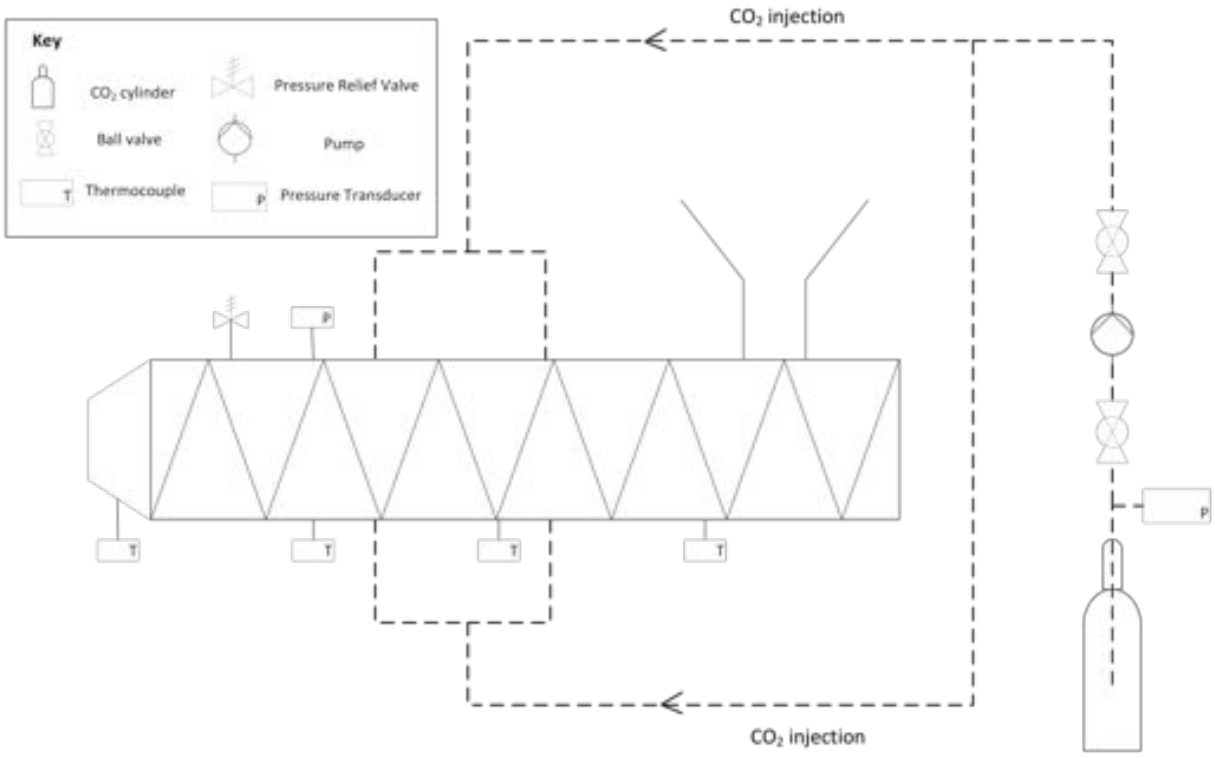

Figure 4.6. Schematic of extruder and carbon dioxide set-up.

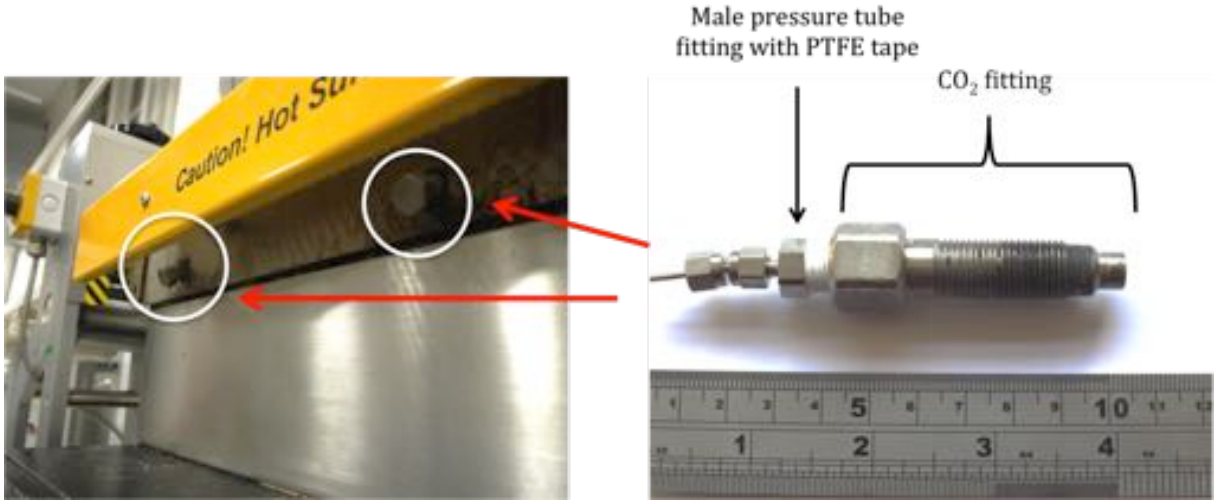

Figure 4.7. Photographic illustration of injection ports, set to run without CO_2 (left) and an example of a CO_2 injection fitting (right).

4.3 Results and discussion

4.3.1 The influence of carbon dioxide on the reptation of poly(ε-caprolactone)

Initial viscosity measurements indicated that the Newtonian region of PCL occurred between shear rates of 0.02 and 0.32 s^{-1}. The strain sweeps performed to determine the strain required to maintain a shear rate within the Newtonian region (0.02 and 0.32 s^{-1}) demonstrated the strain needed to be adjusted between 100 and 0.2% throughout the experiment.

4.3.1.1 Effect of temperature on the atmospheric rheological properties of poly(ε-caprolactone)

Figure 4.8 shows the influence of temperature (80, 100 and 120 ˚C) on the average storage (G') and loss (G") modulus plots of PCL at atmospheric pressure. The results of the frequency sweeps indicate a horizontal shift (illustrated in Figure 4.8) along the angular frequency axis corresponding with an increase in temperature. During an oscillation measurement, a constant shear strain and set angular frequency is applied to the sample. The resultant shear stress required in order to produce this strain enables the calculation of the complex shear modulus (G^*):

$$G^* = \frac{shear\ stress}{shear\ strain} \qquad \text{Equation 4.13}$$

The complex shear modulus is related to both the real (') and imaginary (") moduli:

$$G^* = \sqrt{G'^2 + G"^2} \qquad \text{Equation 4.14}$$

The horizontal shift, seen in Figure 4.8, is caused by a decrease in both G' and G" at a given frequency for low angular frequencies. Upon increasing the temperature, thermal

expansion and consequently an increase in the free volume of the polymer occurs, resulting in the ability for increased translational motion. Additionally, the mobility of the polymer chains is enhanced as more thermal energy is supplied. Therefore, the force required to shear the material is reduced, corresponding with a reduction in the complex shear modulus (*G**). This means there is also a reduction in both the G' and G" components, established by the horizontal shift present. Horizontal shifts may also be seen for polymers varying in molecular weight. A polymer with a higher molecular weight will exhibit G' and G" values at lower angular frequencies. This is due to the longer and less flexible chains being unable to respond with a fast motion at the higher frequencies [13].

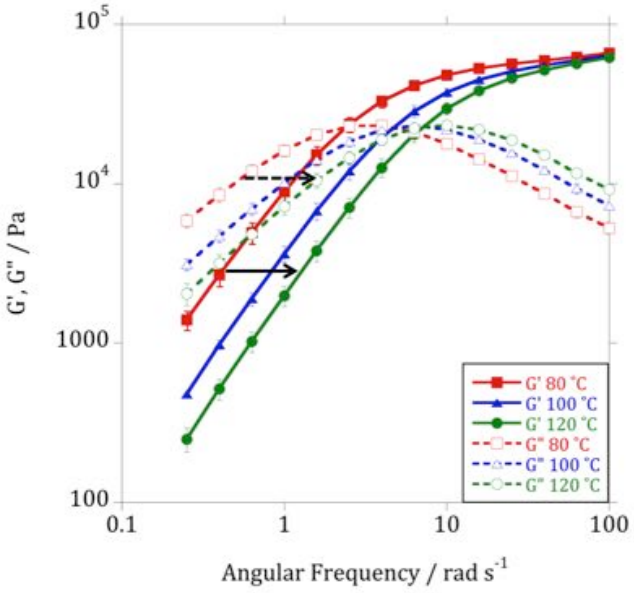

Figure 4.8. The storage (G') and loss (G") modulus plots for PCL at atmospheric pressure for 80, 100 and 120 ˚C. Standard deviation is denoted by error bars.

The results generated from the oscillation experiments exhibit ideal responses as governed by the simplest model of viscoelastic behaviour, the Maxwell model [14]. This model consists of an elastic component (spring) connected in series with a viscous component (dashpot) [15]. The storage and loss moduli are represented mathematically by the Maxwell model as:

$$G' = \frac{G\omega^2\tau^2}{1 + \omega^2 + \tau^2} \qquad \text{Equation 4.15}$$

$$G'' = \frac{\eta\omega}{1 + \omega^2 + \tau^2} \qquad \text{Equation 4.16}$$

where G is the spring modulus of the model, η is the viscous component, ω is the angular frequency and τ is the reptation time. In all results obtained, a plateau in G' is present at high frequencies and follows a sharp transition to the terminal region at low angular frequencies. This model predicts that G' is proportional to ω^2 and G" is proportional to ω for polymers with a linear structure and a relatively narrow molecular weight distribution [16].

The Maxwell model can also used to determine the reptation time. It is expressed as the reciprocal frequency of the intersect of the storage and loss moduli:

$$\tau = \frac{1}{\omega_{(G'=G'')}} \qquad \text{Equation 4.17}$$

The results for the calculated reptation times can be seen in Table 4.1. Upon heating from 80 ˚C to 100 ˚C the reptation time is reduced by 50%. Increasing the temperature to 120 ˚C, reduces the reptation time by another 36%. The addition of thermal energy into the system causes both an increase in free volume, an increase in energy and

mobility of the polymer chains. This means that the network of entanglements (the confinements of the tube) surrounding the reptating chain are able to relax and the diameter of the tube is increased. This allows the chain within the tube an extra degree of freedom that was previously denied at lower temperatures. The increased temperature provides the chain with extra energy to drive the conformational changes that cause the chain to reptate. Therefore, there is a corresponding reduction in reptation time with a raise in temperature.

The time-temperature superposition can be employed in order to determine temperature dependent properties from the known properties of a reference temperature. The procedure involves shifting each of the curves along the horizontal axis to the reference curve. The horizontal shift required, known as the 'shift factor', is calculated using Equation 4.18:

$$shift\ factor\ (a_T) = \frac{\omega_{TExperimental}}{\omega_{TReference}} \qquad \text{Equation 4.18}$$

where $\omega_{TExperimental}$ is the angular frequency at the experimental temperature and $\omega_{TReference}$ is the angular frequency at the reference temperature. The chosen reference temperature was 100 ˚C, previously used in other studies on the rheological properties of PCL [17, 18].

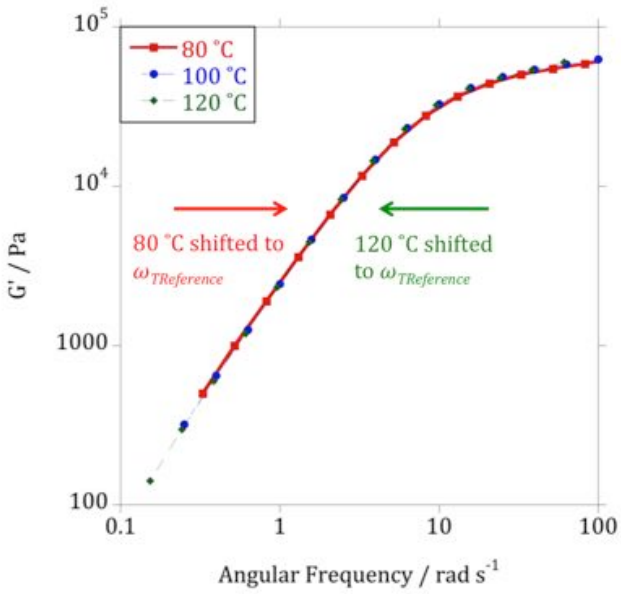

Figure 4.9. Example of the shifted storage moduli to $\omega_{TReference}$ (100 ˚C) in order to calculate the shift factor. Determining the shift factor enables the calculation of activation energy to flow.

In order to calculate the activation energy to flow, the Arrhenius equation (Equation 4.19) was used:

$$lna_T = \left(\frac{E_a}{R}\right)\left[\left(\frac{1}{T}\right) - \left(\frac{1}{T_0}\right)\right] \qquad \text{Equation 4.19}$$

where E_a is the activation energy to flow, T_0 is the reference temperature (in Kelvin), T is the experimental temperature (in Kelvin) and R is the universal gas constant (8.314 J mol^{-1} K^{-1}). Using the above equation, the activation energy to flow for PCL at ambient pressure was calculated to be 31.3 kJ mol^{-1}. This result is consistent with previous publications that report activation energy values between 32 and 41 kJ mol^{-1}

for varying molecular weight grades of PCL [17-19]. An example Arrhenius plot can be seen in Figure 4.14.

4.3.1.2 Effect of carbon dioxide pressure on the rheological properties of poly(ε-caprolactone)

In order to establish the influence of carbon dioxide on the reptation time of PCL, oscillation measurements were similarly performed at 80, 100 and 120 ˚C, with the addition of 60, 80 and 100 bar CO_2. Figure 4.10 shows the average storage and loss moduli plots of PCL with different pressures of CO_2 at 80 ˚C. Upon the addition of 60 bar of carbon dioxide there is a significant horizontal shift to higher angular frequencies, similar to that exhibited by increasing the temperature. This indicates a decrease in the complex shear modulus resulting from a reduction in the torque required to produce the required shear strain.

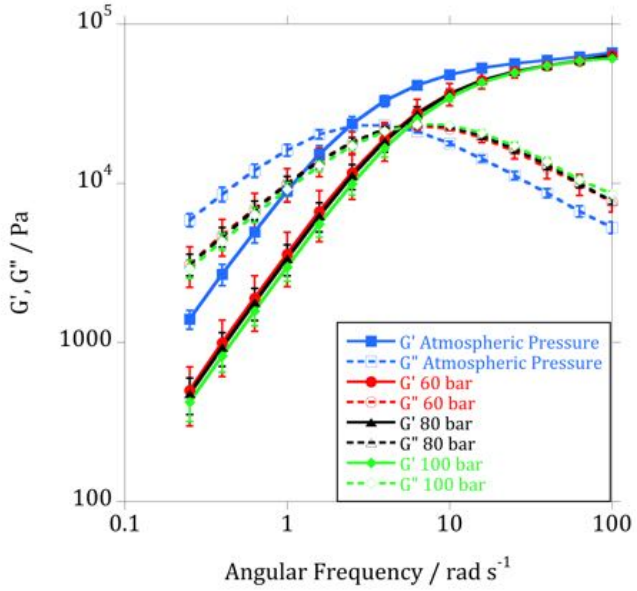

Figure 4.10. Plots of the storage modulus (G') and loss modulus (G") against angular frequency for PCL at 80 ˚C over a range of CO_2 pressures. Standard deviation is denoted by error bars.

The influence of pressure on shear modulus is commonly reported in the literature. A corresponding increase is seen in the shear modulus of a polymer as the pressure is raised [20]. This pressure compresses the free volume between the polymer chains, consequently hindering their mobility. In contrast however, through the addition of 60 bar of CO_2, a shift to higher frequencies is observed, indicating the opposite effect.

The gaseous properties of CO_2 enable its diffusion into the free volume of a polymer, between the individual chains. Once inside, CO_2 forms Lewis acid-base interactions with carbonyl groups (present in PCL). This disrupts the inter/intra molecular interactions, decreasing the number of chain entanglements, thereby increasing the free volume and the mobility of the polymer chains [21]. This influence of carbon dioxide on the mobility of the polymer chains results in the reduction of the complex shear modulus and subsequent horizontal shift in the results. Elevating the pressure subsequently increases the amount of CO_2 present and therefore the dissolved concentration within PCL [22]. Therefore, it was expected that a further reduction in complex shear modulus would arise from additional free volume as a consequence of increased CO_2 concentration. However, this expectation is not apparent; there is little successive shift upon raising the pressure to 80 and 100 bar. This is evidence that the pressure effects upon the polymer chains (compressing and reducing free volume) is competing with the influences that carbon dioxide poses upon the chains. It is apparent that the effects of carbon dioxide are only mildly dominating, therefore resulting in a subtle horizontal shift for both 80 and 100 bar. This result is also present in the comparison of pressure at 100 and 120 ˚C seen in Figure 4.11 and Figure 4.12 respectively. It can also be noted that the same trends observed regarding horizontal shifts with increasing temperature are consistent within each pressure set. Figure 4.11 shows that 80 bar exhibits a greater shift than

100 bar demonstrating the pressure effects are dominating at 100 bar. However, larger standard deviations are also present in these experiments.

Comparison of the calculated reptation times can be seen in Table 4.1 (graphically represented in Figure 4.13). It is evident that upon increasing both temperature and pressure there is a reduction in reptation time. For example, the addition of 60 bar of carbon dioxide exhibits a decrease in reptation time equivalent to that of raising the temperature by 20 ˚C (from 80 to 100 ˚C) at atmospheric pressure. This suggests that processing conditions for PCL can be reduced by 20 ˚C in the presence of 60 bar of CO_2, reducing the risk of thermal degradation and resulting in a more economical procedure.

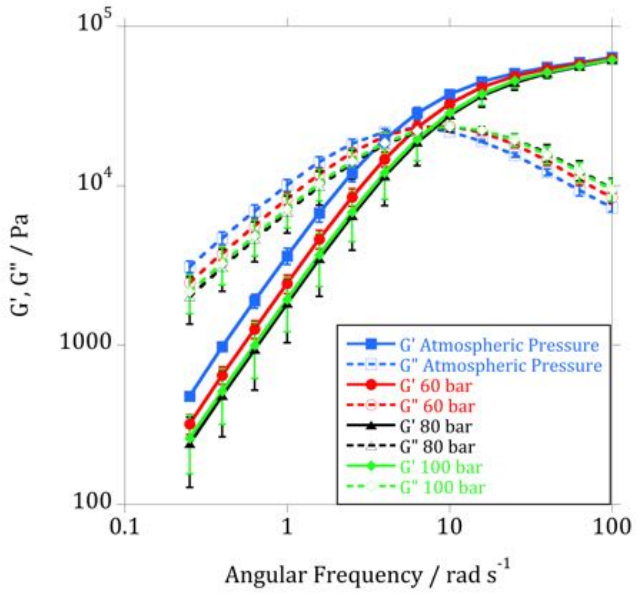

Figure 4.11. Plots of the storage modulus (G') and loss modulus (G") against angular frequency for PCL at 100 ˚C over a range of CO_2 pressures. Standard deviation is denoted by error bars.

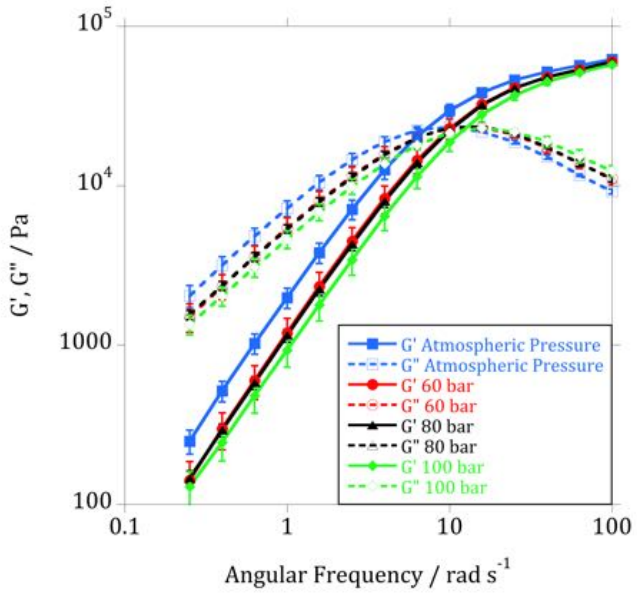

Figure 4.12. Plots of the storage modulus (G') and loss modulus (G") against angular frequency for PCL at 120 ˚C over a range of CO_2 pressures. Standard deviation is denoted by error bars.

Despite the significant initial reduction in reptation time through the addition of 60 bar of carbon dioxide, a further increase in the pressure has a minimal effect across all experimental temperatures. However, the effect of carbon dioxide has less significance as the experimental temperature is raised. For example, at 120 ˚C there is only a 29% reduction in reptation time through the addition of CO_2, in contrast to the 52% reduction observed at 80 ˚C. At higher temperatures, PCL chains possess a greater mobility and therefore the influence of carbon dioxide has less significance.

Experiment	Average cross over / ω	Average reptation time / Seconds
Atmospheric 80°C	2.41	0.44 ± 0.04
Atmospheric 100°C	4.67	0.22 ± 0.02
Atmospheric 120°C	7.18	0.14 ± 0.01
60 bar CO_2 80°C	5.03	0.21 ± 0.05
60 bar CO_2 100°C	6.42	0.16 ± 0.01
60 bar CO_2 120°C	10.17	0.10 ± 0.01
80 bar CO_2 80°C	5.17	0.20 ± 0.03
80 bar CO_2 100°C	8.11	0.13 ± 0.03
80 bar CO_2 120°C	10.47	0.10 ± 0.01
100 bar CO_2 80°C	5.69	0.18 ± 0.02
100 bar CO_2 100°C	7.94	0.13 ± 0.03
100 bar CO_2 120°C	12.20	0.08 ± 0.01

Table 4.1. Reptation times for atmospheric, 60, 80 and 100 bar for 80, 100 and 120 ˚C.

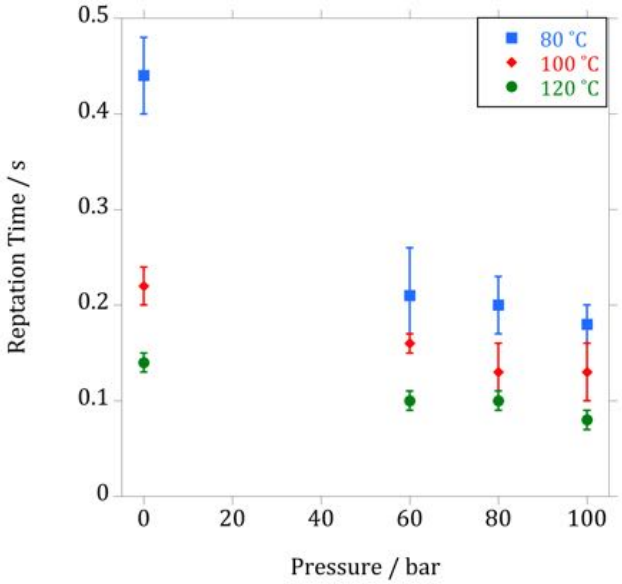

Figure 4.13. The influence of CO_2 pressure and temperature on the reptation time of PCL. Standard deviation is denoted by error bars.

The activation energies to flow are presented in Table 4.2. It is evident that the activation energy is reduced in the presence of carbon dioxide, with a decrease from 31.56 (atmospheric) to 20.74 kJ mol^{-1} (80 bar). This reduction results from increased chain mobility and free volume corresponding with lower energy required for molecular motion and hence for the polymer melt to flow.

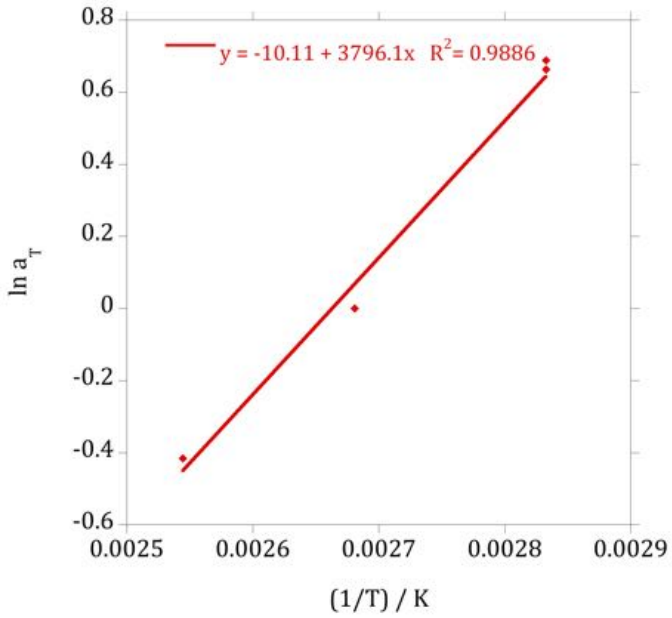

Figure 4.14. Example of an Arrhenius plot (a precursor to calculating the activation energy to flow) for ambient pressure.

CO_2 pressure / bar	**Activation energy to flow / mol^{-1}**	**R^2 value of Arrhenius plot**
Atmospheric	31.56	0.9886
60	21.48	0.9542
80	20.74	0.9835
100	22.90	0.9709

Table 4.2. Activation energy to flow of PCL for varying pressures of carbon dioxide.

4.3.2 Investigations of interactions of poly(lactic acid) and poly(ε-caprolactone) with carbon dioxide using Fourier Transform Infrared (FTIR) Spectroscopy

The interaction between carbon dioxide and polymers has often been investigated using FTIR. Different molecular structures of polymers can transpire to different interactions with CO_2 [23]. Polymers containing carbonyl groups may exhibit Lewis acid-base interactions between the "electron poor" carbon atom of CO_2 (electron acceptor) and the "electron rich" oxygen atom of the carbonyl group (electron donor) [24]. In the presence of dissolved CO_2, for a variety of pressures (sub and supercritical), shifts of the carbonyl stretching band are commonly observed. Polymers include PMMA (up to 89.7 bar) [24], PLGA (up to 40 bar) [25], PLA (up to 80 bar) [26] and PCL (up to 75 bar) [26].

Figure 4.15 and Figure 4.16 illustrate the FTIR spectra and analysis of the carbonyl band of PLA 2002D at 150 ˚C. As the pressure is increased from atmospheric to 120 bar of CO_2 it is evident that there is a reduction in maximum peak absorbance of the carbonyl band with a corresponding shift to higher wavenumbers. The intensity is reduced from an absorbance around 0.59 at atmospheric pressure to 0.48 at 120 bar. As the content of carbon dioxide is increased into the supercritical fluid cell it 'dilutes' the spectrum of PLA, resulting in a reduction in absorbance. The C=O band also exhibits a total horizontal shift over 2 cm^{-1} to higher wavenumbers. Note that only the carbonyl band exhibited wavenumber shifts, no other spectral shifts were observed in these experiments. This corresponds with numerous reports in the literature which present similar shifts for other polymers containing a carbonyl group; PMMA, PLGA, PLA and PCL [24-27]. The associating shifts are attributed to Lewis acid-base interactions between CO_2 and the polymer, consequently the frequency of the vibration of the carbonyl group is reduced and the wavenumber is shifter to a higher value [26].

Similar trends in the intensity and position of the carbonyl band were also exhibited by PLA 4060D. These results are displayed in Figure 4.17 and Figure 4.18. PLA 4060D exhibited a slightly greater shift in comparison to 2002D which could be attributed to its amorphous nature, thus having a greater affinity towards carbon dioxide at this temperature. The noise generated on the spectra during the PCL experiments interfered with subsequent analysis and accurate determination of the maximum peak position of the carbonyl band, therefore PCL results will not be presented.

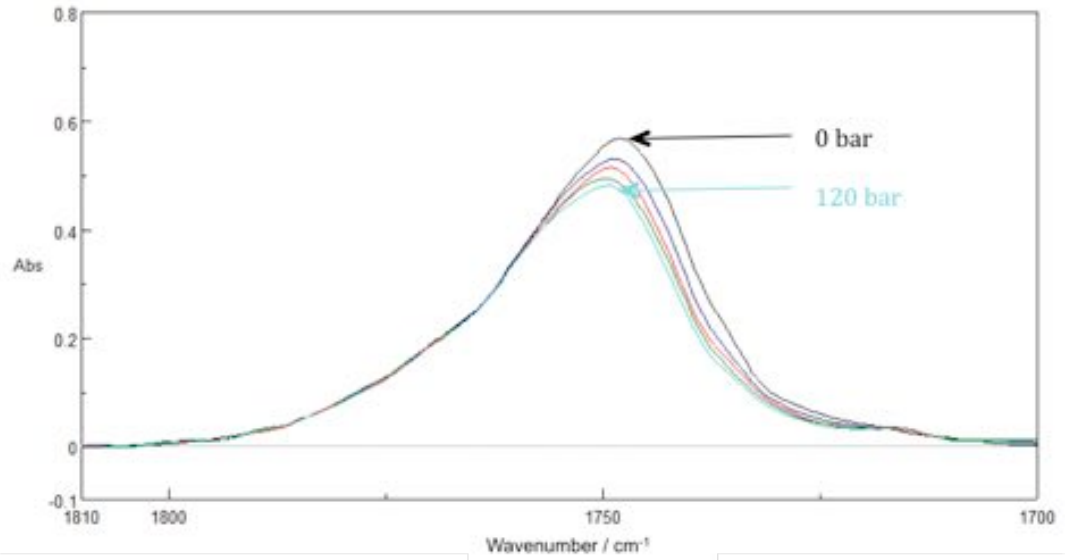

Figure 4.15. FTIR spectra of the carbonyl band of PLA 2002D at 150 ˚C and varying pressures of carbon dioxide.

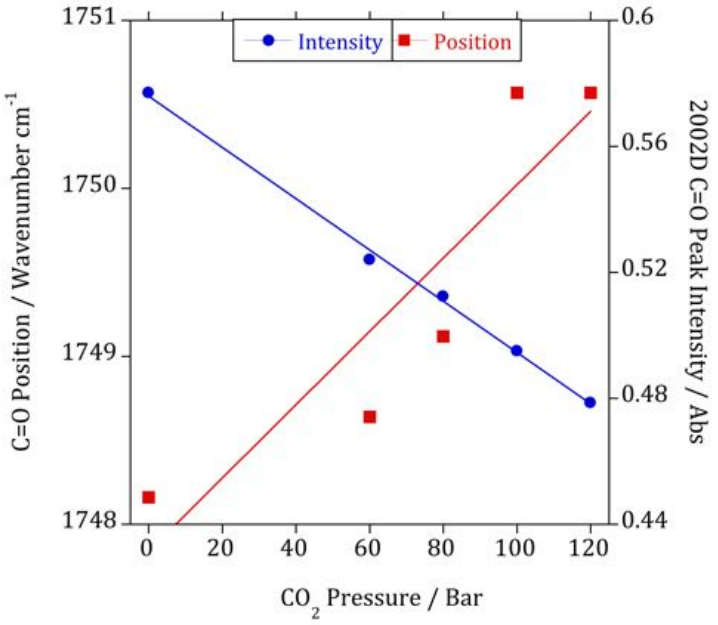

Figure 4.16. The influence of carbon dioxide pressure on the maximum peak position and intensity of the carbonyl band in PLA 2002D.

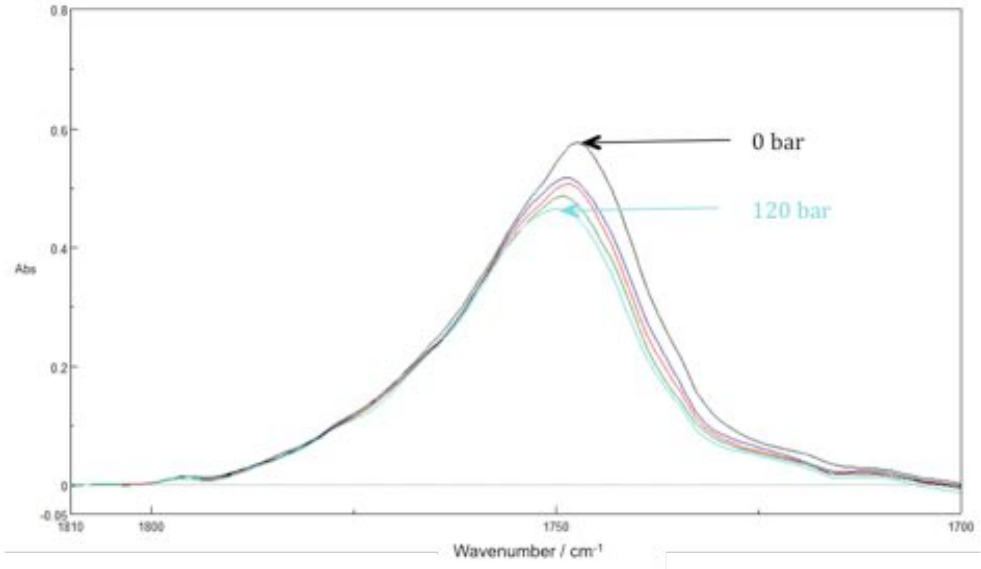

Figure 4.17. FTIR spectra of the carbonyl band of PLA 4060D at 150 ˚C and varying pressures of carbon dioxide.

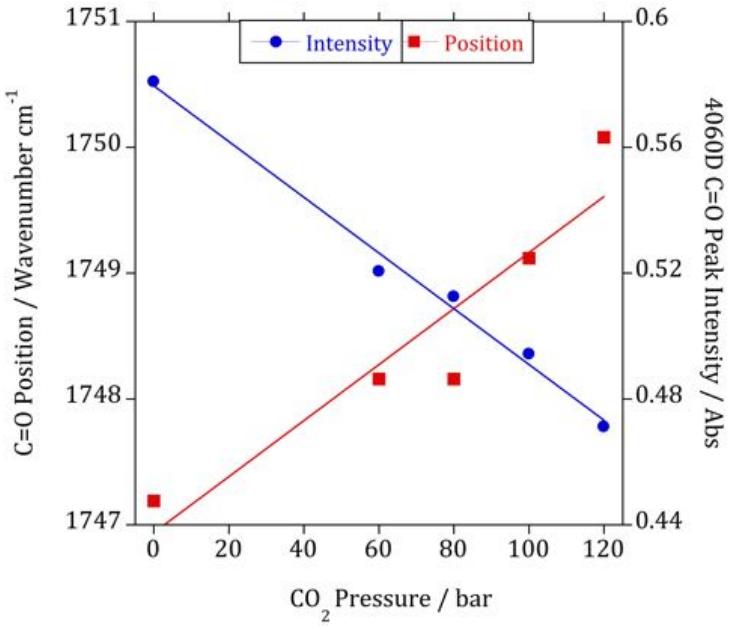

Figure 4.18. The influence of carbon dioxide pressure on the maximum peak position and intensity of the carbonyl band in PLA 4060D.

4.3.3 Carbon dioxide assisted extrusion of poly(lactic acid) and poly(ε-caprolactone) blends

Utilising a pressure transducer for the extrusion experiments in the presence of carbon dioxide allowed the pressure in the barrel to be monitored. Unfortunately, across all experimental variables the pressure did not reach supercritical conditions. Therefore, all presented results and analysis on blends produced in the presence of carbon dioxide have been produced at subcritical pressures.

4.3.3.1 Scanning Electron Microscopy (SEM)

As mentioned previously, various combinations of CO_2 concentrations and screw speeds were used to produce the PLA/PCL blends. SEM was then used to provide initial analysis and indication of the influence of experimental conditions on the blend morphology. It was clearly evident that superior morphologies were observed with a CO_2 concentration of 10% and a screw speed of 30 rpm for PLA 2002D and 20 rpm for PLA 4060D blends. These blends are presented in Figure 4.19 and Figure 4.20 respectively. It is apparent that the composition exhibiting the finest size and distribution of droplets is the 75/25 PLA/PCL blend in both systems. Due to the porosity and difficulty discerning droplet diameter for some blends prepared in the presence of carbon dioxide, the droplet diameter analysis (performed previously for the melt and solvent cast blends) could not be accurately completed and therefore are not presented. However, droplet diameters, where discernable, have been estimated. The PLA2002D/PCL blends show droplet diameters around 0.2, 0.6 and 0.6 μm for the 75/25, 50/50 and 25/75 blends, respectively. PLA4060D/PCL blends exhibit droplet diameters around 0.6, 0.8 and 1 μm for the 75/25, 50/50 and 25/75 blends, respectively. The creation of additional free

volume and increased chain mobility enables better interaction and mixing between the two polymers.

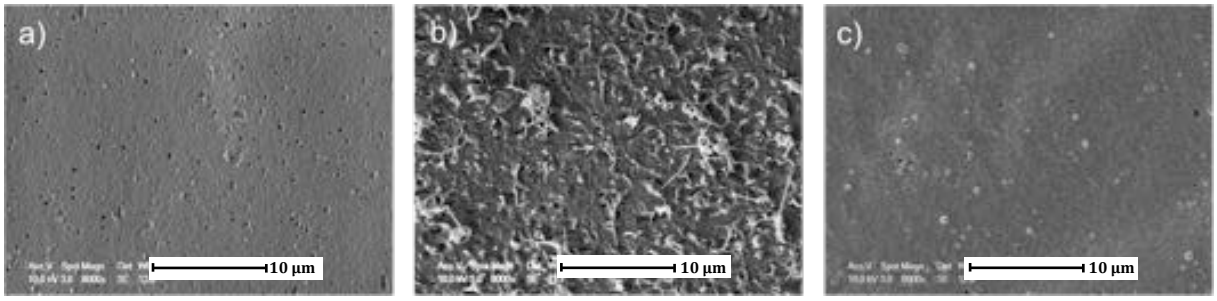

Figure 4.19. PLA2002D/PCL carbon dioxide assisted blends at 30 rpm and 10% CO_2 at 150 ˚C. Image a) 75/25 b) 50/50 and c) 25/75 PLA/PCL.

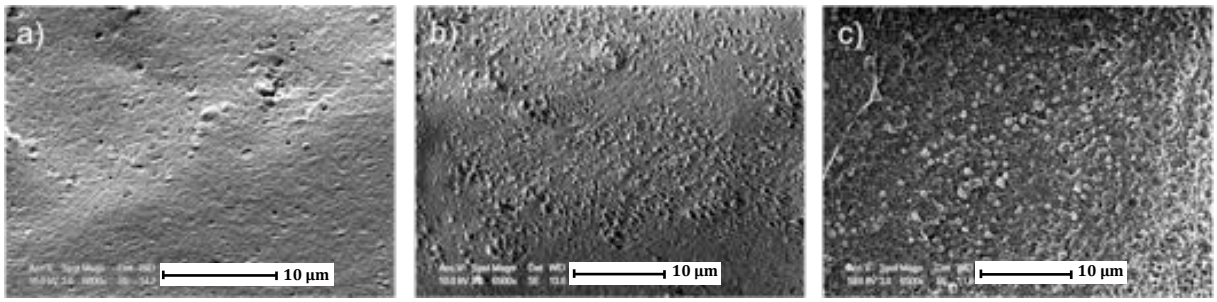

Figure 4.20. PLA4060D/PCL carbon dioxide assisted blends at 20 rpm and 10% CO_2 at 150 ˚C. Image a) 75/25 b) 50/50 and c) 25/75 PLA/PCL.

A comparison of the 75/25 PLA/PCL composition across different blend preparation methods can be seen in Figure 4.21 and Figure 4.22. It is clearly evident that the morphology improves, through a reduction in droplet size and dispersion, across blending techniques. The solvent cast blends exhibit droplet sizes up to 10 µm in diameter, reducing to 0.4 and 0.2 (in the PLA 2002D system) through melt blending and CO_2 assisted blending, respectively. These results are supported in the literature where the blend morphology was investigated in other polymer systems such as PE/PS blends and PS/PMMA using carbon dioxide [28-30]. These blends also showed a significant

decrease in the size of the dispersed phase from a few microns to submicron by injecting CO_2.

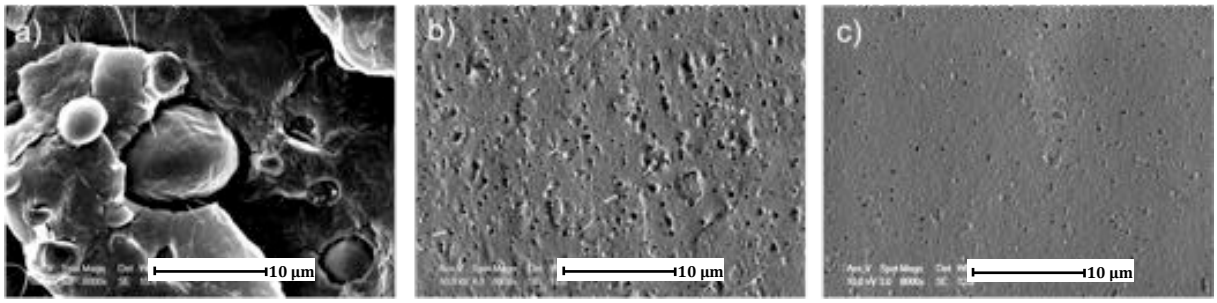

Figure 4.21. A comparison of 75/25 PLA2002D/PCL blends produced by a) solvent casting, b) melt blending at 160 ˚C and 30 rpm and c) CO_2 assisted blending at 150 ˚C, 30 rpm and 10% CO_2.

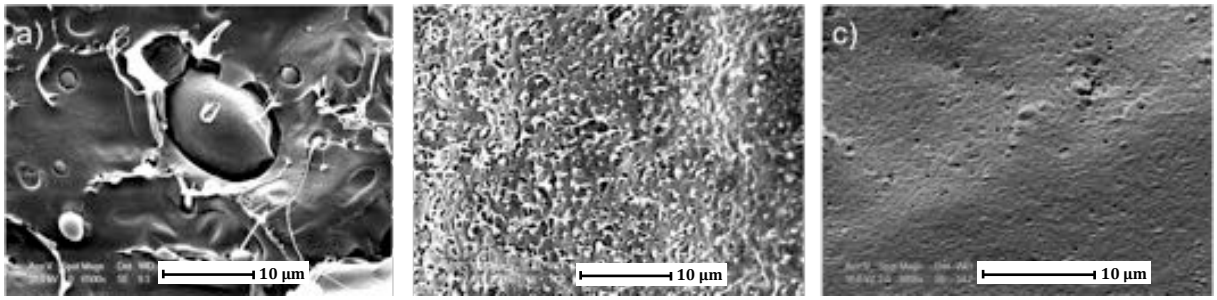

Figure 4.22. A comparison of 75/25 PLA4060D/PCL blends produced by a) solvent casting, b) melt blending at 160 ˚C and 20 rpm and c) CO_2 assisted blending at 150 ˚C, 20 rpm and 10% CO_2.

4.3.3.2 Mechanical testing

Figure 4.23 to Figure 4.25 display the mechanical properties for the PLA2002D/PCL blends prepared by solvent casting, melt blending (160 ˚C and 30 rpm) and CO_2 assisted blending (150 ˚C, 30 rpm and 10% CO_2). It is evident there is a significant improvement in properties from solvent casting to melt blending. Blending in the presence of carbon dioxide exhibits similar mechanical properties to those produced by melt blending. However there are a number of instances where this preparation method of blending exhibits superior properties (such as for the yield stress of 25/75, 50/50 and 75/25 blends and the Young's modulus for 50/50 and 75/25 PLA/PCL blends). This corresponds with the improved morphology observed by SEM, despite the increased porosity in the samples produced with carbon dioxide.

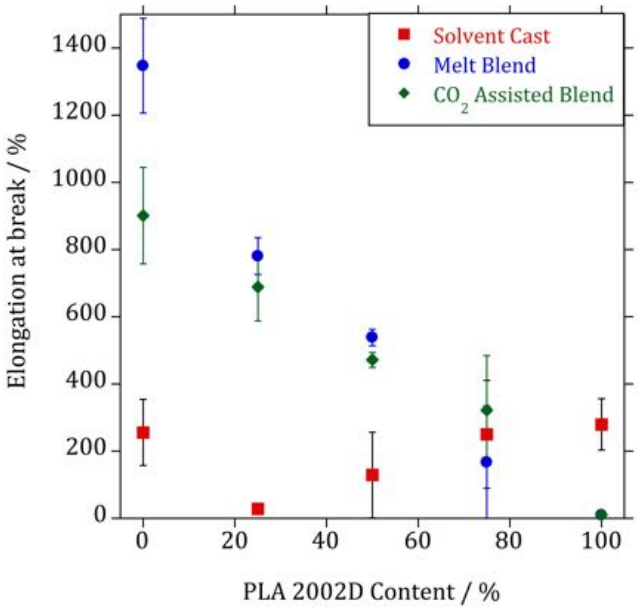

Figure 4.23. Comparison of the elongation at break for PLA2002D/PCL blends prepared by solvent casting, melt blending and CO_2 assisted extrusion.

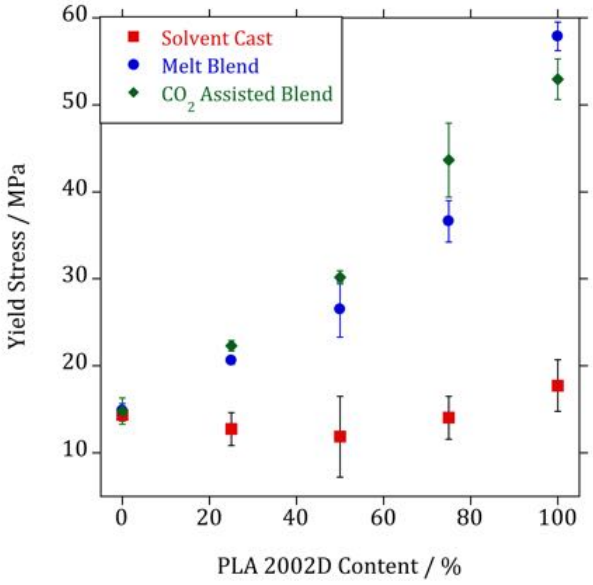

Figure 4.24. Comparison of the yield stress for PLA2002D/PCL blends prepared by solvent casting, melt blending and CO_2 assisted extrusion.

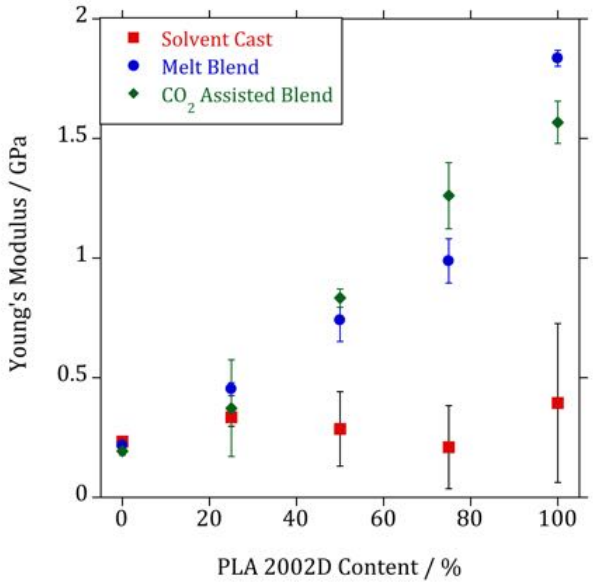

Figure 4.25. Comparison of the Young's modulus for PLA2002D/PCL blends prepared by solvent casting, melt blending and CO_2 assisted extrusion.

There are numerous theoretical prediction models for the mechanical properties of blends. Such models assume different interfacial behaviours between blend components, for example perfect adhesion or no adhesion. The rule of mixtures (Equation 4.20) assumes perfect adhesion between the dispersed phase and the blend matrix, in addition to perfect dispersion of the minor component:

$$\mathrm{E}_b = \left(\left[\frac{\mathrm{E}_d}{\mathrm{E}_m} - 1\right] \times \phi_d + 1\right) \times \mathrm{E}_m \qquad \text{Equation 4.20}$$

where E_b is the Young's modulus of the blend, E_d is the Young's modulus of the dispersed phase, E_m is the Young's modulus of the matrix and ϕ_d is the volume fraction of the dispersed phase [31]. Figure 4.26 presents the Young's modulus for PLA2002D/PCL blends prepared with and without the presence of carbon dioxide and the theoretical predictions assuming perfect adhesion. Greater deviation from the prediction model is observed in the melt blends in comparison to the blends produced in the presence of carbon dioxide. The melt blends show a greater deviation corresponding with increasing PLA content, indicating the potential for enhanced interaction within the blends is at lower compositions of PLA. Conversely, the Young's modulus for the CO_2 assisted blends exhibit greater conformity with the model corresponding with increasing content of PLA in the blends. This indicates a greater interaction is occurring within these blends which is in agreement with the improvement in mechanical properties seen for 75/25 PLA/PCL and the significantly improved morphology observed by SEM.

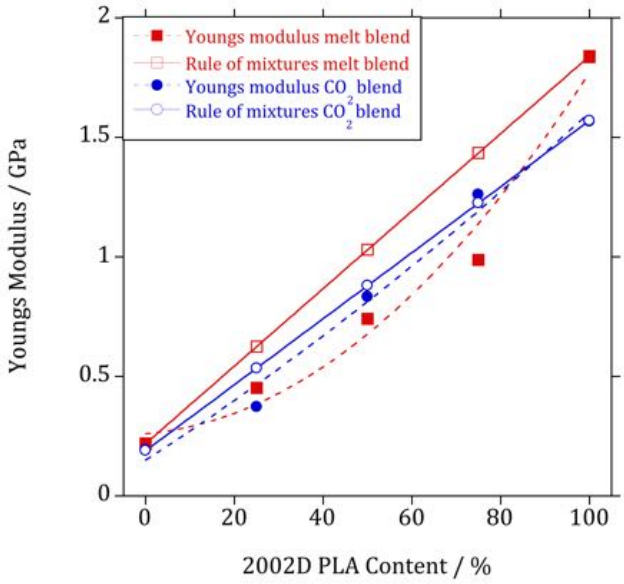

Figure 4.26. Comparison of the prediction model rule of mixtures to the Young's modulus results for both PLA2002D/PCL blends with and without carbon dioxide.

Figure 4.27 to Figure 4.29 display the mechanical properties for the PLA4060D/PCL blends prepared by solvent casting, melt blending (160 ˚C and 20 rpm) and CO_2 assisted blending (150 ˚C, 20 rpm and 10% CO_2). This blend system also exhibits a significant improvement from solvent casting to melt blending. The CO_2 assisted blends display similar or slightly lower mechanical properties to the melt blends, with only one improvement seen in this system (75/25 PLA/PCL for elongation at break) in comparison to the PLA2002D/PCL blends. Figure 4.30 presents the comparison of the Young's modulus for PLA4060D/PCL blends prepared with and without the presence of carbon dioxide and the theoretical predictions assuming perfect adhesion. In contrast to the results displayed for the PLA2002D system, the Young's modulus of the melt blends

increasingly deviate from the theoretical model with lower contents of PLA. Similarly, an improvement between model values and results is observed for the CO_2 assisted blends.

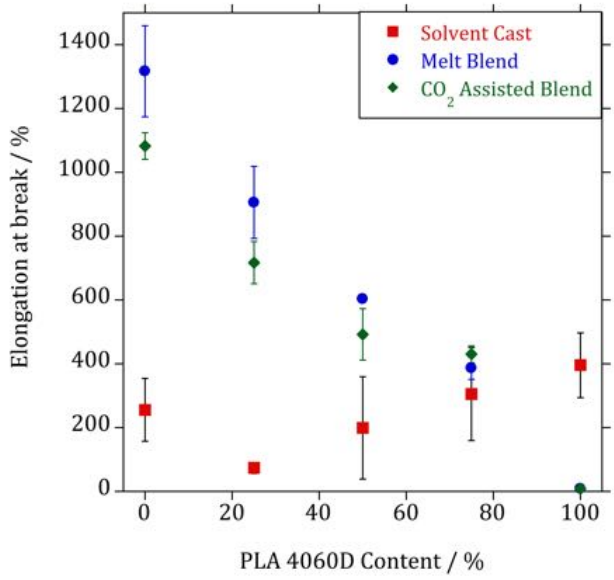

Figure 4.27. Comparison of the elongation at break for PLA4060D/PCL blends prepared by solvent casting, melt blending and CO_2 assisted extrusion.

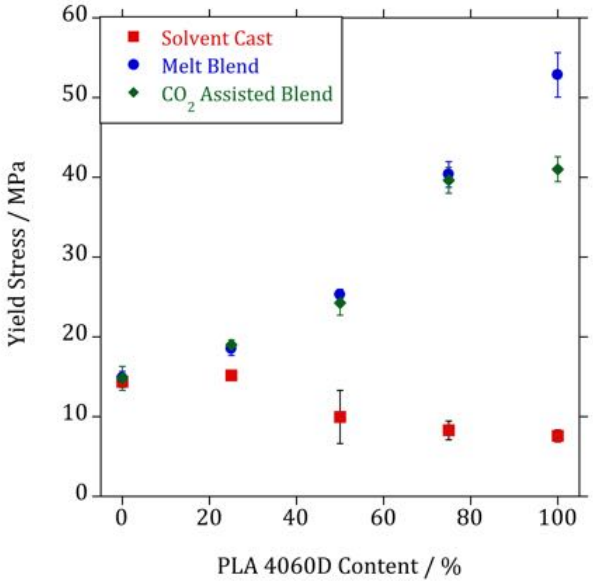

Figure 4.28. Comparison of the yield stress for PLA4060D/PCL blends prepared by solvent casting, melt blending and CO_2 assisted extrusion.

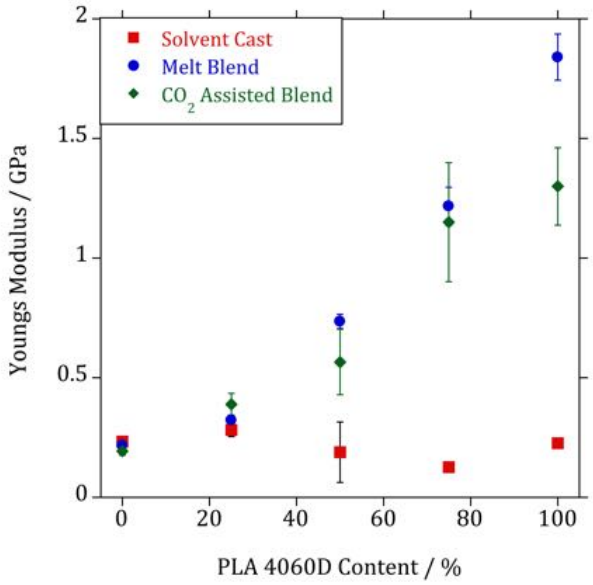

Figure 4.29. Comparison of the Young's modulus for PLA4060D/PCL blends prepared by solvent casting, melt blending and CO_2 assisted extrusion.

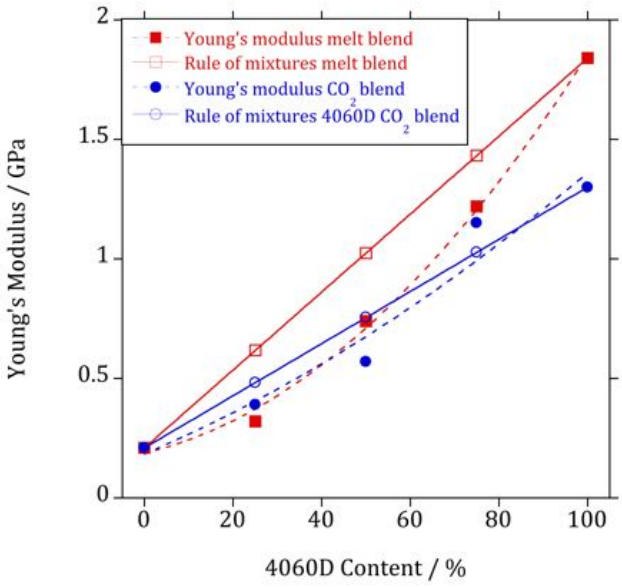

Figure 4.30. Comparison of the prediction model rule of mixtures to the Young's modulus results for both PLA4060D/PCL blends with and without carbon dioxide.

4.3.3.3 Fourier Transform Infrared (FTIR) Spectroscopy

Figure 4.31 and Figure 4.32 present the carbonyl FTIR spectra of the PLA2002D and 4060D/PCL blends produced in the presence of a 10% flow rate of carbon dioxide at 30 rpm and 20 rpm respectively. Both 50/50 and 25/75 PLA/PCL blends exhibit identical behaviour to that observed in the spectra of the melt blends (presented in chapter 3). That is, a greater absorbance of the major component is apparent according to blend composition. However, the 75/25 PLA/PCL blends exhibit less definition associated with composition, appearing as one predominant peak in the PLA region. This could suggest a compositional inaccuracy, that these samples somehow are not representative of a 75/25 PLA/PCL composition. This result however, was consistent for all samples collected at these experimental conditions. DSC analysis (presented in a subsequent section) of these blends confirms PCL is present in these blends, although with a significant reduction in crystallinity. Additionally, a much higher absorbance would be expected to be observed for the carbonyl band representing the homopolymer. It has been previously reported that the carbonyl band of PCL is split into two components; a crystalline band at 1724 cm^{-1} and an amorphous band at 1737 cm^{-1} [32]. A close correlation is present between DSC and FTIR in determining melting and crystallisation of PCL through analyses of the carbonyl band. The reduction in crystallinity for the PCL component in the 75/25 PLA/PCL blends may explain the absence of a dominant peak around 1724 cm^{-1}. The amorphous band of PCL however, is present at higher wavenumbers and therefore would be obscured by the presence of the PLA carbonyl peak. Similar to the measurements reported for the melt blends (chapter 3), the maximum peak position of the carbonyl corresponding to each component is

seen to shift to higher wavenumbers with its decreasing content in the blend (Table 4.3 and Table 4.4). This indicates the presence of an interaction between both components.

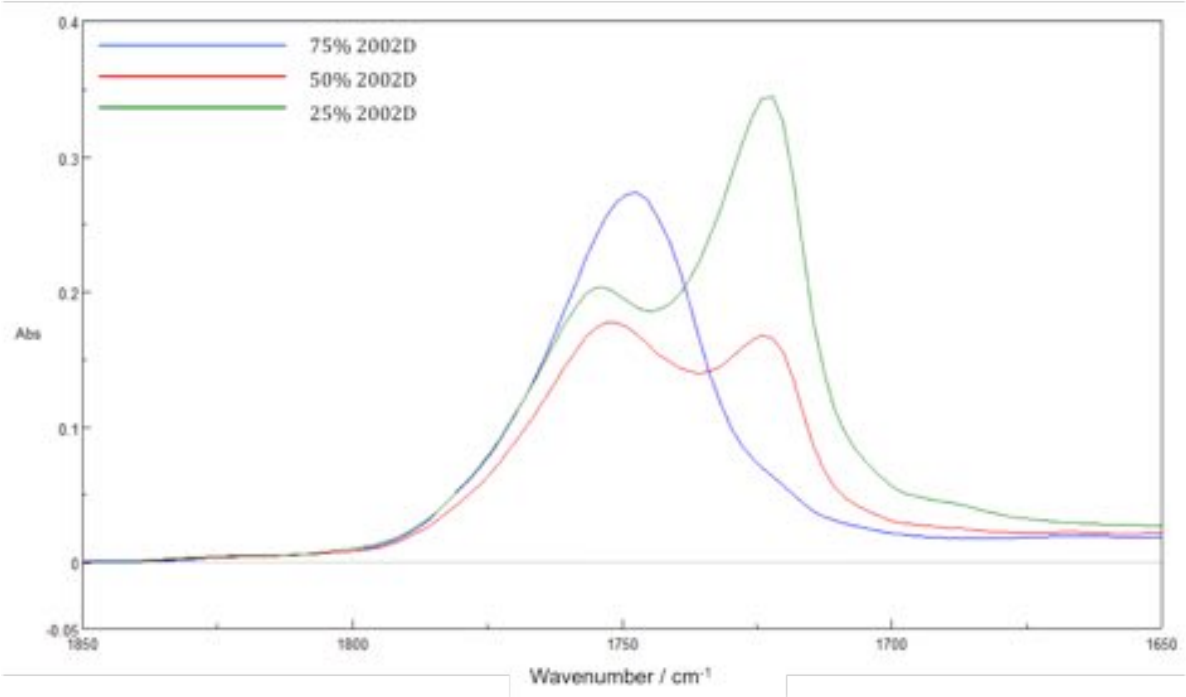

Figure 4.31. FTIR carbonyl spectra of PLA2002D/PCL blends produced in the presence of 10% CO_2 at 150 ˚C and 30 rpm.

PLA/PCL	PLA 2002D / cm $^{-1}$	PCL / cm $^{-1}$
25/75	1755	1722
50/50	1753	1724
75/25	1747	-

Table 4.3. The variance of PLA 2002D and PCL carbonyl peak position with composition.

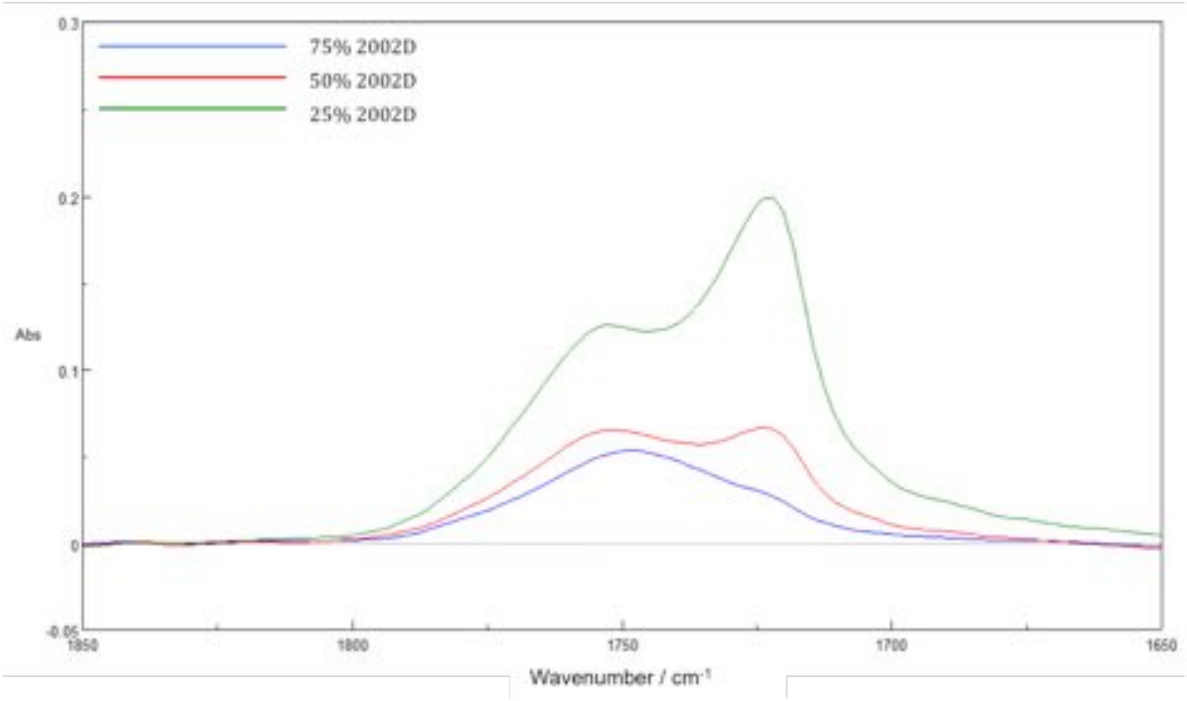

Figure 4.32. FTIR carbonyl spectra of PLA4060D/PCL blends produced in the presence of 10% CO_2 at 150 ˚C and 20 rpm.

PLA/PCL	PLA 4060D / cm $^{-1}$	PCL / cm $^{-1}$
25/75	1753	1722
50/50	1753	1724
75/25	1749	-

Table 4.4. The variance of PLA 4060D and PCL carbonyl peak position with composition.

4.3.3.4 Rheology

The comparison of viscosity for the hotpressed homopolymers with and without carbon dioxide (80 bar) can be seen in Figure 4.33. It is evident that at atmospheric pressure and 140 ˚C, the highest viscosity is possessed by PLA 2002D. Limitations of the high pressure rheometer meant that 140 ˚C was the maximum experimental temperature and therefore the atmospheric experiments were undertaken at the same temperature to preserve some consistency. At this temperature partially crystalline PLA 2002D is not yet in the melt and therefore it is understandable why a substantially higher viscosity is inherent in this polymer. Therefore, the predicted viscosity ratio (Table 4.5) for the 25/75 PLA2002D/PCL blend is significantly higher than the 75/25 blend ratio. Amorphous PLA 4060D (T_g at 52 ˚C) possesses a viscosity only slightly higher than partially crystalline PCL (melt at 58 ˚C) at atmospheric pressure. The viscosity ratios for this blend system therefore present values significantly closer to unity than the 2002D system.

In contrast to the viscosity of PLA 2002D measured at atmospheric pressure in the presence of 80 bar of carbon dioxide, this polymer now possesses the lowest viscosity. This is attributed to the effect of carbon dioxide interacting with PLA 2002D and subsequently depressing the melting point. A less significant reduction in viscosity, through the addition of CO_2, is observed for PLA 4060D. At 140 ˚C (significantly above the glass transition temperature of 52 ˚C) the temperature is already predominantly influencing the viscosity of this polymer and therefore carbon dioxide does not largely contribute to the resulting viscosity. The same is true of PCL, moreover the viscosity of PCL in the presence of carbon dioxide slightly increases. Although it must be noted that the error bars on most of the results overlap due to the similar viscosities, the increase

observed in PCL may be due to pressure effects. The pressure of carbon dioxide forces the polymer chains closer together thereby, reducing the free volume and consequently increases the viscosity. This effect is therefore dominating over the any interactions occurring between polymer and CO_2.

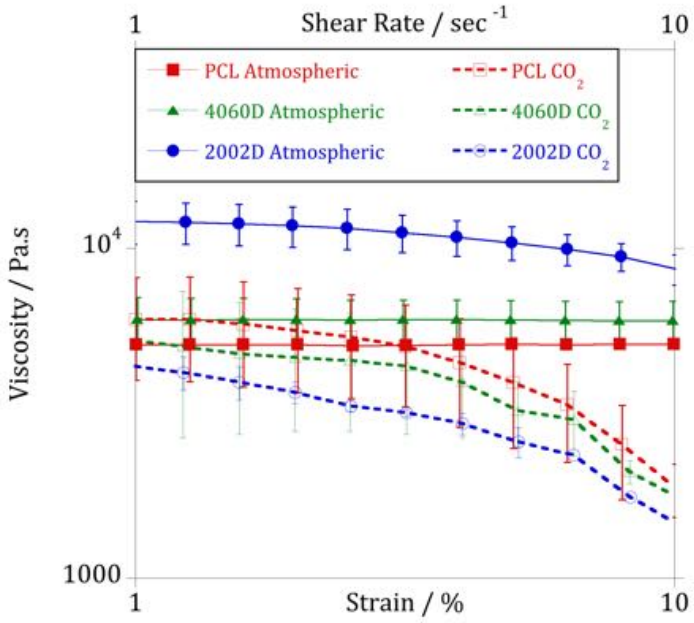

Figure 4.33. Comparison of the viscosity of the homopolymers with and without the presence of carbon dioxide (80 bar) at 140 ˚C. Error bars denote the standard deviation.

PLA/PCL	PLA 2002D / PCL	PLA 4060D / PCL
25/75 Atmospheric	2.36	1.19
75/25 Atmospheric	0.42	0.84
25/75 CO_2	0.73	0.87
75/25 CO_2	1.37	1.15

Table 4.5. Comparison of viscosity ratios at 140 ˚C for PLA2002D/PCL and PLA4060D/PCL blend systems with and without carbon dioxide.

4.3.3.5 Differential Scanning Calorimetry (DSC)

Figure 4.34 shows the comparison of the PLA2002D/PCL blends produced in the presence of carbon dioxide (10% CO_2 and 30 rpm). It is evident that with decreasing PCL content in the blends a corresponding reduction in the enthalpy of fusion is seen for the melting peak of PCL. All calculations of crystallinity were normalised and weighted to the corresponding composition of the blend. PLA crystallinity was calculated according to the presence of a cold crystallisation peak using Equation 3.12 (presented in chapter 3). Calculations of the crystallinity of the PCL component gave values of 60, 45 and 12% for the 25/75, 50/50 and 75/25 PLA/PCL blends, respectively. Cold crystallisation is observed for all three blends and the crystallinity values for the PLA component are 0.6, 2.34 and 3.11% for the 25/75, 50/50 and 75/25 PLA/PCL blends, respectively. Cold crystallisation is largely contributing to the final crystallinity developed in the PLA component. The cold crystallisation is much more pronounced in the blends than exhibited by 100% PLA (see Figure 4.35). This indicates that PCL is behaving as a nucleating agent for PLA. Additionally all three PLA melting endotherms exhibit double melting peaks. The appearance of multiple melting peaks is reported in numerous partially crystalline polymers [33] such as poly(ether ether ketone) PEEK [34, 35], poly(ethylene terephthalate) PET [36], poly(butylene napthalate) PBN [37], nylon-6 [38] and biodegradable polymers such as poly($_L$-lactide-*co*-glycolide) PLGA [39], poly (lactic acid) PLA [40]. Many explain the double melting behaviour using the melt-recrystallisation model [41]. According to this model, the low temperature and high temperature endothermic peaks in the DSC melting trace are attributed to melting of original crystals (formed upon previous cooling) and to the melting of crystals formed within the heating scan of the experiment.

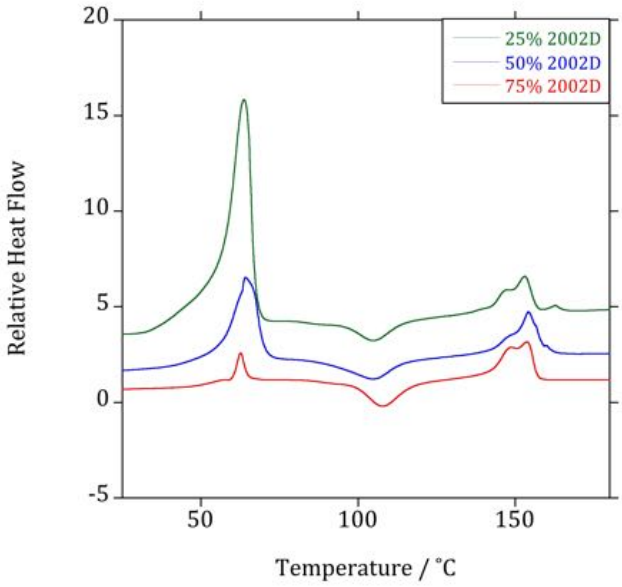

Figure 4.34. Comparison of the PLA2002D/PCL blends produced in the presence of 10% carbon dioxide at 150 ˚C and 30 rpm.

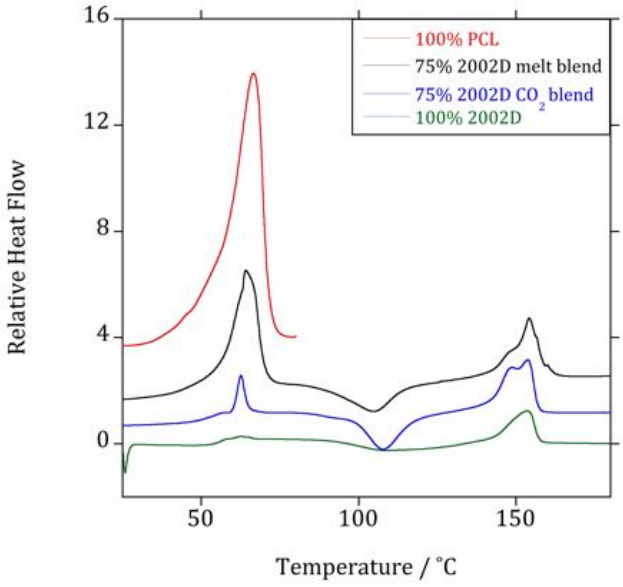

Figure 4.35. Comparison of the 75/25 PLA2002D/PCL blends with and without carbon dioxide and their constituent homopolymers.

At lower heating rates the small and imperfect crystals are able to change successively into more stable crystals as the temperature is increased. Therefore, the melting and recrystallisation process are competing during heating. The endothermic peak appears when the melting process dominates the recrystallisation process. At higher heating rates (examples presented in chapter 5), there is insufficient time for the sample to reorganise and recrystallise into new crystals, thereby supressing this recrystallisation process. The results presented here were obtained at heating rates of 10 ˚C min^{-1}, clearly slow enough for recrystallisation to occur.

Figure 4.35 shows the comparison of the 75/25 PLA2002D/PCL melt blend and blend produced in the presence of carbon dioxide with their constituent homopolymers. It is apparent that the melt blend exhibits a much larger melting endotherm for the PCL component than that observed for the CO_2 assisted blend. The corresponding crystallinity values are 45% for 100% PCL, 34% for the melt blend and 12% for the blend produced in the presence of carbon dioxide. There is a surprisingly low degree of crystallinity in the CO_2 assisted blend and this may be attributed to a reduction in the nucleation density of the sample. This is supported by the finer dispersion of droplets observed in the corresponding sample by SEM. The reduction in crystallinity may be associated with a mechanism called fractionated crystallisation, influenced by a decreased number of nuclei per droplet, the crystallinity of this component sees a drastic reduction [42]. Similar results were observed for PCL/PHB blends, where fractionated crystallisation also occurs in the PCL component. This result was attributed to the dispersion of PCL into isolated droplets, greater in number than the available active heterogeneities usually present in the bulk homopolymer [43].

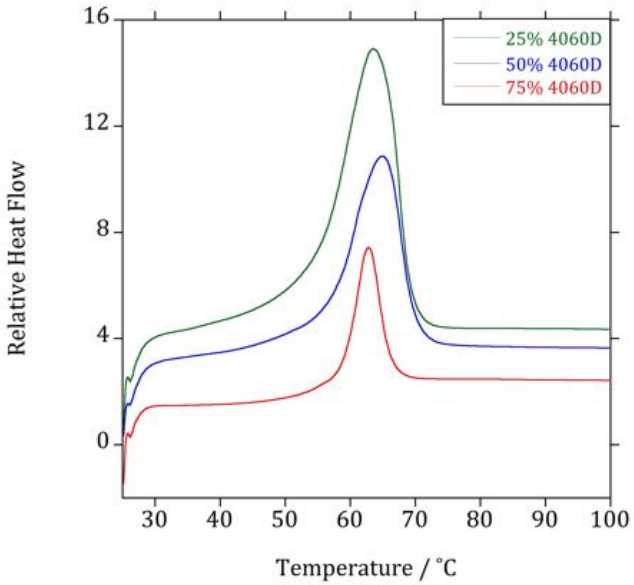

Figure 4.36. Comparison of the PLA4060D/PCL blends produced in the presence of 10% carbon dioxide at 150 °C and 20 rpm.

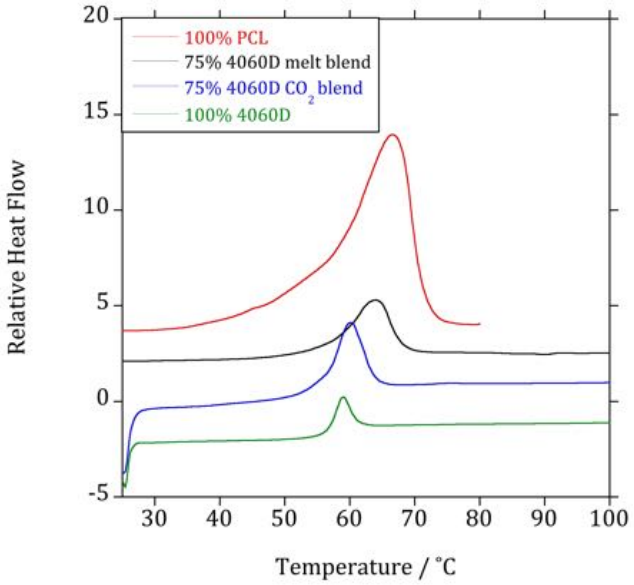

Figure 4.37. Comparison of the 75/25 PLA4060D/PCL blends with and without carbon dioxide and their constituent homopolymers.

A reduction in PCL crystallinity corresponding with decreased droplet size has also been reported in PLLA/PCL blends [44]. Additional to this result (Figure 4.35), the exposure of a glass transition can now be observed in the 75/25 PLA2002D/PCL blend produced in the presence of carbon dioxide. The PLA glass transition midpoint for this blend is measured at 52 ˚C compared to 56 ˚C exhibited by the homopolymer. This reduction does not obey the Fox equation (calculated in chapter 3 as 15 ˚C) however, the slight reduction indicates the presence of partial miscibility.

Figure 4.36 exhibits the PLA4060D/PCL blends produced in the presence of carbon dioxide (10% CO_2 and 20 rpm). Similar to the PLA 2002D blend system, these blends also exhibit a reduction in PCL crystallinity for decreasing PCL content (35, 24 and 14% for 25/75, 50/50 and 75/25 PLA/PCL blends, respectively). The glass transition for PLA cannot be determined due to the overlapping transition corresponding to the melting of PCL. The comparison of the 75/25 PLA4060D/PCL blends produced with and without the presence of carbon dioxide can be seen in Figure 4.37. 100% extruded PCL exhibits a peak melting point at 63 ˚C, this value is also exhibited by the 75/25 PLA/PCL melt blend. However, a reduction of 4 ˚C in the peak melting point of PCL (59 ˚C) is clearly apparent in the 75/25 PLA/PCL blend produced in the presence of carbon dioxide, indicating partial miscibility is present. The calculated relative crystallinity for the PCL components in these blends is 42 and 14% for the melt and CO_2 assisted blend, respectively. This demonstrates that fractionated crystallisation is occurring in the PCL component of the CO_2 assisted blend, resulting in the reduction of crystallinity. This is supported by the presence of a finer dispersion of PCL (as shown by SEM) in this blend, resulting in a reduction in the number of nuclei within each droplet.

4.3.3.6 Size Exclusion Chromatography (SEC)

Size exclusion chromatography (SEC) analysis was carried out on the PLA and PCL homopolymers before and after processing in order to establish any occurrence of thermal degradation. Table 4.6 shows the comparisons of molecular weight measured by SEC on the 'as received' pellets and extruded homopolymers produced with and without the presence of carbon dioxide.

Polymer	**M_w / g mol^{-1}**	**M_n / g mol^{-1}**	**M_w/M_n**
PLA 2002D	193,948	102,602	1.89
PLA 4060D	181,356	95,545	1.90
PCL 6800	212,116	60,859	3.49
PLA 2002D extruded	183,129	75,469	2.43
PLA 4060D extruded	160,730	58,907	2.73
PCL 6800 extruded	220,886	135,079	1.64
PLA 2002D extruded with CO_2	191,819	100,878	1.90
PLA 4060D extruded with CO_2	179,009	94,106	1.90
PCL 6800 extruded with CO_2	218,731	133,454	1.64

Table 4.6. SEC analysis of PLA and PCL homopolymers 'as received' and post extrusion (with and without the presence of carbon dioxide).

Previous research has reported a moderate decrease in molecular weight (M_w) for PLA (117,300 to 82,400 g mol^{-1}) after extrusion, however PCL exhibited very little change (126,100 to 127,900 g mol^{-1}) [45]. This corresponds to the results presented in Table 4.6 where the weight-average molecular weight of both PLA 2002D and 4060D decrease

from 193,948 to 183,129 g mol^{-1} and 181,356 to 160,730 g mol^{-1}, respectively. A broadening of the molecular weight distribution (polydispersity) is also observed for both grades of PLA. At the processing temperatures for PLA, unzipping and chain scission reactions leading to the loss of molecular weight and thermal degradation are known to transpire [46]. The SEC analysis for PCL indicates an increase in molecular weight from 212,116 to 220,886 g mol^{-1}, although this exhibits a greater increase than that found in previous research [45]. It has been reported that an increase in molecular weight in an alternative polyester; poly(-D-β–hydroxybutyric acid) (PHB) is associated with esterification [47]. The rise in molecular weight occurs early in the reaction and is attributed to a reaction between the carboxyl and hydroxyl terminal groups. This results in an increase in the concentration of carboxyl groups formed during the chain scission process and only proceeds until all the carboxyl groups are consumed. This mechanism may explain why a slight increase in molecular weight and decrease in the polydispersity is observed after thermally processing PCL. Consequently, it may add to the higher viscosity seen in the rheology measurements [48] and contribute to the lower crystallinity for the PCL homopolymer and component in the blend [49].

Extruding with carbon dioxide and the associated reductions in viscosity allowed the processing temperature to be decreased from 160 ˚C to 150 ˚C. This lower temperature meant there was a significant prevention in decreasing the molecular weight, compared to processing without carbon dioxide. Both PLA grades exhibited a much smaller decrease in molecular weight processing in the presence of CO_2; approximately 2,000 g mol^{-1} compared to around 10,000 g mol^{-1} (PLA 2002D) and 20,000 g mol^{-1} (PLA 4060D) for processing without CO_2. In addition, the molecular weight distributions are restored to their original values.

4.4 Conclusions

Rheological studies with carbon dioxide indicated both reptation time and activation energy were reduced in PCL upon addition of 60 bar CO_2; a result equivalent to raising the temperature by 20 ˚C in this polymer. This demonstrated carbon dioxide was able to interact with PCL, increasing the free volume and energy required that drives the conformational change for chain reptation. This work was supported through FTIR analysis with a supercritical fluid attachment and showed that carbon dioxide is also interacting with both grades of PLA, demonstrated by a horizontal shift to higher wavenumbers.

Blending in the presence of carbon dioxide exhibited an improvement in blend morphology observed by SEM, indicating a significant reduction in droplet size and dispersion (for example from up to 10 μm in solvent cast blends to 0.2 μm in carbon dioxide assisted blends in the 75/25 PLA2002D/PCL composition). Despite the porosity observed in the blends produced with CO_2, the mechanical properties of numerous blend compositions produced in the presence of carbon dioxide showed an improvement. Applying the model rule of mixtures (assuming perfect adhesion) for the Young's modulus of both melt and CO_2 assisted blends, it was observed that blends produced in the presence of carbon dioxide exhibited greater conformity with the model predictions.

The viscosity ratio calculated at atmospheric pressure and in the presence of carbon dioxide showed that carbon dioxide lowers the viscosity ratio for both 25/75 and 75/25 PLA/PCL compositions.

Analysis using DSC showed a significant reduction in the relative crystallinity of the PCL component for the 75/25 PLA/PCL blends produced in the presence of carbon dioxide,

suggesting that fractionated crystallisation is occurring in the PCL component due to a reduction in nucleation density attributed to a decrease in PCL droplet size. The presence of a depressed PLA T_g and PCL melting point for the 75/25 PLA2002D and 75/25 PLA4060D/PCL CO_2 assisted blends indicated the presence of partial miscibility. FTIR demonstrated that only one carbonyl peak was present for the 75/25 PLA/PCL blends (in contrast to the two inherent corresponding compositional peaks commonly observed). The significant reduction in crystallinity for the PCL component in these blends indicated FTIR was exhibiting the absence of the crystalline band and any presence of the amorphous band would be obscured by the PLA peak. SEC analysis on the 'as received' and extruded homopolymers with and without the presence of carbon dioxide indicated a reduction in molecular weight caused by extruding, however less of a reduction is observed after processing with carbon dioxide. This can be attributed to the ability to process at lower temperatures in the presence of CO_2.

4.5 References

[1] L. H. Sperling, *Introduction to Physical Polymer Science*, Third ed. USA: John Wiley & Sons, 2001.

[2] R. J. Young and P. A. Lovell, *Introduction to Polymers*, 3rd ed. London: CRC Press, 2011.

[3] P. E. Rouse, "A Theory of the Linear Viscoelastic Properties of Dilute Solutions of Coiling Polymers," *The Journal of Chemical Physics,* vol. 21, pp. 1272-1280, 1953.

[4] U. W. Gedde, *Polymer Physics*. London: Chapman & Hall, 1995.

[5] J. M. G. Cowie and V. Arrighi, *Polymers: chemistry and physics of modern materials*, 3rd ed.: CRC Press Taylor & Francis Group, 2008.

[6] P. G. de Gennes, "Reptation of a Polymer Chain in the Presence of Fixed Obstacles," *The Journal of Chemical Physics,* vol. 55, pp. 572-579, // 1971.

[7] M. Rubinstein and R. H. Colby, *Polymer Physics*: Oxford University Press, 2003.

[8] A. E. Likhtman and T. C. B. McLeish, "Quantitative Theory for Linear Dynamics of Linear Entangled Polymers," *Macromolecules,* vol. 35, pp. 6332-6343, 2002/07/01 2002.

[9] D. J. Read, K. Jagannathan, and A. E. Likhtman, "Entangled Polymers: Constraint Release, Mean Paths, and Tube Bending Energy," *Macromolecules,* vol. 41, pp. 6843-6853, 2008/09/23 2008.

[10] S. T. Milner and T. C. B. McLeish, "Reptation and Contour-Length Fluctuations in Melts of Linear Polymers," *Physical Review Letters,* vol. 81, pp. 725-728, 07/20/ 1998.

[11] M. Doi and S. F. Edwards, *The Theory of Polymer Dynamics*. Oxford: Clarendon, 1986.

[12] NIST. (2011). *NIST Chemistry WebBook*. Available: http://webbook.nist.gov/chemistry/fluid/

[13] T. G. Mezger, *The Rheology Handbook*, 3rd ed. Hanover: Vincentz Network, 2011.

[14] H. A. Barnes, *A Handbook of Elementary Rheology*. Wales, UK: The University of Wales Institute of Non-Newtonian Fluid Mechanics, 2000.

[15] T. Annable, R. Buscall, R. Ettelaie, and D. Whittlestone, "The rheology of solutions of associating polymers: Comparison of experimental behavior with transient network theory," *Journal of Rheology (1978-present),* vol. 37, pp. 695-726, 1993.

[16] J. F. Vega, S. Rastogi, G. W. M. Peters, and H. E. H. Meijer, "Rheology and reptation of linear polymers. Ultrahigh molecular weight chain dynamics in the melt," *Journal of Rheology (1978-present),* vol. 48, pp. 663-678, 2004.

[17] N. Noroozi, J. Thomson, N. Noroozi, L. Schafer, and S. Hatzikiriakos, "Viscoelastic behaviour and flow instabilities of biodegradable poly (ε-caprolactone) polyesters," *Rheologica Acta,* vol. 51, pp. 179-192, 2012/02/01 2012.

[18] D. H. S. Ramkumar and M. Bhattacharya, "Steady shear and dynamic properties of biodegradable polyesters," *Polymer Engineering & Science,* vol. 38, pp. 1426-1435, 1998.

[19] J. Gimenez, P. Cassagnau, and A. Michel, "Bulk polymerization of ε-caprolactone: Rheological predictive laws," *Journal of Rheology (1978-present),* vol. 44, pp. 527-547, 2000.

[20] E. Jones Parry and D. Tabor, "Pressure dependence of the shear modulus of various polymers," *Journal of Materials Science,* vol. 9, pp. 289-292, 1974/02/01 1974.

[21] Z. Shen, M. A. McHugh, J. Xu, J. Belardi, S. Kilic, A. Mesiano*, et al.*, "CO2-solubility of oligomers and polymers that contain the carbonyl group," *Polymer,* vol. 44, pp. 1491-1498, 2003.

[22] G. A. Leeke, J. Cai, and M. Jenkins, "Solubility of Supercritical Carbon Dioxide in Polycaprolactone (CAPA 6800) at 313 and 333 K," *Journal of Chemical & Engineering Data,* vol. 51, pp. 1877-1879, 2006/09/01 2006.

[23] Y.-T. Shieh and K.-H. Liu, "The effect of carbonyl group on sorption of CO2 in glassy polymers," *The Journal of Supercritical Fluids,* vol. 25, pp. 261-268, 4// 2003.

[24] S. G. Kazarian, M. F. Vincent, F. V. Bright, C. L. Liotta, and C. A. Eckert, "Specific Intermolecular Interaction of Carbon Dioxide with Polymers," *Journal of the American Chemical Society,* vol. 118, pp. 1729-1736, 1996/01/01 1996.

[25] Y. Yuan and A. S. Teja, "Quantification of specific interactions between CO2 and the carbonyl group in polymers via ATR-FTIR measurements," *The Journal of Supercritical Fluids,* vol. 56, pp. 208-212, 3// 2011.

[26] S. P. Nalawade, F. Picchioni, L. P. B. M. Janssen, D. W. Grijpma, and J. Feijen, "Investigation of the interaction of CO2 with poly (L-lactide), poly(DL-lactide) and poly(ε-caprolactone) using FTIR spectroscopy," *Journal of Applied Polymer Science,* vol. 109, pp. 3376-3381, 2008.

[27] J. R. Fried and W. Li, "High-pressure FTIR studies of gas–polymer interactions," *Journal of Applied Polymer Science,* vol. 41, pp. 1123-1131, 1990.

[28] M. Lee, C. Tzoganakis, and C. B. Park, "Extrusion of PE/PS blends with supercritical carbon dioxide," *Polymer Engineering & Science,* vol. 38, pp. 1112-1120, 1998.

[29] M. Lee, C. Tzoganakis, and C. B. Park, "Effects of supercritical CO2 on the viscosity and morphology of polymer blends," *Advances in Polymer Technology,* vol. 19, pp. 300-311, 2000.

[30] M. D. Elkovitch, D. L. Tomasko, and L. J. Lee, "Supercritical carbon dioxide assisted blending of polystyrene and poly(methyl methyacrylate)," *Polymer Engineering & Science,* vol. 39, pp. 2075-2084, 1999.

[31] C. L. Simões, J. C. Viana, and A. M. Cunha, "Mechanical properties of poly(ε-caprolactone) and poly(lactic acid) blends," *Journal of Applied Polymer Science,* vol. 112, pp. 345-352, 2009.

[32] S. H. Murphy, G. A. Leeke, and M. J. Jenkins, "A Comparison of the use of FTIR spectroscopy with DSC in the characterisation of melting and crystallisation in polycaprolactone," *Journal of Thermal Analysis and Calorimetry,* vol. 107, pp. 669-674, 2012/02/01 2012.

[33] S. Z. D. Cheng and B. Wunderlich, "Thermal analysis of thermoplastic polymers," *Thermochimica Acta,* vol. 134, pp. 161-166, 10// 1988.

[34] S. Z. Cheng, M. Cao, and B. Wunderlich, "Glass transition and melting behavior of poly (oxy-1, 4-phenyleneoxy-1, 4-phenylenecarbonyl-1, 4-phenylene)(PEEK)," *Macromolecules,* vol. 19, pp. 1868-1876, 1986.
[35] B. B. Sauer, W. G. Kampert, E. Neal Blanchard, S. A. Threefoot, and B. S. Hsiao, "Temperature modulated DSC studies of melting and recrystallization in polymers exhibiting multiple endotherms," *Polymer,* vol. 41, pp. 1099-1108, 2// 2000.
[36] P. J. Holdsworth and A. Turner-Jones, "The melting behaviour of heat crystallized poly(ethylene terephthalate)," *Polymer,* vol. 12, pp. 195-208, 3// 1971.
[37] M. Yasuniwa, S. Tsubakihara, and T. Fujioka, "X-ray and DSC studies on the melt-recrystallization process of poly(butylene naphthalate)," *Thermochimica Acta,* vol. 396, pp. 75-78, 2003.
[38] M. Todoki and T. Kawaguchi, "Origin of double melting peaks in drawn nylon 6 yarns," *Journal of Polymer Science: Polymer Physics Edition,* vol. 15, pp. 1067-1075, 1977.
[39] Y. Wang and J. F. Mano, "Multiple melting behaviour of poly(l-lactide-co-glycolide) investigated by DSC," *Polymer Testing,* vol. 28, pp. 452-455, 2009.
[40] M. Yasuniwa, S. Tsubakihara, Y. Sugimoto, and C. Nakafuku, "Thermal analysis of the double-melting behavior of poly(L-lactic acid)," *Journal of Polymer Science Part B: Polymer Physics,* vol. 42, pp. 25-32, 2004.
[41] B. Wunderlich, *Macromolecular Physics* vol. 3. London: Academic Press, 1980.
[42] L. A. Utracki, *Polymer Blends* vol. 11: Rapra Technology, 2000.
[43] D. Lovera, L. Márquez, V. Balsamo, A. Taddei, C. Castelli, and A. J. Müller, "Crystallization, Morphology, and Enzymatic Degradation of Polyhydroxybutyrate/Polycaprolactone (PHB/PCL) Blends," *Macromolecular Chemistry and Physics,* vol. 208, pp. 924-937, 2007.
[44] N.-S. Choi, C.-H. Kim, K. Y. Cho, and J.-K. Park, "Morphology and hydrolysis of PCL/PLLA blends compatibilized with P(LLA-co-ϵCL) or P(LLA-b-ϵCL)," *Journal of Applied Polymer Science,* vol. 86, pp. 1892-1898, 2002.
[45] R. Dell'Erba, G. Groeninckx, G. Maglio, M. Malinconico, and A. Migliozzi, "Immiscible polymer blends of semicrystalline biocompatible components: thermal properties and phase morphology analysis of PLLA/PCL blends," *Polymer,* vol. 42, pp. 7831-7840, 8// 2001.
[46] D. Garlotta, "A Literature Review of Poly(Lactic Acid)," *Journal of Polymers and the Environment,* vol. 9, pp. 63-84, 2001.
[47] N. Grassie, E. J. Murray, and P. A. Holmes, "The thermal degradation of poly(-(d)-β-hydroxybutyric acid): Part 3—The reaction mechanism," *Polymer Degradation and Stability,* vol. 6, pp. 127-134, // 1984.
[48] M. P. Grosvenor and J. N. Staniforth, "The effect of molecular weight on the rheological and tensile properties of poly(ϵ-caprolactone)," *International Journal of Pharmaceutics,* vol. 135, pp. 103-109, 6/17/ 1996.
[49] M. J. Jenkins and K. L. Harrison, "The effect of molecular weight on the crystallization kinetics of polycaprolactone," *Polymers for Advanced Technologies,* vol. 17, pp. 474-478, 2006.

CHAPTER 5 – FLASH DSC

5.1 Flash DSC

5.1.1 Background on the experimental technique

The Flash DSC (Figure 5.1) is a relatively new thermal analysis instrument, commercially available from Mettler Toledo in October 2010 [1]. It is a fast scan, power-compensation DSC, utilising a chip sensor (Figure 5.2) based on MEMS (micro-electro-mechanical systems) technology, requiring extremely small sample sizes. Conventional DSCs, like that discussed in chapter 2, have heating and cooling scanning rates typically up to 60 ˚C min^{-1} (3,600 ˚C s^{-1}) with the capability to accept samples masses between 0.1 mg and 100 mg. A standard polymer sample however, is usually around 5 mg. In contrast, typical sample masses required for experimentation in the Flash DSC are between 100 ng and 10 μg. The Flash is capable of scanning at rates up to 40,000 ˚C s^{-1} on heating and up to 4,000 ˚C s^{-1} on cooling [2].

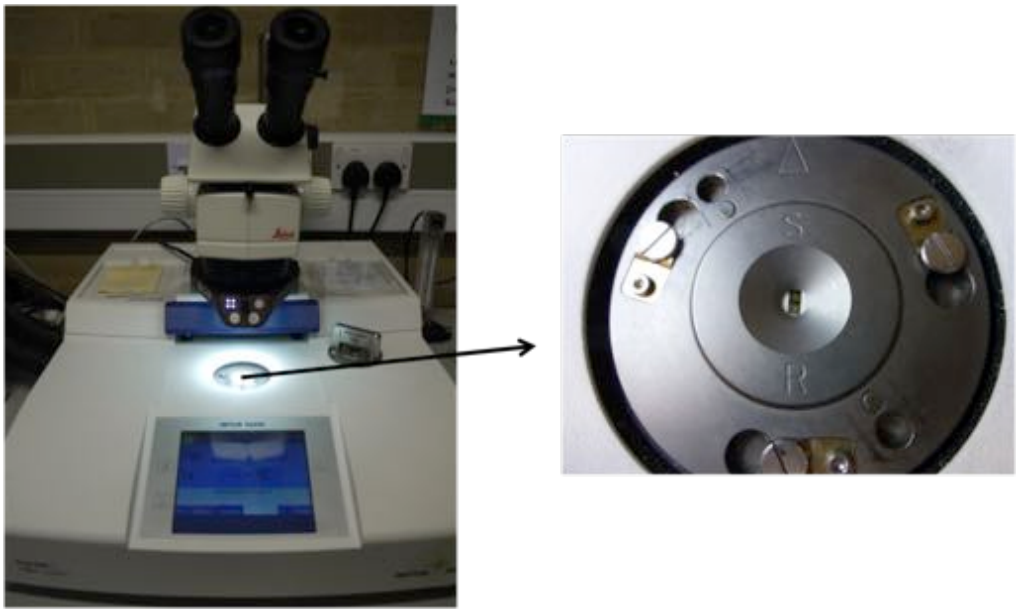

Figure 5.1. Mettler Toledo Flash DSC 1.

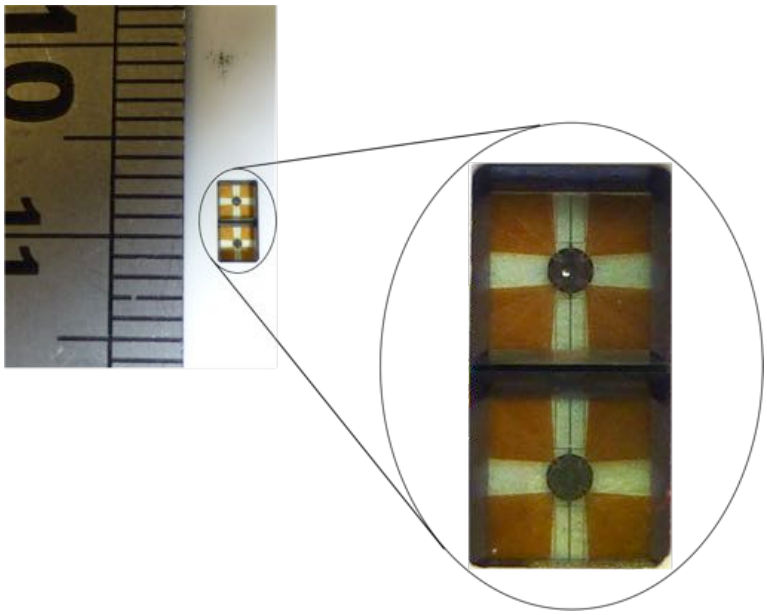

Figure 5.2. Mettler Toledo Flash DSC 1 chip sensor.

5.1.2 The Flash DSC chip sensor

A schematic cross-section of the UFS1 chip sensor can be seen in Figure 5.3. The dimensions of the UFS1 Flash DSC chip sensor are 5.0 x 3.3 x 0.3 mm mounted on a ceramic base plate (24 x 24 x 0.6 mm) with 14 connection sites using wire bonding (as seen in Figure 5.4) [1]. Like conventional DSC, the Flash DSC chip sensors also have sample and reference segments (Figure 5.5) consisting of twin silicon nitride membranes (about 2 µm thick) with an active zone (sample area) that is 0.5 mm in diameter. This sample area is coated with approximately 0.5 µm of aluminum in order to provide a uniform temperature across this region. The sample area temperature is measured using a thermopile consisting of 8 poly-silicon thermocouples. Two heating resistors are also situated within the sample area, a main heater maintains the desired temperature, and a compensation heater that compensates the temperature differences between the sample and reference cells.

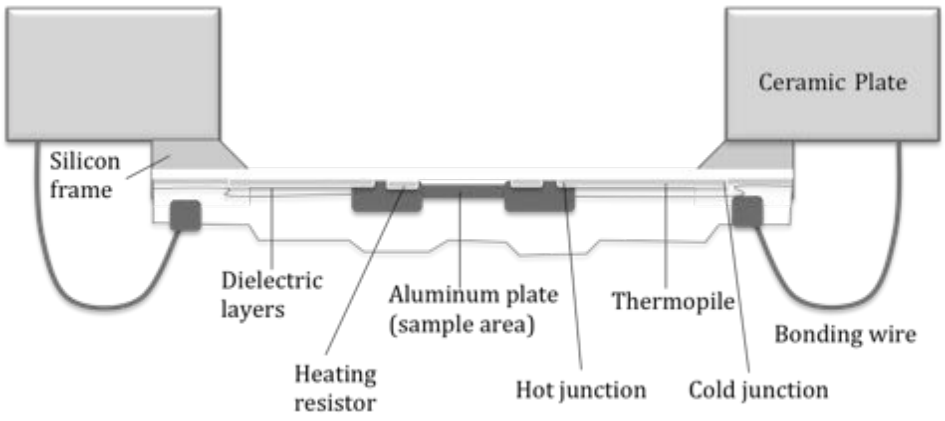

Figure 5.3. Cross-section schematic of the UFS1 Flash DSC chip sensor and ceramic base plate [1].

Prior to the Flash DSC, Perkin Elmer [3] developed a technique based on conventional DSC (without MEMS technology) called the HyperDSC (reaching scanning rates up to 45,000 ˚C s^{-1}). Perkin Elmer subsequently released a second-generation HyperDSC, commercially available as the DSC 8500. Following this, TA instruments released the RHC calorimeter which operates at rates up to 120,000 ˚C s^{-1} [4]. Both Perkin Elmer and TA instruments require sample masses between 1 μg and 1 mg. Due to the small sample masses, these fast scanning calorimeters allow polymers (and metals) to be analysed under fast heating and cooling rates with minimal thermal lag. Heating rates in conventional DSC instruments are not high enough to prevent reorganisation processes in certain partially crystalline polymers that possess fast crystallisation kinetics, or meta-stable crystallinity, for example; polyether ether ketone (PEEK) or poly(ε-caprolactone) (PCL). Therefore, Flash DSC enables investigation of the reorganisation and formation of structure on heating and cooling, measurement of crystallisation kinetics at a wide range of cooling rates and simulation of technical cooling processes at

the corresponding cooling rate.

5.1.3 Method

A Mettler Toledo Flash DSC1 [5] was used to conduct fast heating and cooling experiments, which were subsequently analysed using the STARe software (version 11). The Flash DSC was connected to a T-100 intracooler allowing operation between -100 ˚C and 450 ˚C.

Each chip sensor has a unique identification number (e.g. XEN W11 23741) as illustrated in Figure 5.4, including its individual set of calibration data to be imported prior to experimenting. Electronic calibration has been performed by the manufacturer of the sensors (Xensor Integration, Netherlands) [6]. Following chip sensor selection, and before sample preparation, the sensor undergoes a number of 'conditioning' cycles, heating and cooling from 45 ˚C to 450 ˚C. Satisfied the sensor is behaving in the correct manner, with a linear and reproducible baseline, a 'correction' method is applied to the sensor. This method heats the chip sensor in stepped isothermal segments, covering the temperature range of the instrument. The correction performs a calibration of the thermopile and the difference in temperature at the cold-junction. The sample support temperature programmed for the instrument to maintain is recorded during the correction method. Consequently, all subsequent experiments performed using this chip sensor must be performed at the corresponding sensor support temperature.

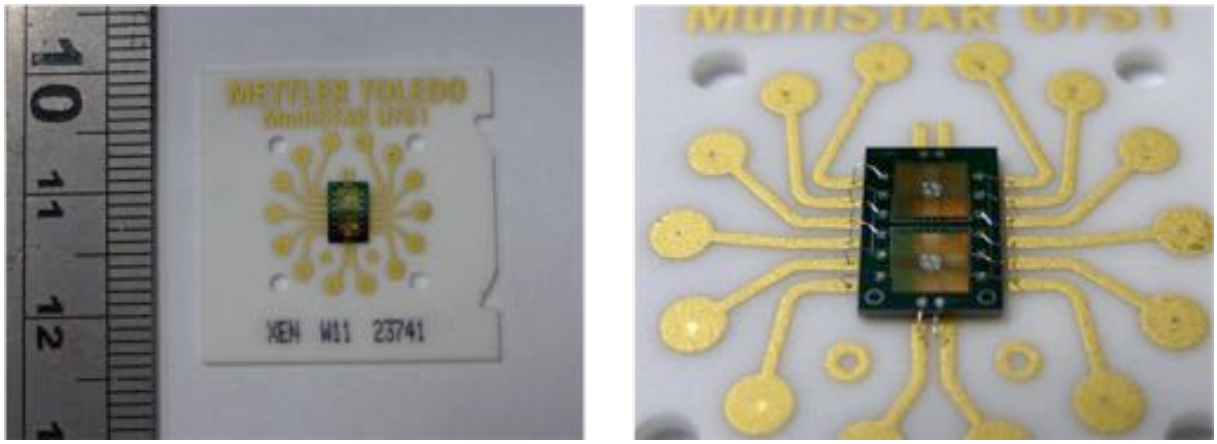

Figure 5.4. The underside of the Mettler Toledo Flash DSC 1 chip sensor, illustrating the unique chip identification number. The right image shows the 14 connection sites using bonding wire.

Due to the nature and small scale of the Flash DSC, sample preparation can be extremely time consuming. Those samples that were not powders needed to be microtomed as thinly as possible, and subsequently cut smaller with a scalpel under the Flash microscope. Once the sample was small enough, it was applied using a single human hair to the centre of the sample side of the chip sensor (as indicated in Figure 5.5). As with conventional DSC, the reference side of the sensor is left empty. However, a calibration substance can be applied to the reference at the end of a set of experiments in order to check the calibration of the chip sensor. The Flash DSC was connected to a cylinder of argon, regulated with a flow meter set between 20 and 50 mL min^{-1}. The gas is the cooling mechanism for the instrument, and by using the intracooler, creates an extremely cool environment around the sensor, enabling quenching of samples at rates up to 20,000 ˚C sec^{-1}. It also purges the instrument, preventing internal ice formation due to the extremely cold temperatures employed when experimenting.

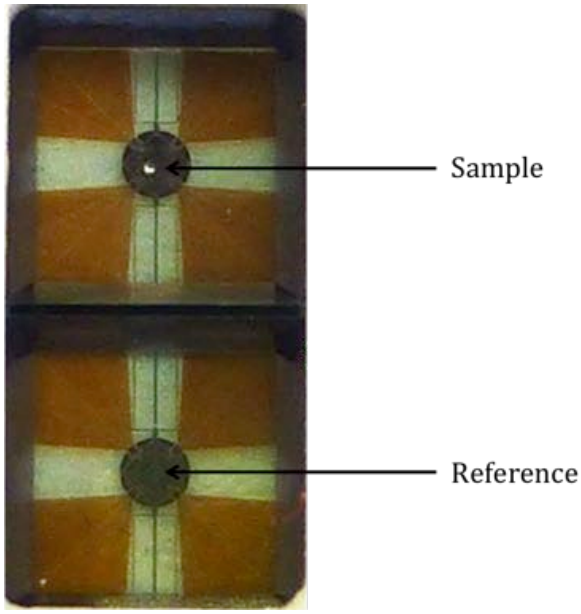

Figure 5.5. Mettler Toledo Flash DSC 1 chip sensor sample and reference segments, indicating the 'active' furnace areas.

Once the sample was in place, a slow heating rate was applied to the chip, heating to temperatures above the melting point or glass transition (depending on the morphology of the polymer) in order for the sample to make good contact with the surface of the sensor. The heating rate applied (usually at 1 $^{\circ}C\ s^{-1}$) prevented the sample from 'jumping' off the sensor; this commonly occurred with faster rates. It is important to reduce the sample height (influencing thermal lag) as much as possible. This can be done once the sample is in the melt, using a hair to 'smear' the sample thinly across the active furnace area. Throughout the series of measurements, samples were frequently cooled and reheated at 100 $^{\circ}C\ s^{-1}$ as a reference rate, to check their stability and any indication of degradation.

5.2 Materials and methods

5.2.1 Materials

5.2.1.1 Poly(ε-caprolactone)

Poly(ε-caprolactone) (PCL) grade 6800 was supplied in pellet form by Perstorp Caprolactones (Warrington, UK). Details on this polymer is presented in chapter 2.

5.2.1.2 Poly(lactic acid)

Poly(lactic acid) grades 3051D, 2002D and 4060D were supplied in pellet form by Natureworks LLC (Nebraska, USA). Detailed information on PLA 2002D and 4060D grades are presented in chapter 2. PLA 3051D is partially crystalline with a molecular weight of 151,000 g mol^{-1}. It exhibits a glass transition around 60 ˚C and a peak melting temperature at 156 ˚C. A comparison of the different PLA grades can be seen in Table 5.1.

	PLA 3051D	**PLA 2002D**	**PLA 4060D**
T_g °C	60	55	52
T_m °C	156	154	-
T_c °C (onset)	-	-	-
% crystallinity	39	37	-
M_w	151,000	194,000	181,000
D-lactide content (wt %)	3.3	4*	11-13**
		*[7]	**[8]

Table 5.1. A comparison of the properties of PLA grades 3051D, 2002D and 4060D.

5.2.1.3 Polyetherimide

Polyetherimide (PEI), commercial grade Ultem 1000 was supplied by Gilbert Curry Industrial plastics co. Ltd (Coventry, UK) in sheet form. Ultem 1000 is an amorphous polymer with a molecular weight around 39,000 g mol^{-1} [9] and a T_g of 220 ˚C.

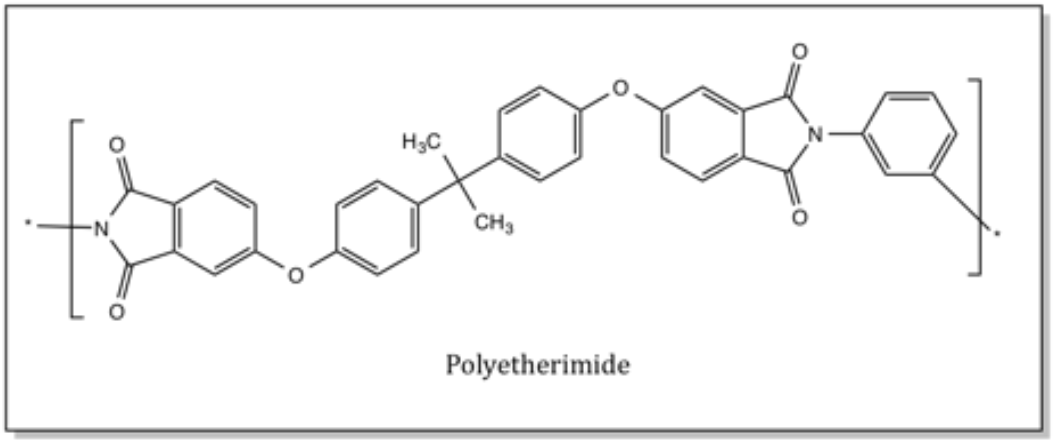

Figure 5.6. The chemical structure of polyetherimide.

5.2.1.4 Poly(ether-ether-ketone)

Poly(ether-ether-ketone) (PEEK) grade 150 PF was supplied by Victrex (Lancashire, UK) in fine powder form. It has a peak melting and crystallisation temperature of 344 ˚C and 295 ˚C respectively. The relative crystallinity is around 38% with a weight average molecular weight of 26,800 g mol^{-1} [10].

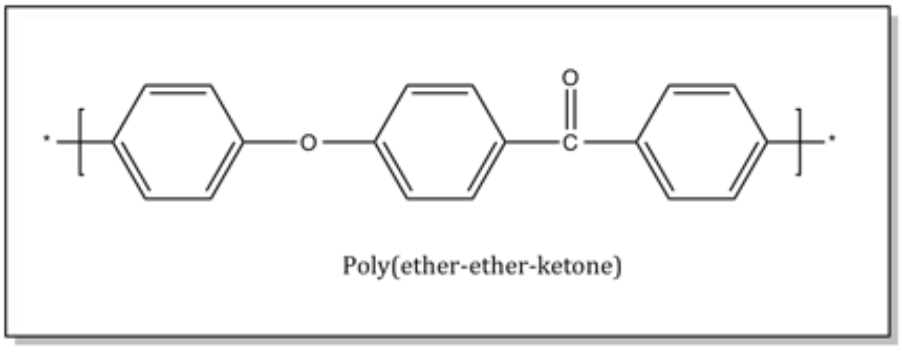

Figure 5.7. The chemical structure of poly(ether-ether-ketone).

5.2.1.5 Indium

Indium was supplied by Mettler Toledo (Leicestershire, UK) and is 99.999% pure. Indium has a specific melting onset of 156.6 ˚C.

5.2.2 Methods

5.2.2.1 Chip conditioning

As mentioned in the introduction, prior to sample preparation, the empty chip sensors must be subjected to 2 or 3 'conditioning' runs, a method pre-set into the software, that heats and cools the sensor from 45 ˚C to 450 ˚C. Observations of the chip sensor's behaviour can indicate the presence of any abnormalities, suggesting a faulty chip. Figure 5.8 demonstrates the ideal response of a chip sensor. Heating and cooling exhibit symmetrical traces with no unusual abnormalities. However, Figure 5.9 displays the response of a chip sensor that would subsequently be discarded from experimental measurements due to the presence of large 'spikes' in the trace. These spikes represent that an electrical malfunction is present in this chip sensor and these abnormalities would therefore also occur during sample measurements.

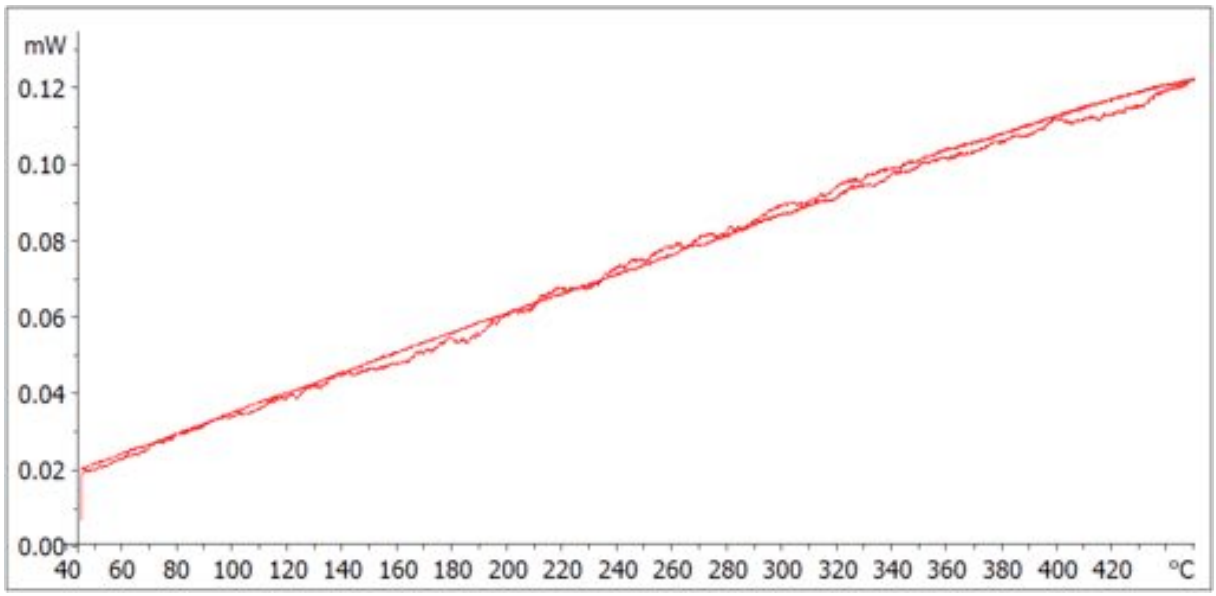

Figure 5.8. The heating and cooling cycle (45 to 450 ˚C) of chip sensor conditioning. This trace represents a typical chip sensor response, indicating that the chip can be used for experimental measurements.

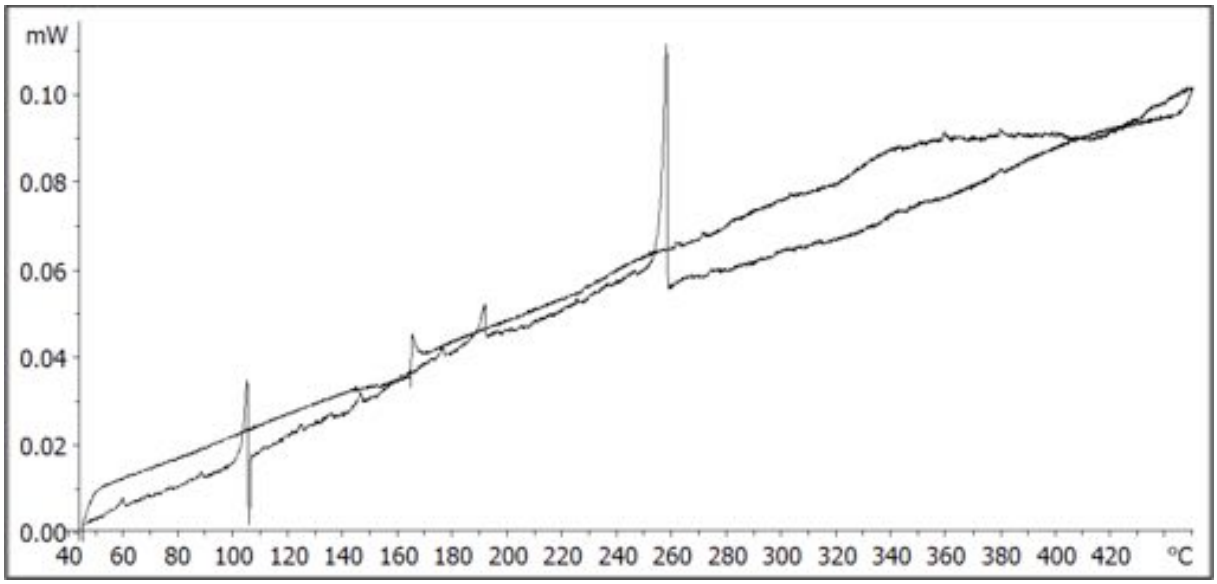

Figure 5.9. The heating and cooling cycle (45 to 450 ˚C) of chip sensor conditioning. This trace represents a faulty chip sensor response, indicating that the chip should be discarded from further use.

5.2.2.2 Effect of heating rate and thermal lag on the melting onset of indium

To investigate the influence of heating rate on thermal lag using Flash DSC, a small slice of indium was prepared onto the sample side of a chip sensor. The indium sample was melted to make contact with the chip by heating from 25 to 170 ˚C at 1 ˚C s^{-1}, (a slower rate is initially selected to prevent the sample from 'jumping' off the sensor). Once melted and in good contact with the surface of the sensor, a cyclic method is applied where the sample is heated from 25 to 350 ˚C from 0.05 ˚C s^{-1} through to 10,000 ˚C s^{-1}. The sample was cooled to 25 ˚C at a fixed rate of 100 ˚C s^{-1}. At each temperature extreme, an isothermal of 0.1 seconds was applied. The melting onset was measured for each melting endotherm corresponding to the different heating rates and plotted in graphical form. To accommodate for the large range of heating rates, the horizontal axis is displayed logarithmically.

Increasing scanning rates corresponds with more apparent and obvious changes in heat flow, therefore the endothermic and exothermic events are also increased in size [11, 12]. The heat flow equation is expressed in Equation 5.1 as:

$$Q = m \times C_p \times \beta \qquad \text{Equation 5.1}$$

where Q is the heat flow, m is the sample mass, C_p is the specific heat and β is the heating rate. In some instances in this chapter, where the comparison of a variety of heating or cooling rates are presented, the traces have been normalised so that the influence of increasing the scanning rate on the sample can be observed without interference from the increasing heat flow.

5.2.2.3 Identification of the heating and cooling rates to prevent crystallisation in poly(ε-caprolactone)

PCL was chosen as a model polymer to investigate and explore the different capabilities of the Flash DSC. An extremely small sample was prepared on to the chip sensor using a microscope and a single synthetic hair. The sample was then heated from 25 to 100 ˚C heating rate of 1 ˚C s^{-1} with an isothermal of around 20 seconds in the melt. During the isothermal, the sample is spread across the sensor surface with a thick human hair. The smearing / spreading of the polymer reduces the sample height (reducing thermal lag) and distributes a more even contact across the sensor surface.

Due to the relatively fast crystallisation kinetics of PCL [13], the cooling rate to suppress crystallisation, resulting with an amorphous sample, was investigated. This was carried out by fixing the heating rate to 100 ˚C s^{-1} from -80 ˚C to 80 ˚C. An isothermal of 0.1 seconds was applied between heating and cooling. The sample was then subjected to various cooling rates, incrementally increasing until the crystallisation exotherm was no longer observed. Once established, the cooling rates and window where crystallisation ceases were then 'finely tuned' to more accurately refine the specific cooling rate. The cooling rate required to prevent crystallisation in PCL was then used to identify the heating rate that will suppress cold crystallisation on the reheat. In a similar experiment to that previously described, PCL was subjected to a fixed cooling rate whilst varying the heating rates until cold crystallisation was no longer observed.

5.2.2.4 Determination of the activation energy of T_g

In contrast to PCL, the partially crystalline grades of PLA (3051D and 2002D) have extremely slow crystallisation kinetics [14, 15] and will not crystallise within the timescales of conventional DSC (e.g. 10 ˚C min^{-1}). Therefore, once the 'as received' samples have passed through the melt, these polymers will remain amorphous.

Sample preparation of amorphous polymers onto chip sensors were typically more challenging than partially crystalline samples. Dependent upon their melt viscosity, amorphous polymers do not necessarily 'flow', therefore the samples need to be taken to an elevated temperature, significantly above their glass transition temperatures (around 50-100 ˚C higher) in order to allow the samples to make sufficient contact with the sensors. Therefore the process of spreading the sample with a human hair needed to be conducted quickly to prevent the occurrence of thermal degradation.

All grades of PLA were subjected to the same heating and cooling rates using the Flash DSC. The samples were heated and cooled between -50 to 100 ˚C with a 0.1 s isothermal applied after each heat and cool. Cooling rates were between 50 and 600 ˚C s^{-1} with a constant reheat of 100 ˚C s^{-1}. The amorphous grade of PLA 4060D was also investigated using conventional DSC in order to subject the polymer to comparatively slower cooling rates. The sample was heated and cooled between 25 and 100 ˚C, cooled at 0.1, 1 and 10 ˚C min^{-1} and reheated at 10 ˚C min^{-1}. An isothermal of 2 minutes was applied between each heat and cool.

A comparison of the different grades of PLA was conducted through the investigation into the activation energy of the glass formation. Arrhenius plots of the reciprocal T_g of each grade of PLA against the logarithm of the cooling rate was used to calculate the activation energy.

An alternative amorphous polymer, polyetherimide (PEI - Ultem 1000) was also studied over an extensive range of cooling rates, from extremely slow rates in a conventional DSC at 0.008 ˚C s^{-1} (0.5 ˚C min^{-1}) to considerably faster rates in the Flash DSC at 400˚C s^{-1}. The heating rate was fixed at 10 ˚C min^{-1} and 100 ˚C s^{-1} for conventional and Flash DSC respectively. Isothermals of 2 minutes (DSC) and 0.1 s (Flash DSC) were applied between each heat and cool. These rates were chosen in accordance to the typical capabilities of each instrument. The sample was heated and cooled from 150 to 270 ˚C and 25 to 300 ˚C for DSC and Flash DSC respectively. To examine the effect of the cooling rate upon the glass formation, the T_g on the succeeding heat is measured. An Arrhenius plot of the logarithm of the cooling rate against the reciprocal T_g of Ultem 1000 was used to calculate the activation energy.

5.2.2.5 Characterisation of poly(ether-ether-ketone) using chip calorimetry

Another polymer possessing fast crystallisation kinetics [16] is poly(ether-ether-ketone). This polymer was supplied as a powder and therefore no sample preparation (microtoming and cutting) was required. Using the synthetic hair, a small amount of powder was collected and deposited into the centre of the chip sensor. To melt the powder onto the chip, it was heated at 1 ˚C s^{-1} from 25 to 400 ˚C to make an initial melt contact with the sensor. Subsequent measurements were conducted between 25 to 400 ˚C with isothermals of 0.1 s after each heat and cool. Cooling rate was varied and the heating rate was kept constant at 100 ˚C s^{-1}.

5.2.2.6 Estimation of sample mass

In order to calculate the relative crystallinity of a sample using calorimetry, there must be a known sample mass to provide an accurate reading for the enthalpy of fusion (ΔH_f), the area under the melting peak. The samples prepared for the Flash DSC, are too small and cannot be weighed using a balance. Therefore, in order to calculate the sample mass when using Flash DSC, an alternative method can be employed. The capabilities of both conventional DSC and Flash DSC overlap, enabling the application of identical cooling rates to develop the same crystallinity providing the material is homogeneous and isotropic [17]. It is also assumed that the contrasting sample dimensions and masses do not instigate differences in crystallisation behaviours. Therefore, if the crystallinities of both samples are equal, so must the specific enthalpies of melting for both conventional and Flash DSC:

$$\Delta h_{DSC} = \Delta h_{FDSC} \qquad \text{Equation 5.2}$$

Using a quantified mass of the same material, the sample should be subjected to a heat and cool in a conventional DSC using a heating rate that the Flash is able to replicate. Samples in both techniques were cooled at 30 °C min^{-1} to establish a thermal history. The cooling rate must provide sufficient time for the polymers to crystallise so that no cold crystallisation occurs upon heating. They were subsequently heated at typical rates associated with each technique, 20 °C min^{-1} and 100 °C s^{-1} for conventional DSC and Flash DSC, respectively. The specific enthalpy of melting, Δh (J g^{-1}) and ΔH_{FDSC} (J) is determined from the melting peak using conventional DSC and Flash DSC, respectively.

The sample mass is calculated from Equation 5.3:

$$m = \frac{\Delta H_{FDSC}}{\Delta h} \qquad \text{Equation 5.3}$$

For an amorphous sample, the step height of the specific heat capacity, $\Delta C_{p,}$ was established by measuring the glass transition of the polymer. This value can be used to determine the sample mass. Similarly to the process for a partially crystalline sample, the amorphous sample is also characterised by conventional DSC, so that the ΔC_p is established. Then, for the Flash DSC measurement, a sample mass of 1 ng is entered. Therefore, evaluation of the glass transition exhibited by Flash DSC yields an apparent specific heat capacity change of ΔC_{pa}. The true sample mass can then be obtained from Equation 5.4:

$$m = \frac{\Delta C_{pa}}{\Delta C_p}\ 1\ \text{ng} \qquad \text{Equation 5.4}$$

Alternatively, if the glass transition cannot be measured using conventional DSC, the ΔC_p values can be obtained from the ATHAS data bank [18]. It is important to keep sample mass less than 500 ng [19] for measurements with the Flash DSC. Applying a sample mass that is too great or a scanning rate that is too high, thermal lag increases beyond acceptable values [4]. Alternatively, when concerned with the sensitivity of the machine, in order to achieve a heat flow rate signal sample masses and scanning rates must be sufficiently high enough.

5.2.2.7 Chip calibration

Within a batch of chips produced, a small number of randomly selected chip sensors are pre-calibrated using an electrical method during manufacturing [6]. This provides an indicative temperature calibration for all chip sensors in this batch. On another small number of chip sensors, the measurements of the onset temperatures of adamantane, indium, tin and zinc are then used to determine the accuracy of the electrical pre-calibration. This combination of calibration procedures covers the temperature range of -65 to 450 ˚C with a typical maximum error of ±5 ˚C [6].

The factory calibration can be checked in the laboratory following experimental measurements with each chip sensor using the melting onset of standard reference materials. For this work, indium was used to check the temperature calibration. A small sample of indium is placed on the reference side of the chip and run at a relatively slow heating rate (0.5 ˚C s^{-1}). The onset of melting can be measured and corresponding adjustments can be applied to results obtained from this chip sensor only.

5.2.2.8 Machine characterisation – performance check

Inert purge gas is used in the operation of the Flash DSC in order to avoid any condensation of water from the environment and prevent possible oxidative degradations. Additionally, it enhances the heat transfer between sensor and surroundings. Argon, nitrogen and helium are purge gases commonly employed in thermal analysis techniques and the gas selected has quite an important influence on the performance of fast scanning calorimeters [4].

Vanden Poel *et al.* characterise their Flash DSC using nitrogen and helium [17]. They show that nitrogen is superior for heating, demonstrating that the scan rates are achieved across a greater range of temperatures. However, the temperature ‘operating

window' (where scan rates are achieved) strongly depends upon the cooling rate. In contrast, helium improves the cooling capability, enabling scan rates to be achieved at lower temperatures. Helium possesses higher heat conductivity compared to nitrogen and may be used when an increased heat transfer is required. These authors also investigate a variety of flow rates (1, 10 and 20 mL min^{-1}) for both gases. They found that flow rate does not influence the performance of the Flash DSC when using nitrogen, but increasing the flow rate when using helium, shifts the 'window-to-operate' to lower temperatures. Therefore, the maximum temperature of the machine can only be met with helium at a flow rate of 1 mL min^{-1}. They conclude by recommending using nitrogen (with a flow rate of 20 mL min^{-1}) as the purge gas for the Flash DSC due to the drawbacks of a reduced operating temperature window seen with helium.

For the measurements presented in this thesis, argon was selected as the purge gas and therefore the machine capabilities using argon were established. The flow rate of argon was set to 20 mL min^{-1} and scanning rates between 1,000 and 20,000 ˚C s^{-1} were employed to an empty chip sensor covering the temperature limitations of the machine (from -90 to 450 ˚C).

In order to establish the performance of the Flash DSC, the following steps were implemented: A variety of heating and cooling rates are programmed into a method and an empty chip sensor is subjected to this method. The four steps below correspond to the steps presented in Figure 5.10 and Figure 5.11.

- Upon evaluation of the results, the heating and cooling traces are plotted in mW versus time (in seconds) to establish how the heat flow changes per unit time (Step 1 in Figure 5.10).

- Each individual curve is then converted to sample temperature to provide a plot of sample temperature variation (˚C) versus time (seconds). (Step 2 in Figure 5.10).
- Using these results, the 1st derivative is derived for each curve providing an overall plot of the change in scanning rate as a function of time. (Step 3 in Figure 5.11).
- Finally, each individual curve is re-plotted to give the performance of the machine; scanning rate as a function of temperature. (Step 4 in Figure 5.11).

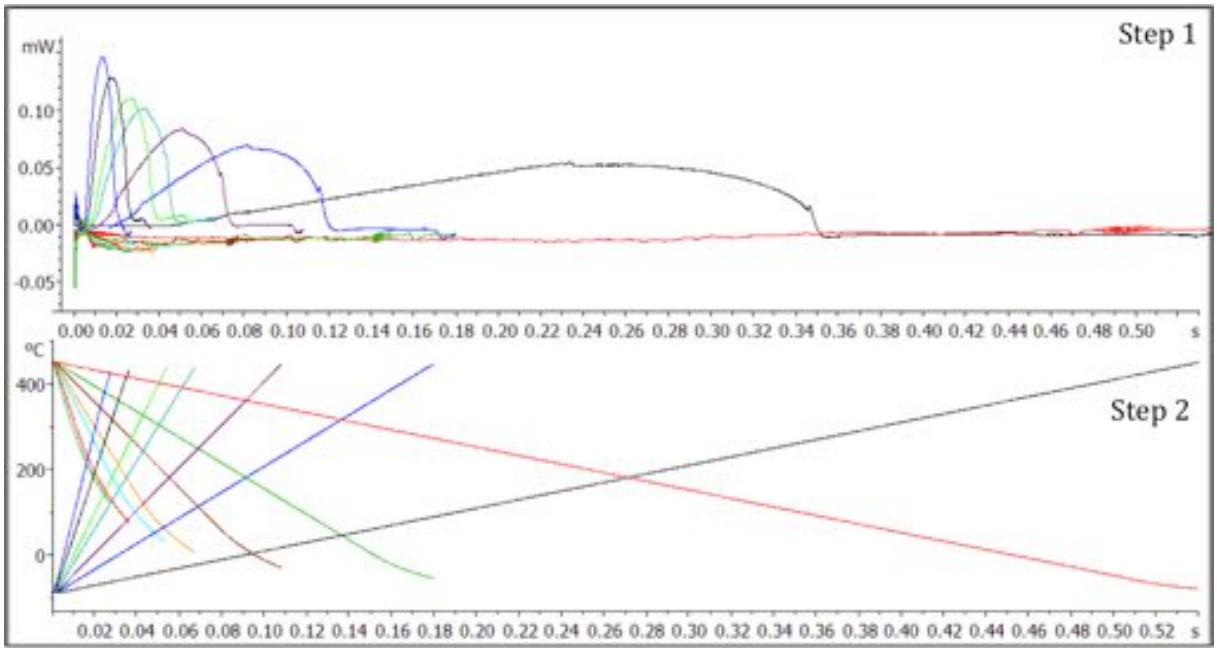

Figure 5.10. First two steps of the procedure to determine the performance of the Flash DSC over a variety of scanning rates between -90 and 450 ˚C.

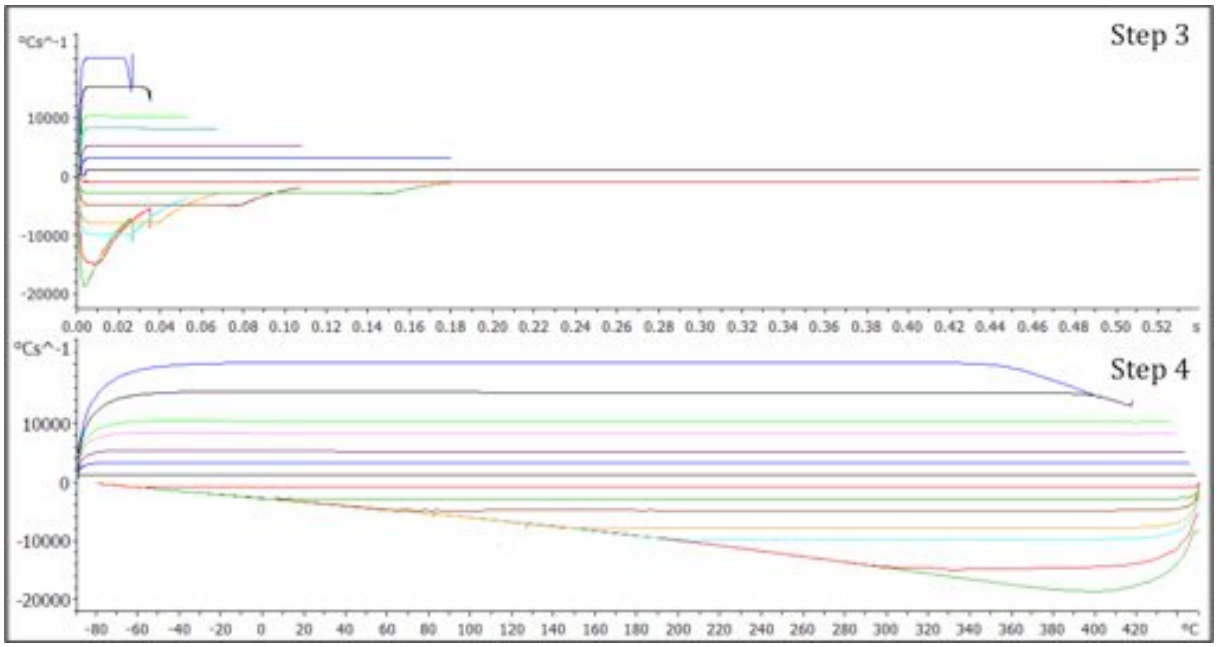

Figure 5.11. Final two steps of the procedure to determine the performance of the Flash DSC over a variety of scanning rates between -90 and 450 ˚C.

Figure 5.12 illustrates the performance of the Flash DSC using argon as a purge gas. It is apparent that the Flash DSC is able to control the heating rates across the entire temperature range at 1000 ˚C s^{-1}. The maximum programmed temperature of 450 ˚C can be achieved for heating rates up to 10,000 ˚C s^{-1}. Rates 15,000 and 20,000 ˚C s^{-1} reach maximum temperatures of 400 and 345 ˚C, respectively. Both these rates exhibit an overall narrower operating window, reaching starting temperatures of -60 ˚C when the rate is 15,000 ˚C s^{-1} and -45 ˚C for 20,000 ˚C s^{-1} instead of the programmed -90 ˚C.

The operating window appears to demonstrate a more significant dependency upon cooling rates. In particular, the operating window is restricted to the higher temperatures and a narrower temperature range is achieved corresponding to faster rates. For example 15,000 ˚C s^{-1} exhibits a operating window of approximately 120 ˚C temperature range. Therefore, the lower temperatures are not achieved for the majority of cooling rates investigated.

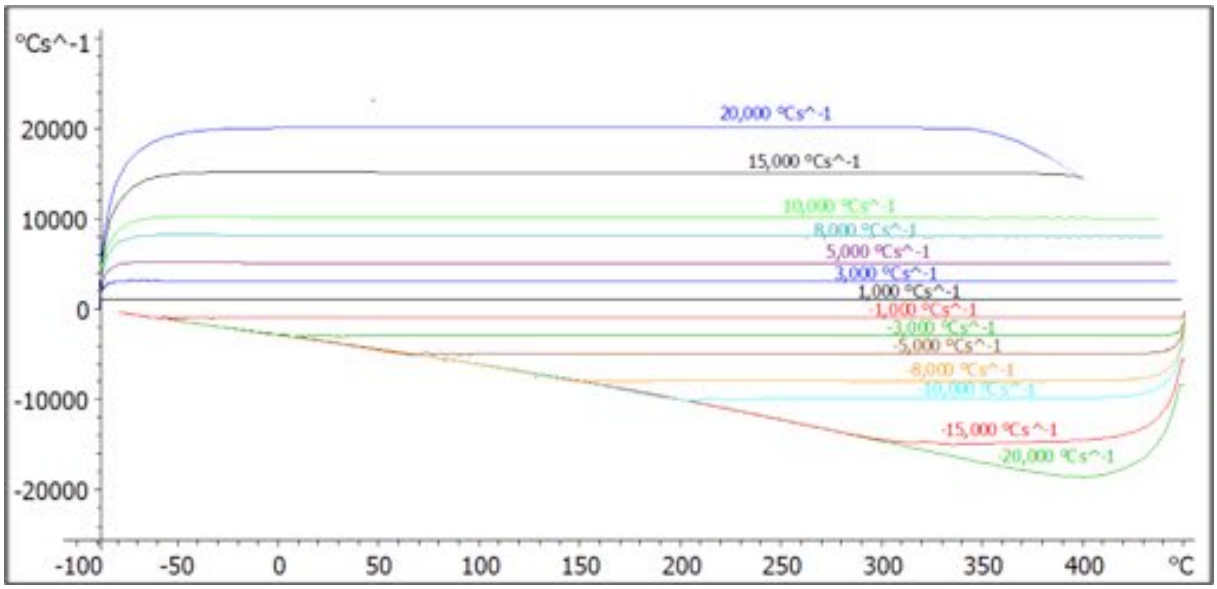

Figure 5.12. The performance of the Flash DSC between -90 ˚C and 450 ˚C using argon as a purge gas at 20 mL min^{-1}.

In comparison to the results obtained by Vanden Poel *et al.* for helium [17], argon shows a superior heating capability and is therefore able to reach much higher temperatures upon heating. Despite helium being able to achieve lower temperatures upon cooling, it exhibits similar or narrower operating windows in comparison to argon. For example, heating at 20,000 ˚C s^{-1} using helium as a purge gas, the temperature range achieved is -50 to 200 ˚C in comparison to -45 to 345 ˚C with argon. Cooling at 15,000 ˚C s^{-1} achieves an operating window with helium of 125 to 275 ˚C, whereas the operating window for argon is from 300 to 420 ˚C. Comparing the performance of the machine using argon and nitrogen as a purge gas at 20 mL min^{-1} shows that nitrogen is able to achieve higher temperatures on heating at 20,000 ˚C s^{-1}, -50 to 410 ˚C (-45 to 345 ˚C with argon). Cooling at 15,000 ˚C s^{-1} the operating window for nitrogen is 260 to 400 ˚C and 300 to 420 ˚C for argon so exhibits a similar performance when cooling.

5.3 Results and discussion

5.3.1 Effect of heating rate and thermal lag on the melting onset of indium

Figure 5.13 shows the influence of thermal lag upon the melting onset of indium. The heating rates investigated were between 0.05 and 10,000 ˚C s^{-1} on a sample with a mass calculated as 118 ng. Similar to conventional DSC, the conduction of heat between the sensor and the sample (thermal lag) influences the melting onset temperature of the sample. The thermal lag originates from two influences: the combination of the sample size and mass (as mentioned previously), and the scanning rate. Thermal lag arises during heating when the sample is at a lower temperature than the temperature sensor of the instrument and conversely at a higher temperature when cooling [1]. It is therefore important to keep sample height to a minimum in order to reduce thermal lag, in particular for polymeric samples, which are more susceptible as they are thermal insulators [20]. It is for this reason all polymer samples were smeared in the melt across the active sample zone with a single hair.

The melting onset of indium increases linearly with heating rate and Figure 5.13 shows there is a progressive thermal lag in the instrument at rates in excess of 100 ˚C s^{-1}. The onset temperature and the use of different heating rates to account for thermal lag, T_{on} can be derived using the following equation:

$$T_{on} = T_{on,0} + \tau_{lag}\beta \qquad \text{Equation 5.5}$$

where $T_{on,0}$ is the original onset temperature uninfluenced by τ_{lag}, thermal lag, and β is the heating rate. This equation shows that the apparent temperature increase is given by

the time in lag (s) multiplied by heating rate (˚C s^{-1}) to give an onset temperature lag (˚C). The τ_{lag} derived from the results in Figure 5.13 is 0.86 ms. This thermal lag should be accounted for when conducting experiments using heating rates above 1000 ˚C s^{-1}. In the work by Vanden Poel *et al.* [17] a correction factor was successfully calculated and applied to measured onset temperatures of indium as a function of heating rate and sample mass. They found that no correction factor was required for heating rates between 0-10 ˚C s^{-1} and sample masses of 0.1 to 4 µg. Vanden Poel *et al.* also noted that the maximum correction factor of -2.6 ˚C for a heating rate of 1000 ˚C s^{-1} for a 4 µg sample mass is low in comparison to other fast scanning calorimeters (the Perkin Elmer Diamond HyperDSC and TA Instrument's RHC DSC) .

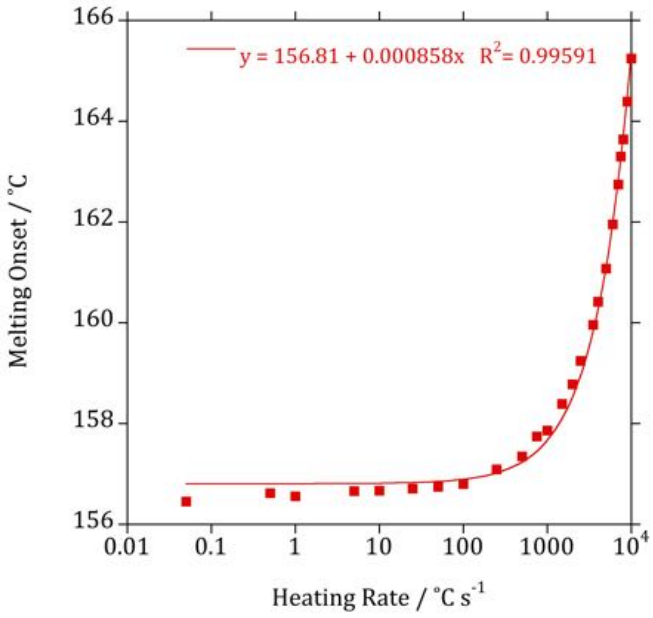

Figure 5.13. The effect of thermal lag on melting onset of indium when heating between 0.05 and 10,000 ˚C s^{-1}. τ_{lag} is 0.86 ms. The horizontal axis is displayed logarithmically to account for the large range in heating rates.

5.3.2 Identification of the heating and cooling rates to prevent crystallisation in poly(ε-caprolactone)

Crystallisation in polymers typically occurs via heterogeneous nucleation and examples of such heterogeneities are processing enhancers, stabilisers or catalyst residues [21]. The nucleation activity of these heterogeneities can only be supressed by cooling at sufficiently fast cooling rates. Therefore, to investigate the suppression of crystallisation, PCL was subjected to progressively increasing cooling rates until the observation of the crystallisation exotherm disappeared.

A sample mass of approximately 107 ng was calculated for PCL. Figure 5.14 and Figure 5.15 show the cooling (between 100 and 420 ˚C s^{-1}) and heating curves (at 100 ˚C s^{-1}) respectively. Figure 5.14 shows that as the cooling rate is increased the corresponding crystallisation is gradually reduced until complete suppression is observed at 420 ˚C s^{-1}. This is exhibited by a decrease in the area and intensity of the exothermic peak. Additionally, there is a depression in the onset of crystallisation with increasing cooling rate. Due to the reduction of crystallisation on cooling, increasing cooling rates shows a more pronounced glass transition on the reheat (Figure 5.15). Crystallisation prevented upon cooling was accompanied by a cold crystallisation peak that appears and grows corresponding with increasing cooling rates (Figure 5.15). The enthalpy of the cold crystallisation peak is dependent on the number of active nuclei and heating rate, which determines the time for growth. As a constant heating rate of 100 ˚C s^{-1} was applied in these measurements, reportedly the cold crystallisation enthalpy can be considered as a relative measure of the number of nuclei present in the sample [13].

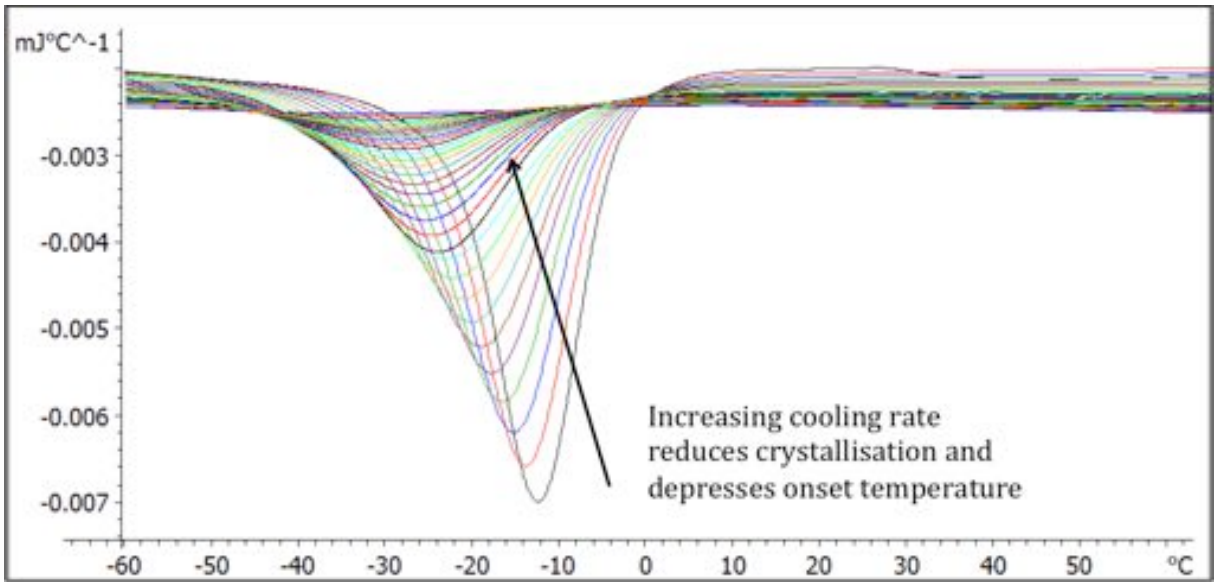

Figure 5.14. The normalised cooling rates depicting the prevention of crystallisation in PCL.

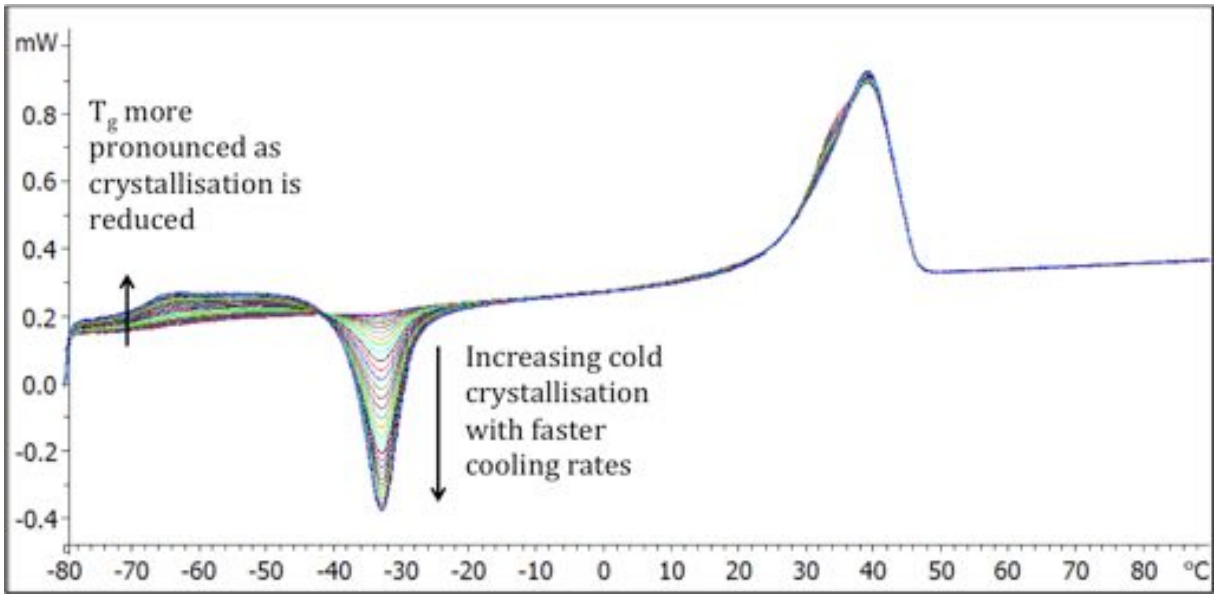

Figure 5.15. The reheat of PCL at 100 ˚C s^{-1} after cooling at various rates. Where crystallisation has been prevented upon cooling at increasing scanning rates, the reheat allows cold crystallisation to occur. Increased cold crystallisation is observed corresponding to faster cooling rates.

The subsequent melting peak remains consistent in size indicating that a heating rate of 100 ˚C s^{-1} is sufficient to account for the original crystallinity in the sample to be restored via cold crystallisation. These results are consistent with the literature [13, 21] on alternative fast scanning calorimeter instruments investigating the crystallisation and nucleation kinetics on PCL.

After establishing the cooling rate required to supress crystallisation (420 ˚C s^{-1}) the heating rates required to prevent cold crystallisation can be explored. Selecting a cooling rate of 1000 ˚C s^{-1}, well above 420 ˚C s^{-1} ensures confidence that the sample will be completely amorphous and that homogeneous nucleation in PCL is prevented. The heating rates were then varied between 100 and 3500 ˚C s^{-1} (Figure 5.16 and Figure 5.17) until cold crystallisation could no longer be detected. Figure 5.17 displays the heating curves separated indicating that cold crystallisation is reducing with increasing heating rate. The onset of cold crystallisation is also shifted to higher temperatures. The lowest temperature and largest amount of cold crystallisation is exhibited at 100 ˚C s^{-1} due to a longer time for nucleation near the glass transition. As the heating rates increase, the time for nucleation reduces and cold crystallisation is completely prevented. The reduction and prevention of cold crystallisation corresponds with a reduction in the subsequent melting peak.

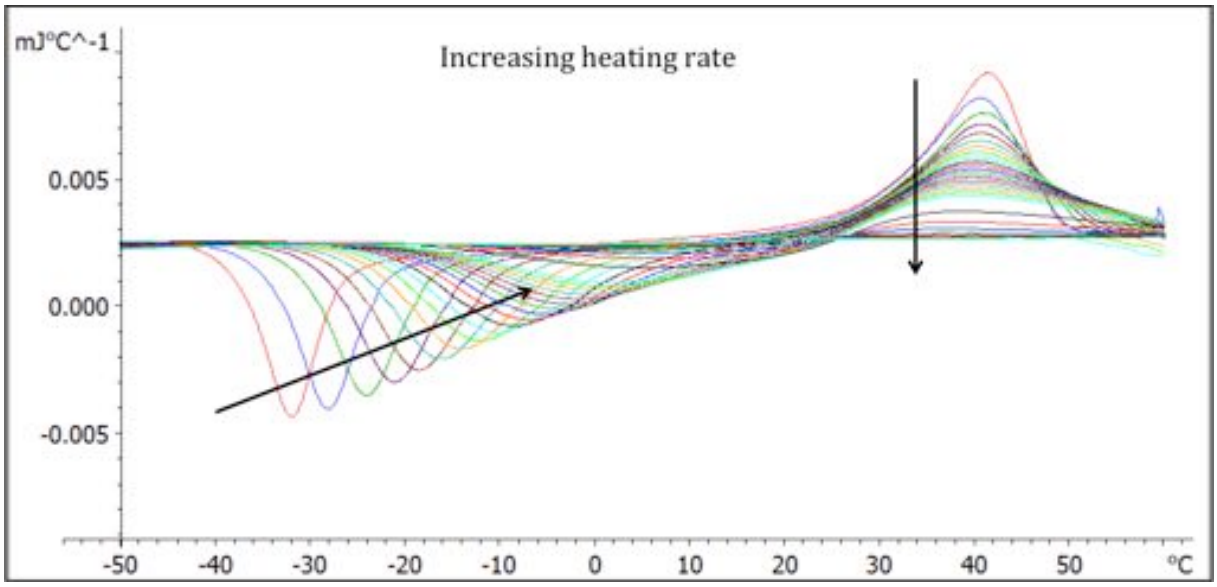

Figure 5.16. The normalised heating curves of PCL. The heating rate varied from 100 to 3500 ˚C s^{-1} with cooling at 1000 ˚C s^{-1}.

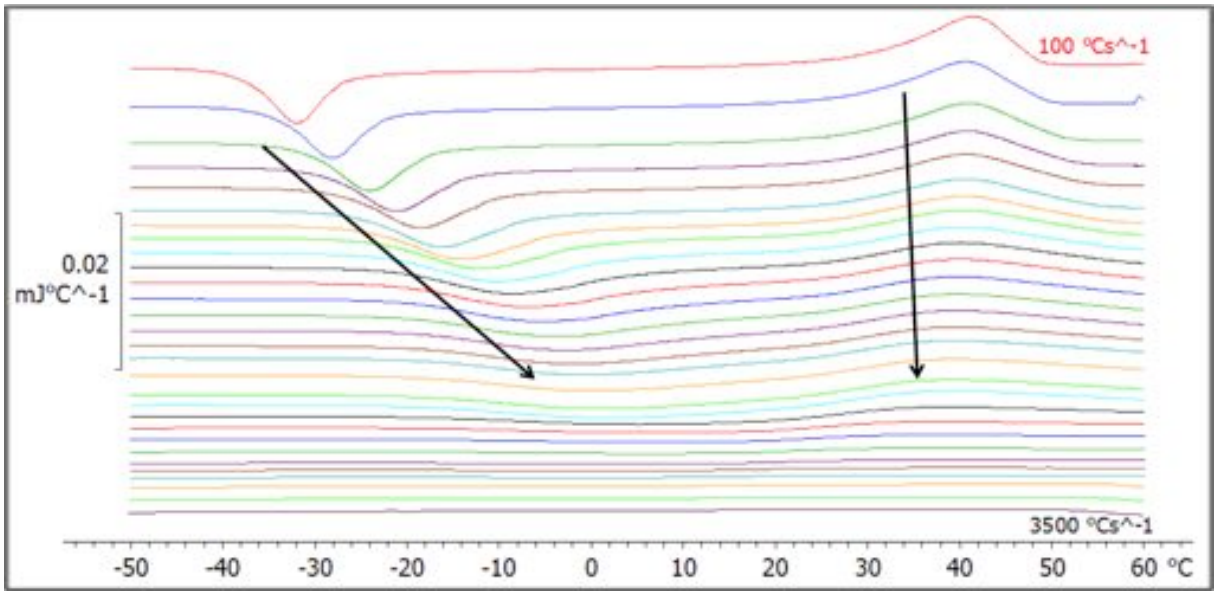

Figure 5.17. The normalised heating curves of PCL separated to illustrate the suppression of cold crystallisation and subsequent reduction in melting peak. The heating rate varied from 100 to 3500 ˚C s^{-1} with cooling at 1000 ˚C s^{-1}.

5.3.3 Determination of the activation energy of T_g

5.3.3.1 Activation energy of the glass transition of polyetherimide

The glass transition of polyetherimide (commercial grade Ultem 1000) was subjected to a variety of overlapping cooling rates (from 0.008 to 400 ˚C s^{-1}) across both conventional DSC and Flash DSC. The calculated sample mass for Ultem 1000 was 215 ng. Figure 5.18 shows the reheat of the sample after being previously cooled at the specified cooling rates (0.5 to 30 ˚C min^{-1}) using conventional DSC. Upon cooling the sample at slower rates the glass transition exhibits an increasing endothermic peak. An amorphous polymer above its glass transition temperature is in thermodynamic equilibrium and when cooled below this transition, a non-equilibrium glass is formed. This peak imposed upon T_g is attributed to the recovery of enthalpy during structural relaxation towards the equilibrium and is commonly referred to as physical ageing [22]. Ageing depends upon the annealing temperature, or more specifically, this temperature distance from the T_g. The bigger the temperature difference, the rate at which the system approaches equilibrium is increased. Cooling Ultem 1000 at slower rates through the glass enables increased molecular mobility, enhancing the relaxation process and subsequently results in an enthalpy relaxation peak upon the corresponding reheat.

Glass transitions exhibiting an ageing peak were therefore measured using the Richardson method (detailed in chapter 2) and it was found that T_g moved to a higher temperature corresponding to faster cooling rates (Figure 5.20). It should be noted that in order to be consistent in measuring the glass transition across both instruments for all curves, a strict procedure was followed ensuring the analysis was identical (see appendix 1 for an example). Figure 5.19 shows the glass transitions on the reheat following cooling rates of 0.5 to 400 ˚C s^{-1}.

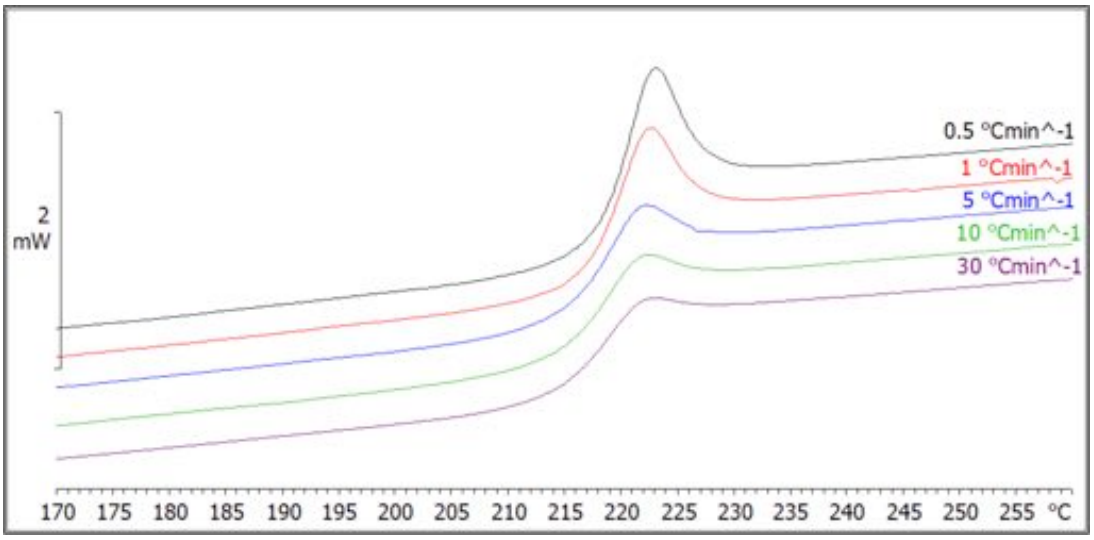

Figure 5.18. The glass transition of Ultem 1000 measured by conventional DSC. The cooling rate was varied between 0.5 and 30 °C min^{-1} (0.008, 0.016, 0.083, 0.16 and 0.5 °C s^{-1}) and subsequently reheated at 10 °C min^{-1}. The glass transitions presented above are the glasses formed on the reheat (labelled corresponding to the previous cool).

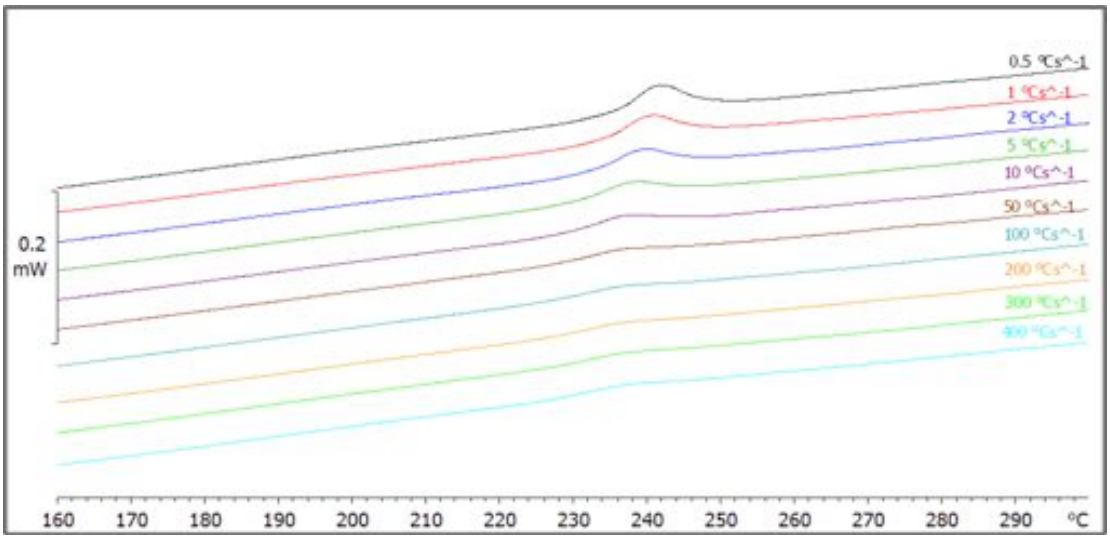

Figure 5.19. The glass transition of Ultem 1000 measured by Flash DSC. The cooling rate was varied between 0.5 and 400 °C s^{-1} and subsequently reheated at 100 °C s^{-1}. The glass transitions presented above are the glasses formed on the reheat (labelled corresponding to the previous cool).

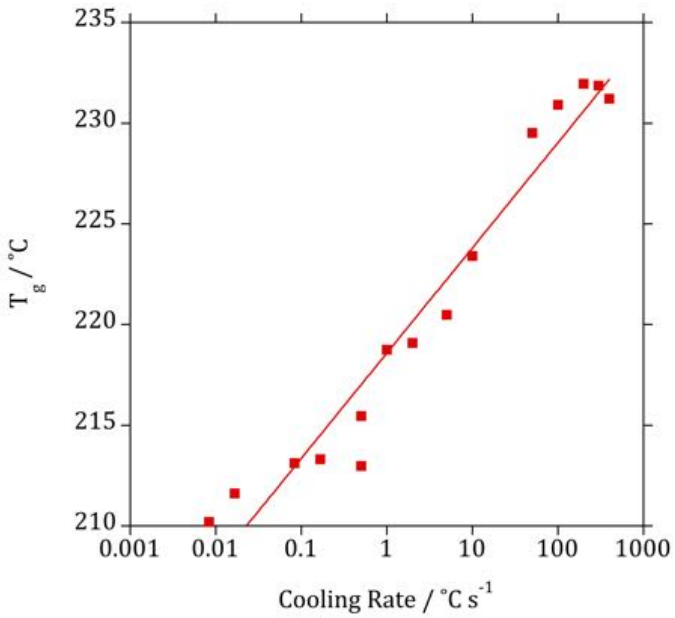

Figure 5.20. The glass transition of Ultem 1000 for a range of cooling rates (0.008 to 400 ˚C s^{-1}). The horizontal axis is displayed logarithmically to account for the wide range of cooling rates.

These results are consistent with a previous study on Ultem 1000 [23], which also shows shifted T_g to lower values with slower rates of cooling. This study reported an activation energy of 1150 ± 200 kJ mol^{-1}.

The activation energy of the glass transition for results in this thesis was calculated using the Arrhenius equation (Equation 5.6):

$$\ln K = \ln A - \frac{E_a}{RT} \qquad \text{Equation 5.6}$$

where K is the cooling rate (in K s^{-1}), E_a is the activation energy (in kJ mol^{-1}), R is the universal gas constant (8.314 J mol^{-1} K^{-1}) and T is the temperature (in Kelvin). Figure 5.21 shows the Arrhenius plot of the logarithm of the cooling rate against the reciprocal

T_g of Ultem 1000. The activation energy was calculated as 854 kJ mol^{-1}. By employing both Flash and conventional DSC (and therefore a larger range of cooling rates) only a slightly lower activation energy was found compared to that reported previously (1150 ± 200 kJ mol^{-1} [23]).

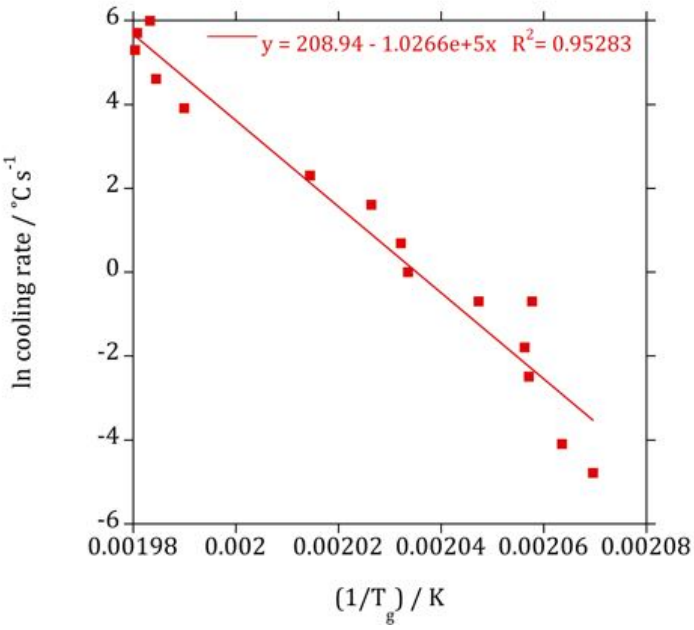

Figure 5.21. The Arrhenius plot of the logarithm of the cooling rate against the reciprocal T_g of Ultem 1000. Activation energy was calculated as 854 kJ mol^{-1}.

5.3.3.2 Activation energy of the glass transition of poly(lactic acid)

PLA grades 4060D, 2002D and 3051D were subjected to a range of cooling rates (from 50 to 600 ˚C s^{-1}) using the Flash DSC to determine the activation energy of the glass transition temperature. The calculated sample masses were 83, 295 and 329 ng for PLA 4060D, 2002D and 3051D respectively.

PLA 4060D is an amorphous grade of PLA enabling the glass transition temperature to be investigated across both conventional and Flash DSC. Both PLA 2002D and 3051D are partially crystalline and although have extremely slow crystallisation kinetics [14], in order to eliminate the potential for crystallisation influencing the glass transition, only Flash DSC measurements were conducted for these grades. Similar to the results presented for Ultem 1000, PLA also exhibited an enthalpy relaxation peak upon the glass transition. Therefore, the Richardson method was also employed when measuring the glass transition temperatures for these polymers.

As seen in Figure 5.22, the Arrhenius plot shows different behaviours corresponding to measurements with the two different instruments. The faster rates achieved with the Flash DSC produces broader glass transitions and therefore E_a is reduced corresponding with a lower gradient in the Arrhenius plot. Therefore the Flash DSC activation energy results are expected to be lower in comparison to conventional DSC. This is consistent for the results presented in Figure 5.22 which shows that the Flash DSC has an activation energy of 489 kJ mol^{-1} in comparison to conventional DSC which gives 1108 kJ mol^{-1}. The Arrhenius plots for PLA 2002D and 3051D are shown in Figure 5.23 and Figure 5.24 respectively.

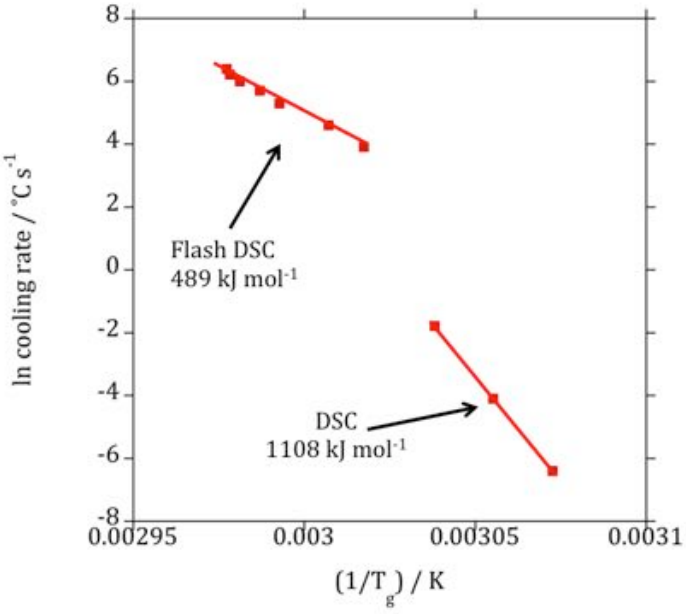

Figure 5.22. The Arrhenius plot of the logarithm of the cooling rate against the reciprocal T_g of PLA 4060D measured by conventional and Flash DSC. The activation energy was calculated as 489 and 1108 kJ mol^{-1}.

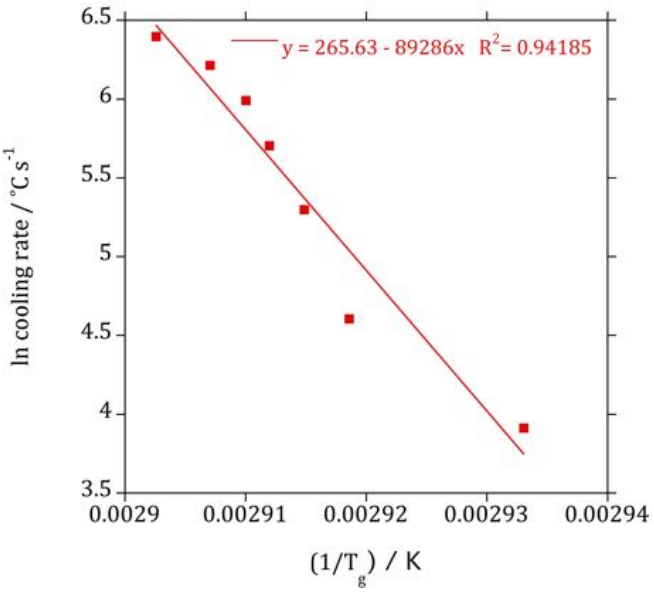

Figure 5.23. The Arrhenius plot of the logarithm of the cooling rate against the reciprocal T_g of PLA 2002D measured by Flash DSC. Activation energy was calculated as 742 kJ mol^{-1}.

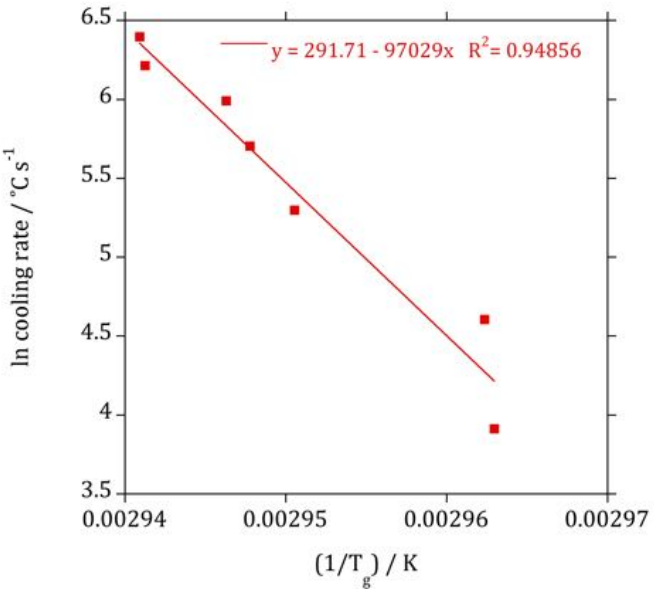

Figure 5.24. The Arrhenius plot of the logarithm of the cooling rate against the reciprocal T_g of PLA 3051D measured by Flash DSC. The activation energy was calculated as 807 kJ mol^{-1}.

As detailed in chapter 1, D-lactide content of PLA influences its crystallinity. This is a consequence of the introduction of macromolecular imperfections into the stereoregular architecture of PLA. These imperfections may hinder close chain packing to an extent (depending on the amount of D-lactide content) that either reduces the crystallinity of PLA or prevents it completely [24]. Table 5.2 shows the different grades of PLA and their corresponding D-lactide contents. It can be seen that with increasing D-lactide content of the polymer, the activation energy is correspondingly reduced (see Figure 5.25). This result indicates that by reducing or preventing the crystallinity of PLA, the glass transition has greater molecular mobility and lower activation energy. The lower molecular weight in a polymer results in more end groups and consequently greater free volume. This corresponds with greater mobility of polymer chains, reducing the glass transition and activation energy. However, the molecular weight value for PLA 3051D is confounding, providing scope for further work in this area to be undertaken.

	PLA 4060D	**PLA 2002D**	**PLA 3051D**
$_D$-lactide content / %	12	4.25	3.3
M_w / g mol^{-1}	181,356	193,948	151,114
T_g / ˚C	50.21	53.23	58.23
Activation energy / kJ mol^{-1}	489	742	807

Table 5.2. The comparison of PLA grades 4060D, 2002D and 3051D and their calculated activation energies, average-weight molecular weight and D-lactide content. The activation energy is seen to decrease corresponding to increasing D-lactide content in the polymer.

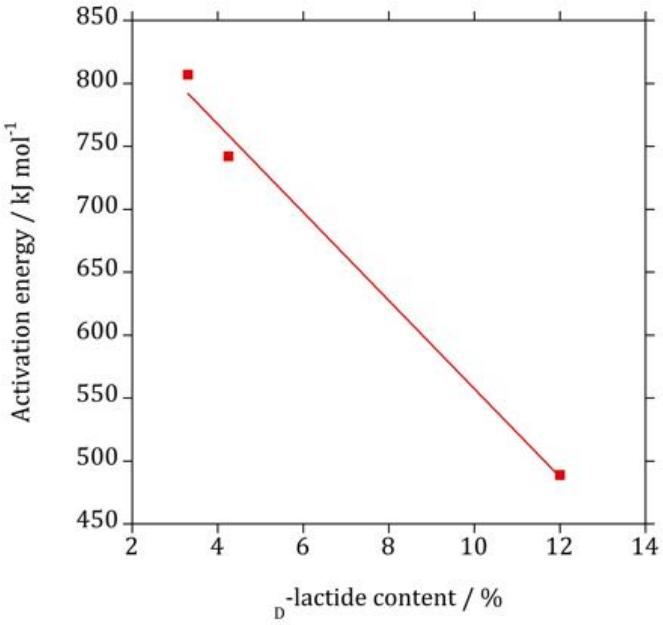

Figure 5.25. The influence of $_{D}$-lactide content in PLA on the activation energy of $T_{g.}$

5.3.4 Investigations on poly(ether-ether-ketone)

The behaviour of PEEK was initially examined using Flash DSC providing a basis for further work and developments. A variety of cooling rates were selected from 0.5 to 40 ˚C s^{-1} whilst reheating remained constant at 100 ˚C s^{-1}. A sample mass of 1052 ng was calculated for PEEK. A larger sample mass was required for PEEK in order to detect thermal transitions, particularly for slower rates or isothermal measurements [25].

The reheat is shown in Figure 5.26, depicting that as the cooling rate is decreased, a double melting peak is observed. Both peaks are seen to shift to higher temperatures with decreasing cooling rate. This double melting behaviour has been observed by many previous studies [16, 26-28] where it is thought that the double melting peaks are attributed to melting of two different crystal populations, differing from each other in respect to their lamellar thicknesses. Double melting peaks can be caused by the growth of different crystal populations during isothermal crystallisation or from reorganisation during heating. There are discrepancies within the literature as to the origins of the double melting peak phenomenon in PEEK; whether it is attributed to melt-recrystallisation during heating in DSC or differing lamellar thicknesses. Cebe and Dong have investigated the crystallisation behaviour of PEEK using conventional DSC. They show that slower cooling treatments of the melt exhibit a low temperature shoulder on the melting endotherm [27]. The location of the shoulder was sensitive to cooling rate. It is thought that the lower melting peak / shoulder may be attributed to melting of crystalline regions formed on the previous cool [29]. This peak reduces as the cooling rate increases as a result of reducing the time for nucleation. The higher peak therefore, is attributed to the melt-recrystallisation process occurring during the heating scan, suggesting that 100 ˚C s^{-1} is slow enough to allow recrystallisation to occur for PEEK.

Fast scanning calorimetry is able to achieve heating rates fast enough in order to suppress any melt-recrystallisation during heating. Increasing the heating rate to observe the effect it has on the double melting behaviour provides scope for further work. Many of the previous studies that examine the double melting behaviour of PEEK often perform isothermal crystallisation experiments. This is also something for future work and to further investigate double melting with isothermal crystallisation experiments on the Flash DSC.

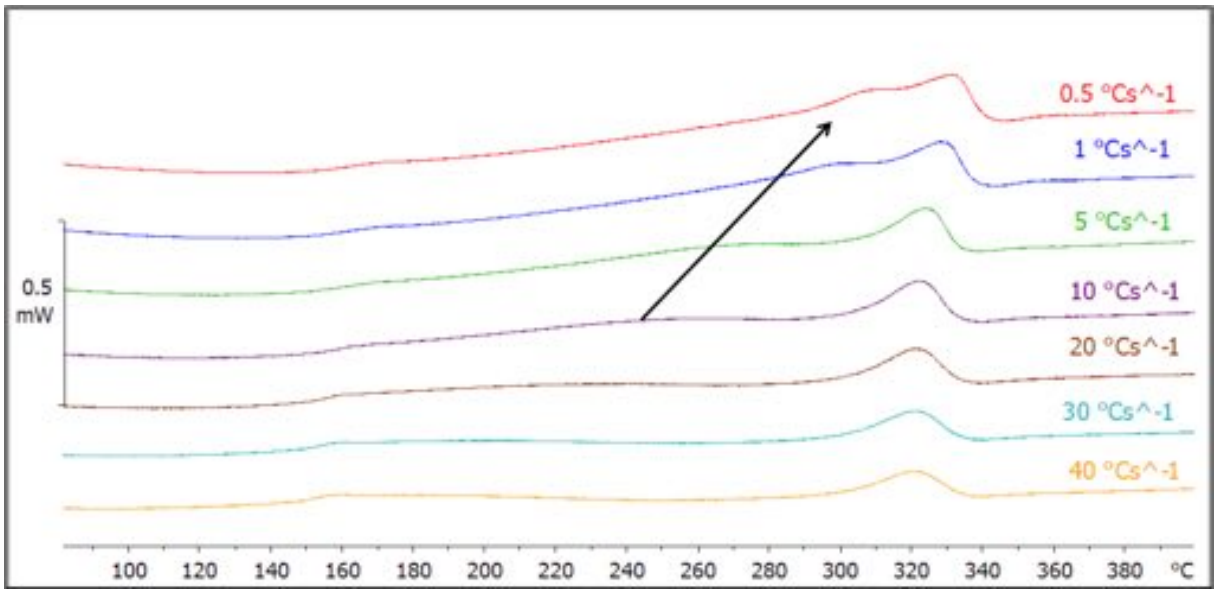

Figure 5.26. The reheat of PEEK at 100 ˚C s^{-1} after cooling at a variety of scanning rates.

5.4 Conclusions

The performance of the Flash DSC was determined using argon as a purge gas at 20 mL min^{-1}. This allowed the operating windows for various heating and cooling rates to be established for the instrument. Flash DSC is capable of mimicking cooling rates of polymer processing techniques such as extrusion (100 ˚C min^{-1}/6000 ˚C s^{-1}), the core of injection moulding (50 to 250 ˚C min^{-1}/3000 to 15,000 ˚C s^{-1}) and rotation moulding (5 to 50 ˚C min^{-1}/300 to 3000 ˚C s^{-1}) [30].

The influence of heating rate on the thermal lag of indium was explored using a range of heating rates (0.05 and 10,000 ˚C s^{-1}) and the melting onset was shown to linearly increase with corresponding increasing heating rate. Thermal lag was calculated to be 0.86 ms for a sample mass of 118 ng.

PCL was used as a model polymer to study the suppression of crystallisation with increasing cooling rate. It was shown that crystallisation is prevented with cooling rates of 420 ˚C s^{-1} and that increasing cooling rates gradually reduces the crystallisation exotherm which is accompanied by a depression in the onset. In order to establish the heating rates required to prevent cold crystallisation from occurring, a cooling rate of 1000 ˚C s^{-1} was selected to ensure homogeneous nucleation in PCL was prevented. The subsequent heating rates were varied showing that at 3500 ˚C s^{-1} cold crystallisation can no longer be observed. The slowest heating rate (100 ˚C s^{-1}) shows the greatest amount of cold crystallisation at the lowest temperature. This onset temperature shifted to higher temperatures as the heating rate was increased.

Ultem 1000 was used to study the activation energy of the glass transition by varying the cooling rates using both conventional and Flash DSC.

Different grades of PLA with varying $_D$-lactide content were all subjected to increasing cooling rates in order to compare the activation energy of the glass transition. It was found that with increasing $_D$-lactide content (and a reduction of crystallinity) within the polymer, the glass transition exhibits a lower activation energy. The activation energy of the glass transition of PLA 4060D (an amorphous grade) was explored using both conventional and Flash DSC. As expected, the Arrhenius plot displayed two distinct behaviours of activation energy. The Flash DSC produced lower activation energies in comparison to conventional DSC. This was attributed to the broadening of the glass transition due to the increased cooling rates achieved by the Flash DSC.

An initial investigation into the double melting behaviour of PEEK was undertaken. PEEK was cooled at different rates whilst the reheat remained constant. The appearance of a double melting peak is present for lower cooling rates. These experiments showed that by increasing the cooling rate the lower melting peak is reduced and finally inhibited at 40 ˚C s^{-1}. It was suggested that the lower peak was attributed to melting of crystalline regions formed on the previous cool and the higher peak was associated with melt-recrystallisation occurring during the heating scan. This indicates that 100 ˚C s^{-1} is slow enough to allow reorganisation of the polymer chains. Further work such as isothermal crystallisation studies and varying and increasing heating rate measurements to analyse the effect on the double melting behaviour of PEEK should be considered.

5.5 References

[1] S. van Herwaarden, E. Iervolino, F. van Herwaarden, T. Wijffels, A. Leenaers, and V. Mathot, "Design, performance and analysis of thermal lag of the UFS1 twin-calorimeter chip for fast scanning calorimetry using the Mettler-Toledo Flash DSC 1," *Thermochimica Acta,* vol. 522, pp. 46-52, 2011.

[2] M. Toledo. *Flash Differential Scanning Calorimeter*. Available: http://us.mt.com/us/en/home/products/Laboratory_Analytics_Browse/TA_Family_Browse/Flash_DSC.html

[3] PerkinElmer. Available: http://www.perkinelmer.com/catalog/product/id/n5340501

[4] V. Mathot, M. Pyda, T. Pijpers, G. Vanden Poel, E. van de Kerkhof, S. van Herwaarden*, et al.*, "The Flash DSC 1, a power compensation twin-type, chip-based fast scanning calorimeter (FSC): First findings on polymers," *Thermochimica Acta,* vol. 522, pp. 36-45, 8/10/ 2011.

[5] M. TOLEDO. Available: http://uk.mt.com/gb/en/home/products/Laboratory_Analytics_Browse/TA_Family_Browse/Flash_DSC.tabs.models-and-specs.html

[6] E. Iervolino, A. W. van Herwaarden, F. G. van Herwaarden, E. van de Kerkhof, P. P. W. van Grinsven, A. C. H. I. Leenaers*, et al.*, "Temperature calibration and electrical characterization of the differential scanning calorimeter chip UFS1 for the Mettler-Toledo Flash DSC 1," *Thermochimica Acta,* vol. 522, pp. 53-59, 2011.

[7] M. Mihai, M. A. Huneault, and B. D. Favis, "Crystallinity development in cellular poly(lactic acid) in the presence of supercritical carbon dioxide," *Journal of Applied Polymer Science,* vol. 113, pp. 2920-2932, 2009.

[8] P. Krishnamachari, J. Zhang, J. Lou, J. Yan, and L. Uitenham, "Biodegradable Poly(Lactic Acid)/Clay Nanocomposites by Melt Intercalation: A Study of Morphological, Thermal, and Mechanical Properties," *International Journal of Polymer Analysis and Characterization,* vol. 14, pp. 336-350, 2009/05/19 2009.

[9] R. Scarlet, L. R. Manea, I. Sandu, L. Martinova, O. Cramariuc, and I. G. Sandu, "Study on the solubility of polyetherimide for nanostructural electrospinning," *Revista de Chimie (Bucharest),* vol. 63, pp. 688-692, 2012.

[10] A. Jonas and R. Legras, "Thermal stability and crystallization of poly(aryl ether ether ketone)," *Polymer,* vol. 32, pp. 2691-2706, // 1991.

[11] J. L. Ford and T. E. Mann, "Fast-Scan DSC and its role in pharmaceutical physical form characterisation and selection," *Advanced Drug Delivery Reviews,* vol. 64, pp. 422-430, 4// 2012.

[12] J. C. Van Miltenburg and M. A. Cuevas-Diarte, "The influence of sample mass, heating rate and heat transfer coefficient on the form of DSC curves," *Thermochimica Acta,* vol. 156, pp. 291-297, 12/30/ 1989.

[13] E. Zhuravlev, J. W. P. Schmelzer, B. Wunderlich, and C. Schick, "Kinetics of nucleation and crystallization in poly(ε-caprolactone) (PCL)," *Polymer,* vol. 52, pp. 1983-1997, 4/19/ 2011.

[14] M. Salmerón Sánchez, V. B. F. Mathot, G. Vanden Poel, and J. L. Gómez Ribelles, "Effect of the Cooling Rate on the Nucleation Kinetics of Poly(l-Lactic Acid) and

Its Influence on Morphology," *Macromolecules,* vol. 40, pp. 7989-7997, 2007/10/01 2007.

[15] W. T. Zhai, Y. Ko, W. L. Zhu, A. S. Wong, and C. B. Park, "A Study of the Crystallization, Melting, and Foaming Behaviors of Polylactic Acid in Compressed CO2," *International Journal of Molecular Sciences,* vol. 10, pp. 5381-5397, Dec 2009.

[16] G. Crevecoeur and G. Groeninckx, "Binary blends of poly(ether ether ketone) and poly(ether imide): miscibility, crystallization behavior and semicrystalline morphology," *Macromolecules,* vol. 24, pp. 1190-1195, 1991/03/01 1991.

[17] G. Poel, D. Istrate, A. Magon, and V. Mathot, "Performance and calibration of the Flash DSC 1, a new, MEMS-based fast scanning calorimeter," *Journal of Thermal Analysis and Calorimetry,* vol. 110, pp. 1533-1546, 2012/12/01 2012.

[18] (2014). *ATHAS Data Bank*. Available: http://web.utk.edu/~athas/databank/

[19] J. Schawe. (2012). *Practical aspects of the Flash DSC 1: Sample preparation for measurements of polymers*. Available: http://uk.mt.com/gb/en/home/supportive_content/usercom/TA_UserCom36.html

[20] G. Wang and I. R. Harrison, "Polymer melting: thermal resistance effects in a DSC," *Thermochimica Acta,* vol. 230, pp. 309-317, 12/15/ 1993.

[21] A. Wurm, E. Zhuravlev, K. Eckstein, D. Jehnichen, D. Pospiech, R. Androsch*, et al.*, "Crystallization and Homogeneous Nucleation Kinetics of Poly(ε-caprolactone) (PCL) with Different Molar Masses," *Macromolecules,* vol. 45, pp. 3816-3828, 2012/05/08 2012.

[22] A. D'Amore, G. Caprino, L. Nicolais, and G. Marino, "Long-term behaviour of PEI and PEI-based composites subjected to physical aging," *Composites Science and Technology,* vol. 59, pp. 1993-2003, 10// 1999.

[23] F. Biddlestone, A. A. Goodwin, J. N. Hay, and G. A. C. Mouledous, "The relaxation spectrum and physical ageing of polyetherimide," *Polymer,* vol. 32, pp. 3119-3125, // 1991.

[24] L. Averous and E. Pollet, "Biodegradable Polymers," in *Environmental Silicate Nano-Biocomposites*, L. Averous and E. Pollet, Eds., ed London: Springer, 2012.

[25] X. Tardif, B. Pignon, N. Boyard, J. W. P. Schmelzer, V. Sobotka, D. Delaunay*, et al.*, "Experimental study of crystallization of PolyEtherEtherKetone (PEEK) over a large temperature range using a nano-calorimeter," *Polymer Testing,* vol. 36, pp. 10-19, 6// 2014.

[26] D. C. Bassett, R. H. Olley, and I. A. M. Al Raheil, "On crystallization phenomena in PEEK," *Polymer,* vol. 29, pp. 1745-1754, 10// 1988.

[27] P. Cebe and S.-D. Hong, "Crystallization behaviour of poly(ether-ether-ketone)," *Polymer,* vol. 27, pp. 1183-1192, 1986.

[28] C.-L. Wei, M. Chen, and F.-E. Yu, "Temperature modulated DSC and DSC studies on the origin of double melting peaks in poly(ether ether ketone)," *Polymer,* vol. 44, pp. 8185-8193, 12// 2003.

[29] D. J. Blundell and B. N. Osborn, "The morphology of poly(aryl-ether-ether-ketone)," *Polymer,* vol. 24, pp. 953-958, 8// 1983.

[30] G. Vanden Poel and V. B. F. Mathot, "High performance differential scanning calorimetry (HPer DSC): A powerful analytical tool for the study of the metastability of polymers," *Thermochimica Acta,* vol. 461, pp. 107-121, 9/15/ 2007.

CHAPTER 6 – CONCLUSIONS AND FURTHER WORK

6.1 Conclusions

Blends of poly(lactic acid) grade 2002D and 4060D with poly(ε-caprolactone) at various compositions (25/75, 50/50 and 75/25 PLA/PCL) were produced by solution casting, melt blending and blending in the presence of carbon dioxide. These blends were characterised and compared using SEM, mechanical testing, FTIR, DSC, rheology and SEC.

Solution cast blends were prepared from dichloromethane. In some blends, large-scale phase separation was observed prior to analysis. SEM confirmed that all blends were immiscible by the presence of droplets dispersed throughout a matrix. Both DSC and FTIR spectroscopy demonstrated the absence of adhesion and partial miscibility. The presence of large droplets acted as stress initiation sites and severely hindered the mechanical properties within the blends. There was extreme variation in mechanical properties seen by the large error within the majority of the compositions, this was attributed to porosity (caused by solvent evaporation) and large-scale phase separation within the blends.

The melt blends were extruded at 160 ˚C with screw speeds of 20, 30 and 40 rpm. SEM analysis indicated a significantly improved microstructure was present in the melt blends compared to solution cast blends. Using SEM images the number and weight average droplet diameters were calculated for the solution cast and melt blends. Improvements in dispersion and droplet size from solution casting to melt blending was

observed, with reductions as great as 9 μm to 1 μm. This corresponded to an improvement in mechanical properties in the melt blends. Despite the absence of miscibility in the blends, the results show that PCL is able to influence the mechanical properties of PLA. Reducing the screw speed has a small but positive effect on the mechanical properties, particularly in the 75/25 PLA/PCL blends. It was evident that the 40 rpm samples possessed inferior properties to 20 and 30 rpm samples. FTIR analysis of the melt blends exhibited clear changes in carbonyl band absorbance with composition. Additionally, the carbonyl bands assigned to both PLA and PCL were seen to shift to higher wavenumbers corresponding to decreasing content of each component, indicating an interaction between the polymers. However, DSC showed there were no shifts in the melting points corresponding to either component, although it was noted that there was an increase in the crystallinity of PLA 2002D upon the addition of PCL indicating that PCL was acting as a nucleating agent. Rheological analysis of the homopolymers illustrated a higher viscosity for PCL than PLA, signifying mixing will be preferred in the 25/75 PLA/PCL blends (where the matrix possesses the higher viscosity). The average viscosity ratios calculated at 1% strain confirmed the lowest ratios were for the 25/75 PLA/PCL blend for both systems, although 75/25 PLA2002D/PCL also exhibited a relatively low viscosity ratio.

The blends produced in the presence of carbon dioxide were extruded at 150 ˚C at 20 and 30 rpm. SEM showed that these blends exhibited an improvement in morphology, indicating a significant reduction in droplet size and dispersion from up to 10 μm in solvent cast blends to 0.2 μm in the blends produced in the presence of carbon dioxide. An increased porosity was also observed however, despite this porosity, the mechanical

properties of numerous blend compositions produced in the presence of carbon dioxide showed an improvement. The rule of mixtures model (assuming perfect adhesion) was calculated for the Young's modulus of both melt and CO_2 assisted blends. It was observed that blends produced in the presence of carbon dioxide exhibited greater conformity with the model predictions. The viscosity ratio calculated at atmospheric pressure and in the presence of carbon dioxide showed that carbon dioxide lowers the viscosity ratio for both 25/75 and 75/25 PLA/PCL compositions. DSC analysis showed a significant reduction in the crystallinity of PCL in the 75/25 PLA/PCL blends. This was attributed to fractionated crystallisation in PCL as a result of a reduction in nucleation density associated with a significant decrease in droplet size. Additionally, partial miscibility was observed in the 75/25 PLA/PCL blends by a reduction in the glass transition and melting temperature for PLA and PCL respectively. Corresponding to the reduction in PCL crystallinity, FTIR showed an absence of the crystalline band. SEC analysis indicated that processing with carbon dioxide inhibits the reduction in molecular weight that is observed by extruding without CO_2.

The findings of blending in the presence of carbon dioxide indicate that by injecting CO_2 into the polymer melt, it is able to act as a molecular lubricant, thereby reducing their viscosities and encouraging increased molecular interaction between the two polymers. Consequently it is able to improve the adhesion between phases at the microscale and induce partial miscibility.

Rheological studies with carbon dioxide were undertaken to investigate the influence of CO_2 on the reptation time of poly(ε-caprolactone). Introducing carbon dioxide into the polymer melt resulted in a reduction in reptation time equivalent to that of raising the temperature by 20 ˚C. This result confirmed that CO_2 was interacting with the polymer by diffusing into the free volume between the individual chains. CO_2 formed Lewis acid-base interactions with the carbonyl groups present in PCL, disrupting the inter/intra molecular interactions. As a consequence, the number of chain entanglements decreased, resulting in an increase in the free volume and the mobility of the polymer chains. By further increasing the pressure it was seen that carbon dioxide had a less significant effect on reptation time. This was attributed to the competing pressure effects, where raising the pressure subsequently forced the polymer chains closer together, reducing the viscosity. Further analysis of the data showed that the activation energy to flow was reduced, which was consistent with the reduction in the reptation times.

Flash DSC, a relatively new calorimetry technique, enabling extremely fast scanning rates in comparison to conventional DSC, was used to undertake measurements that conventional DSC cannot achieve. The performance of the instrument was first characterised, followed by some initial measurements with a variety of different materials; PLA, PCL, PEI, PEEK and indium. The operating window of heating and cooling rates of the instrument was determined using argon as a purge gas at 20 mL min^{-1}. Thermal lag was also studied using the melting onset of indium (T_{on}). T_{on} increases linearly with heating rate and shows a progressive thermal lag in the instrument at rates in excess of 100 ˚C s^{-1}. Poly(ε-caprolactone) was chosen as a 'model'

partially crystalline polymer, used to demonstrate the suppression of crystallisation by increasing the cooling rate. It was shown that it is possible to prevent crystallisation at rates under 500 ˚C s^{-1}. Additionally, at constant cooling rates of 1000 ˚C s^{-1}, the cold crystallisation exotherm was prevented with heating rates of 3500 ˚C s^{-1}. Both PEI and PLA were used to study the activation energy of the glass transition. Three different grades of PLA with varying $_{D}$-lactide content were calculated and compared from Arrhenius plots. It was found that with increasing $_{D}$-lactide content (and a reduction of crystallinity) within the polymer, the glass transition exhibits a lower activation energy. An initial investigation into the double melting behaviour of PEEK showed that the appearance of a double melting peak is present for lower cooling rates. By increasing the cooling rate, the lower melting peak is reduced and finally inhibited at 40 ˚C s^{-1}. It was suggested that the lower peak was attributed to melting of crystalline regions formed on the previous cooling scan and the higher peak was associated with melt-recrystallisation occurring during the heating scan.

6.2 Further Work

Extruded blends within this study were created using a single-screw. Twin-screw extruders have a greater efficiency of blending polymers and therefore an improvement in blends could be obtained by using a twin-screw by enhanced mixing between components. This enhanced mixing coupled with achieving supercritical conditions for CO_2 could lead to increased reactions between the two polymers. Further investigations could be undertaken focusing on a narrower composition window (selecting blends around 75/25 PLA/PCL). This would establish whether a more specific composition could enhance the final morphology and properties of the blends. Alternative blends with different grades of PCL could be prepared in addition to incorporating a co-polymer compatibiliser.

The novel technique of Flash DSC was explored and initially characterised to determine the capabilities of the machine. Therefore, there is undoubtedly considerable further work to be undertaken using the Flash DSC. The results presented in chapter 5 were primarily an initial performance and characterisation check of the instrument. Further characterisation of operating windows with alternative gases (helium and nitrogen) should be considered. Expanding upon the research into activation energy of T_g with varying $_D$-lactide content by experimenting on additional grades of PLA, will help to provide a greater insight on the influence of $_D$-lactide.

Alternative methods of sample preparation could be looked into, such as spin coating and ink jet printing to deposit even and consistent sample sizes and masses. Replication of polymer processing heating and cooling rates could be studied. Additionally, the

instrument can be used to probe alternative materials such as metals or pharmaceutical substances. However, the care and awareness should always remain regarding appropriate heating and cooling rates and their limitations.

APPENDIX 1

In addition to the blends of PLA 4060D and 2002D with PCL, two alternative PLA/PCL blends were created with different PLA grades; PLA 3051D and PLA 3801X. Some examples of the analysis and characterisation of these blends are presented below. PLA3051D/PCL and PLA3801X/PCL blends exhibited immiscibility across all compositions with transcrystallinity present within the solution cast PLA3801X/PCL blends.

PLA 3051D is a partially crystalline polymer with a molecular weight of 151,000 g mol^{-1}, it exhibits a glass transition around 60 ˚C and a peak melting temperature at 156 ˚C.

PLA 3801X is a relatively new grade of PLA from NatureWorks LLC, designed for applications that require high heat and high impact performance. Due to the addition of talc acting as a nucleating agent, this grade of PLA has faster crystallisation kinetics than other PLA grades readily available to purchase. PLA 3801X is comprised of; 71% 3001D matrix with 10% impact modifier, 9% accelerant, 9% reinforcing agent and 1% nucleating agent [1]. It possesses a glass transition temperature of 54 °C and a melting temperature of 170 °C.

Figure A.1 and Figure A.2 show the solution cast blend samples of PLA3051D/PCL and PLA3801X/PCL respectively. No obvious large-scale phase separation was observed within these samples. However, SEM indicated these blends produced by all preparation methods were immiscible by the presence of droplets within a matrix (see Figure A.3 to Figure A.5). Comparable with the PLA2002D/PCL and PLA4060D/PCL blends presented in this thesis, the PLA 3051D blends also exhibit a reduced in droplet size by blending in the presence of carbon dioxide.

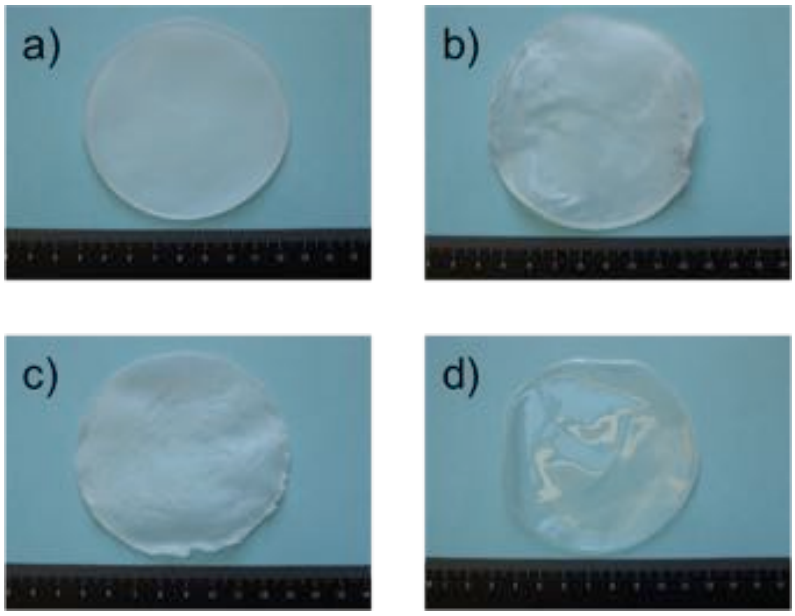

Figure A.1. PLA 3051D / PCL 6800 solvent cast blends: a) 25/75 PLA/PCL, b) 50/50 PLA/PCL, c) 75/25 PLA/PCL, d) 100 PLA.

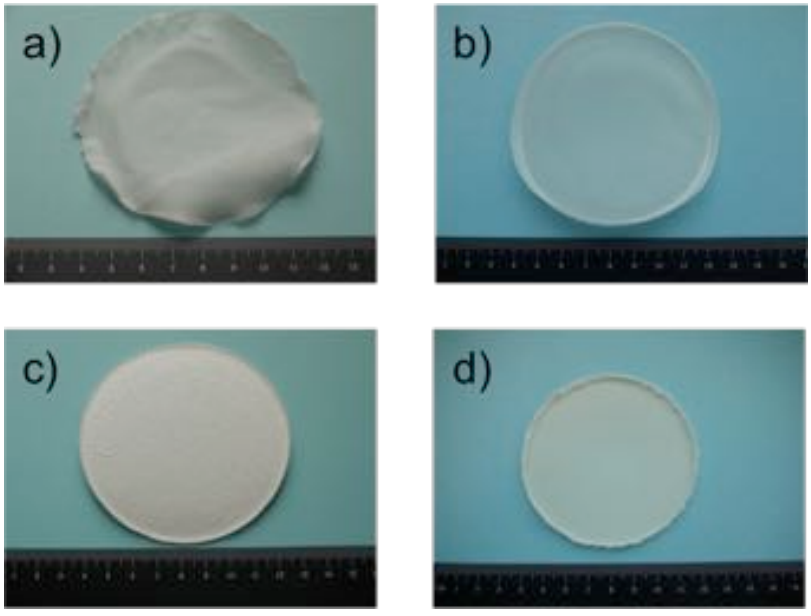

Figure A.2. PLA 3801X / PCL 6800 solvent cast blends: a) 25/75 PLA/PCL, b) 50/50 PLA/PCL, c) 75/25 PLA/PCL, d) 100 PLA.

Difficulties in extruding and conveying PLA 3051D blends frequently occurred in both preparation methods with and without the presence of carbon dioxide. Therefore, limited results were produced and the alternative PLA 4060D and 2002D grades (presented in the main body of the thesis) were carried forward for a more detailed investigation.

Due to the higher melting temperature of PLA 3801X, blends were extruded at 170 ˚C in the absence of carbon dioxide. These blends exhibit a significant reduction in droplet size (see Figure A.6 to Figure A.8). Despite the transcrystallinity observed in the solution cast 25/75 PLA/PCL sample (Figure A.6 image a), this characteristic was not present in the melt blend samples.

Unfortunately PLA3801X/PCL blends would not extrude and convey in the presence of carbon dioxide at 160 ˚C at all screw speeds investigated. This could be investigated as further work, changing the temperature in order to convey the polymer melt in the presence of CO_2. Alternatively, these blends would benefit from being produced using an intermeshing twin-screw extruder, where the polymer melt cannot undergo slip at the barrel wall [2, 3].

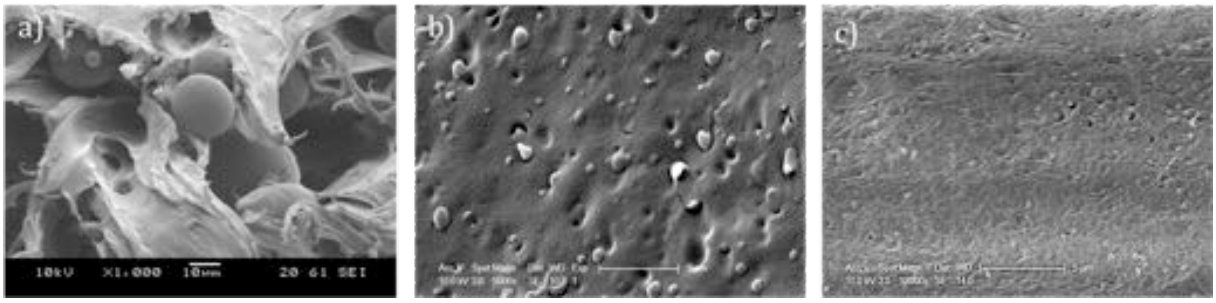

Figure A.3. A comparison of 25/75 PLA3051D/PCL blends produced by: a) solvent casting, b) melt blending at 160 ˚C and 30 rpm and c) CO_2 assisted blending at 150 ˚C, 30 rpm and 5% CO_2.

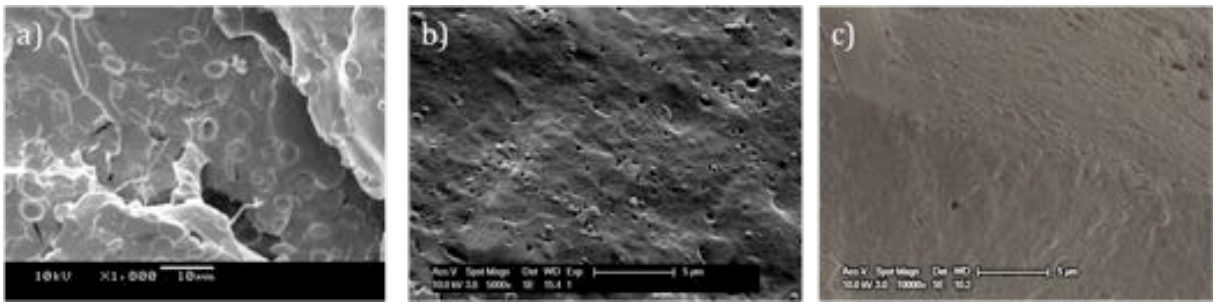

Figure A.4. A comparison of 50/50 PLA3051D/PCL blends produced by: a) solvent casting, b) melt blending at 160 ˚C and 30 rpm and c) CO_2 assisted blending at 150 ˚C, 30 rpm and 5% CO_2.

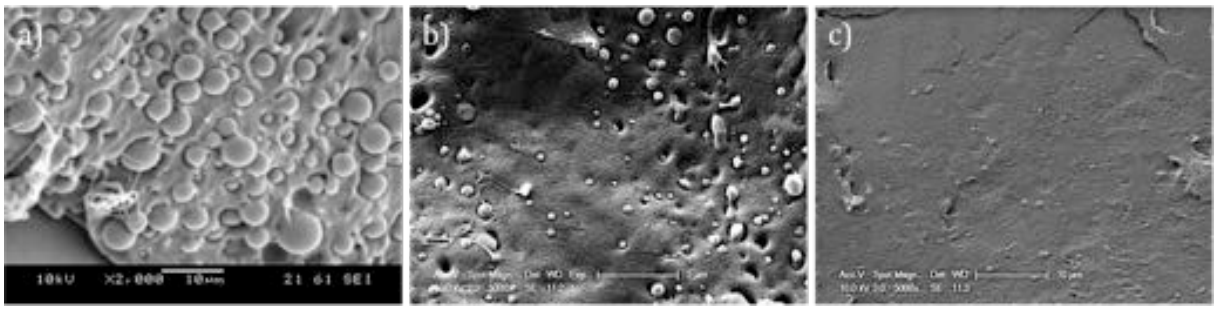

Figure A.5. A comparison of 75/25 PLA3051D/PCL blends produced by: a) solvent casting, b) melt blending at 160 ˚C and 30 rpm and c) CO_2 assisted blending at 150 ˚C, 30 rpm and 5% CO_2.

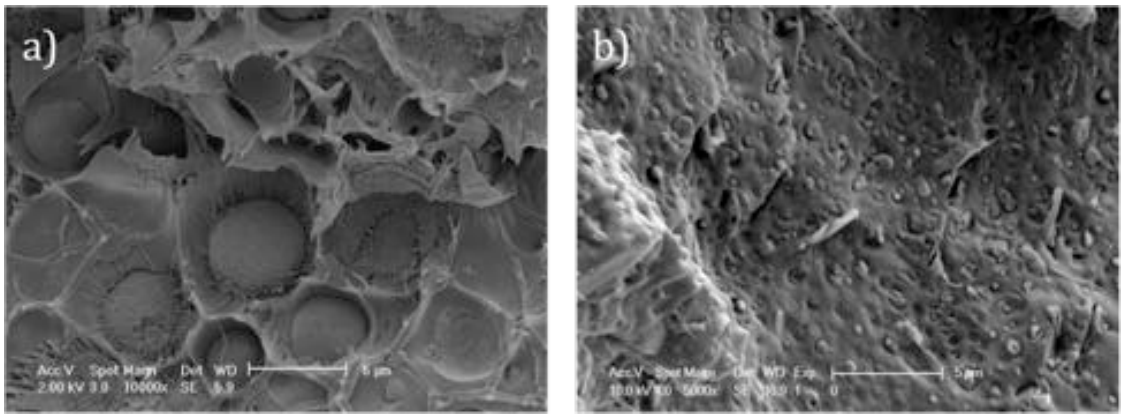

Figure A.6. A comparison of 25/75 PLA3801X/PCL blends produced by: a) solvent casting, b) melt blending at 170 ˚C and 30 rpm.

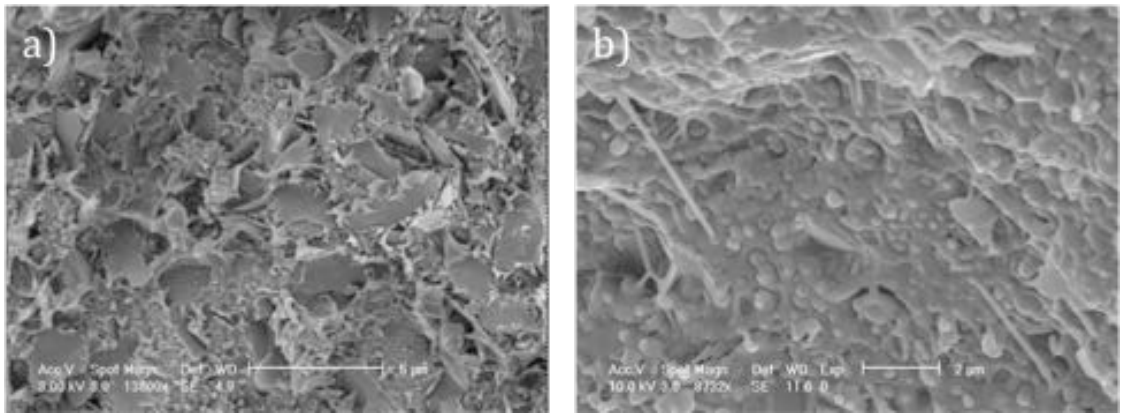

Figure A.7. A comparison of 50/50 PLA3801X/PCL blends produced by: a) solvent casting, b) melt blending at 170 ˚C and 30 rpm.

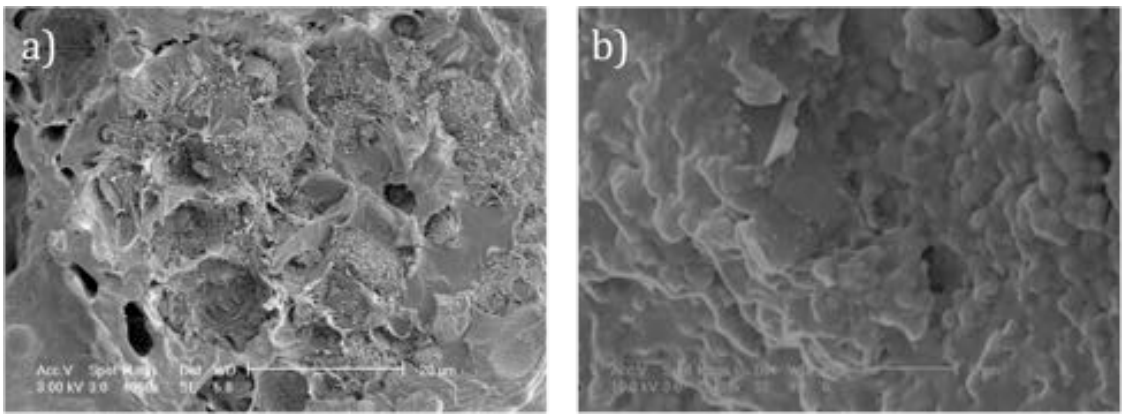

Figure A.8. A comparison of 75/25 PLA3801X/PCL blends produced by: a) solvent casting, b) melt blending at 170 ˚C and 30 rpm.

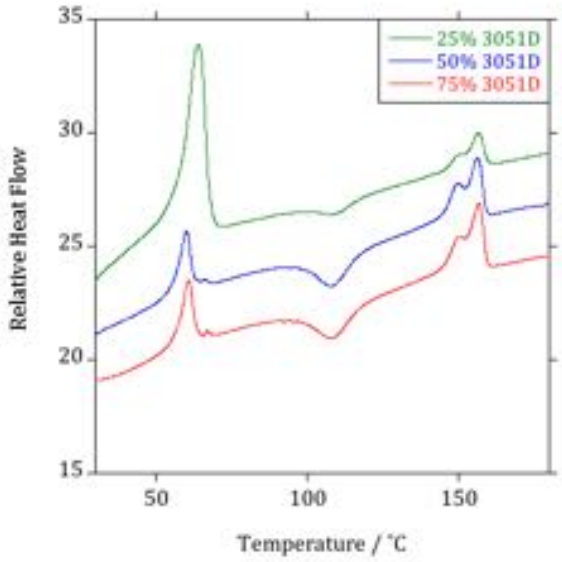

Figure A.9. Comparison of the PLA3051D/PCL blends produced at 160 ˚C and 30 rpm.

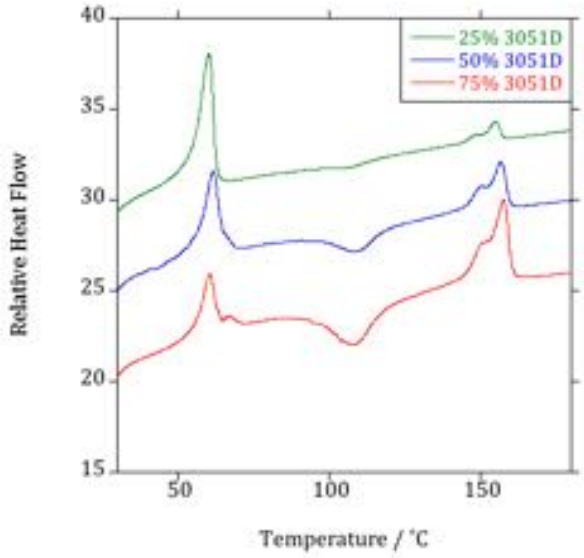

Figure A.10. Comparison of the PLA3051D/PCL blends produced in the presence of 5% carbon dioxide at 150 ˚C and 30 rpm.

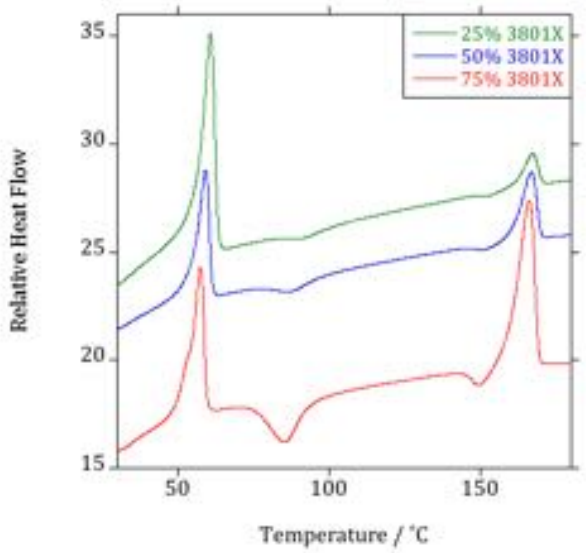

Figure A.11. Comparison of the PLA3801X/PCL blends produced at 170 °C and 30 rpm.

Polymer	**M_w / g mol^{-1}**	**M_n / g mol^{-1}**	**M_w/M_n**
PLA 3051D	151,114	81,543	1.85
PLA 3801X	130,275	60,412	2.16

Table A.1. SEC analysis of PLA 3051D and 3801X 'as received'.

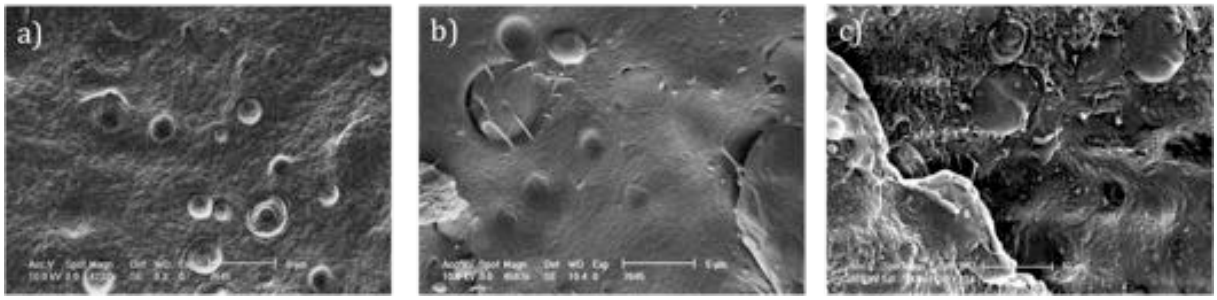

Figure A.12. Examples of alternative compositions of PLA4060D/PCL blends produced at 160 °C and 30 rpm: a) 15/85, b) 20/80 and c) 25/75 PLA/PCL. Images show that increasing the content of the dispersed phase, the size of the droplets increase due to coalescence of the relative increase in volume [4, 5].

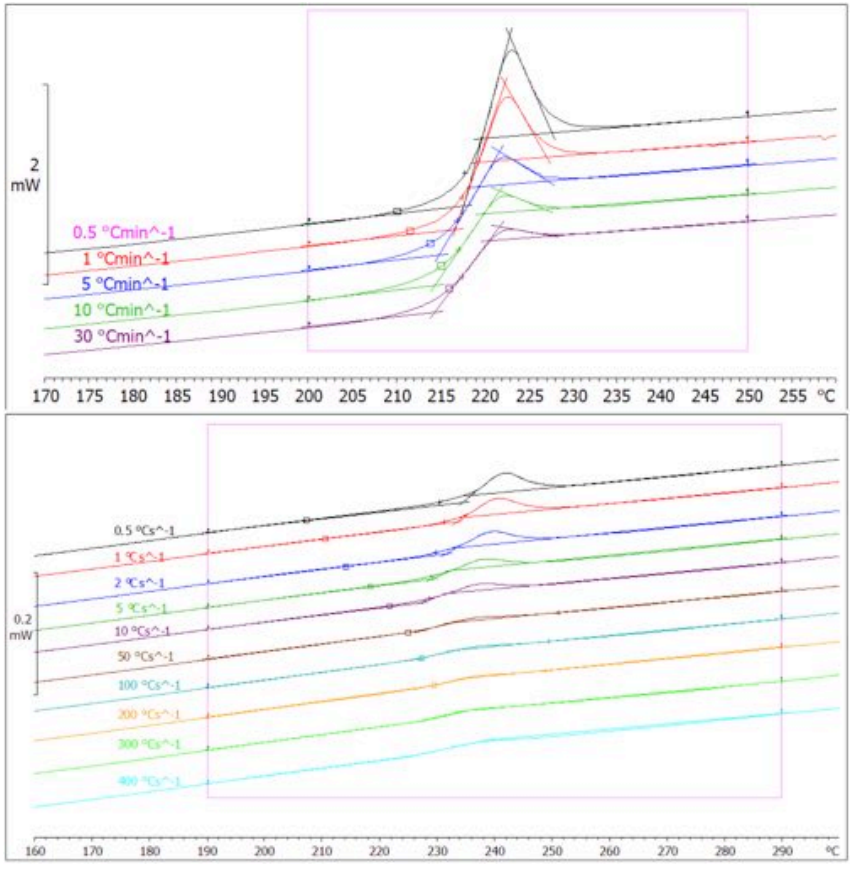

Figure A.13. An example of the consistent measurement procedure of the glass transitions across conventional and Flash DSC.

References

[1] NatureWorksLLC. (2010). *Collaborative Research to Advance Bioplastics: Developing Higher Value Bioplastic Applications* Available: http://www.biocom.iastate.edu/workshop/2010workshop/presentations/dan_sawyer.pdf

[2] P. Prentice, *Rheology and its Role in Plastics Processing*. Shropshire, UK: Rapra Techology Ltd., 1997.

[3] L. P. B. M. Janssen, *A phenomenological study on twin screw extruders*. Meppel: Krips Repro B.V., 1976.

[4] N. Noroozi, L. L. Schafer, and S. G. Hatzikiriakos, "Thermorheological properties of poly (ε-caprolactone)/polylactide blends," *Polymer Engineering & Science,* vol. 52, pp. 2348-2359, 2012.

[5] M. Todo, S. D. Park, T. Takayama, and K. Arakawa, "Fracture micromechanisms of bioabsorbable PLLA/PCL polymer blends," *Engineering Fracture Mechanics,* vol. 74, pp. 1872-1883, 2007.

APPENDIX 2

Article 1:

Murphy, S.H., Leeke, G.A. and Jenkins, M.J. “A Comparison of the use of FTIR spectroscopy with DSC in the characterisation of melting and crystallisation in polycaprolactone”. Journal of Thermal Analysis and Calorimetry. 107.2 (2012). DOI: 10.1007/s10973-011-1771-7

Article 2:

Kelly, C.A., Murphy, S.H., Leeke, G.A., Howdle, S.M., Shakesheff, K.M. and Jenkins, M.J. “Rheological studies of polycaprolactone in supercritical CO2”. European Polymer Journal. 49.2 (2013). DOI: 10.1016/j.eurpolymj.2012.11.021

Article 3:

Kelly, C.A., Murphy,S.H., Hillerström, A., Gilling, J., Massoudi, S., Jenkins, M.J. and Leeke, G.A. “Production of biodegradable foams using supercritical CO2”. Polymer-Plastics Technology and Engineering. 53.11 (2014). DOI: 10.1080/03602559.2014.886114

CO_2 ASSISTED BLENDING OF BIODEGRADABLE POLYESTERS

S.H. Murphy[1] J.J. Marsh[1], C.A. Kelly[1] , G.A. Leeke[2] and M.J. Jenkins[1*].

*[1] School of Metallurgy and Materials, University of Birmingham, Birmingham, B15 2TT – m.j.jenkins@bham.ac.uk**

[2] School of Chemical Engineering, University of Birmingham, Birmingham, B15 2TT

**corresponding author*

Abstract

High pressure CO_2 was utilised during blending to encourage miscibility between two normally immiscible polymers: poly(ε-caprolactone) (PCL) and poly(lactic acid) (PLA). Blends were prepared by a variety of different methods; solution casting from di-chloromethane, melt blending with a single-screw extruder and melt blending in the presence of carbon dioxide. High pressure CO_2 plasticises polymers, reducing their viscosities, encouraging increased molecular interaction between polymer chains. As a result, CO_2 assisted blends demonstrate improvements in mechanical properties and a significant reduction in the size and number of PCL droplets in a PLA matrix. Consequently, it is able to improve the adhesion between phases at the microscale.

Keywords: Poly(lactic acid), Poly(ε-caprolactone), blends, carbon dioxide, extrusion.

1. Introduction

The use of biodegradable polymers is becoming increasingly widespread as their applications broaden both into the biomedical [1] and food packaging industries [2]. Persistent rapid growth in the consumption of biodegradable plastics is forecast for the foreseeable future [3]. Among biopolymers, poly(lactic acid) (PLA) is the most prevalent in the market place, due to availability and having the most attractive cost structure [4]. It is extensively used in various medical applications, such as drug delivery [5] and scaffolds in tissue engineering [6]. Additionally, there is a growing interest in the use of PLA as food packaging because PLA can be derived from natural sustainable resources and it does not persist in landfill as it is biodegradable. PLA is produced from lactic acid which can be obtained from renewable (sustainable) resources such as corn and

sugarcane [7, 8]. It has therefore attracted attention as an alternative to synthetic non-biodegradable polymers. However, it has been reported that PLA is relatively brittle [9] and this has limited its range of applications. Accordingly, there have been a number of attempts to improve the mechanical properties of PLA through blending with other biodegradable (and less brittle) polymers: inclusion of a soft elastomeric heteropolymer into PLA has been identified as a method to yield improved mechanical properties of polymer blend [10, 11].

Poly(ε-caprolactone) (PCL) is a partially crystalline, biodegradable aliphatic polyester with a low T_g in the region of -60°C. PCL is a low modulus polymer and is ductile at room temperature, PCL can exhibit elongation-to-break values in the region of 800%. The ductility of PCL has made it a viable blend component for PLA [13].

PLA/PCL blends produced through solution casting from chloroform [10, 14] and methylene chloride [15] were found to be immiscible using DSC, DMA and SEM. Choi *et al.* studied the effect of compatibilsers; P(LLA-*co*-εCL) and P(LLA-*b*-εCL), on the morphology of PLA/PCL blends. Miscibility was not obtained, however there was a reduction in size of the dispersed PCL domains.

Broz *et al.* [15] found poor adhesion at the phase boundary interface and confirmed immiscibility and phase separation through NMR. It was hypothesised that to improve the mechanical properties of the blend, the samples should be annealed in the single-phase region of the LCST phase-diagram to enhance interfacial adhesion. They concluded that interfacial adhesion may occur when the majority phase is PCL [10] .

PLLA/PCL blends have also been produced through a conventional melt-mixer followed by reprocessing into plaques [9, 16]. Improvements were seen in the mechanical properties and the fracture toughness of PLA with the addition of just 5% PCL. The improvement is a result of multiple craze formation, nucleated by debonding of spherulite interfaces. SEM and DSC confirmed phase separation using this production method, although some adhesion was seen between phases.

In other polymer blend systems, high pressure and supercritical carbon dioxide (CO_2) assisted blending has been exploited in the production of PCL/PHB [17], PE/PS [18, 19] and PLA/PEG blends [20]. However, it has yet to be explored in the blending of PCL and PLA. The introduction of CO_2 into the melt has been seen to promote miscibility in polymer systems [17-19]. CO_2 is able to diffuse into the free volume of the system allowing Lewis acid-base reactions to occur, reducing the chain entanglements by inhibiting the secondary interactions between the chains [21]. This

expands the chain separations and facilitates chain motions. Blends of PE/PS prepared in the presence of CO_2 demonstrated a reduction in the size of the dispersed phase from a few microns to submicrons [18].

It can be seen from previous research that the blending of PCL and PLA has been found to be immiscible when prepared through solution and melt blending. Blending PLA and PCL in the presence of CO_2 has not been reported. Therefore, the aim of this work is to compare solution, melt and CO_2 assisted blending methods for the creation of PLA/PCL blends. More specifically, to determine whether scCO2 can induce miscibility is a polymer blend systems that has been shown otherwise to be immiscible.

2. Experimental

2.1 Materials

Poly(lactic acid) (PLA) grades; 2002D (M_w 194,000 g mol^{-1}) and 4060D (M_w 181,000 g mol^{-1}) in the form of pellets were supplied by NatureWorks LLC (Nebraska, USA). Poly(ε-caprolactone) (PCL) grade CAPA 6800 (M_w 212,000 g mol^{-1}) was supplied by Perstorp UK Ltd (Warrington, UK). CO_2 (purity 99.9 %v/v) was obtained from BOC (Birmingham, UK) and used as received.

2.2 Blend Preparation

Blends were prepared by solution casting and extrusion with and without the presence of CO_2. The following compositions were produced for each preparation method; 0/100, 25/75, 50/50, 75/25 and 100/0 by weight.

2.2.1 Solution Blending

Dichloromethane was chosen as a common solvent to dissolve both poly(lactic acid) and poly(ε-caprolactone). The required masses of each polymer (totalling 4 g) were dissolved in dichloromethane (40 ml) to give a 10 wt% solution. The solutions were then covered and stirred for 2 hours to ensure complete dissolution of both polymers. Films were cast into petri dishes, 9 cm in diameter, covered with glass lids and left to slowly evaporate for 2-3 days. It was found to be important to prevent the rapid evaporation of solvent in order to prevent the development of voids in the blend samples.

2.2.2 Production of Melt Blends by Extrusion

Prior to extrusion, the PLA grades were dried to remove any residual moisture. Drying temperatures and times were selected in accordance with the processing data sheets provided by Natureworks. Consequently, PLA 4060D was subjected to 4 hours at 45 °C and 2002D for 2 hours at 90 °C. The dried polymer was subsequently stored in desiccators with silica gel (previously dried).

The melt blends were produced using a Rondol (Staffordshire, UK) bench top linear 25 mm rotating single-screw extruder with a L/D (length/diameter) ratio of 25:1. The screw possesses a general purpose profile of 3:1 compression ratio. It was made of high strength carbon steel, heat-treated, polished and removable to enable cleaning. The screw speed was infinitely variable between 0 and 120 rpm. The barrel was also composed of heat-treated high strength carbon steel, fitted with bursting discs for over pressure protection. The temperature was controlled through a series of heaters, one in each of the three zones. The barrel and die temperatures were controlled between 0-300 ˚C and cooled using a tangential water cooling system. A stainless steel two roll take-off unit (with cooling / polishing rolls) placed after the die, cooled the extrudate before passing onto a conveyor belt.

Blends of pre-mixed pellets were added to the hopper of the extruder in 200g batches. Barrel and die temperatures were set to 160 ˚C and 170 ˚C respectively. The pressure in the screw was monitored using an external pressure transducer. Samples were extruded through a 1 mm slit die and passed through the cooled rollers onto a conveyor belt. Screw speeds of 20 and 30 rpm were selected.

2.2.3 Production of Carbon Dioxide Assisted Blends

Blends were also produced in the presence of CO_2 using the same extruder as discussed above, however the extruder was modified to allow the injection of CO_2 into the polymer melt.

CO_2 was injected via a custom made design of 4 injection ports, 2 on either side of the barrel, into zones 2 and 3 (see figure 1 for extruder set-up). A Jasco pump (Model PU-2086 Plus) fitted with a chiller head enabled CO_2 to be pumped in liquid form. A pressure relief valve was installed to

prevent over pressurisation in the extruder. The pressure in the extruder was monitored using a pressure transducer.

In order to calculate the CO_2 concentration for addition into the extruder, each polymer was extruded at both 20 and 30 rpm and the average of three extruded masses per minute was calculated for each screw speed. The CO_2 flow rate (g/min) was then calculated as a wt% of the measured polymer mass extruded per minute using equation 1. This enabled the input of a given concentration of CO_2, in relation to the polymer, into the extruder. This calculated value was converted into ml/min as CO_2 was injected as liquid. Equation 2 shows this conversion. The density of CO_2 was calculated by NIST web-book [22] as 0.91898 g ml^{-1} based on the CO_2 pressure and temperature in the pump.

$$\boldsymbol{Flow\ rate_{CO2}\ (g/min)} = \frac{\boldsymbol{CO_2\ Concentration\ (wt\%)}}{\mathbf{100}} \times \boldsymbol{Flow\ rate_{polymer}\ (g/\mathrm{min}\ )} \qquad \textbf{[Eq. 1]}$$

$$\boldsymbol{Flow\ rate_{CO2}\ (ml/\mathrm{min})} = \frac{\boldsymbol{Flow\ rate_{CO2}\ (g/\mathrm{min})}}{\boldsymbol{Density_{CO2}\ (g/\mathrm{min})}} \qquad \textbf{[Eq. 2]}$$

Since CO_2 is known to depress the melting point of semi-crystalline polymers, it was found that blends of PLA and PCL could be readily extruded at reduced barrel and die temperatures of 150 °C and 160 °C, respectively.

2.3 Microstructural, Mechanical and Thermal Analysis

Fracture surfaces were produced by a flexural loading of the blend samples following immersion in liquid nitrogen. The fracture surfaces were mounted on an aluminium stub using conductive carbon adhesive discs and coated in gold using a Polaron SC7640 sputter coater. Coating the samples for 3 minutes deposited approximately 10 to 12 nm of gold, which provided sufficient conductivity to minimize charging of the sample surface. Samples were imaged using a Phillips (XL30 ESEM) scanning electron microscope. An accelerating voltage of 10 kV was selected.

Tensile tests were carried out using a mechanical test instrument (Instron 5566) interfaced to a PC. The instrument was controlled using proprietary Instron Merlin software. Samples were cut into a

standard 25 mm (L_o) 'dog-bone' shape. The width of the narrow central section was 4 mm and the thickness was recorded from a three-point average. Stress-strain curves were recorded at 25 ˚C and at a strain rate of 10 mm/min. Young's modulus, elongation to break and yield stress were determined from the resulting stress-strain curves. A minimum of 5 repeats were performed for each blend system.

Thermal analysis of the blends was performed using a Mettler Toledo DSC1 (Greifensee, Switzerland) purged with nitrogen at a gas flow rate of 100 cm^3/min. The instrument was interfaced to a personal computer and controlled using proprietary STARe software (version 11). The thermal response of the instrument was calibrated from the enthalpy of fusion of a known mass of indium (99.999% pure). The temperature of the calorimeter was calibrated using the melting point of tin. Samples of around 5-7 mg were contained in aluminium pans with an empty pan used as a reference. The glass transition temperature (T_g), melting point (T_m) and enthalpy of fusion (ΔH_f) of the blends were measured from the initial heating run at 10 ˚C/min.

3. Results and Discussion

3.1 Microstructural Characterisation

The blends created by solution casting from dichloromethane showed clear evidence of gross phase separation with relatively large droplets (up to 10 µm) as observed by SEM (Figure 2a and 2b). This observation is in accordance with other studies in which clear phase separation is reported, although it should be noted that these observations were made in blends produced from different grades of PLA and PCL.

Melt blending with a single screw extruder was also found to yield a phase separated system at all compositions and screw speeds investigated. However, a clear improvement in dispersion and droplet size (reduced from 10 µm by solution casting to around 1 µm by melt blending) was observed in the 75/25 PLA/PCL composition (Figures 3a and 3b).

A further improvement in the dispersion was observed when the blends were prepared in the presence of CO_2 (Figures 4a and 4b). Similar to the melt blends, the blend composition that

showed the greatest reduction in size and dispersion of droplets was 75/25 PLA/PCL. Droplet sizes in these blends were around 0.2 μm in diameter. However, all blends produced in the presence of CO_2 showed a high degree of porosity (around 100 nanometers in diameter) due to the effect of depressurisation of the blend system on exit from the extruder.

Solution casting from dichloromethane dissolves both polymers allowing constituent polar groups to interact. However, slow evaporation of the solvent (which was required in order to reduce the formation of voids) allows time for the polymers to phase separate and encourages crystallinity to develop causing further phase separation to occur. The observation of phase separation in previous PLA/PCL solution-cast blends was attributed to crystallisation of PCL and expulsion of PLA in these crystalline regions through spherulitic growth [23]. It was noted that phase separation may also be induced by the presence of a third component, the solvent. Solution-casting these blends promotes phase separation and may not reflect the true morphology of the two component systems.

The application of heat (160 °C which is above the melting points of both polymers) combined with the shear forces of mechanical mixing during melt blending, initially creates a higher level of dispersion allowing the blends to transform from the two phase into the one phase region of the LCST curve [13].

The polymer blend solution was initially transparent and no interfacial boundary layers were observed as a result of any solution density differences. Therefore, molecular level mixing was assumed to have taken place. Subsequently, no boundary layers were observed to develop on evaporation of the solvent, yet the final blend was grossly phase separated. Clearly, the phase separation observed in this preparation method was induced by crystallisation of the homopolymers from solution.

In the case of the melt blend preparation, the high shear forces encountered in the barrel encourage dispersion of the blend components. The morphology of the blend system is stabilised on cooling after the exit from the die at the end of the barrel. If there is vitrification of the PLA component prior to the crystallisation-induced phase separation of PCL from the blend, a miscible

system will be retained. However, in this case, the cooling rate was insufficient to limit the phase separation of PCL, although an enhanced dispersion was still evident.

Low interfacial tension, high shear rates and similar viscosities of both polymers contribute to the size and homogeneity of the dispersed phase and final sample morphology [24]. The situation in the blends produced in the presence of CO2 was somewhat improved.

The gaseous properties of CO_2 enables its diffusion into the free volume of polymers, between the individual chains. Once inside, CO_2 forms Lewis acid-base interactions with the carbonyl groups (present in both PLA and PCL). This disrupts the inter/intra molecular interactions, decreasing the number of chain entanglements within the polymers and consequently reduces their melting point and viscosity [21]. The creation of additional free volume and increased chain mobility enables better interaction and mixing between the two polymers, enhancing the potential for miscibility in this system.

Blend morphology has been investigated in other polymer systems: PE/PS blends and PS/PMMA using carbon dioxide [18, 19, 25]. These blends showed a significant decrease in the size of the dispersed phase from a few microns to submicron by injecting CO_2. In summary, the introduction of CO_2 into a blend, reduces the viscosity and also the interfacial tension between the two polymers. As a result, an improvement is seen in droplet size and dispersion when producing immiscible blends in the presence of carbon dioxide.

Figure 5 shows a representative example of the engineering stress-strain curves for all the PLA4060D/PCL blends produced by melt blending. The curve for 100% PLA is shown as an inset due to the dramatic change in elongation-to-break across composition. It is clear that with increasing PCL content in the blend, the tensile behaviour of the blend system changed dramatically: the reduction in yield stress was compensated by a significant increase in elongation at break. The same trend was also apparent in the PLA 2002D system.

Figures 6, 7 and 8 illustrate the variation of mechanical properties with composition of both blend systems for all three preparation methods. The mechanical properties of the blends produced by melt and CO_2 assisted extrusion generally change linearly with composition, suggesting that they

are obeying the rule of mixtures. PCL has a higher elongation than PLA and by blending these polymers together the properties combine resulting in a higher elongation for the blend. It is evident there is a significant improvement in properties from solution casting to melt blending. For example, the 25/75 PLA2002D/PCL solvent casting sample had an elongation to break of 25% in contrast to the same composition produced by melt blending, with elongation around 780% (figure 6b). Blending in the presence of carbon dioxide exhibits similar mechanical properties to those produced by melt blending. However, there are a number of instances where this preparation method of blending exhibits superior properties. For example, in the PLA 2002D system, the CO_2 assisted blends have the highest elongation to break for the 75/25 PLA/PCL samples, the greatest Young's Modulus for both 50/50 and 75/25 PLA/PCL, and the highest yield stress demonstrated in the compositions 25/75, 50/50 and 75/25 PLA/PCL. This corresponds with the improved dispersion observed by SEM, despite the increased porosity in the samples produced with carbon dioxide.

The improvement in mechanical properties indicates that CO_2 has influenced the interfacial tension between both polymers enabling better mixing and dispersion of phases. As a result, partial miscibility developed between both phases subsequently improves the mechanical properties. The finer dispersion of droplets results in lower number of stress concentration points throughout the sample. This result is consistent with Todo *et al.* [9] who found that larger PCL domains within PCL/PLA blends hasten the initiation of fracture by inducing more severe stress concentrations than smaller phases within the blends.

3.2 Thermal Analysis

Figures 9a and 9b show the DSC traces of 75/25 PLA/PCL and respective homopolymers for the PLA4060D/PCL and PLA2002D/PCL blends produced with and without the presence of carbon dioxide. The observation of two melting peaks in figure 9b confirms that phase separation has taken place in blends made by both techniques, and that any interactions in the melt were not significant enough to develop / retain miscibility on cooling.

The melt blend exhibits a much larger melting endotherm for the PCL component (figure 9a and 9b) than that observed for the CO_2 assisted blend. The corresponding ΔH_f PCL values are 62.66 Jg^{-1}

for 100% PCL, 46.6 Jg^{-1} for the melt blend and 17.14 Jg^{-1} for the blend produced in the presence of carbon dioxide. There is a surprisingly low degree of crystallinity in the CO_2 assisted blend and this may be attributed to a reduction in the nucleation density in the droplet as the droplet size decreases. The reduction in crystallinity may be associated with fractionated crystallisation of the PCL component, influenced by a decreased number of nuclei per droplet, the crystallinity sees a drastic reduction [26]. Similar results have been observed in PCL/PHB blends, where fractionated crystallisation also occurs in the PCL component. This result was attributed to the dispersion of PCL into isolated droplets, greater in number than the available active heterogeneities usually present in the bulk homopolymer [27]. A reduction in PCL crystallinity corresponding with decreased droplet size has also been reported in PLLA/PCL blends [14]. Furthermore, (figure 9b), the glass transition of PLA can now be partially observed immediately prior to the melting endotherm of PCL (in the 75/25 PLA2002D/PCL blend produced in the presence of carbon dioxide). The PLA glass transition midpoint for this blend is 52 ˚C compared to 56 ˚C exhibited by the homopolymer. This slight reduction in Tg of PLA suggests the development of partial miscibility. The PLA4060D/PCL blends (figure 9a) produced in the presence of carbon dioxide also exhibit a reduction in PCL crystallinity. The glass transition for PLA 4060D cannot be determined due to the overlapping transition corresponding to the melting of PCL. 100% extruded PCL and the 75/25 PLA4060D/PCL melt blend exhibits a peak melting point at 63 ˚C. However, a reduction of 4 ˚C in the peak melting point of PCL (59 ˚C) is apparent in the 75/25 PLA/PCL blend produced in the presence of carbon dioxide, again indicating partial miscibility.

Cold crystallisation is observed between the melting peak of PCL and PLA (figure 9b) suggesting that PCL may be acting as a nucleating agent for PLA. The finer distribution of PCL droplets (acting as more nucleating points) within the CO_2 assisted blend may allow additional crystallisation to occur upon heating. It has been commonly reported [28, 29] that PLA exhibits relatively slow crystallisation kinetics and it has been found that within the time-scales of a conventional DSC experiment run at 10 ˚C/min, PLA will not undergo crystallisation (on cooling) from the melt. Therefore, it is unusual to observe a melting endotherm post processing. The double melting peak on the PLA component for the CO_2 assisted blend indicates the formation of different lamellae sizes, often explained by the melt-recrystallisation model [8, 9]. The appearance of multiple

melting peaks is reported in numerous partially crystalline polymers [30] such as poly(ether-ether-ketone) PEEK [31, 32], poly(ethylene terephthalate) PET [33], poly(butylene napthalate) PBN [34], nylon-6 [35] and biodegradable polymers such as poly($_L$-lactide-*co*-glycolide) PLGA [36], poly (lactic acid) PLA [37]. Many explain the double melting behaviour using the melt-recrystallisation model [38]. According to this model, the low temperature and high temperature endothermic peaks in the DSC melting trace are attributed to melting of original crystals (formed upon previous cooling) and to the melting of crystals formed within the heating scan of the experiment.

4. Conclusions

Blends produced by solution casting display immiscibility across all compositions. A significant improvement in mechanical properties and droplet size was observed through melt blending using a single screw extruder. Although the mechanical properties of the CO_2 assisted blends showed little improvement on those samples made by melt blending, the SEM images clearly indicate an improvement at the microscale. However, porous structures have been observed which explain the lack of a significant improvement in mechanical properties. Regardless of the porosity within these samples, it must be noted that an improvement in mechanical properties is found, particularly for the 75/25 PLA/PCL blends. For this blend composition, CO_2 assisted extrusion provides the most effective method of blending (with the greatest elongation to break and a finer dispersed phase) compared to the other blending techniques.

The findings of CO_2 assisted extrusion indicate that by injecting CO_2 into the polymer melt, the CO_2 is able to act as a molecular lubricant by reducing the polymer viscosity and encouraging increased molecular interaction of the polymer chains. Consequently resulting in adhesion and partial miscibility between phases at the microscale.

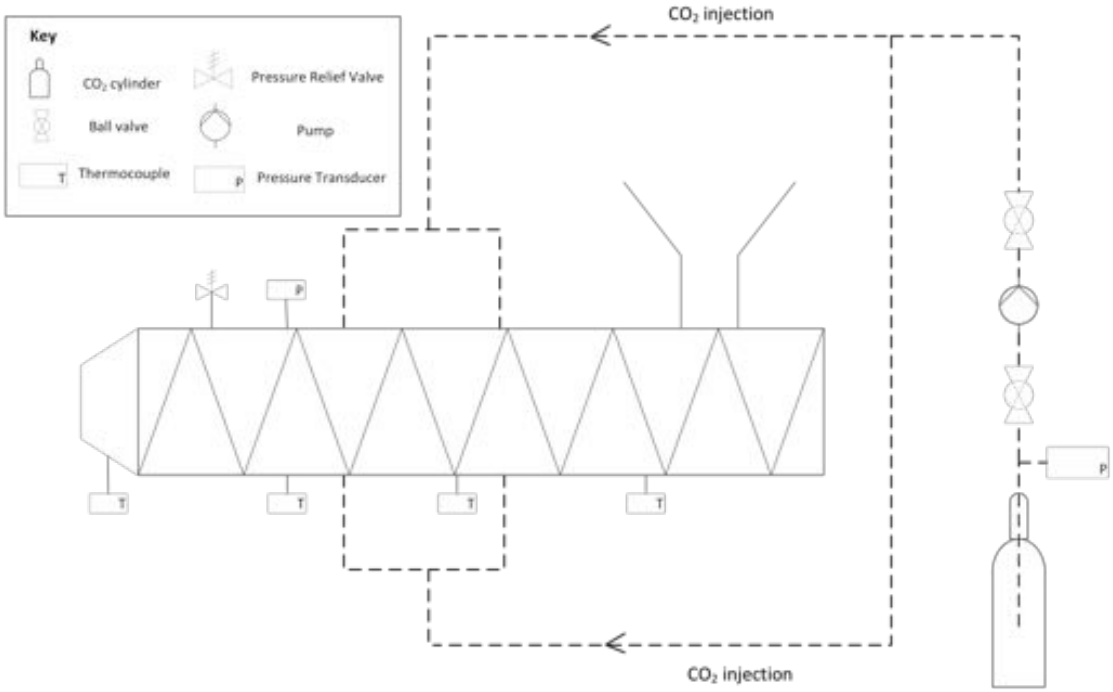

Figure 1. Schematic of the extruder set-up illustrating the injection of CO_2.

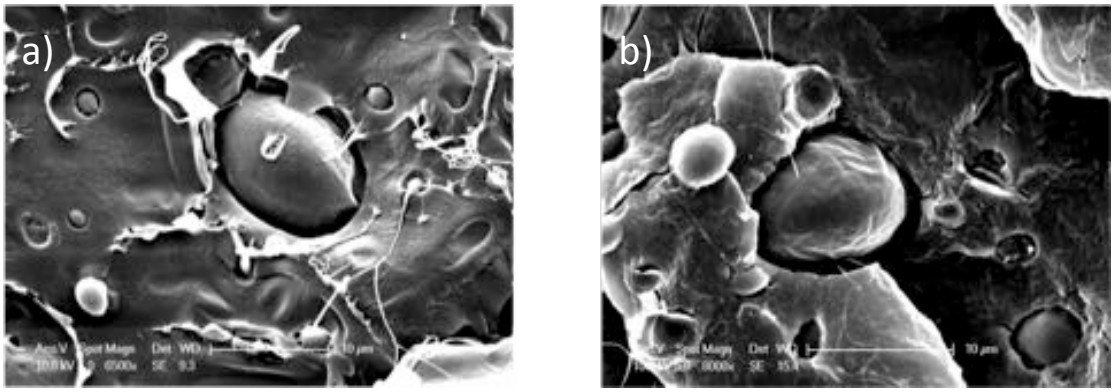

Figure 2a and b. SEM images of solution cast **(2a):** 75/25 PLA4060D/PCL and **(2b):** 75/25 PLA2002D/PCL.

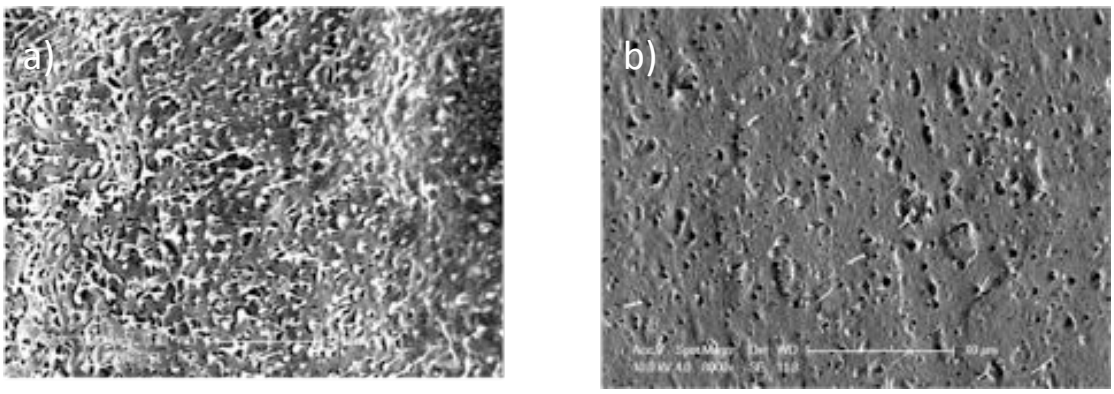

Figure 3a and b. SEM images of melt blends produced with a single screw extruder at 160 °C. **(3a):** 75/25 PLA4060D/PCL at 20 rpm. **(3b):** 75/25 PLA2002D/PCL at 30 rpm.

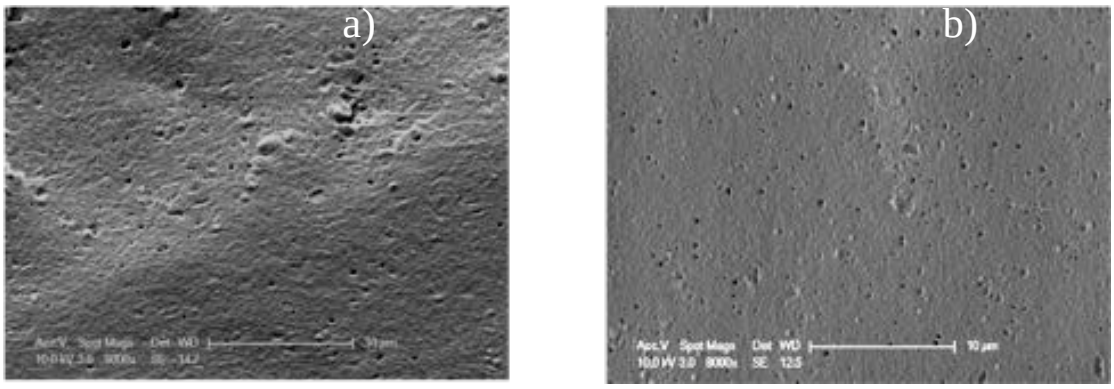

Figure 4a and b. SEM images of blends produced in the presence of 10% carbon dioxide at 150 ˚C. **(4a):** 75/25 PLA4060D/PCL at 20 rpm. **(4b):** 75/25 PLA2002D/PCL at 30 rpm.

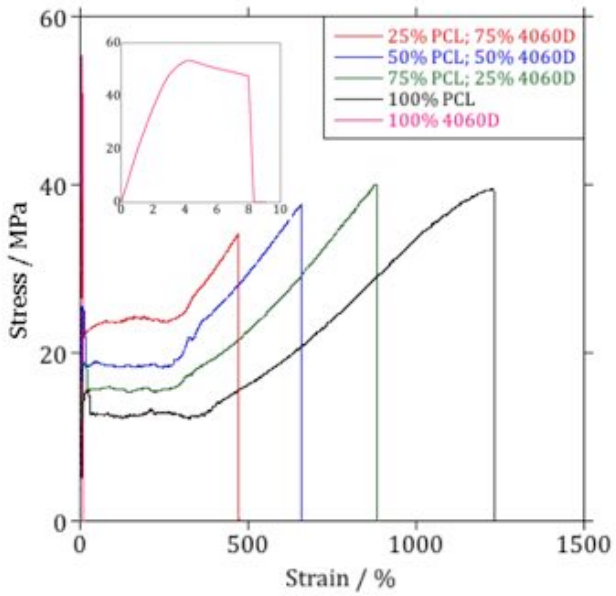

Figure 5. An example of the engineering stress-strain curves for the mechanically blended PLA4060D/PCL blend system. Inset top left is the result for 100% PLA.

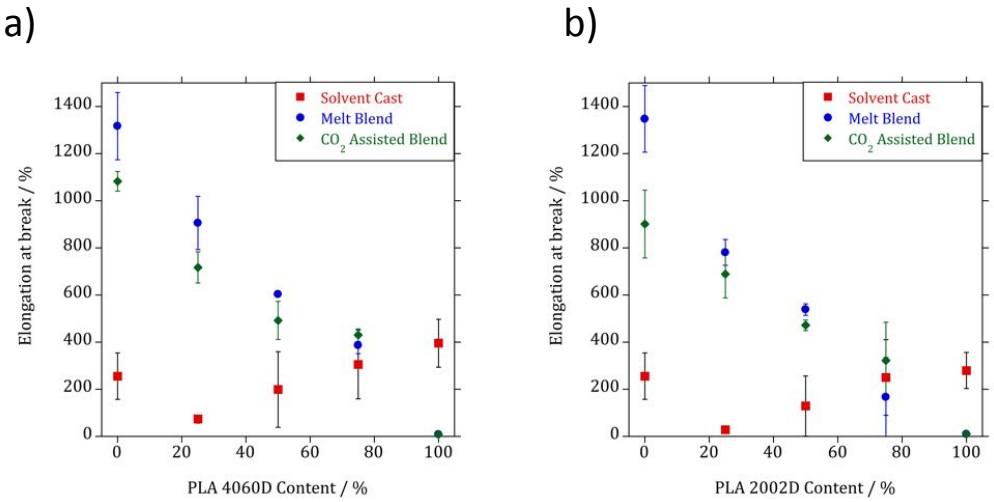

Figure 6a and 6b. A comparison of elongation at break for solution cast, melt and CO_2 assisted blends of **(6a):** PLA 4060D and **(6b):** PLA 2002D/PCL at various compositions. The standard uncertainty is denoted by error bars, which represents the standard deviation averaged over multiple experiments.

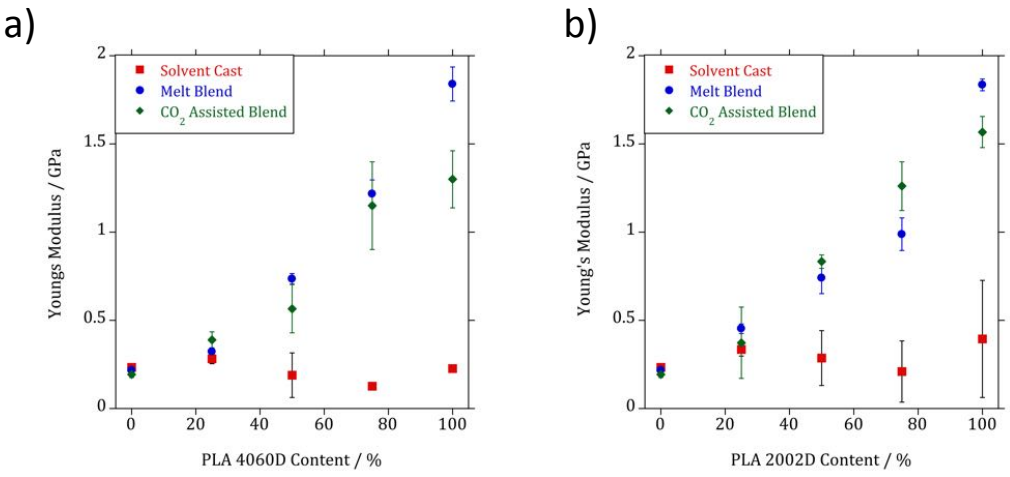

Figure 7a and 7b. A comparison of Young's Modulus for solution cast, melt and CO_2 assisted blends of **(7a):** PLA 4060D and **(7b):** PLA 2002D/PCL at various compositions. The standard uncertainty is denoted by error bars, which represents the standard deviation averaged over multiple experiments.

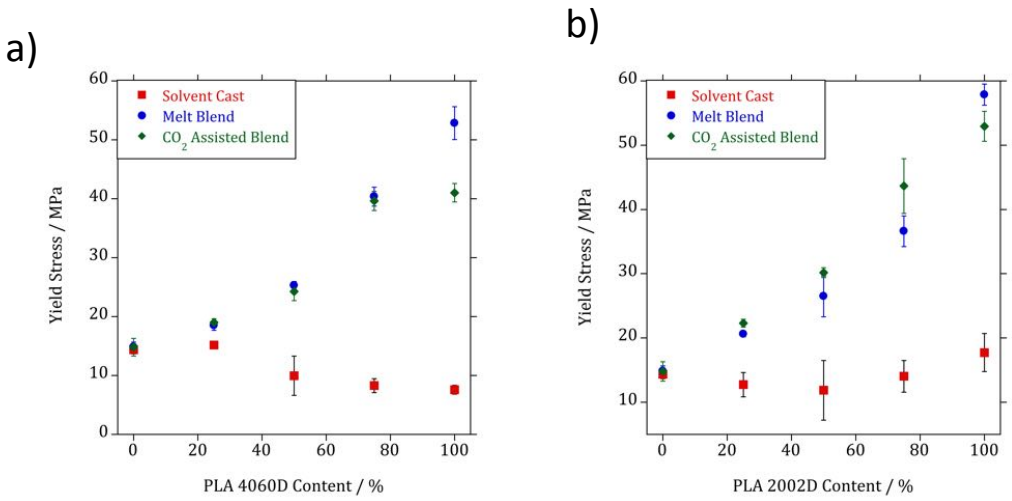

Figure 8a and 8b. A comparison of yield stress for solution cast, melt and CO_2 assisted blends of **(8a):** PLA 4060D and **(8b):** PLA 2002D/PCL at various compositions. The standard uncertainty is denoted by error bars, which represents the standard deviation averaged over multiple experiments.

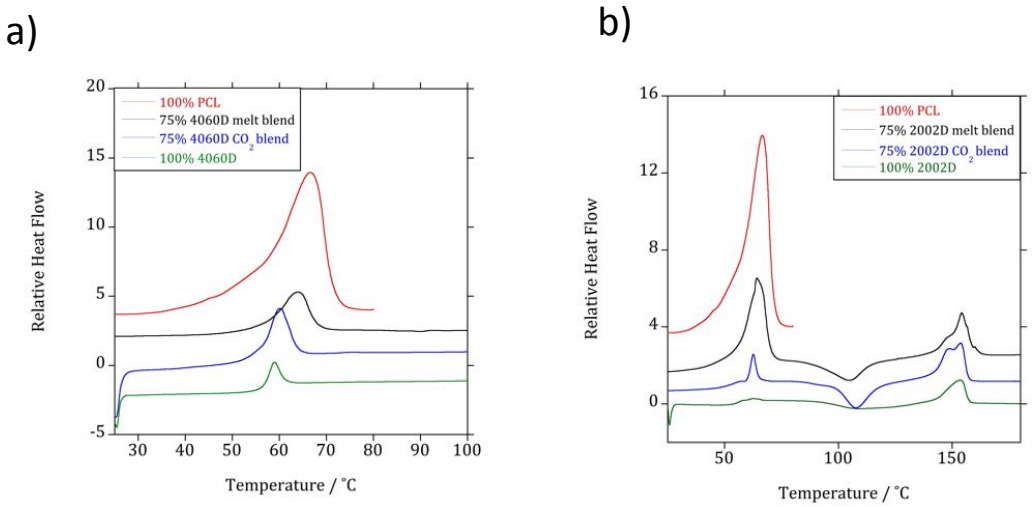

Figure 9a and 9b. A comparison of DSC traces of **(9a):** 75/25 PLA4060D/PCL and **(9b):** 75/25 PLA2002D/PCL produced by melt and CO_2 assisted blending with their homopolymers.

5. References

[1] Z. Zhang, O. Ortiz, R. Goyal, and J. Kohn, "Biodegradable Polymers," in *Handbook of Polymer Applications in Medicine and Medical Devices*, K. Modjarrad and S. Ebnesajjad, Eds., ed Oxford: William Andrew Publishing, 2014, pp. 303-335.

[2] M. Bhattacharya, R. L. Reis, V. Correlo, and L. Boesel, "Material properties of biodegradable polymers," in *Biodegradable polymers for industrial applications*, R. Smith, Ed., ed Cambridge: Woodhead Publishing Limited, 2005.

[3] IHS. (2012). *Biodegradable Polymers*. Available: http://www.ihs.com/products/chemical/planning/ceh/biodegradable-polymers.aspx

[4] W. Groot, J. V. Krieken, O. Sliekersl, and S. De Vos, "Production and Purification of Lactic Acid and Lactide," in *Poly(lactic acid) Synthesis, Structures, Properties, Processing, and Applications*, R. Auras, L.-T. Lim, S. E. M. Selke, and H. Tsuji, Eds., ed New Jersey: Wiley, 2010.

[5] K. S. Soppimath, T. M. Aminabhavi, A. R. Kulkarni, and W. E. Rudzinski, "Biodegradable polymeric nanoparticles as drug delivery devices," *Journal of Controlled Release,* vol. 70, pp. 1-20, 1/29/ 2001.

[6] V. Guarino, F. Causa, P. Taddei, M. di Foggia, G. Ciapetti, D. Martini*, et al.*, "Polylactic acid fibre-reinforced polycaprolactone scaffolds for bone tissue engineering," *Biomaterials,* vol. 29, pp. 3662-3670, 9// 2008.

[7] D. Garlotta, "A Literature Review of Poly(Lactic Acid)," *Journal of Polymers and the Environment,* vol. 9, pp. 63-84, 2001.

[8] NatureWorksLLC. (2013). *How Ingeo Is Made*. Available: http://www.natureworksllc.com/The-Ingeo-Journey/Eco-Profile-and-LCA/How-Ingeo-is-Made

[9] M. Todo, S. D. Park, T. Takayama, and K. Arakawa, "Fracture micromechanisms of bioabsorbable PLLA/PCL polymer blends," *Engineering Fracture Mechanics,* vol. 74, pp. 1872-1883, 2007.

[10] N. López-Rodríguez, A. López-Arraiza, E. Meaurio, and J. R. Sarasua, "Crystallization, morphology, and mechanical behavior of polylactide/poly(ε-caprolactone) blends," *Polymer Engineering & Science,* vol. 46, pp. 1299-1308, 2006.

[11] J. Zhao, X. Yuan, Y. Cui, Q. Ge, and K. Yao, "Preparation and characterization of poly(L-lactide)/ poly(ϵ-caprolactone) fibrous scaffolds for cartilage tissue engineering," *Journal of Applied Polymer Science,* vol. 91, pp. 1676-1684, 2004.

[12] D. Wu, D. Lin, J. Zhang, W. Zhou, M. Zhang, Y. Zhang*, et al.*, "Selective Localization of Nanofillers: Effect on Morphology and Crystallization of PLA/PCL Blends," *Macromolecular Chemistry and Physics,* vol. 212, pp. 613-626, 2011.

[13] J. C. Meredith and E. J. Amis, "LCST phase separation in biodegradable polymer blends: poly(D,L-lactide) and poly(ϵ-caprolactone)," *Macromolecular Chemistry and Physics,* vol. 201, pp. 733-739, 2000.

[14] N.-S. Choi, C.-H. Kim, K. Y. Cho, and J.-K. Park, "Morphology and hydrolysis of PCL/PLLA blends compatibilized with P(LLA-co-ϵCL) or P(LLA-b-ϵCL)," *Journal of Applied Polymer Science,* vol. 86, pp. 1892-1898, 2002.

[15] M. E. Broz, D. L. VanderHart, and N. R. Washburn, "Structure and mechanical properties of poly(,-lactic acid)/poly([var epsilon]-caprolactone) blends," *Biomaterials,* vol. 24, pp. 4181-4190, 2003.

[16] C. L. Simões, J. C. Viana, and A. M. Cunha, "Mechanical properties of poly(ε-caprolactone) and poly(lactic acid) blends," *Journal of Applied Polymer Science,* vol. 112, pp. 345-352, 2009.

[17] M. J. Jenkins, Y. Cao, L. Howell, and G. A. Leeke, "Miscibility in blends of poly(3-hydroxybutyrate-co-3-hydroxyvalerate) and poly(ε-caprolactone) induced by melt blending in the presence of supercritical CO2," *Polymer,* vol. 48, pp. 6304-6310, 2007.

[18] M. Lee, C. Tzoganakis, and C. B. Park, "Extrusion of PE/PS blends with supercritical carbon dioxide," *Polymer Engineering & Science,* vol. 38, pp. 1112-1120, 1998.

[19] M. Lee, C. Tzoganakis, and C. B. Park, "Effects of supercritical CO2 on the viscosity and morphology of polymer blends," *Advances in Polymer Technology,* vol. 19, pp. 300-311, 2000.

[20] C. A. Kelly, A. Naylor, L. Illum, K. M. Shakesheff, and S. M. Howdle, "Supercritical CO2: A Clean and Low Temperature Approach to Blending PDLLA and PEG," *Advanced Functional Materials,* vol. 22, pp. 1684-1691, 2012.

[21] Z. Shen, M. A. McHugh, J. Xu, J. Belardi, S. Kilic, A. Mesiano*, et al.*, "CO2-solubility of oligomers and polymers that contain the carbonyl group," *Polymer,* vol. 44, pp. 1491-1498, 2003.

[22] NIST. (2011). *NIST Chemistry WebBook*. Available: http://webbook.nist.gov/chemistry/fluid/

[23] H. Tsuji and Y. Ikada, "Blends of aliphatic polyesters. I. Physical properties and morphologies of solution-cast blends from poly(DL-lactide) and poly(ε-caprolactone)," *Journal of Applied Polymer Science,* vol. 60, pp. 2367-2375, 1996.

[24] L. P. B. M. Janssen and S. Nalawade, P., "Polymer Extrusion with Supercritical Carbon Dioxide," in *Supercritical Carbon Dioxide: in Polymer Reaction Engineering*, M. F. Kemmere and T. Meyer, Eds., ed Germany: WILEY-VCH, 2005.

[25] M. D. Elkovitch, D. L. Tomasko, and L. J. Lee, "Supercritical carbon dioxide assisted blending of polystyrene and poly(methyl methyacrylate)," *Polymer Engineering & Science,* vol. 39, pp. 2075-2084, 1999.

[26] L. A. Utracki, *Polymer Blends* vol. 11: Rapra Technology, 2000.

[27] D. Lovera, L. Márquez, V. Balsamo, A. Taddei, C. Castelli, and A. J. Müller, "Crystallization, Morphology, and Enzymatic Degradation of Polyhydroxybutyrate/Polycaprolactone (PHB/PCL) Blends," *Macromolecular Chemistry and Physics,* vol. 208, pp. 924-937, 2007.

[28] M. Salmerón Sánchez, V. B. F. Mathot, G. Vanden Poel, and J. L. Gómez Ribelles, "Effect of the Cooling Rate on the Nucleation Kinetics of Poly(l-Lactic Acid) and Its Influence on Morphology," *Macromolecules,* vol. 40, pp. 7989-7997, 2007/10/01 2007.

[29] W. T. Zhai, Y. Ko, W. L. Zhu, A. S. Wong, and C. B. Park, "A Study of the Crystallization, Melting, and Foaming Behaviors of Polylactic Acid in Compressed CO2," *International Journal of Molecular Sciences,* vol. 10, pp. 5381-5397, Dec 2009.

[30] S. Z. D. Cheng and B. Wunderlich, "Thermal analysis of thermoplastic polymers," *Thermochimica Acta,* vol. 134, pp. 161-166, 10// 1988.

[31] S. Z. Cheng, M. Cao, and B. Wunderlich, "Glass transition and melting behavior of poly (oxy-1, 4-phenyleneoxy-1, 4-phenylenecarbonyl-1, 4-phenylene)(PEEK)," *Macromolecules,* vol. 19, pp. 1868-1876, 1986.

[32] B. B. Sauer, W. G. Kampert, E. Neal Blanchard, S. A. Threefoot, and B. S. Hsiao, "Temperature modulated DSC studies of melting and recrystallization in polymers exhibiting multiple endotherms," *Polymer,* vol. 41, pp. 1099-1108, 2// 2000.

[33] P. J. Holdsworth and A. Turner-Jones, "The melting behaviour of heat crystallized poly(ethylene terephthalate)," *Polymer,* vol. 12, pp. 195-208, 3// 1971.

[34] M. Yasuniwa, S. Tsubakihara, and T. Fujioka, "X-ray and DSC studies on the melt-recrystallization process of poly(butylene naphthalate)," *Thermochimica Acta,* vol. 396, pp. 75-78, 2003.

[35] M. Todoki and T. Kawaguchi, "Origin of double melting peaks in drawn nylon 6 yarns," *Journal of Polymer Science: Polymer Physics Edition,* vol. 15, pp. 1067-1075, 1977.

[36] Y. Wang and J. F. Mano, "Multiple melting behaviour of poly(l-lactide-co-glycolide) investigated by DSC," *Polymer Testing,* vol. 28, pp. 452-455, 2009.

[37] M. Yasuniwa, S. Tsubakihara, Y. Sugimoto, and C. Nakafuku, "Thermal analysis of the double-melting behavior of poly(L-lactic acid)," *Journal of Polymer Science Part B: Polymer Physics,* vol. 42, pp. 25-32, 2004.

[38] B. Wunderlich, *Macromolecular Physics* vol. 3. London: Academic Press, 1980.